Regioselective, Nucleophilic Activation of C-F Bonds in *o*-Fluoroanilines

Sarita Elizabeth Hough

Thesis submitted to the faculty of Virginia Polytechnic Institute and State University
in partial fulfillment of the requirements for the degree of

Master of Science

in

Chemistry

Paul A. Deck, Chair

Harry C. Dorn

Joseph S. Merola

Amanda J. Morris

13 May 2019

Blacksburg, Virginia

Keywords: titanium amide, S_NAr, defluorination, anilines, organometallic, nucleophiles

Regioselective, Nucleophilic Activation of C-F Bonds in *o*-Fluoroanilinee

Sarita Elizabeth Hough

Abstract

Reactions of fluorinated anilines with stoichiometric $Ti(NMe_2)_4$ in mesitylene (typically for 23 h at 120 °C) afforded moderate to high yields of the corresponding *N*,*N*-dimethyl-*o*-phenylenediamine derivatives resulting from defluoroamination of a fluorine atom *ortho* to the NH_2 of the starting aniline. Reactivity increased with additional ring fluorination in general accordance with established regiochemical (activating and deactivating) trends. Based on results, we propose a metal-mediated, S_NAr-based mechanism. We report the scope and limitations of this reaction and discuss trends in reactivity according to a putative mechanistic scheme.

Regioselective, Nucleophilic Activation of C-F Bonds in *o*-Fluoroanilines

Sarita Elizabeth Hough

General Audience Abstract

This thesis describes reactions of fluorinated anilines with titanium amides to make fluorinated 1,2-phenylenediamines. The reaction gives high to moderate yields, and is highly selective for *ortho* substitution. The scope of the reaction, trends in reactivity among substrates, product characterization, and reaction mechanism are discussed. This reaction is of interest because fluorinated aniline derivatives are a privileged structural motif in pharmaceuticals and agricultural chemicals. The first chapter presents an overview of C-F bond activation and key background information. Chapter 2 is a description of the experiments and an in-depth analysis of their results. Chapter 3 presents detailed characterization data for substances generated in this research. Chapter 4 comprises some concluding remarks and plans for possible future extensions of the research.

Acknowledgements

I would like to thank Dr. Deck for his advice, help, and mentoring. I would also like to thank my committee members for their advice and insight. I would like to thank Ken Knott, Geno Iannaccone, Bill Bebout, and Mehdi Ashraf-Khorassani for their invaluable advice and assistance with product characterization, and Joli Huynh for guidance in navigating the administrative side of graduate school. I would like to thank Kevin Kaurich, Loren Brown, Chris Houser, Chad Bernier, and Chrissy DuChane for advice, insight, and assistance, as well as Ophelia Wadsworth, Spencer Schultz, and Brittany Bonnett. Last, but not least, I would like to thank my family for their support and encouragement.

Table of Contents

Attributions

Preliminary experiments of 2-fluoroanilines with $Ti(NMe_2)_4$ were conducted by Willie R. Hargrove, Jr. Willie also carried out the reaction of *o*-chloroaniline with $Ti(NMe_2)_4$ and the reaction of 2,6-difluoroaniline with $Ti(O^iPr)_4$. All other experimental work described in the paper was conducted by Sarita Hough.

Chapter 1: Transition-Metal-Mediated C-F Bond Activation and Its Applications

1.1 Introduction

This thesis describes a reaction in which an *o*-fluoroaniline derivative combines with $Ti(NMe_2)_4$ to afford a defluoroaminated product as shown in Figure 1.1. Chapter 2 will describe the scope and mechanism of this reaction, which we have explored in detail experimentally. Fundamentally, the reaction is a type of C-F bond activation that is directed by an existing ring substituent. Therefore, this introductory chapter will first summarize the importance of fluoroaromatic compounds generally and then review role of transition-metal reagents in C-F processes generally. Toward the end of the chapter, the potential significance of the reaction shown in Figure 1.1 and its products (1,2-phenylenediamine derivatives) will be discussed. Because the reaction shown in Figure 1.1 also represents a form of nucleophilic aromatic substitution, some of the mechanistic theory of S_NAr reactions will also be discussed as a transition to the detailed chemistry described in Chapter 2.

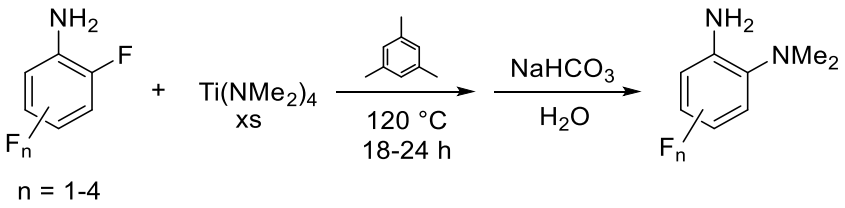

Figure 1.1: C-F activation of *o*-fluoroanilines with $Ti(NMe_2)_4$.

1.2 Significance of fluoroaromatic compounds

A primary application of fluoroaromatic compounds is in medicine. Fluoroaromatic moieties occur widely in successful drugs for the treatment of diseases and disorders ranging from cancer to conjunctivitis.[1–10] Fluorine substituents in pharmaceutically active molecules can influence the molecule's favored conformations via fluorine's interactions with other functional groups, affect the polarity and lipophilicity of the molecule, as well as its ability to permeate membranes.[11] A

few examples of fluorinated drugs are shown in Figure 1.2. There are, of course, a great many more fluorinated drugs; in 2010, nine of the top 30 blockbuster drugs contained a fluorine, likely a persistent trend.[9] The compounds shown below were chosen due to their bearing on the chemistry shown in Figure 1.1—several of these compounds contain *fluorinated aniline functionalities*, while several others contain fluorinated phenylenediamine functionalities. These examples show that there is a potential for these classes of compounds to be biologically active. In addition to pharmaceutically-active compounds, compounds containing radioisotope ^{18}F can be used in the bioimaging technique positron emission tomography (PET).[9,11]

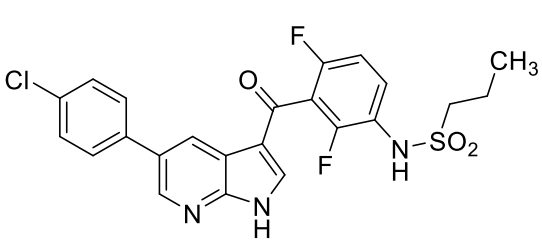

vemurafenib--used against melanoma

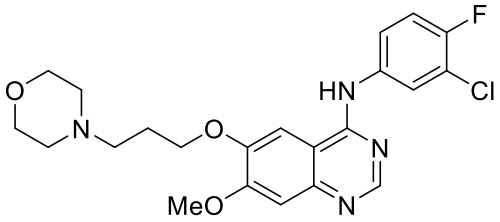

gefitinib--used against lung cancer

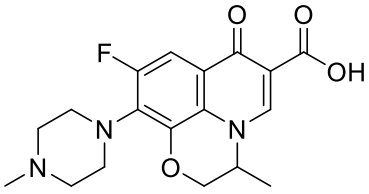

levofloxacin--antibiotic

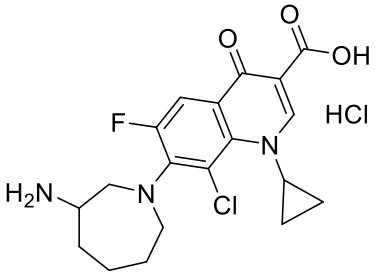

besifloxacin--used to treat bacterial conjunctivitis

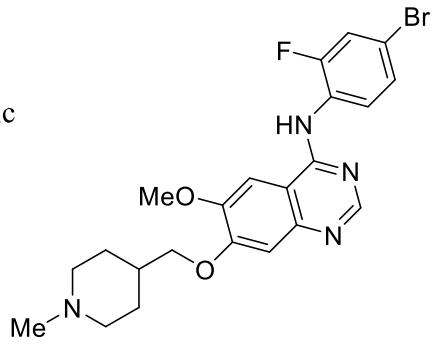

vandetanib--used against thyroid cancer

Figure 1.2: Examples of pharmaceuticals with fluorinated aniline functionalities.[6,12]

Another major application of fluorinated arenes is in agricultural chemicals such as herbicides, insecticides, and fungicides.[8,9,13] Examples of two such compounds with fluorinated aniline functionality are shown in Figure 1.3. As with pharmaceuticals, the design of herbicides, insecticides, and fungicides aspires to selectivity, in this case, the ability to affect only the targeted organism, while leaving the crops under cultivation unharmed.[13] Strategically-located fluorines on such molecules, for the reasons discussed in the preceding paragraph, can help.

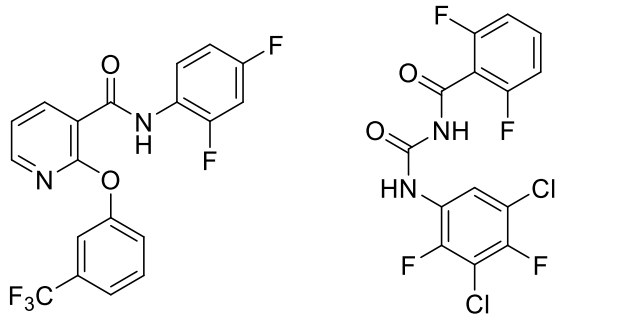

Diflufenican--herbicide Teflubenzuron--insecticide

Figure 1.3: Structures of two examples of fluorinated agricultural compounds.[13]

1.3 Aromatic defluorination reactions

With such promising and lucrative applications in view, new research seeking better, less expensive, more selective methods of fluorination seem worthwhile. With fluoroaromatic compounds, however, an equally viable strategy for selective fluorination is *removal or substitution of fluorine from more highly-fluorinated derivatives*. The latter will be the focus of the discussion here. Much has been written regarding the defluorination chemistry of fluorinated aliphatic compounds,[14–18] but for the purpose of brevity, this introduction will consider only arene defluorinations. An example of an important compound illustrating the importance of this strategy is the quinolone antibiotic *levofloxacin* (Figure 1.2), in which the piperazine substituent and the cyclic ether are installed by selective fluorine displacement reactions.[12]

In defluorination reactions, conjugation and local polarity of reactants, products, and intermediates influence reactivity, selectivity, and procedural efficiency. Chemically, C-F bonds are exceedingly strong, but also highly polar due to fluorine's high electronegativity. Aromatic C-F bonds tend to be easier to activate than corresponding aliphatic C-F bonds, due to the ability of certain intermediates (and the transition states leading to them) to be resonance-stabilized.

Perutz and his co-workers have made extensive studies of the reactions of fluoroarenes with Group 10 compounds (Ni, Pd, and Pt). Starting from $Ni(COD)_2$ (COD = cyclooctadiene) as a generic Ni(0) source and trialkylphosphines as stabilizing ligands, they explored oxidative addition reactions of hexafluorobenzene, pentafluoropyridine, and partially fluorinated pyridines to synthesize products of the form *trans*-$Ni(PEt_3)_2ArF$, as shown in Figure 1.4.[19] In these reactions, which tend to transfer negative charge to the arene, pyridines are always more reactive than comparably fluorinated benzenes because of the higher electronegativity of nitrogen relative to carbon.[19] They also found that the reaction of $Pd(PCy_3)_2$ (Cy = cyclohexyl) with pentafluoropyridine yields *trans*-$Pd(PCy_3)_2(C_5F_4N)F$, with the pentafluoropyridine reacting selectively at the 4-position.[20]

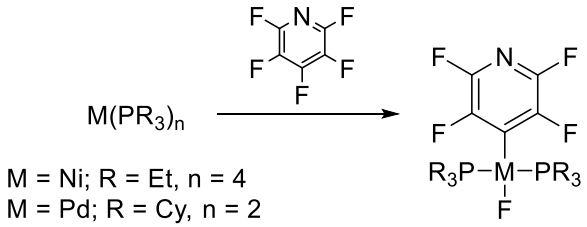

Figure 1.4: Oxidative addition of pentafluoroaniline to a phosphine complex.

The products of these reactions are Ni(II) and Pd(II) species, so an oxidative addition has clearly occurred. However, in this chemistry, there are two mechanistic possibilities to be considered as shown in Figure 1.5. The first option, Pathway A, is an S_NAr process in which the M(0) species (M = Ni, Pd) is the nucleophile. There is solid precedent for oxidative additions that

occur sequentially, often with relatively reactive C-X bonds, such as benzylic bromides, CH_3I, or (as in this case), perfluoroarenes. Especially in the case of highly fluorinated aromatic species, oxidative addition can sometimes be viewed as a nucleophilic aromatic substitution.

The second option (Pathway B in Figure 1.5) is a synchronous oxidative addition in which the C-F sigma bond coordinates to the metal atom through synergistic bonding (a combination of donation from the C-F bonding orbital and back-bonding from the metal to the C-F σ^* orbital), leading to the cleavage of the C-F bond and formation of both the M-Ar and M-F bonds at the same time.

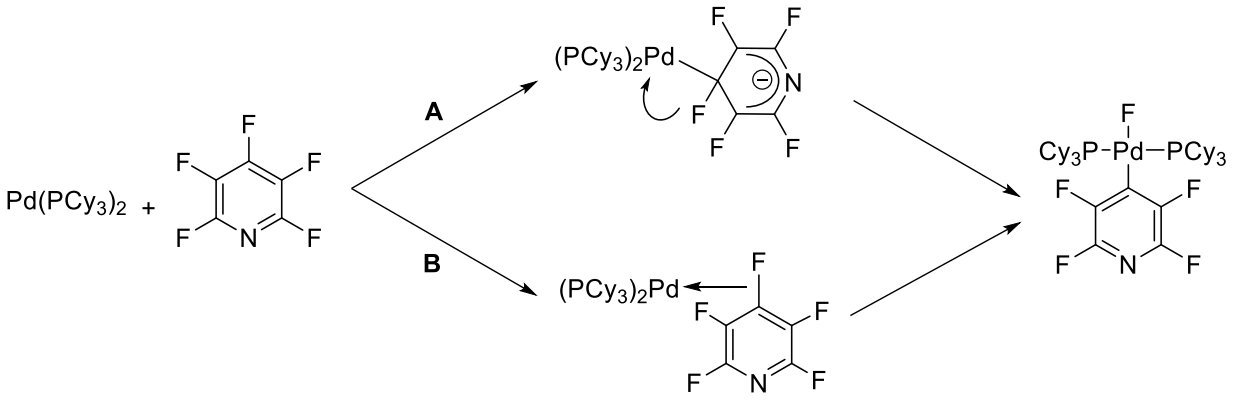

Figure 1.5: Two possible mechanistic pathways to *trans*-$Pd(PCy_3)_2(4\text{-}C_5F_4N)F$.

Both pathways result in a common product because rearrangement of initial *cis* oxidative addition products to the corresponding *trans* isomers is well documented and fairly common. The main differentiator is timing. Lacking more compelling evidence, though, it is difficult to determine which mechanism (or some intermediate alternative) is followed.

When the metal is Pt(0), different reaction pathways open up. For example, the reaction of $Pt(PCy_3)_2$ gives an oxidative addition product in which the Pt-F and P-Cy bonds have exchanged partners (Scheme 1.6).[20] Platinum is also less chemoselective. $Pt(PCy_3)_2$ reacts with 2,3,5,6-tetrafluoropyridine to activate the C-H bond, while $Pd(PCy_3)_2$ does not react with it.[20]

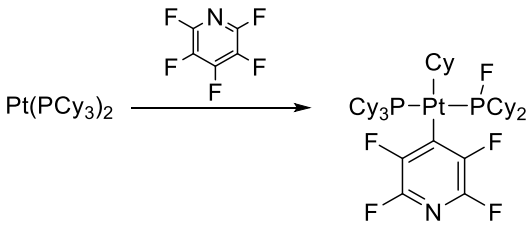

Figure 1.6: Oxidative addition and rearrangement reaction from reaction of pentafluoropyridine and $Pt(Cy_3)_2$.

These reactions provide insight into some of the challenges of catalytic C-F bond activation. The reactions of $Pt(PCy_3)_2$ described above demonstrates the potential for other types of bond activation to compete with C-F activation, which is not particularly surprising considering the strength of the C-F bond. On the other hand, many of Perutz's reactions show strong regioselectivities, which are consistent with trends in S_NAr chemistry, as discussed in Section 1.5 below. Having a basis to predict regioselectivity in aromatic C-F activation is an advantage.

Another significant challenge in C-F bond activation is catalytic turnover. Although Perutz clearly showed that the C-F bond is activated, both the arene and the abstracted fluorine remain bound to the metal. They did not develop their chemistry into a catalytic system. The turnover problem is two-fold. First, metal-fluorine bonds can be quite strong. This problem is traditionally solved using a fluorophilic co-catalyst that can scavenge the fluoride from the metal and replace it with another group such as hydride. Aluminum-, boron-, and silicon-based compounds have found use as fluoride scavengers because they form even stronger bonds with fluorine than many transition metals, driving the transmetallation reaction thermodynamically.[14,21–23] The other issue in catalytic turnover, which has not been addressed in any general way, is the strength of the Ar-M bond. In particular, perfluoroaryl groups can bind very strongly to late transition metal ions which are often electron-rich and can engage in dπ-pπ back-bonding with the low-lying π* orbitals of the fluoroaromatic group. The first problem (M-F bond strength) is the more significant

problem for early transition metals, while the second problem (M-Ar bond strength) is the main issue for late transition metals.

One of the most important classes of organometallic-mediated fluoroarene reactions is hydrodefluorination (HDF), in which a fluorine atom is replaced by a hydrogen atom.[14,24] HDF is desirable because the hydrogen atom can, in theory, be replaced by other groups through electrophilic chemistry. HDF reactions have been reported in a number of different compounds, with a variety of metals, and proceed by a diversity of mechanisms. Many, although not all, reported HDF reagents involve mid- to late transition metals.[24–26] This is presumably because of the M-F bond strength issue described above. HDF has been explored in great detail and, importantly, many catalytic systems have emerged.

$Co(PMe_3)_4$ is an example of an HDF-active compound which, unusually, uses sodium formate as a fluorine scavenger.[27] As seen in Figure 1.7, the aryl halide adds via oxidative addition and the sodium formate exchanges the formate group for the fluorine. The formate then undergoes β-hydride elimination with loss of CO_2 – likely the ultimate driving force in a sequence of reactions that are probably equilibria. The hydride then undergoes reductive elimination with the aryl halide, regenerating the active form of the catalyst.[27] The catalyst turns over, but only poorly (TON < 10), and undergoes an unspecified degradation process .[27]

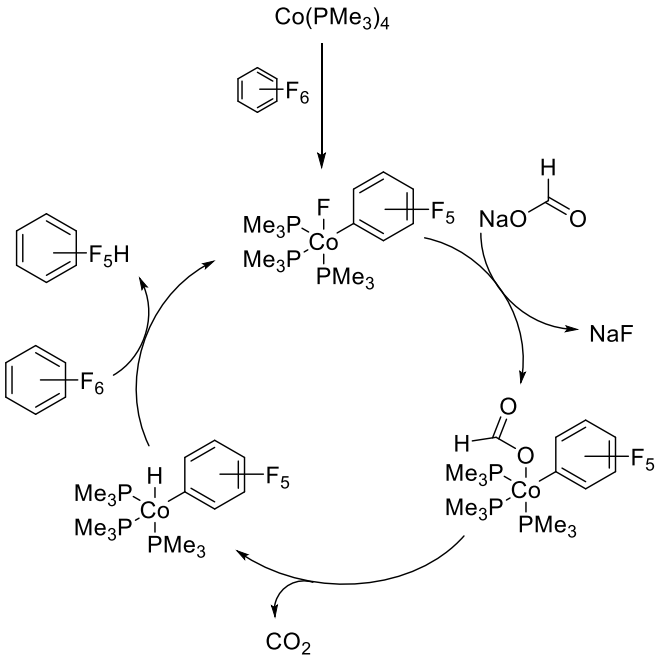

Figure 1.7: Catalytic cycle for HDF reaction via $Co(PMe_2)_4$, shown for hexafluorobenzene. Other substrates used in the article include pentafluoropyridine, octafluorotoluene, and decafluorobiphenyl.

Another example of an HDF catalyst that proceeds via a much different mechanism is the iron-based catalyst shown in Figure 1.8.[28] The pre-catalytic species added to the reaction is a hydride-bridged dimer, but the active form is the monomeric species shown. In this reaction, the Fe(II) center seems unlikely to undergo any type of oxidative addition, because Fe(IV) is a fairly high oxidation state for iron. The authors present quantum-chemical (DFT) calculations suggesting that the hydrodefluorination step occurs by sigma-bond metathesis, sidestepping the oxidation-state issue. However, their "transition state" for sigma-bond metathesis does look very similar to a conventional Meisenheimer intermediate. The catalyst is then turned over with the aid of cocatalyst Et_3SiH. In the absence of Et_3SiH, the Fe-F species evidently dimerizes. Turnover numbers (TONs) varied but were as high as 50 for pentafluoropyridine under optimized conditions, although regioselectivity was inferior to other catalysts.[28]

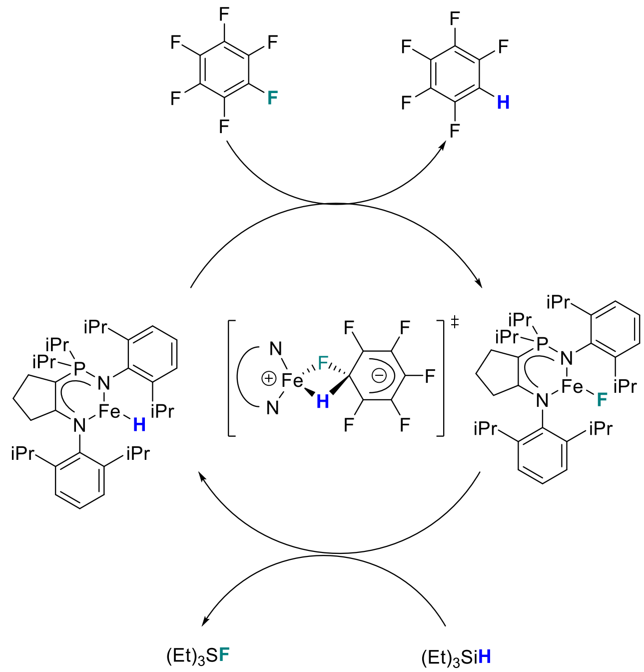

Figure 1.8: Catalytic cycle of an iron-based HDF catalyst with hexafluorobenzene substrate.[28]

Figure 1.9 shows a palladium phosphine-based catalyst that is HDF-active, using pinacolborane (HBpin) as the cocatalyst.[29] The authors confirmed, independent of substrate, that treatment of the catalyst with HBpin in the absence of substrate led to the replacement of the fluorine ligand with a hydride, and that thermolysis of the hydrido complex led to reductive elimination of the hydrodefluorinatated pentafluoropyridine (presumably after isomerization to the *cis* isomer). Under optimized conditions with pentafluoropyridine, TON = 12. When pinacolborane is replaced with an arylboronic acid such as $PhB(OH)_2$, transmetallation affords the Pd-Ph bond, leading to biaryls. Defluorinative aromatic C-C coupling reactions are described in more detail below.

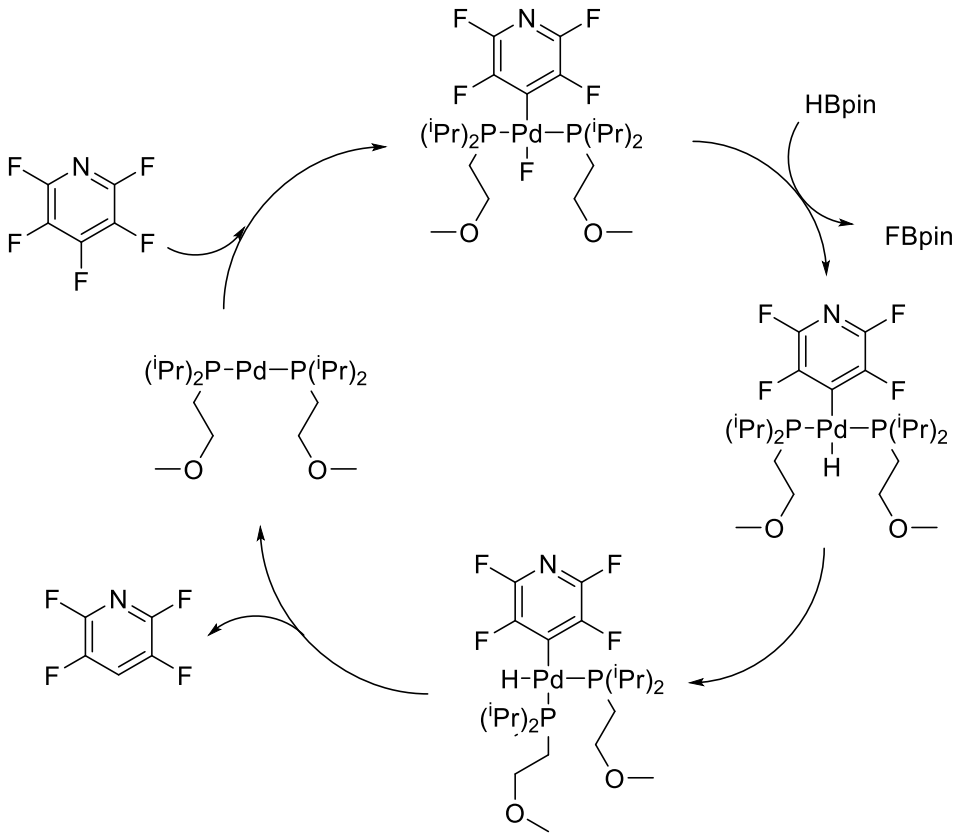

Figure 1.9: Catalytic cycle of palladium-based phosphine catalyst.[29]

As an especially interesting example, Structure C in Figure 1.10 is a bimetallic catalyst that catalyzes HDF of fluorobenzene. Although the mechanism is not discussed in the article, the authors confirm that Structure A is not HDF-active and Structure B is only marginally so, although a mixture of A and B shows moderate activity.[26] These results imply that both metal ions in Structure C are necessary for catalytic action. Thus, Structure C is HDF-active, and the authors report very high catalyst stability, with a TON of up to 660 with respect to fluorobenzene.[26]

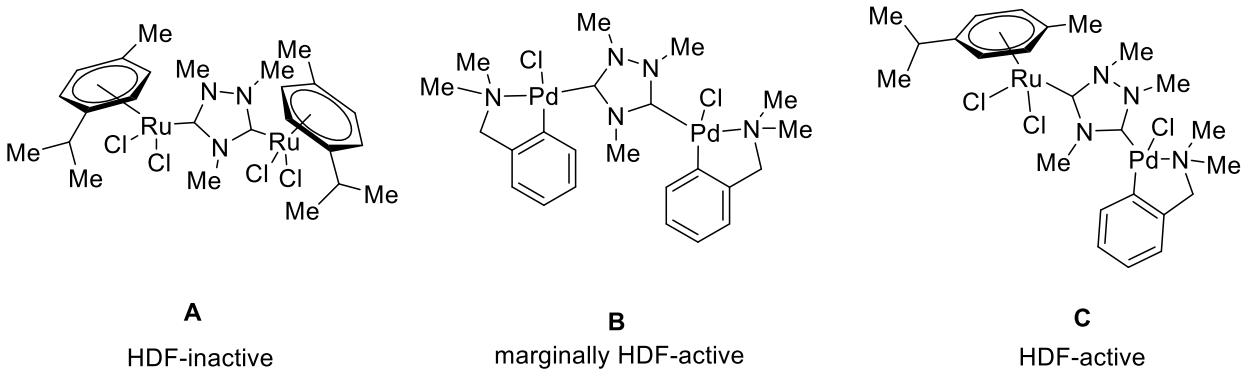

Figure 1.10: Bimetallic C-F activation catalyst.[26]

However, C-F bond activation is not solely confined to mid and late transition metals. Niobium(V) chloride, when activated with LAH, has been reported to catalyze HDF reactions. The authors reporting the reaction suspect that the reduced, active species is niobium metal, but were not able to definitively establish the presence of metallic niobium and were not able to replicate the activity with turnings of niobium.[30] Nevertheless, the catalyst was HDF-active with respect to a variety of fluorinated biphenyls.[30] Based on the results of experiments using deuterated LAH, the article proposes a mechanism in which a niobium hydride nucleophilically attacks the C-F bond.[30]

Another thoroughly-studied set of HDF-active compounds is the Group 4 metallocene dihydrides. Many of these systems are still stoichiometric but might be made catalytic with further study. Zirconocene dihydride and its ring-substituted analogues (e.g., $Cp^*_2ZrH_2$, $Cp^* = \eta^5$–Me_5C_5) perform stoichiometric defluorination reactions, including HDF.[24,31,32] Corresponding hafnocene dihydrides are less reactive,[16] while titanocene dihydrides are highly active toward HDF.[33] A common product is the species Cp_2MArF (M = Ti, Zr, Hf).[32,34] With regard to the mechanism, reported results suggest that that the reaction of $Cp^*_2ZrH_2$ with arenes does not proceed via a radical mechanism,[32,34] although the mechanism of the defluorination of fluoroalkanes by the same compound does seem to be a radical reaction.[16,17,35]

The mechanism proposed by Jones et al. for non-catalytic HDF using zirconocene dihydride is shown in Figure 1.11. First, a fluorine on the fluoroarene is attracted to the zirconocene. An agostic interaction then develops in which both the active carbon and the zirconium atom are simultaneously "bound" to both a hydrogen and a fluorine, until the hydrogen breaks away from the metal, leaving the fluorine bound to the zirconium and a new C-H bond on the arene.[32] This mechanism strongly resembles the classical organometallic sigma-bond metathesis reaction, except that the adduct (**C**) seems to be a metastable intermediate rather than a transition state. Again, this intermediate resembles a classical Meisenheimer complex even though Jones did not draw it that way. It seems reasonable that this mechanism can be extended to other Group 4 metallocenes and to their reactions with fluorinated pyridines and other fluoroarenes.

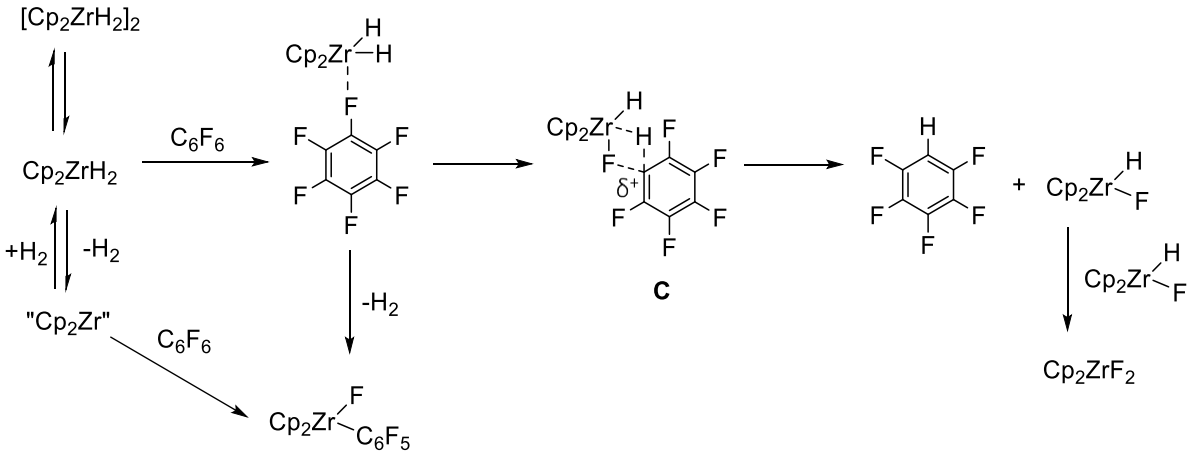

Figure 1.11: Proposed mechanistic pathway for HDF of hexafluorobenzene via Cp_2ZrH_2.[32]

Turning over the mechanism shown in Figure 1.11 requires simply that the Zr-F bonds are exchanged to Zr-H bonds. As discussed above, this requires a co-catalyst that can simultaneously remove fluoride and provide hydride. With early transition metals, this process requires an aggressively fluorophilic hydride reagent. Alane derivatives have predominantly been used for this purpose, including sodium bis(2-methoxyethoxy)aluminum dihydride (Red-Al) and di-isobutylaluminum hydride (DIBAL).[22,33] The two zirconocene-type compounds $[Cp^*_2ZrH(\mu\text{-}H)]_2$

and [*rac*-(ebthi)ZrH(μ-H)]$_2$ (defined in Figure 1.12) both hydrodefluorinate pentafluoropyridine selectively at the 4-position with co-catalytic DIBAL.[22] The latter reaction (who catalyst is shown in Figure 1.12) yields a respectable TON of 67.[22] The mechanism of this HDF reaction seems consistent with Jones's mechanism, but with the DIBAL regenerating the zirconocene hydride and closing the catalytic cycle. Supporting this belief is the fact that when the authors attempt to react C_6F_6 with their catalyst, they report observing Cp*$_2$Zr(C_6F_5)F, which Jones also describes in his mechanism.[22]

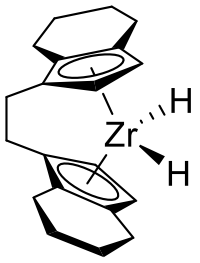

Figure 1.12: Structure of *rac*-(ebthi)ZrH$_2$, active catalyst (monomeric) form.

For reasons that are unclear, pentafluoropyridine seems to be more selective for HDF while hexafluorobenzene tends to divert more toward the oxidative addition product Cp*$_2$Zr(C_6F_5)F. Treatment of hexafluorobenzene with DIBAL would also be problematic because the products would be Cp*$_2$Zr(H)F and *i*Bu$_2$AlC_6F_5, and perfluorophenylaluminum compounds are treacherously unstable.

Aromatic coupling reactions involving an aryl halide reactant that is a fluoroarene may also be viewed as defluorinations. A related example was already mentioned in Figure 1.9 above. Traditionally, aromatic couplings use aryl bromides or iodides, since those are relatively weak bonds and can undergo oxidative addition readily. However, aryl fluorides can also undergo such reactions to form C-C bonds. For instance, Love and co-workers reported the reaction shown in Figure 1.13, in which nickel-catalyzed defluorination was used in a coupling reaction. The

reaction selectively coupled the aryl to the position of the fluorine *ortho* to the imine (in cases where there were two *ortho* fluorines, both were substituted, likely a directing effect involving imine coordination to nickel).[36] The imine was presumably hydrolyzed to an aldehyde during the workup. They report that the reaction was tolerant of ancillary fluorines in a variety of positions on the phenylimine, and of a variety of functional groups, including substituent fluorine, trifluoromethyl, hydroxyl, and methoxy groups on the boronic acid.[36] The mechanism is not discussed in depth, but it seems reasonable to suppose that the boronic acid serves as the fluorine sink in this reactions.

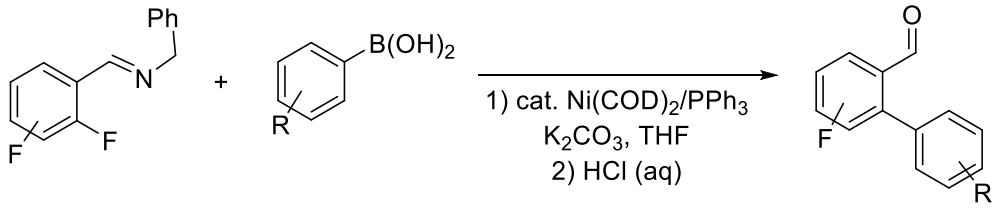

Figure 1.13: An Ni-catalyzed, defluorinative aryl C-C coupling reaction.[36]

Many of these catalytic C-F activation reactions are run at relatively low (< 65 °C) temperatures for long times (> 24 hours). The authors do not discuss the reasons for this, but it seems fair to presume that running the reactions at higher temperatures would result in decreased regioselectivities and possibly also lower TONs via catalyst decomposition.

1.4 S_NAr Reaction and Organometallic Reagents

In addition to envisioning an organometallic reagent as the nucleophile in an S_NAr reaction or undergoing oxidative addition of an Ar-F bond, metal-containing species can have other significant roles in conducting S_NAr reactions. In some cases, the nucleophile and substrate are brought into proximity by being bound to the same metal center.[37] In other cases, metal coordination can enhance the intrinsic reactivity of the substrate, usually by making it more electrophilic. For instance, the $CrCO_3$ moiety is electron-poor enough that if a substituted benzene is bound η^6 to it, the bound ring can undergo S_NAr substitutions under surprisingly mild conditions. For instance,

(*tert*-butyl-4-chlorobenzoate)tricarbonylchromium can undergo S_NAr substitution at room temperature whereas chloride substitution of the free arene would proceed only under forcing conditions under which the ester moiety could also react.[38] In a similar case, chlorobenzene bound in η^6 fashion to the cationic cyclopentadienylruthenium fragment ($CpRu^+$) enables facile substitution of the chloride as a key step in a longer synthetic sequence.[39] The CpRu group was then decomplexed from the arene ring by mild photolysis.[39]

1.5 S_NAr Selectivity

Chambers has published a number of articles over the years discussing fluorine substituent effects on the rate and selectivity of variety of S_NAr reactions.[40–44] He presented a general theory that regioselectivity is due to a combination of fluorine's sigma-accepting and pi-donating abilities. The following paragraphs summarize his findings, which are important to understanding regioselectivity in the reactions presented in Chapter 2. This background is provided here instead of in Chapter 2 because Chapter 2 is presented in its final form as a published article (https://doi.org/10.1016/j.jfluchem.2019.03.009).

The sigma-accepting abilities of fluorine manifest through the inductive effect. As shown in Figure 1.14, ancillary fluorine atoms can make the active site of the S_NAr reaction (the *ipso* carbon) more electron-deficient and thus more reactive. The inductive effect depends on proximity, so *ortho* fluorines have the strongest effect and are therefore the most activating. *Meta* fluorines' inductive effects are weaker, but still activating, while *para* fluorines are too far away to have a significant effect.

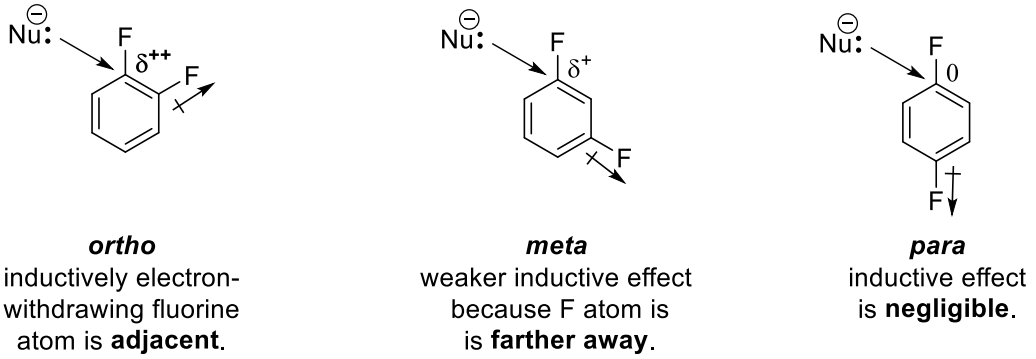

Figure 1.14: Inductive effects of ancillary fluorines on nucleophilic carbons.

The other factor that ancillary fluorines have on selectivity is fluorine's pi-donating abilities, which come into play via the resonance effect, as shown in Figure 1.15. Meisenheimer intermediate formation dislodges a lone pair of electrons. As shown in Figure 1.15, the presence of the lone pair is resonance-stabilized, but if there are fluorines located *ortho* or *para* to the active site, pi-repulsion between fluorine's lone pair and the dislocated lone pair will make that resonance structure more unfavorable, destabilizing the intermediate. Ancillary fluorines *meta* to the active site do not affect the stability of the intermediate.

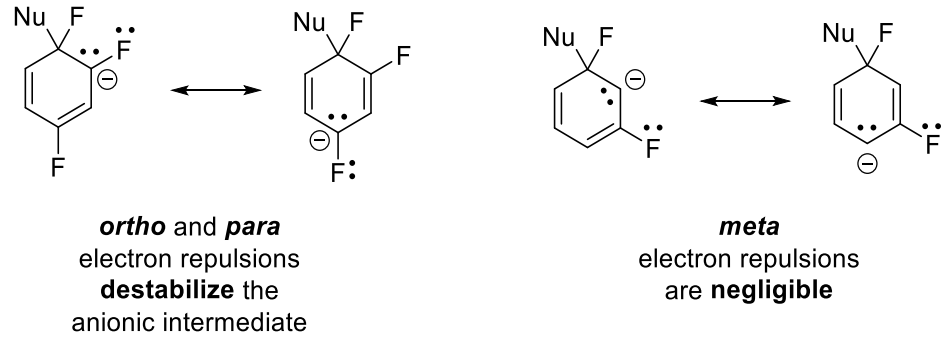

Figure 1.15: Resonance effects of ancillary fluorines on the Meisenheimer intermediate.

The net effects are shown in Table 1.1. For *ortho* fluorines, the activating effect of the inductive effect tends to be a stronger activator than the unfavorable resonance effect, so the net result is that *ortho* fluorines are activating. *Meta* fluorines, by virtue of not having a deactivating resonance effect, are also activating. The question of whether an *ortho* or *meta* fluorine is more

activating is system-dependent. *Para* fluorines have no activating inductive effect and an unfavorable resonance effect, making them overall deactivating. Chambers's predictions seem to do a good job of rationalizing reported results in the context of S_NAr reactions involving common organic nucleophiles such as amines and alkoxides.[45,46]

Table 1.1: Substituent effects of ancillary fluorines on S_NAr reactions.

	Ortho	*Meta*	*Para*
Inductive effect	Activating	Activating	--
Resonance effect	Deactivating	--	Deactivating
Net effect	Activating	Activating	Deactivating

In the next chapter, regioselective C-F bond activation is reported, specifically a reaction between $Ti(NMe_2)_4$ and a variety of *o*-fluoroanilines. This reaction results in the selective installation of a dimethylamino group in moderate to high yield. Results of these reactions, attempts to generalize this reaction, and the implications of the results are discussed, with a mechanism being proposed based on those results.

The reaction's products are of interest both because of their potential as building blocks for future pharmaceutically-active molecules and because phenylenediamines have been reported as integral components of catalysts. Phenylenediamines have been reported as precursors to and components of pincer compounds (Figure 1.16).[47] Nitrogen is a harder base than phosphorus, and as such can be used to stabilize mid-transition metals that adopt high oxidation states in the course of a catalytic cycle. Such pincer compounds have been found to be catalysts for reactions such as transfer hydrogenation of ketones and hydrodehalogenation.[47,48] Additionally, a palladium complex containing a phenylene-1,2,3-triamine functionality (shown in Figure 1.17) has been reported as an ethylene polymerization catalyst that can incorporate polar monomers.[49] Fluorination of the catalyst's phenyl rings could potentially tune the electron density of a catalyst

to make it more selective or reactive. Fluorination could also perhaps be used as a spectroscopic probe (via ^{19}F NMR), to further explore the mechanism and reactions of such catalysts.

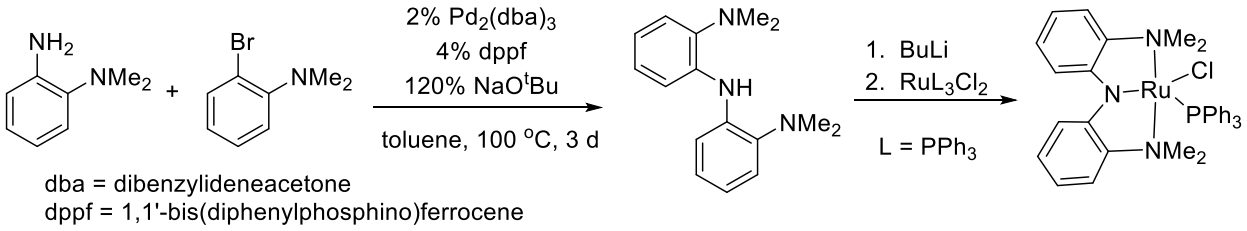

Figure 1.16: Synthesis of an aniline-derived pincer complex that catalyzes transfer hydrogenation of ketones.[47]

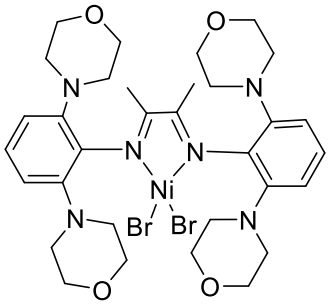

Figure 1.17: Nickel polymerization catalyst containing 1,2,3-trifluoroaniline functionality.[49]

Chapter 2: Regioselective, Nucleophilic Activation of C-F Bonds in *o*-Fluoroanilines

2.0 Article Attributions

Preliminary experiments of 2-fluoroanilines with $Ti(NMe_2)_4$ were conducted by Willie R. Hargrove, Jr., who also carried out the reaction of *o*-chloroaniline with $Ti(NMe_2)_4$ and the reaction of 2,6-difluoroaniline with $Ti(O^iPr)_4$. All other experimental work described in the paper was conducted by Sarita Hough.

2.1 Introduction

Manipulation of C-F bonds in organic compounds has become increasingly important in areas of organic chemistry where physical properties and bioactivity depend sensitively on the placement of fluorine substituents.[6,8,50,51] Fluorination can afford thermal or photolytic stability[52] and help tune local molecular polarities.[8,51–53] Much has also been written about the special hydrophobicity and oleophobicity of highly fluorinated aliphatics.[54–56] In fluorinated arenes, conjugation and local polarity effects play key roles in governing reactivity and properties. Fluorinated aromatic moieties appear in several new drugs and drug candidates ranging from anti-cancer drugs to antipsychotics.[1–7] With that background, new research to identify additional reaction sequences for the installation, substitution, or removal of aromatic fluorine substituents seems justified.[18,57–59]

Aromatic defluorination reactions often involve organometallic species in directing, activating, or stabilizing roles. Processes include oxidative additions, S_NAr-type substitutions, and radical reactions.[8,19,24,26,59–61] Ideally, aromatic defluorinations would be catalytic with respect to the metal.[21–23,30,33,36,62–65] However, with early transition metals, M—F bonds tend to be strong, impeding turnover. A common solution employs a co-catalytic main-group compound (for example, an aluminum hydride like DIBAL) to scavenge fluoride by transmetallation and regenerate the active catalytic species.[22,33]

We have particular interest in reactions of the general form shown in Scheme 2.1, where a Lewis-basic ring substituent coordinates a metal-organic reagent, directing its nucleophilic ligands toward the *ortho* ring position.[37,66,67] Our interest derives from our serendipitous finding that that pentafluorophenyl-substituted cyclopentadienes and indenes undergo *ortho* C-F bond activation upon treatment with $Ti(NMe_2)_4$ (Scheme 2.2).[68]

Scheme 2.1: Aromatic C-F activation using a metal-organic reagent (M−Nu) directed by a ring substituent (G).

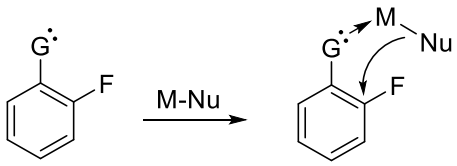

Scheme 2.2: C-F activation of (pentafluorophenyl)cyclopentadiene with $Ti(NMe_2)_4$.

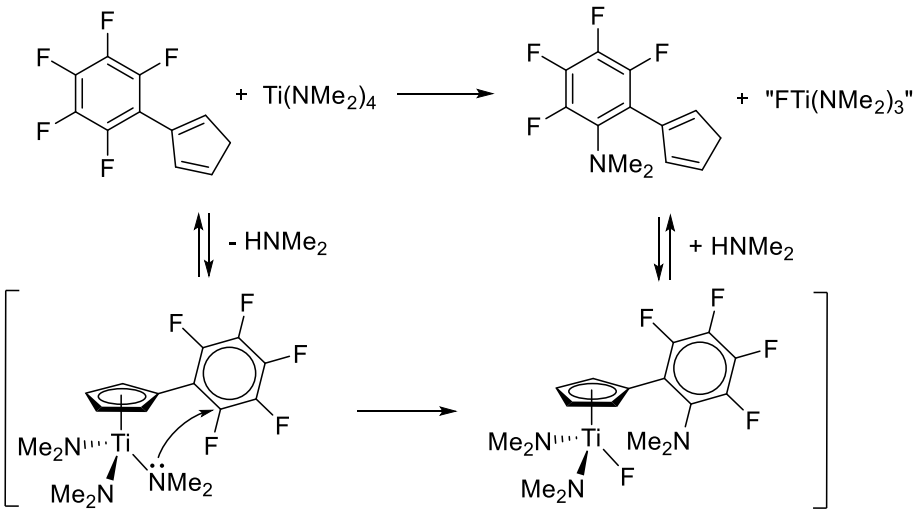

Schrock and co-workers also reported that polydentate ligands containing 2,6-difluorophenyl substituents undergo defluoroaminations when treated with either $Hf(NMe_2)_4$ or $Mo(NMe_2)_4$.[69,70] In all of these cases, the intended synthetic objective involved the installation of new ligands with removal of dimethylamine, but the reactions were accompanied by exchange of M-NMe_2 bonds and aromatic C-F bonds. Therefore, we wondered whether this "side-reaction" could be converted and optimized toward a selective, general, and efficient process in its own right. We now report

reactions of *ortho*-fluorinated anilines with $Ti(NMe_2)_4$ to afford products in which an *ortho* fluorine atom is replaced with NMe_2 to form fluorinated 1,2-phenylenediamine derivatives. *N*,*N*-Dimethyl-1,2-phenylenediamines have found application as precursors to multidentate ligands for various transition metal catalysts.[47,48,71]

2.2 Results & Discussion

In Scheme 2.2, cyclopentadiene played a directing role by coordinating the titanium atom (likely in η^5 fashion) and facilitating an intramolecular substitution process.[68] This proposal neatly rationalized the exclusive *ortho* selectivity. We surmised that the directing role of the cyclopentadiene could be shifted to other acidic ligating groups, such as NH_2 (Scheme 2.3).

Scheme 2.3: Defluoroamination of ortho-fluoroanilines using $Ti(NMe_2)_4$.

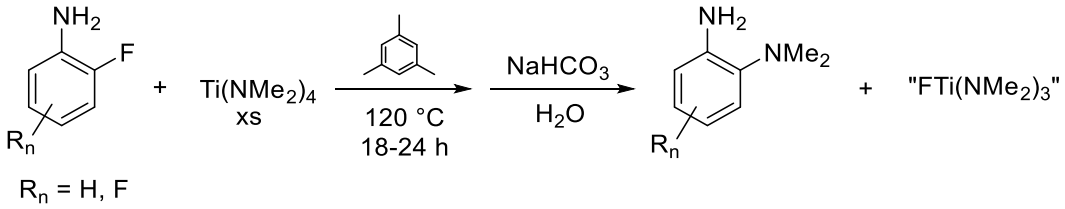

Our experimental approach used ^{19}F NMR to follow reactions and to estimate conversions and yields. We chose substrates having at least two ring fluorine substituents so that we could quantify both the substrate and its defluoroamination product using ^{19}F NMR spectroscopy. The use of mesitylene as the reaction solvent maintained homogeneity of the reaction mixture. (Preliminary studies using *n*-decane led to precipitation of intermediates and very low yields.) Mildly alkaline aqueous workup conditions minimized water-solubility of the aniline products. The crude product mixture still contained the mesitylene solvent and the internal NMR standard, bis(4-fluorophenyl)ether. (We initially chose 3,5-difluoro-1-bromobenzene as the internal standard, but preliminary control experiments showed this compound to be unstable toward the titanium reagent at temperatures above 100 °C.) After ^{19}F NMR spectroscopic analysis to estimate product yields,

the mixture was subjected to liquid chromatography to separate the mesitylene solvent and internal NMR standard and to isolate the products.

Product yields are collected in Table 2.1. Errors of ±5% are conservatively based on the internal reliability of NMR integration method and are reproducible within those limits in multiple trials. Yields are mostly high enough to conclude that the method is general and reasonably efficient. In entries 1, 3, and 4, we still observe some unreacted substrate; likely these reactions could be driven toward higher conversion by increasing the reaction time or temperature. In the case of entries 5, 8, and 9, the substrates are sufficiently reactive to give appreciable yields of products arising from substitution of both *ortho* fluorine atoms.

Table 2.1. NMR yields of defluoroamination products resulting from the reaction shown. Yields (±5%) were estimated by NMR analysis of crude product mixtures.

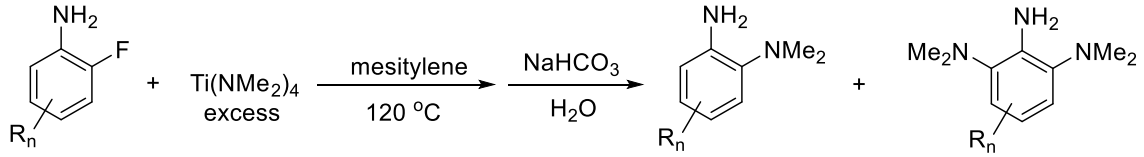

1; R_n = H, F — **2** — **3**

			Yields by ^{19}F NMR, ±5%		
Entry	**Substrate**	**time**	**1**	**2**	**3**
1	2,3-difluoroaniline (**1a**)	20 h	8	86	
2	2,4-difluoroaniline (**1b**)	23 h		92	
3	2,5-difluoroaniline (**1c**)	23 h	31	60	
4	2,6-difluoroaniline (**1d**)	23 h	3	96	
5	2,3,6-trifluoroaniline (**1e**)	23 h		83[a]	13
6	2,3,4- trifluoroaniline (**1f**)	23 h		95	
7	2,4,5- trifluoroaniline (**1g**)	18 h		83	
8	2,3,4,6- tetrafluoroaniline (**1h**)	23 h		14[b]	88
9	2,3,4,5,6-pentafluoroanline (**1i**)	18 h			68

[a] Product **2e** is a 7:1 mixture of 2-dimethylamino-3,6-difluoroaniline (**2e**) and 2,3-difluoro-6-dimethylaminoaniline (***iso*-2e**), respectively. See Scheme 2.5 below.

[b] Product **2h** is 2-dimethylamino-3,4,6-trifluoroaniline.

Mixtures were separated by liquid chromatography, but not particularly efficiently despite our efforts to optimize the eluting solvent. Isolated yields from pure chromatographic fractions were relatively low (ca. 20%) and not particularly reproducible. All new substances were characterized

using NMR spectrometry and exact mass determination (HRMS). We found that ^{1}H and ^{19}F NMR spectra were sufficient for unambiguous identification of all major reaction products, therefore we did not collect ^{13}C NMR spectra, which would likely be quite complex due to extensive long-range couplings to ^{19}F. The ^{1}H and ^{19}F spectra show typical chemical shifts and coupling constants for fluoroaromatic compounds. In the spectra of products having an NMe_2 directly adjacent (vicinal) to a fluorine atom, the methyl groups are split into a doublet with $^{5}J_{HF}$ of ca. 2 Hz. This spectral feature was previously documented for *N*,*N*-dimethyl-2-fluoro-aniline and was useful in making signal assignments.[72]

Reactions of Difluoroanilines. As shown in Table 2.1, difluoroanilines **1a**-**1d** (entries **1**–**4**) reveal an interesting trend in the relative position of the unreactive (ancillary) fluorine atom. Conversion of starting material was lowest when the unreactive and departing fluorine atoms had a *para* relationship (substrate **1c**). Chambers found that fluorines *meta* and *ortho* to the departing fluorine in S_NAr reactions tend to be activating, whereas fluorines *para* to the departing fluorine tend to be deactivating, although the exact (quantitative) kinetic effects are system-dependent.[43,44] Likewise, the first substitution in 2,6-difluoroaniline is activated by the presence of another fluorine in a *meta* position, but after that initial substitution, the remaining fluorine atom has no activating substitution and remains inert under the reaction conditions described in Table 2.1.

Competitive Study of Relative Reaction Rates: All four difluoroanilines were subjected to a ten-fold excess of $Ti(NMe_2)_4$ in a competitive experiment at 80 °C. This lower temperature was chosen to slow down all of the reactions so that we could monitor them conveniently by ^{19}F NMR spectroscopic analysis of small aliquots. As shown in Figure 2.1, 2,6-difluoroaniline had the highest rate of conversion into product, followed closely by 2,4-difluoroaniline. This observation is consistent with Chambers's findings; the fluoroanilines substituted *meta* to the reactive site are

highly activated, while 2,5-difluoroaniline, which has a fluorine atom *para* to the reactive site, is highly deactivated in comparison and is the least reactive of the four substrates. Even though these data were obtained at a lower reaction temperature, we believe they will reflect relative reactivity trends at 120 °C, at least qualitatively.

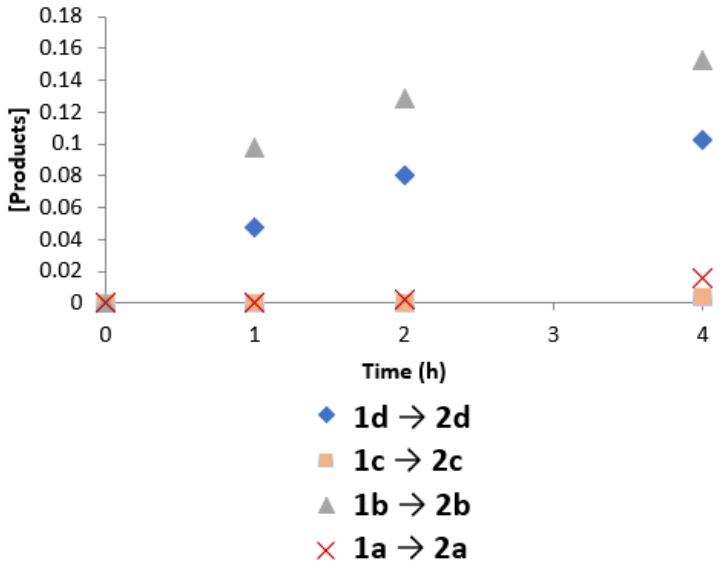

Figure 2.1: Concentrations of products over time in a competitive reaction of four difluoroanilines with a ten-fold excess of $Ti(NMe_2)_4$ in mesitylene at 80 °C.

Reactions of Highly Fluorinated Anilines. As shown in Table 2.1 and Scheme 2.4, aniline **1e** affords a mixture of three products. The major product (**2e**) arises from substitution of F_2, activated by one *ortho* and one *meta* fluorine substituent (F_3 and F_6, respectively). The minor product (***iso*-2e**) results from substitution of F_6, activated by one *meta* fluorine (F_2) but also deactivated by one *para* fluorine (F_3). Substitution of both F_2 and F_6 also afforded **3e**.

Scheme 2.4: Reaction of 2,3,6-trifluoroaniline **1e** with $Ti(NMe_2)_4$.

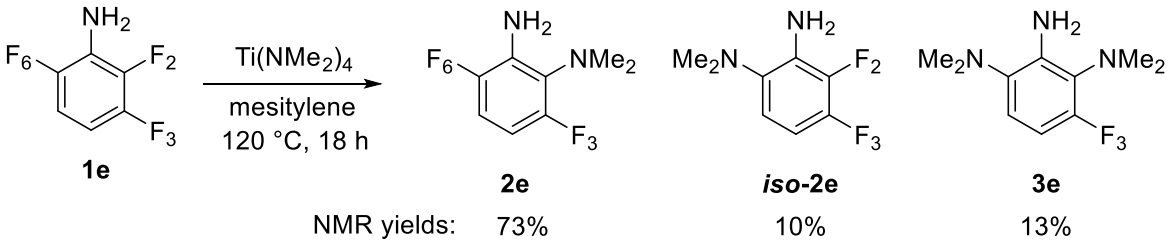

Based on the results with **1e**, we were curious to compare the reactivity of **1f** and **1g** (Scheme 2.5). While the observed NMR yield of **2f** (95%) is higher than the observed yield of **2g** (83%), we wanted a more direct comparison to minimize sources of experimental error. In a competitive reaction with both **1f** and **1g** present in solution at 120 °C for one hour, substrate **1f** underwent 67% conversion to **2f**, whereas substrate **1g** underwent only 33% conversion to **2g**. This result confirms that an ancillary *para* fluorine is deactivating compared to an ancillary *ortho* fluorine.

Scheme 2.5: Reactions of anilines **1f** and **1g** with $Ti(NMe_2)_4$.

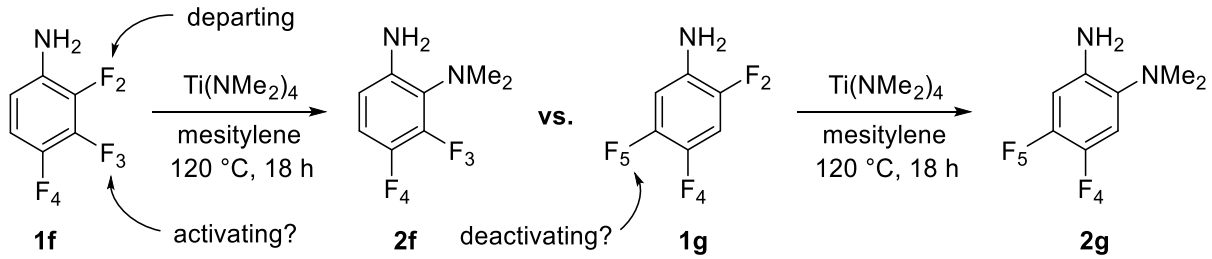

The reaction of the tetrafluorinated aniline **1h**, shown in Scheme 2.6, also featured a substrate with two *o*-fluorines in non-equivalent chemical environments. After 23 h at 120 °C, triamine **3h** was the major product, and the remaining product was **2h**; all of the substrate (**1h**) had been consumed. A separate reaction of substrate **1h** at 90 °C for 3 h afforded not only **2h** and **3h**, but also a third product having three signals in the ^{19}F spectrum. Because some unreacted **1h** was also still present, chromatographic separation was difficult, and we were not able to obtain a fraction containing only the third product. Instead we used a fraction containing some **3h**, which was already well characterized, and we used GCMS to provide a nominal assay of the third product present in that fraction. Following this approach, we assigned the structure ***iso*-2h** to the third product. Based on these results, we suggest that both isomers (**2h** and ***iso*-2h**) are produced early in the reaction, but of the two isomers, the minor component (***iso*-2h**), whose remaining fluorine has both a *meta* and *ortho* fluorine activating the reaction site, undergoes a more facile

defluoroamination, and is thus consumed to form **3h**, compared to **2h**, which has one *meta* fluorine activating and one *para* fluorine deactivating its remaining substitution site.

Scheme 2.6: Temperature-dependent defluoroamination of 2,3,4,6-tetrafluoroaniline.

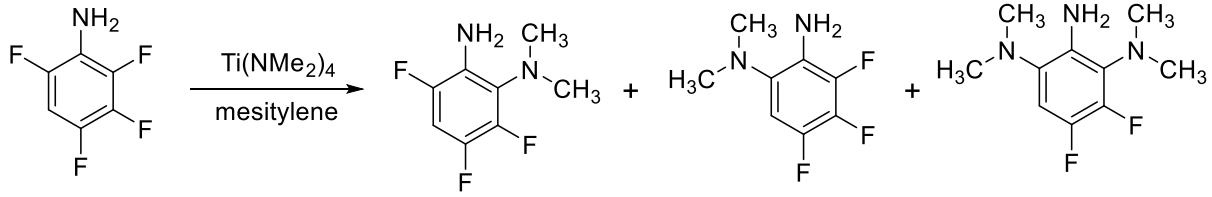

1h **2h** ***iso*-2h** **3h**

NMR yields:				
	at 120 °C	14%	0 %	88%
	at 90 °C	78 %	16 %	<1 %

Pentafluoroaniline (**1i**), as the most activated substrate, afforded exclusively the disubstituted product **3i** in moderate yield at 120 °C. A separate reaction, conducted at 90 °C for 3 h, afforded a product with four signals in the ^{19}F NMR spectrum. We were not able to obtain this product in a pure form, but we assigned the NMR spectrum of the mixture with the aid of simulation software (please see the Supporting Information), and we found the appropriate exact mass upon ESI-MS analysis of the mixture, leading to the assignment of **2i**. Yields are shown in Scheme 2.7.

Scheme 2.7: Temperature-dependent defluoroamination of 2,3,4,5,6-pentafluoroaniline.

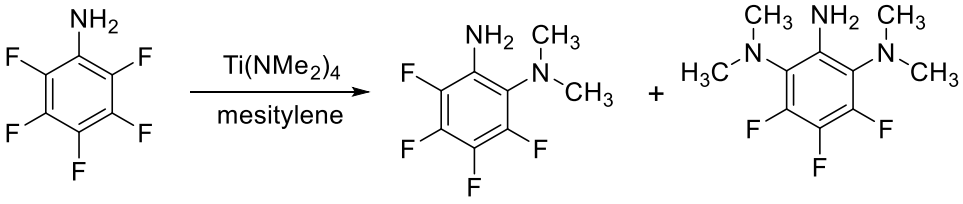

1i **2i** **3i**

NMR yields:				
	at 120 °C	0%	0%	68%
	at 90 °C	14%	75%	<3%

Mechanism and Scope. All of the reactions shown in Table 2.1 involve substitution of fluorine atoms exclusively *ortho* to the NH_2 group. This observation supports a pathway (Scheme 2.8) in which the dimethylamino group is delivered to the *ortho* position of the aromatic ring by means

of prior attachment of the aniline nitrogen to titanium, forming the Meisenheimer intermediate **4** in a process resembling intramolecular S_NAr. We stress, however, that the pathway shown in Scheme 2.7 is largely speculative. Even though there is strong precedent for such pathways in the published literature,[51,69,70,73] none of the putative intermediates (**4**, **5**, and **6**) were observed spectroscopically. A solution of 2,6-difluoroaniline (**1d**) and $Ti(NMe_2)_4$ prepared in C_6D_6 at 25°C (at which temperature the rate of defluoroamination should be negligible) showed a complex ^{19}F NMR spectrum that we could not assign. At least three prominent intermediates are present. In none of our spectra could we identify any Ti-F species, but we did tentatively assign free dimethylamine in the ^1H NMR spectrum. Spectra are provided in the supporting information.

Scheme 2.8: Possible pathway for reactions of *o*-fluoroanilines with $Ti(NMe_2)_4$.

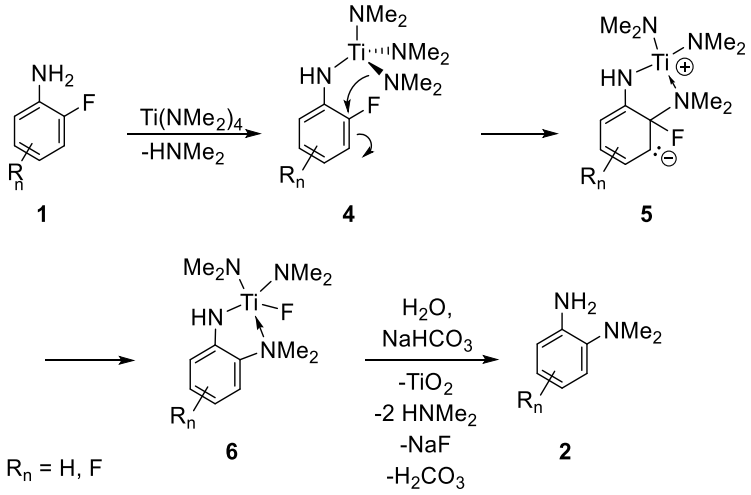

The overall success of the foregoing synthetic method prompted a preliminary investigation of its scope and generality. As shown in Scheme 2.9, we subjected *N*-ethyl-2,6-difluoroaniline [74,75] (**8**) to the same reaction conditions as the other compounds in this study (Table 1) and obtained a 42 percent yield of the defluoroamination product (**8**). This result supports the proposal of putative reaction intermediate **4** which arises from metathesis of one aniline N—H bond with one Ti—

NMe_2 bond. In particular, the reactivity of **7** argues against the intermediacy of arylimidotitanium species, e.g., $ArN{=}Ti(NMe_2)_2$.

Scheme 2.9: Reaction of *N*-ethyl-2,6-difluoroaniline with $Ti(NMe_2)_4$.

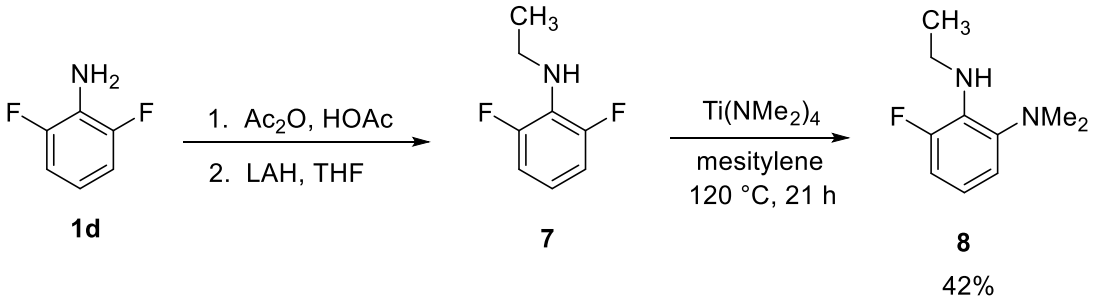

1d **7** **8**

42%

Attempting to cast a wider net, we found that 2,6-dichloroaniline is unreactive toward $Ti(NMe_2)_4$ even at 150 °C, and that the reaction of 2,6-difluoroaniline with titanium(IV) isopropoxide under the same conditions returned only the starting aniline. Treatment of 2,6-difluorophenol (**9**) with $Ti(NMe_2)_4$ at 120 °C (Scheme 2.10) gave a low conversion to the corresponding monosubstitution product (**10**), and the reaction produced additional byproducts that we were not able to identify.

Scheme 2.10: Reaction of 2,6-difluorophenol with $Ti(NMe_2)_4$.

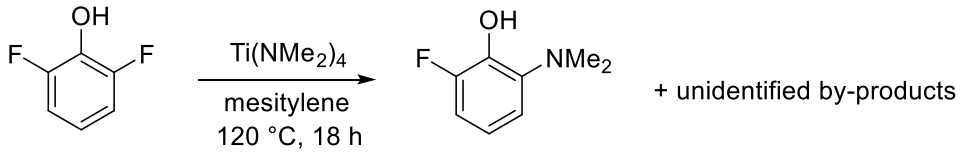

9 **10**

16%

2.3 Conclusions

o-Fluoroanilines undergo defluorodimethylamination when treated with $Ti(NMe_2)_4$. Reactivity increases with added fluorine substituents *ortho* or *meta* to the departing fluorine atom. Trifluoro-, tetra-, and pentafluoroaniline compounds having fluorines in both the 2- and 6-positions undergo substitution at both positions after extended reaction intervals. Preliminary experiments show poor generalization to ortho-fluorinated phenols.

2.4 Experimental

Materials and Methods. $Ti(NMe_2)_4$ (Alfa Aesar), bis(4-fluorophenyl)ether (Oakwood), mesitylene (Acros Organics), and fluoroanilines (various suppliers) were used as received. NMR spectrometry was performed using an Agilent U4-DD2 (proton at 400 MHz) or Varian MR4 instrument (proton at 400 MHz). Exact masses of new substances were determined using an Agilent 6220 ESI-TOF instrument.

General Reaction Procedure. In nitrogen glovebox, a flame-dried Schlenk tube was charged with $Ti(NMe_2)_4$ (0.300 g, 1.30 mmol). Under a nitrogen counterstream, 0.15 g of bis(4-fluorophenyl)ether internal standard, 1.15 mmol of the aniline reactant, and 3.0 mL of mesitylene were added. The tube was then sealed (PTFE valve) and heated at 120 °C in an oil bath for 18-24 hours. After cooling, the mixture was diluted with dichloromethane (ca. 50 mL) and quenched with aqueous 10% sodium bicarbonate solution. The layers were separated, and the aqueous portion was extracted with additional dichloromethane (10 mL). The combined organic portions were dried over anhydrous magnesium sulfate, filtered, and evaporated to afford mostly yellow oils. Yields of products (and unreacted starting aniline, if any) were estimated using ^{19}F NMR spectroscopy. A characteristic signal from each fluorinated aniline was integrated against the bis(4-fluorophenyl)ether internal standard, after correcting for concentration and symmetry factors. Products were isolated using liquid chromatography on silica gel, eluting with dichloromethane or ethyl acetate.

N-Ethyl-2,6-difluoroaniline [74,75] was synthesized by *N*-acylation and LAH-reduction of the acyl as follows. First, a mixture of 2,6-difluoroaniline (2.23 g), acetic anhydride (1.9 mL), and 4 mL of glacial acetic acid reacted at 25 °C for 15 h and then diluted with dichloromethane. The solution was washed with 0.75 M aqueous sodium hydroxide solution, dried over anhydrous

magnesium sulfate, filtered, and solvent was evaporated to afford a white solid, which was recrystallized from ethyl acetate/hexanes (3:1) mixture to afford intermediate *N*-acyl-2,6-difluoroaniline as a colorless crystalline solid. This solid was dissolved in dry THF and cooled using a dry ice bath and then lithium aluminum hydride (1.44 g) was added. The reaction was stirred for 20 h while warming to room temperature and then diluted with dichloromethane. The mixture was washed with aqueous sodium bicarbonate, then with water, dried over magnesium sulfate, filtered, and evaporated to form a pale solid, which was found to be impure by NMR spectroscopic analysis. The crude product was purified by silica gel chromatography, eluting with dichloromethane. After evaporation, 0.67 g of a pale oil was obtained. This procedure was not optimized. Analytical data are provided in Chapter 3.

Chapter 3: Supporting Information

This chapter was published as the "Supporting Information" for the manuscript that is presented in this thesis as Chapter 2. Each set of spectra is followed by a summary describing the peak assignments (noting any ambiguities) and coupling constants. The more complex spectra were modelled using gNMR version 5.1 software (available from Prof. P. H. M. Budzelaar, University of Manitoba). NMR spectrometry was performed using an Agilent U4-DD2 (proton at 400 MHz) or Varian MR4 instrument (proton at 400 MHz) at ambient temperature (20-25 °C). Proton spectra are referenced either to TMS at 0.00 ppm or to residual solvent isotopomer ($CHCl_3$) at 7.26 ppm unless noted below. ^{19}F NMR spectra are referenced to external hexafluorobenzene in $CDCl_3$ at −163.0 ppm. Exact masses of new substances were determined using an Agilent 6220 ESI-TOF instrument.

2-Dimethylamino-3-fluoroaniline

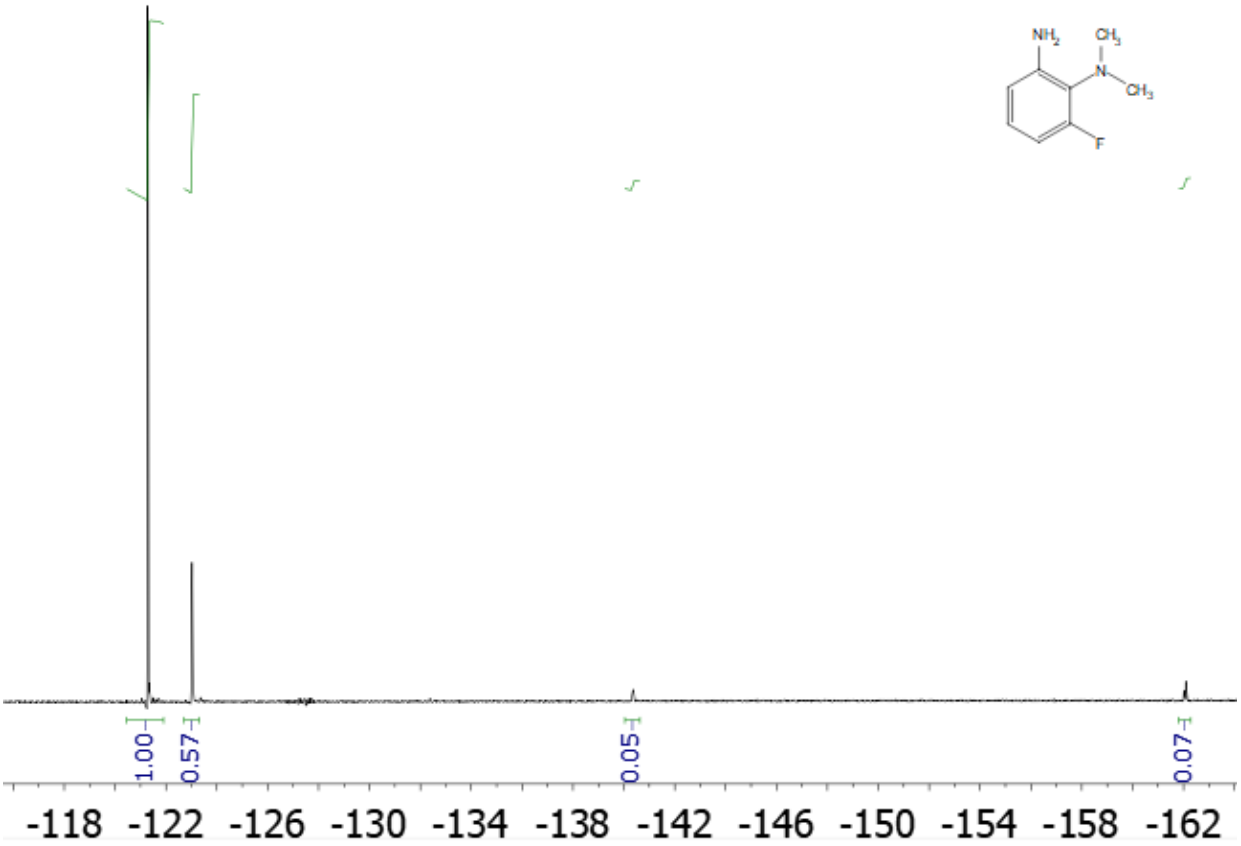

Figure 3.1: ^{19}F NMR spectrum ($CDCl_3$, 376 MHz) of <u>crude</u> 2-dimethylamino-3-fluoroaniline (**2a)**. Unreacted 2,3-difluoroaniline is at –140.4 ppm and −160.1 ppm. Also present is bis(4-fluorophenyl) ether (internal standard), referenced at −121.3 ppm.

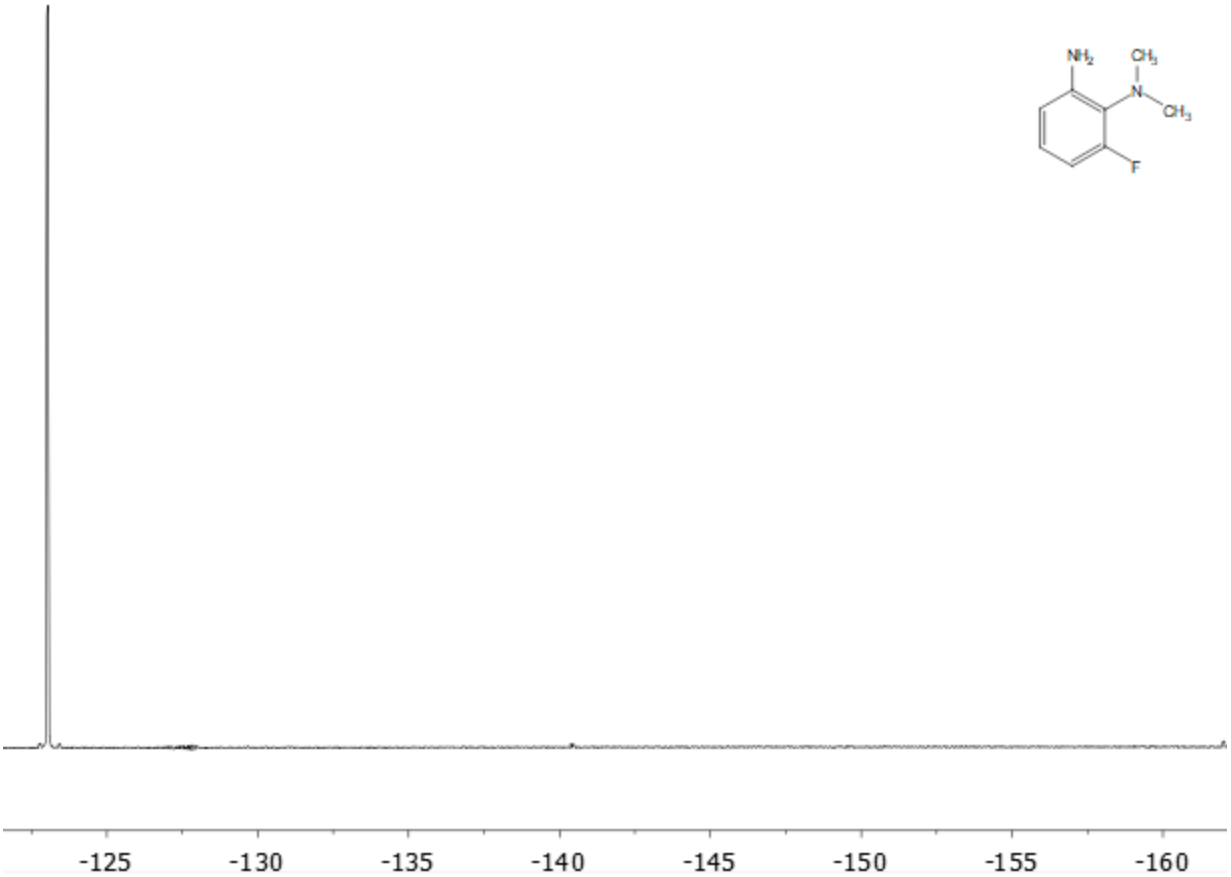

Figure 3.2: ^{19}F NMR spectrum ($CDCl_3$, 376 MHz) of purified 2-dimethylamino-3-fluoroaniline (**2a)**. Comparison to Figure 3.1 above shows that the impurities present in the crude sample have been removed except for traces of unreacted 2,3-difluoroaniline −140.4 ppm and −162.1 ppm.

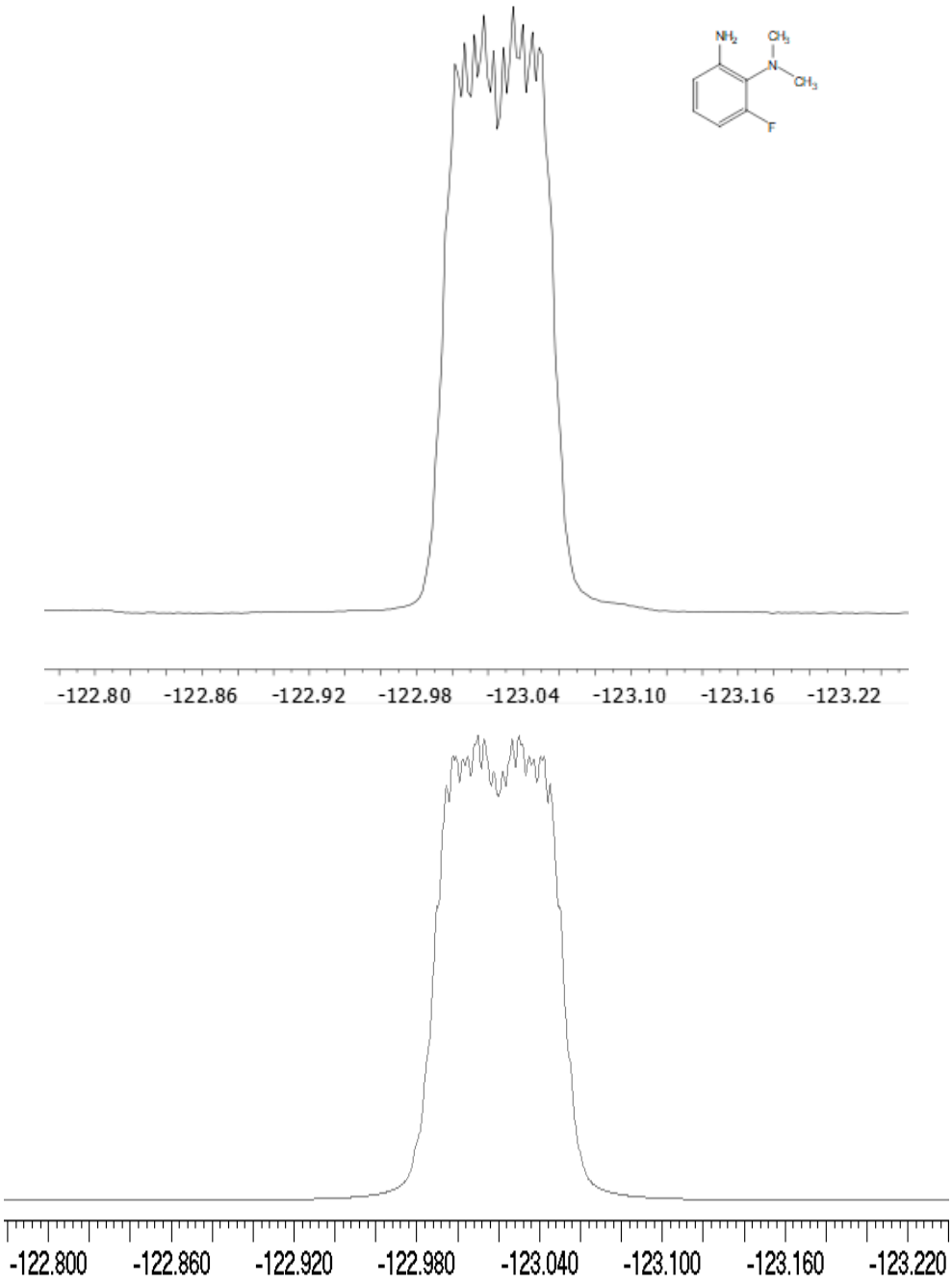

Figure 3.3: ^{19}F NMR spectra ($CDCl_3$, 376 MHz, expansion) of 2-dimethylamino-3-fluoroaniline (**2a)**. Upper: Experimental. Lower: Simulated (A natural linewidth of 1.4 Hz was estimated.) The extensive fine structure arises from coupling to the $N(CH_3)_2$ protons in addition to the three aromatic protons.

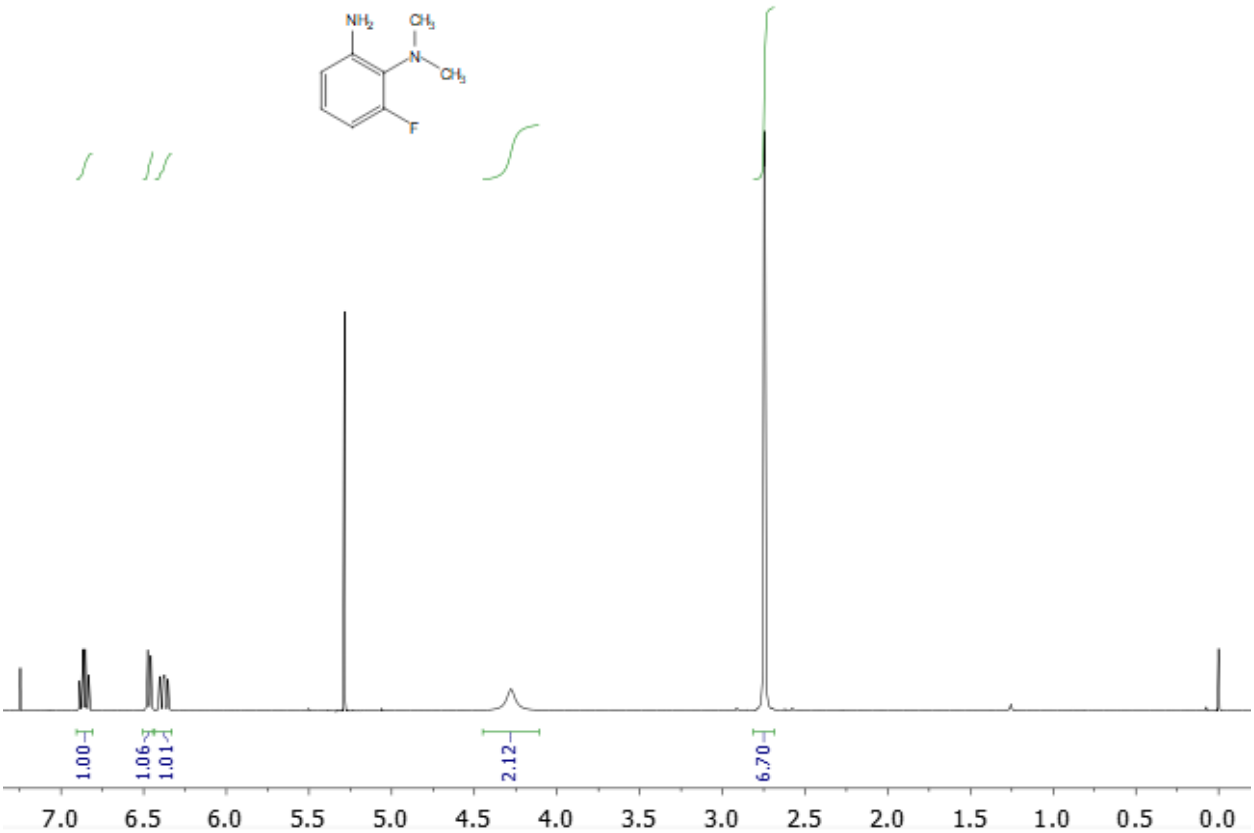

Figure 3.4: ^{1}H NMR spectrum ($CDCl_3$, 400 MHz) of purified 2-dimethylamino-3-fluoroaniline **(2a)**, δ 6.86, 6.47, 6.38 ppm (3 aromatic CH), 4.28 (NH_2), 2.75 ppm (NMe_2). Dichloromethane (chromatography solvent, 5.28 ppm), $CHCl_3$ (NMR solvent residual isotopomer, 7.26 ppm), and TMS (shift standard, 0.00 ppm) are also present. A polynomial baseline correction was applied to the frequency-domain spectrum.

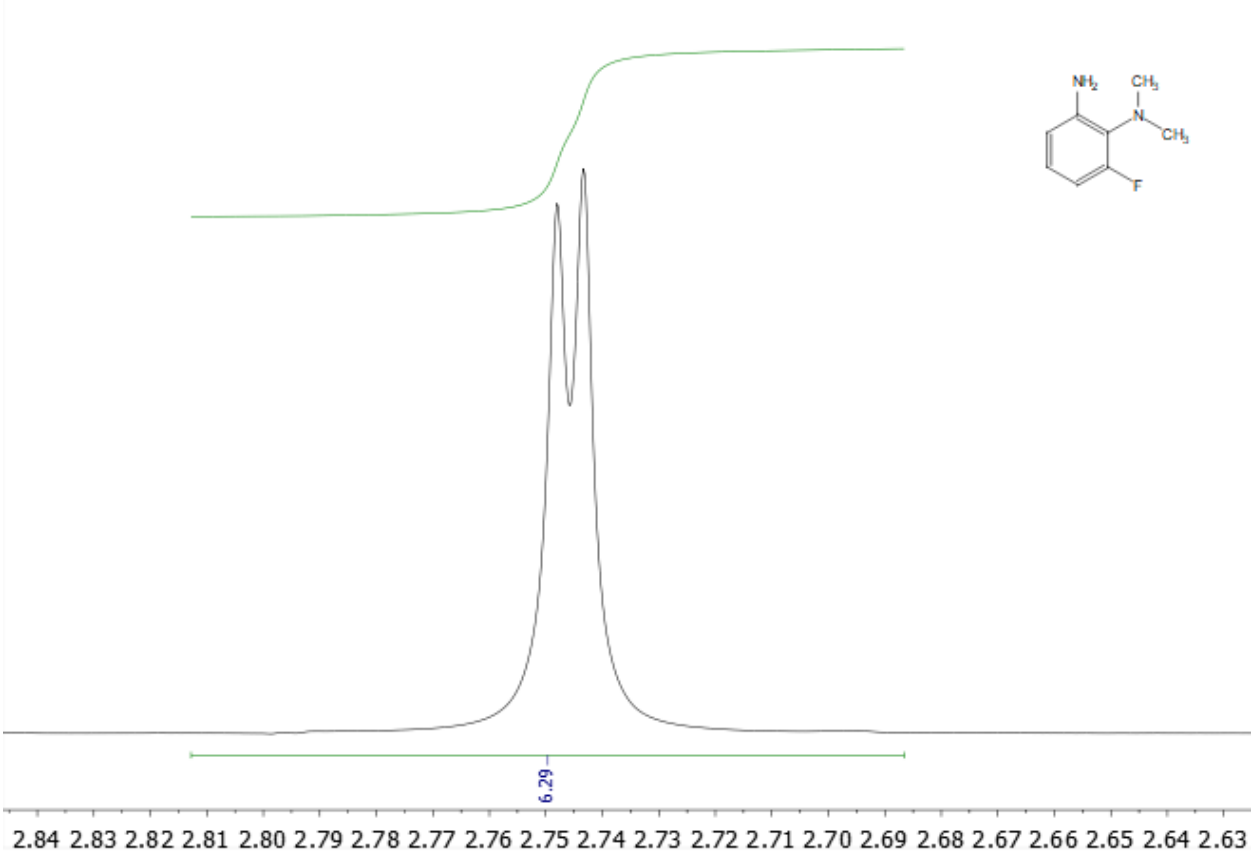

Figure 3.5: ^{1}H NMR spectrum ($CDCl_3$, 400 MHz) of column-purified 2-dimethylamino-3-fluoroaniline (**2a)**. Expansion of NMe_2 signal showing 2-Hz coupling to the 3-fluorine. A multipoint polynomial baseline correction was applied to the frequency-domain spectrum.

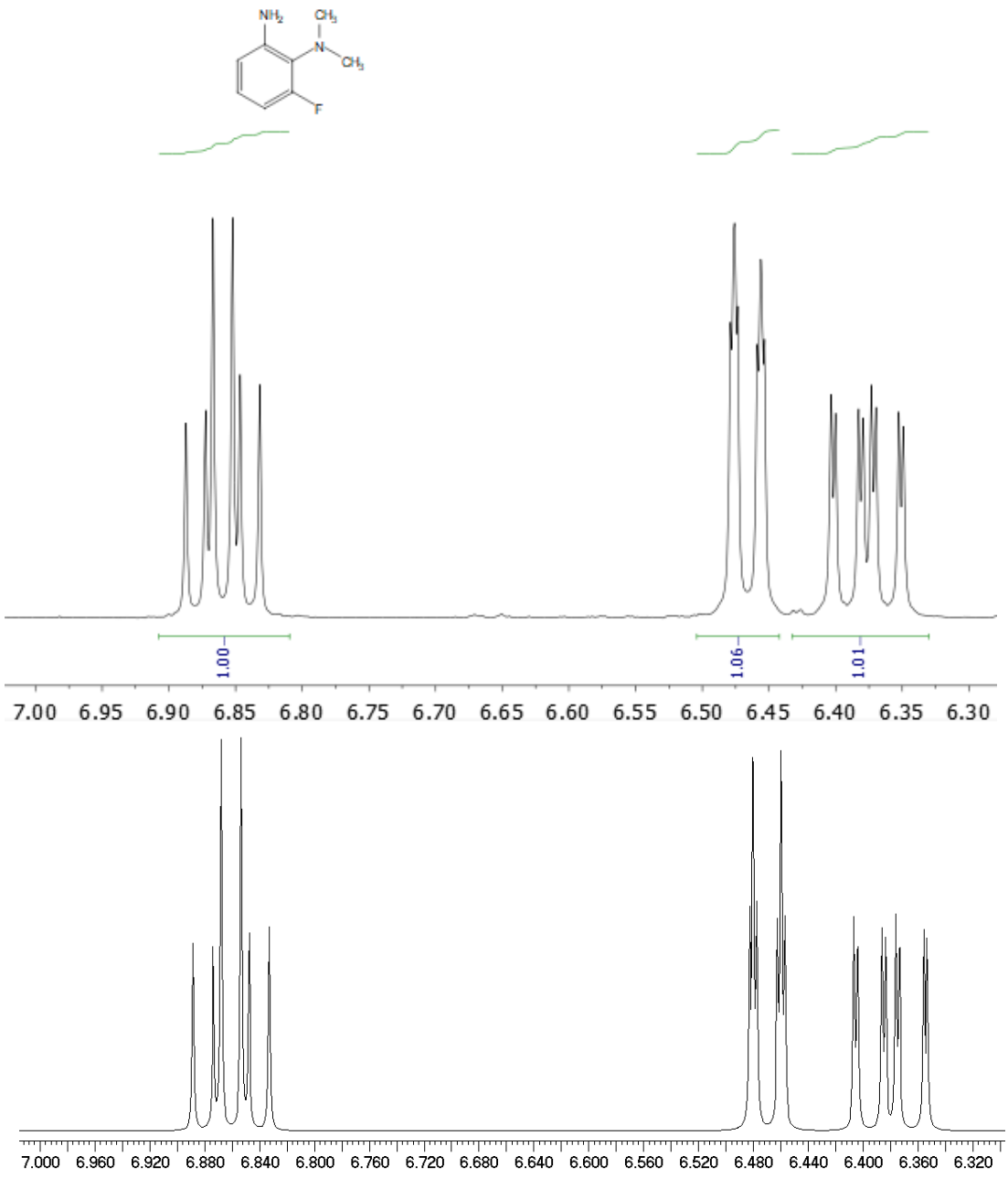

Figure 3.6: ^{1}H NMR spectra ($CDCl_3$, 400 MHz, expansion) of the aromatic region of 2-dimethylamino-3-fluoroaniline **(2a)**. **Upper**: Experimental spectrum with multipoint polynomial baseline correction applied. **Lower**: Simulated; a natural linewidth of 0.5 Hz was estimated.

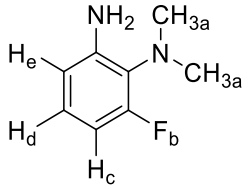

Figure 3.7: Structure of 2-dimethylamino-3-fluoroaniline (**2a)** showing nuclei labeled for the simulation described in Table 3.1.

Table 3.1: Chemical shifts and coupling constants for 2-dimethylamino-3-fluoroaniline used to generate the simulated spectra shown in Figures 3.1 through 3.6.

		Coupling Constants (Hz)				
Nucleus	Chemical Shift (ppm)	a	b	c	d	e
a (NMe_2)	–123.0					
b (F)	2.75	1.9				
c (H)	6.38	0.0	12.2			
d (H)	6.86	0.0	5.9	8.1		
e (H)	6.47	0.0	1.1	1.1	8.2	
NH_2	4.28					

2-Dimethylamino-4-fluoroaniline

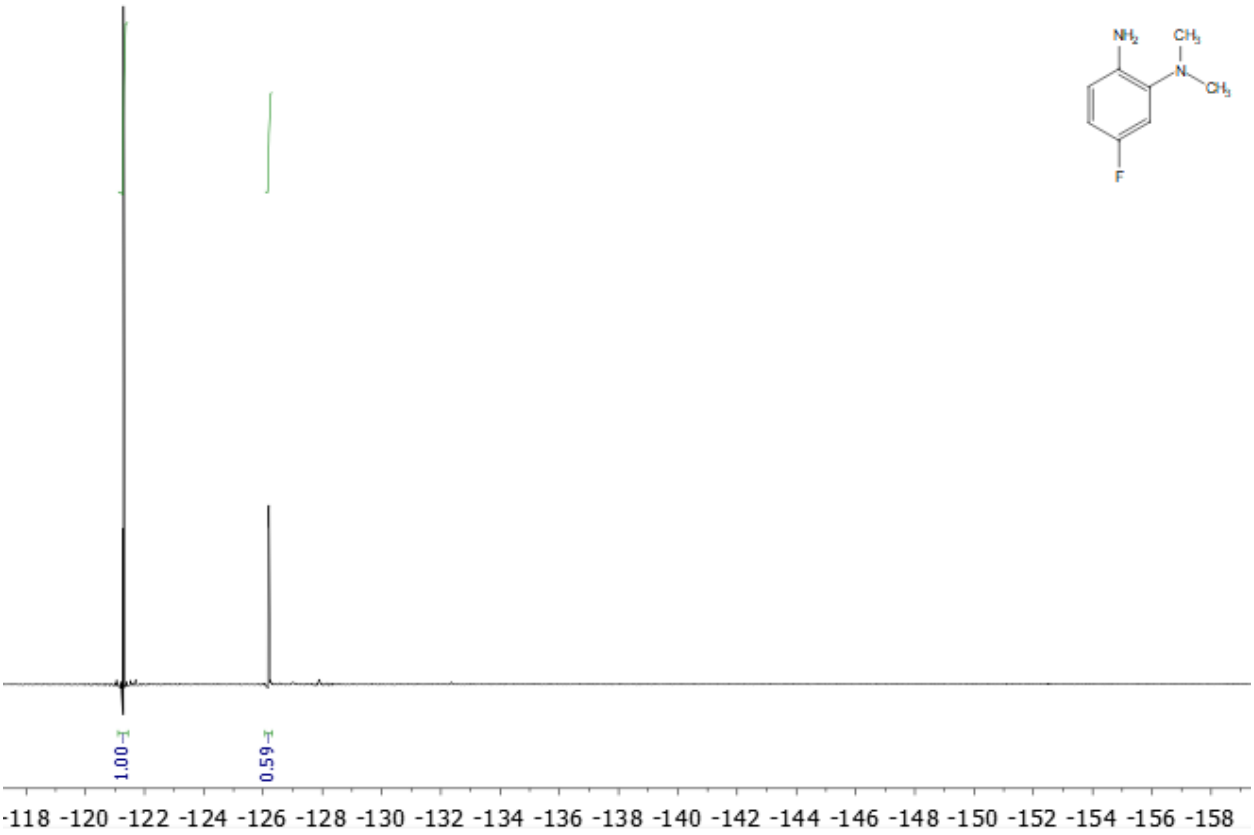

Figure 3.8: ^{19}F NMR spectrum ($CDCl_3$, 376 MHz) of <u>crude</u> 2-dimethylamino-4-fluoroaniline (**2b)**. Also present is bis(4-fluorophenyl) ether (internal standard), referenced at −121.3 ppm.

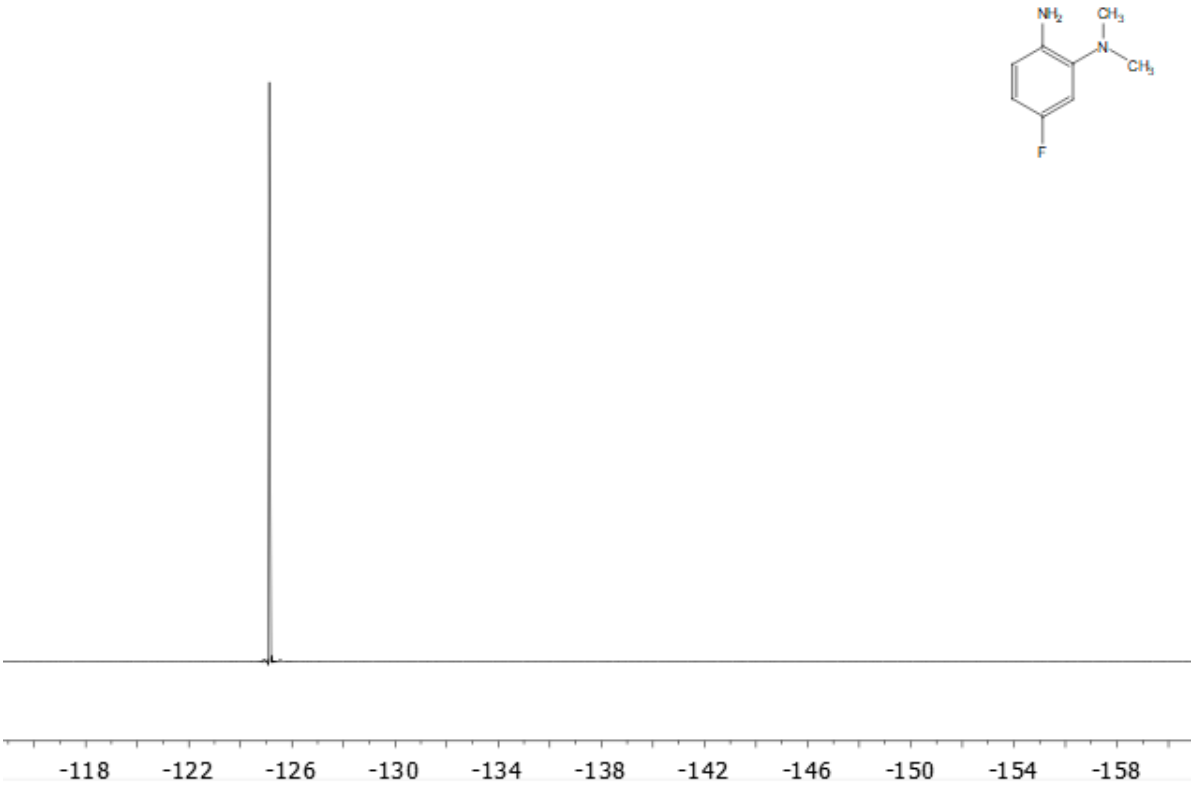

Figure 3.9: ^{19}F NMR spectrum ($CDCl_3$, 376 MHz) of column-purified 2-dimethylamino-4-fluoroaniline (**2b)**. Comparison to Figure 3.8 shows complete removal of the internal standard.

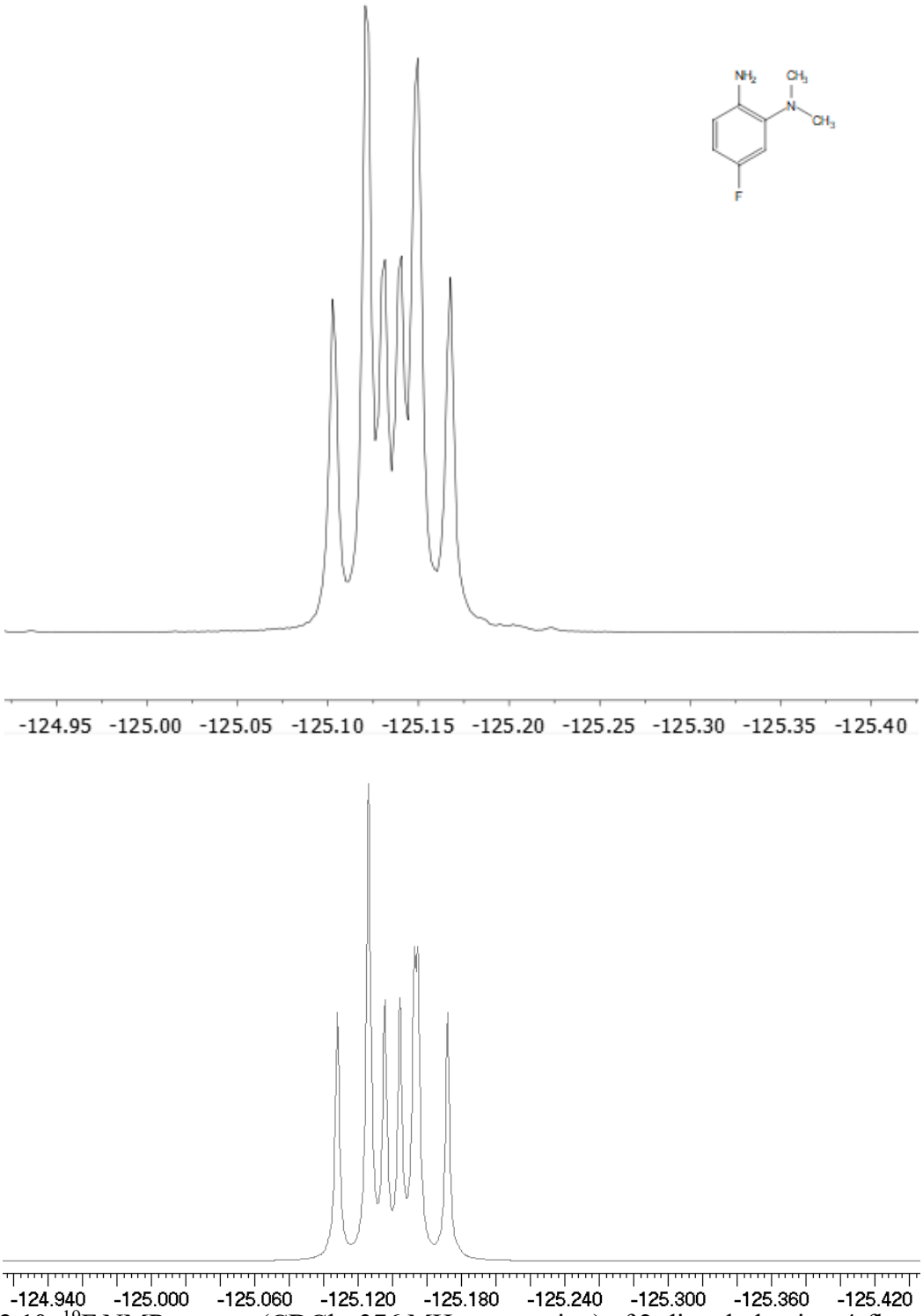

Figure 3.10: ^{19}F NMR spectra ($CDCl_3$, 376 MHz, expansion) of 2-dimethylamino-4-fluoroaniline (**2b)**, with 1.0 Hz of line broadening apodization applied to the FID and a multipoint polynomial baseline correction applied to frequency-domain spectrum. **Upper**: Experimental. **Lower**: Simulated (a natural linewidth of 1.4 Hz was estimated.)

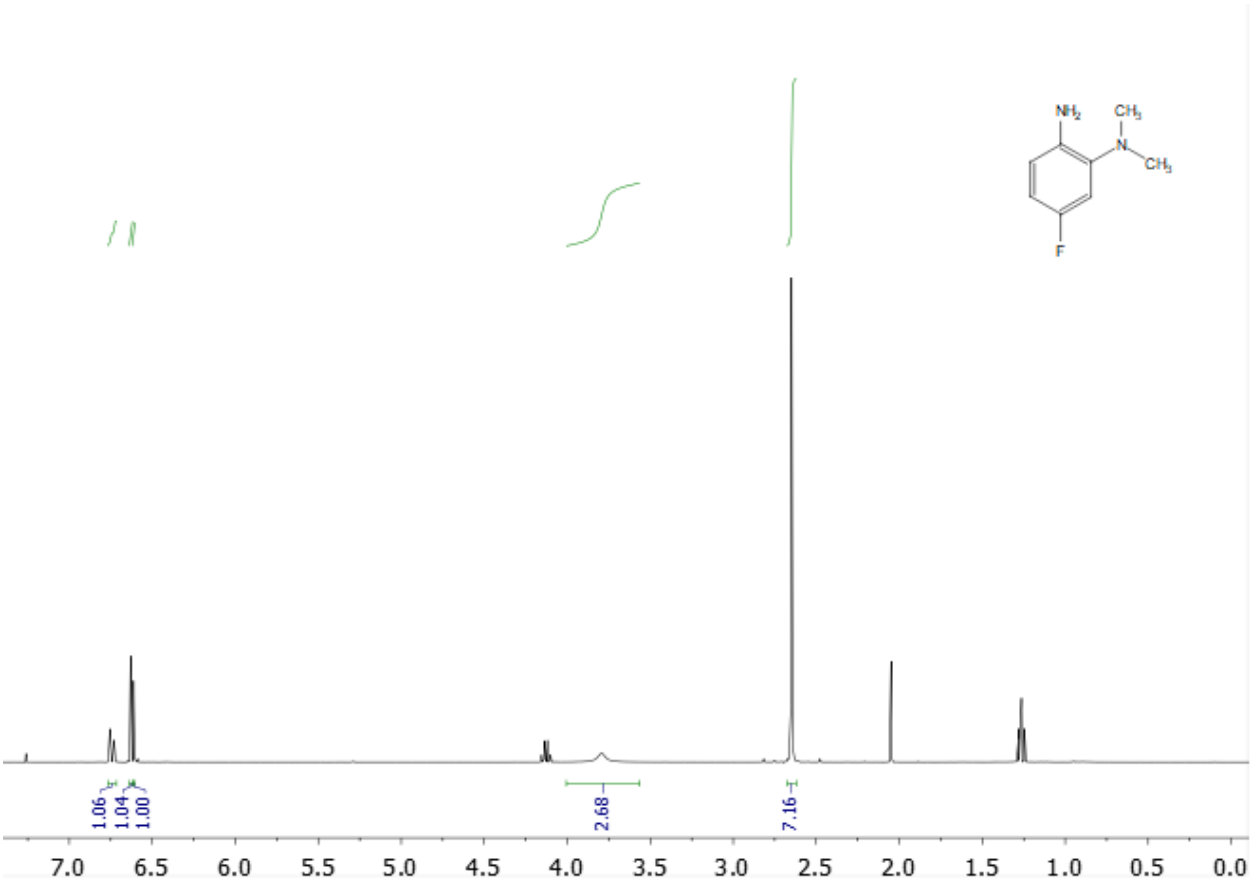

Figure 3.11: ^{1}H NMR spectrum ($CDCl_3$, 400 MHz) of column-purified 2-dimethylamino-4-fluoroaniline (**2b)**, δ 6.74 (CH), 6.63 (CH), 6.61 (CH), 3.79 (NH_2), 2.65 (NMe_2). Also present are ethyl acetate (chromatography solvent, 4.13 ppm, 2.05 ppm, and 1.26 ppm) and $CHCl_3$ (NMR solvent isotopomer). A multipoint polynomial baseline correction was applied to the frequency-domain spectrum.

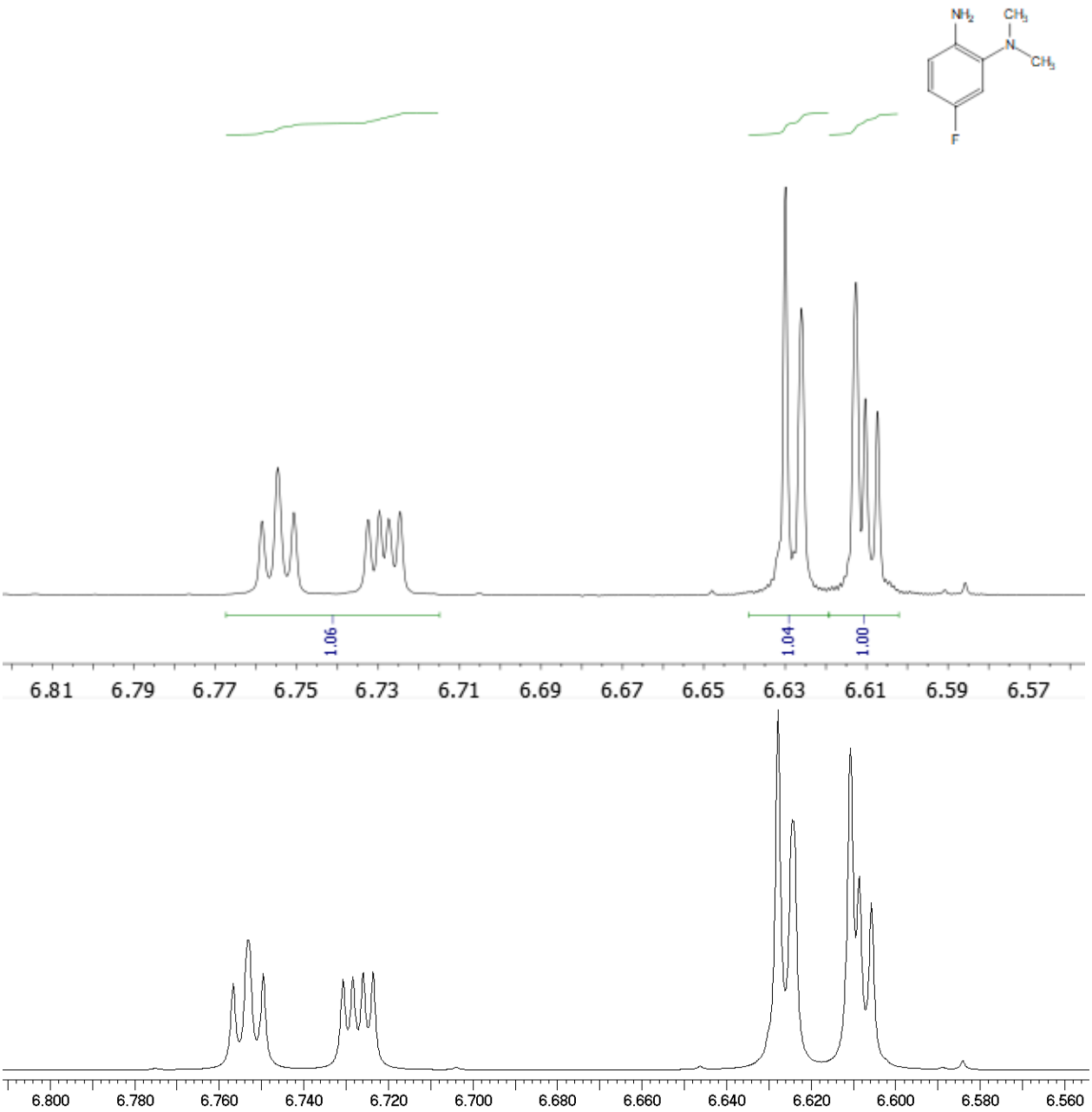

Figure 3.12: ^{1}H NMR spectra ($CDCl_3$, 400 MHz, expansion) of aromatic region of 2-dimethylamino-4-fluoroaniline **(2b)**. **Upper**: Experimental spectrum with multipoint polynomial baseline correction applied. **Lower**: Simulated; a natural linewidth of 0.5 Hz was estimated. Note especially the small features in the simulated spectrum – these are not impurities.

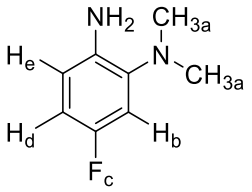

Figure 3.13: Structure of 2-dimethylamino-4-fluoroaniline (**2b)** showing nuclei labeled for the simulation described in Table 3.2.

Table 3.2: Chemical shifts and coupling constants for 2-dimethylamino-4-fluoroaniline used to generate the simulated spectra shown in Figures 3.8 through 3.12.

		Coupling Constants (Hz)				
Nucleus	Chemical Shift (ppm)	a	b	c	d	e
a (NMe_2)	2.65					
b (H)	6.74	0.0				
c (F)	−126.1	0.0	10.4			
d (H)	6.615	0.0	2.8	8.0		
e (H)	6.620	0.0	0.0	5.7	8.7	
NH_2	3.79					

2-Dimethylamino-5-fluoroaniline

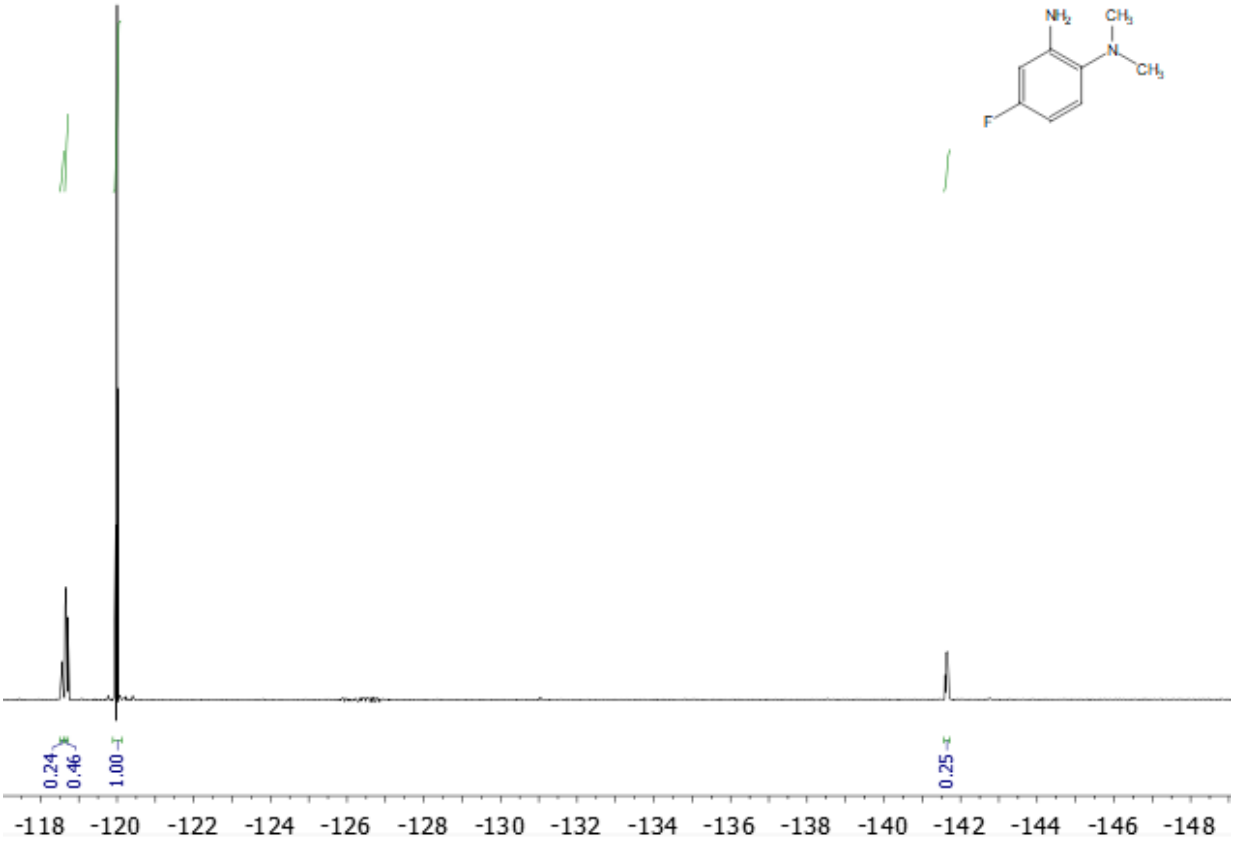

Figure 3.14: ^{19}F NMR spectrum ($CDCl_3$, 376 MHz) of <u>crude</u> 2-dimethylamino-5-fluoroaniline (**2c**) (present at –120.0 ppm). Unreacted 2,5-difluoroaniline is present at –119.9 ppm and -142.9 ppm. Also present is bis(4-fluorophenyl) ether (internal standard) at −121.3 ppm.

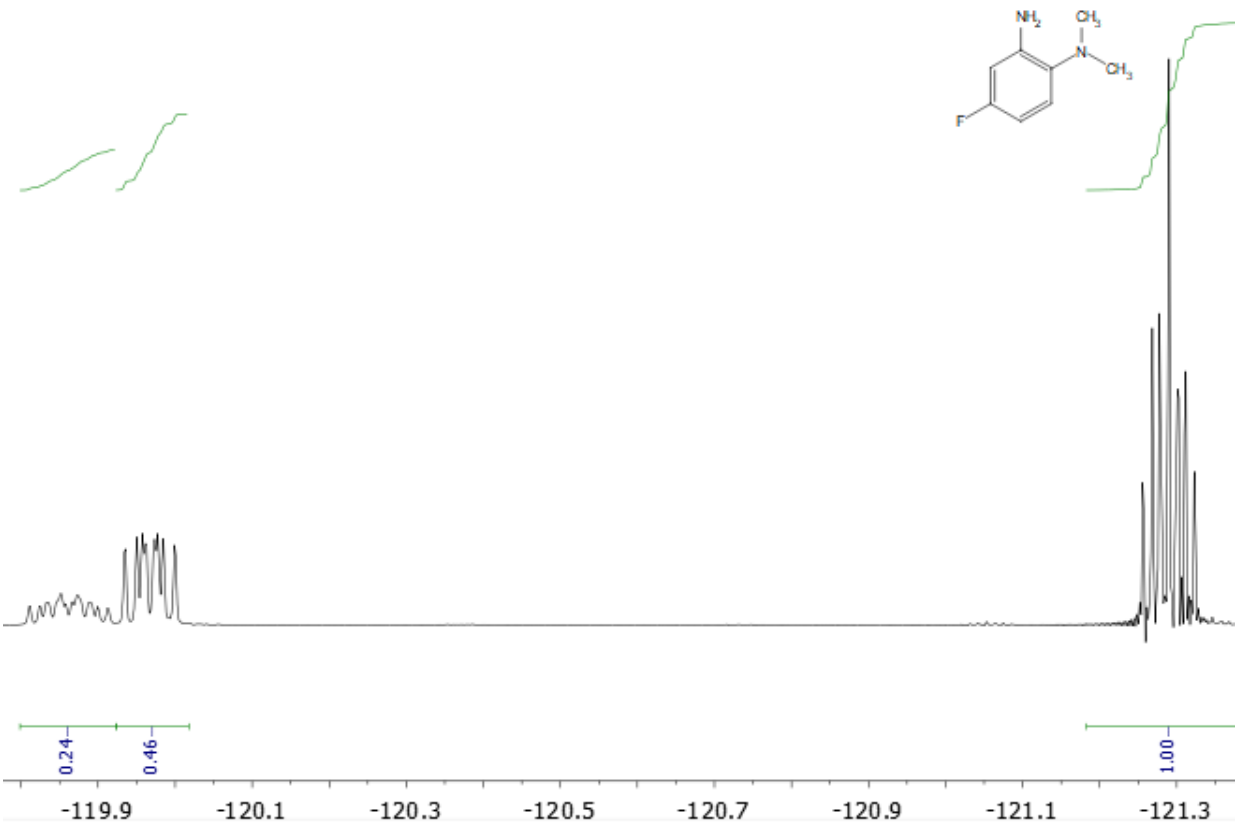

Figure 3.15: Expansion of ^{19}F NMR spectrum ($CDCl_3$, 376 MHz) showing the crude 2-dimethylamino-5-fluoroaniline (**2c**) (present at –120.0 ppm), the downfield peak of unreacted 2,5-difluoroaniline is present at –119.9 ppm, and the bis(4-fluorophenyl) ether (internal standard) at −121.3 ppm.

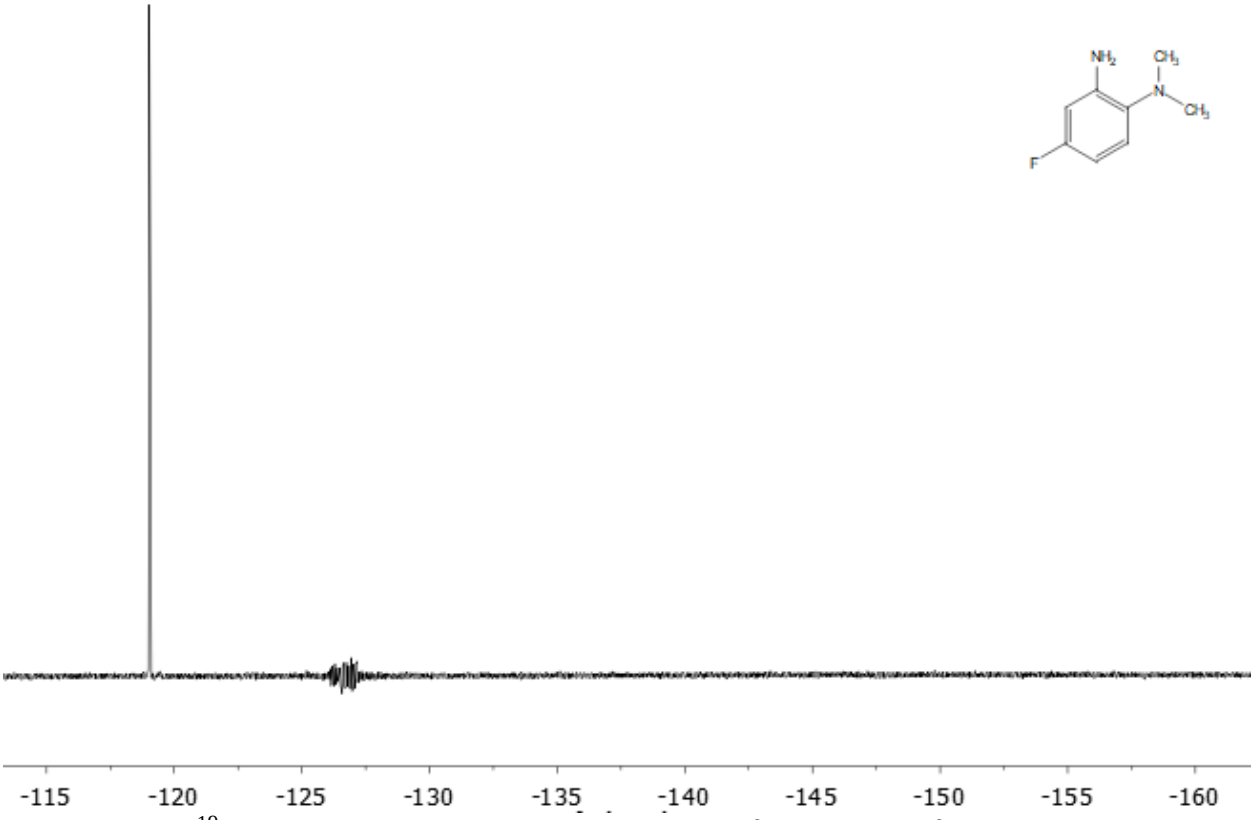

Figure 3.16: ^{19}F NMR spectrum ($CDCl_3$, 376 MHz) of column-purified 2-dimethylamino-5-fluoroaniline (**2c**). The feature at ca. −127 ppm is a Fourier-transform artifact.

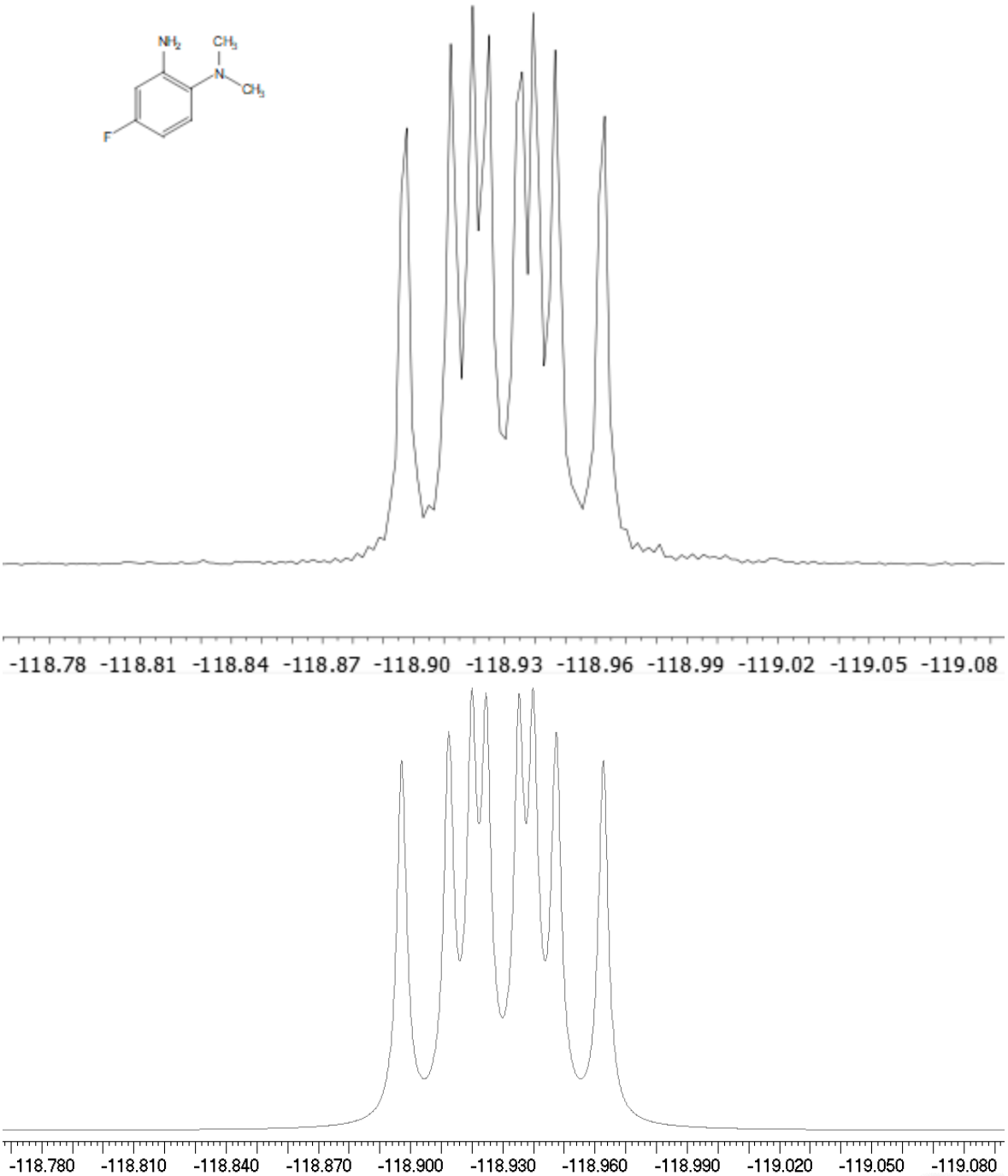

Figure 3.17: ^{19}F NMR spectra (C_6D_6, 376 MHz, expansion) of 2-dimethylamino-5-fluoroaniline (**2c**). **Upper**: Experimental spectrum with 0.5 Hz line broadening applied. **Lower**: Simulated (A natural linewidth of 1.4 Hz was estimated.)

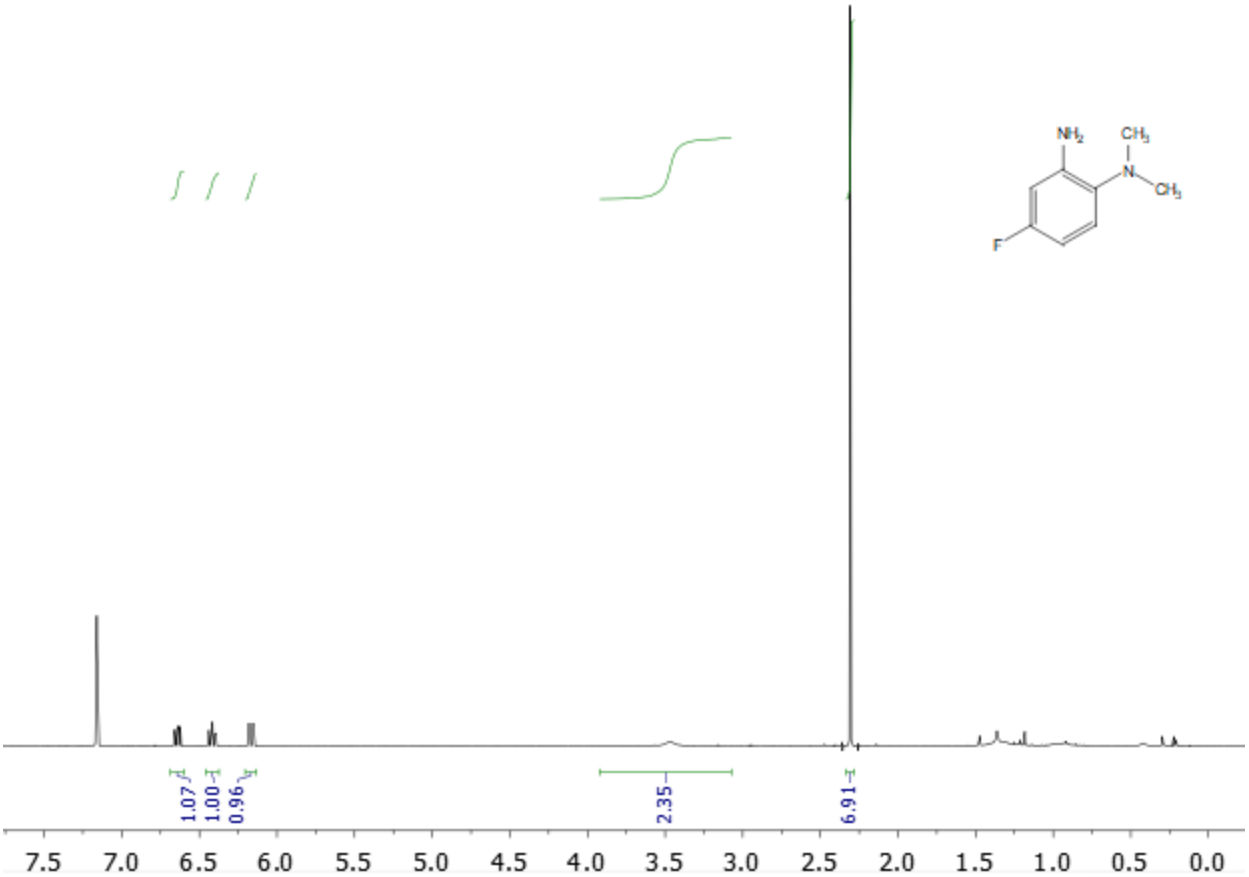

Figure 3.18: ^{1}H NMR spectrum (C_6D_6, 400 MHz) of column-purified 2-dimethylamino-5-fluoroaniline (**2c**), δ 6.64 (CH), 6.42 (CH), 6.17 (CH), 3.47 (NH_2), 2.31 (NMe_2). Chemical shift is referenced to the solvent isotopomer, C_6D_5H at 7.16 ppm. A polynomial baseline correction was applied to the frequency-domain spectrum.

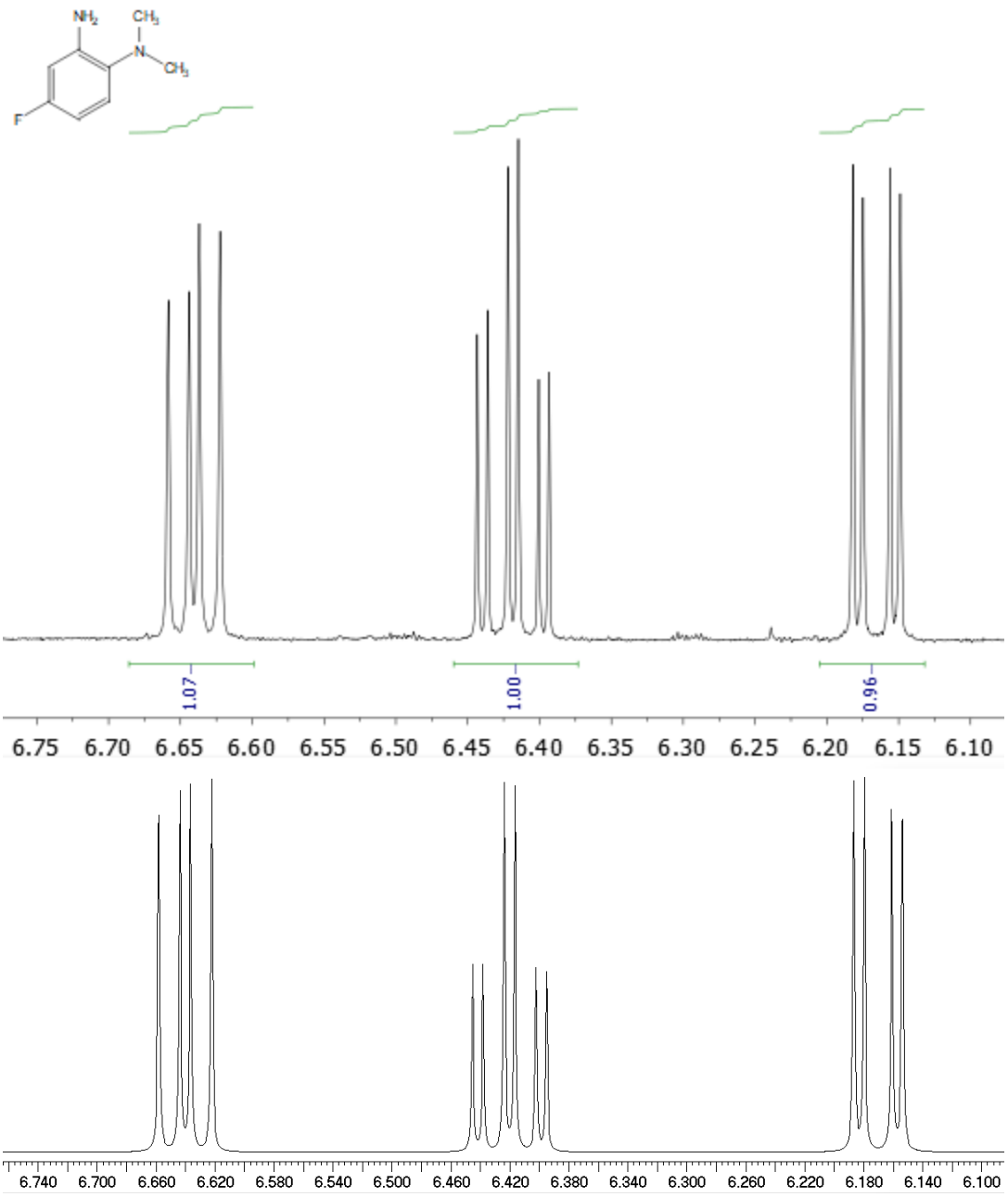

Figure 3.19: ^{1}H NMR spectra (C_6D_6, 400 MHz, expansion) of aromatic region of 2-dimethylamino-5-fluoroaniline (**2c**). **Upper**: Experimental spectrum with polynomial baseline correction applied. **Lower**: Simulated; a natural linewidth of 0.5 Hz was estimated.

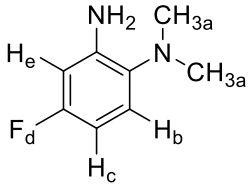

Figure 3.20: Structure of 2-dimethylamino-5-fluoroaniline (**2c**) showing nuclei labeled for the simulation described in Table 3.3. Please note that the corresponding experimental spectra were obtained in C_6D_6 solvent. Spectra that we obtained in $CDCl_3$ solvent showed chemical shift overlap that we were unable to model to our own satisfaction. 2-dimethylamino-5-fluoroaniline is the only compound for which we had to resort to collecting the spectra in a solvent other than chloroform to model the spin system cleanly.

Table 3.3: Chemical shifts and coupling constants for 2-dimethylamino-5-fluoroaniline used to generate the simulated spectra shown in Figures 3.14 through 3.19.

		Coupling Constants (Hz)				
Nucleus	Chemical Shift (ppm)	a	b	c	d	e
a (NMe_2)	2.31					
b (H)	6.64	0.0				
c (H)	6.42	0.0	8.6			
d (F)	-118.9	0.0	5.8	8.9		
e (H)	6.17	0.0	0.0	2.9	10.3	
NH_2	3.47					

2-Dimethylamino-6-fluoroaniline

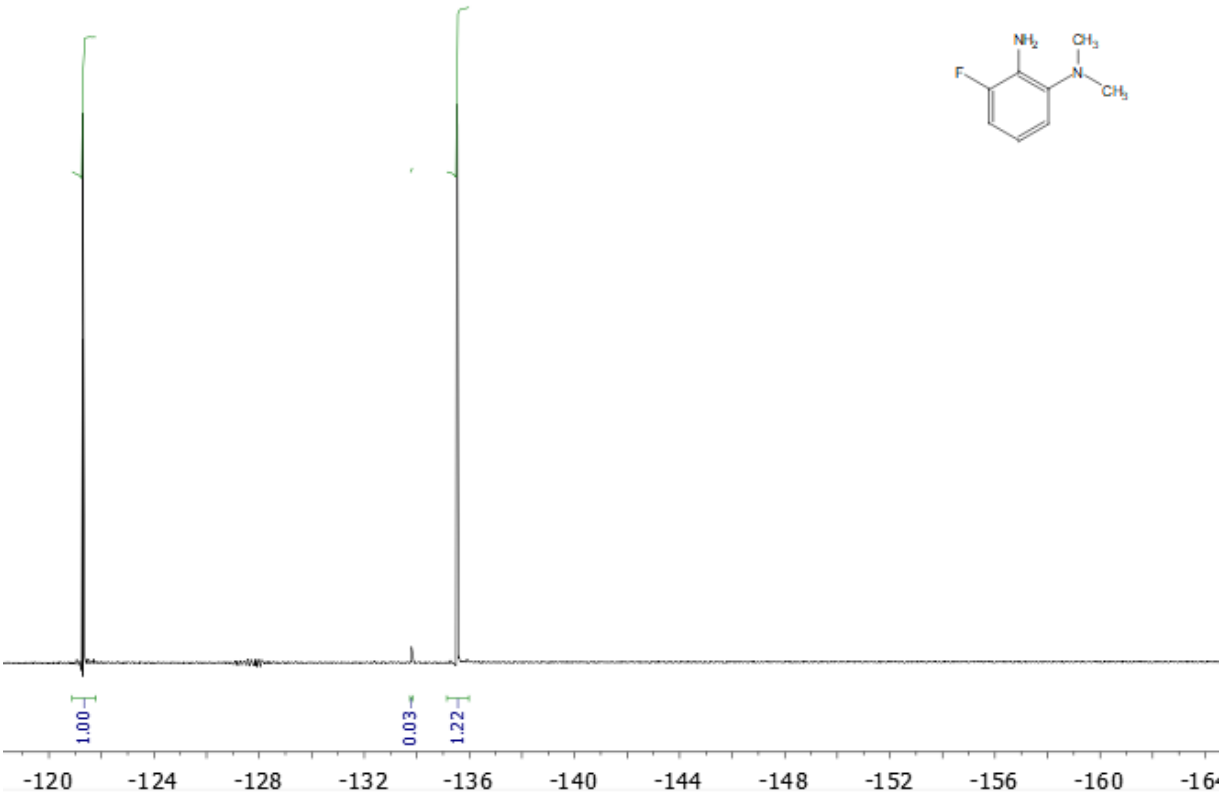

Figure 3.21: ^{19}F NMR spectrum ($CDCl_3$, 376 MHz) of crude 2-dimethylamino-6-fluoroaniline (**2d**) at −135.5 ppm, starting material at −133.8 ppm. Also present is bis(4-fluorophenyl) ether at −121.3 ppm.

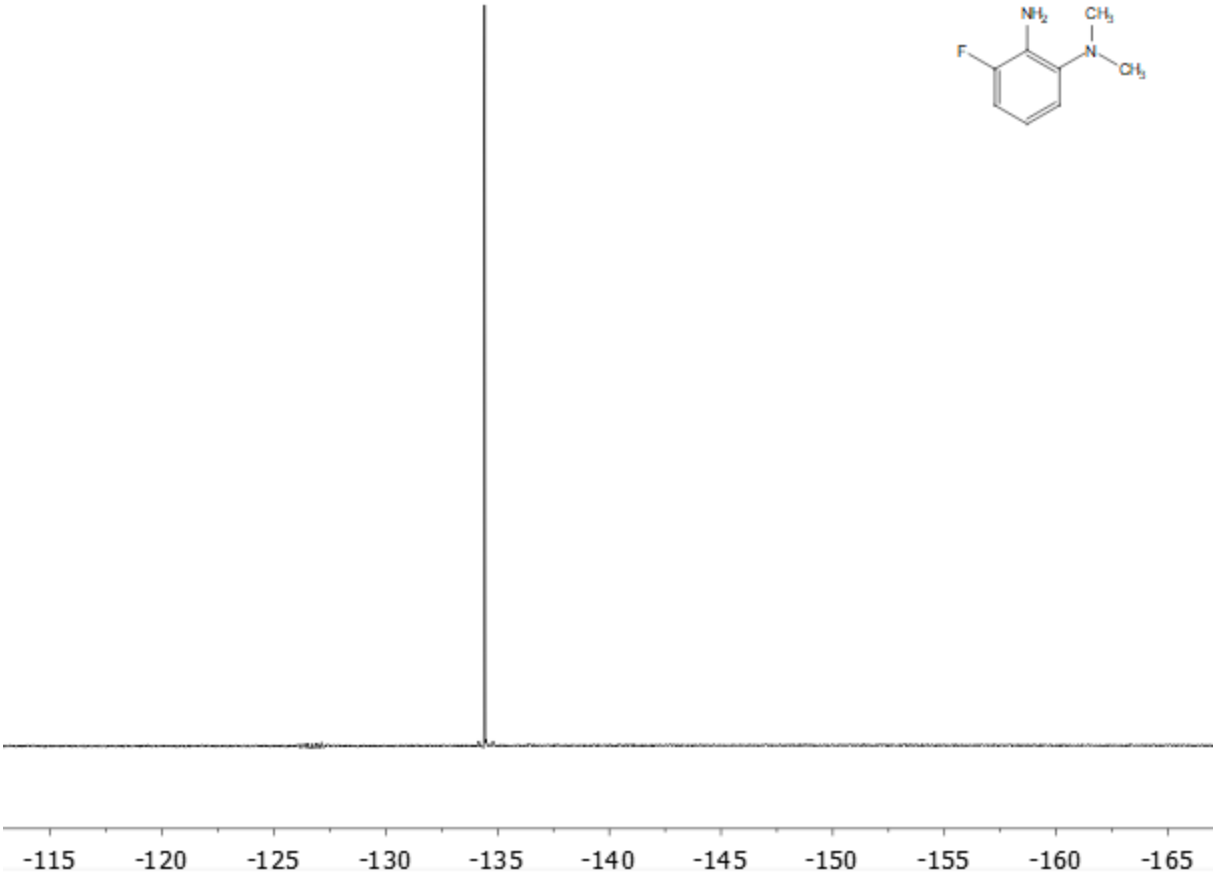

Figure 3.22: ^{19}F NMR spectrum ($CDCl_3$, 376 MHz) of column-purified 2-dimethylamino-6-fluoroaniline (**2d**). A multipoint polynomial baseline correction was applied to the frequency-domain spectrum.

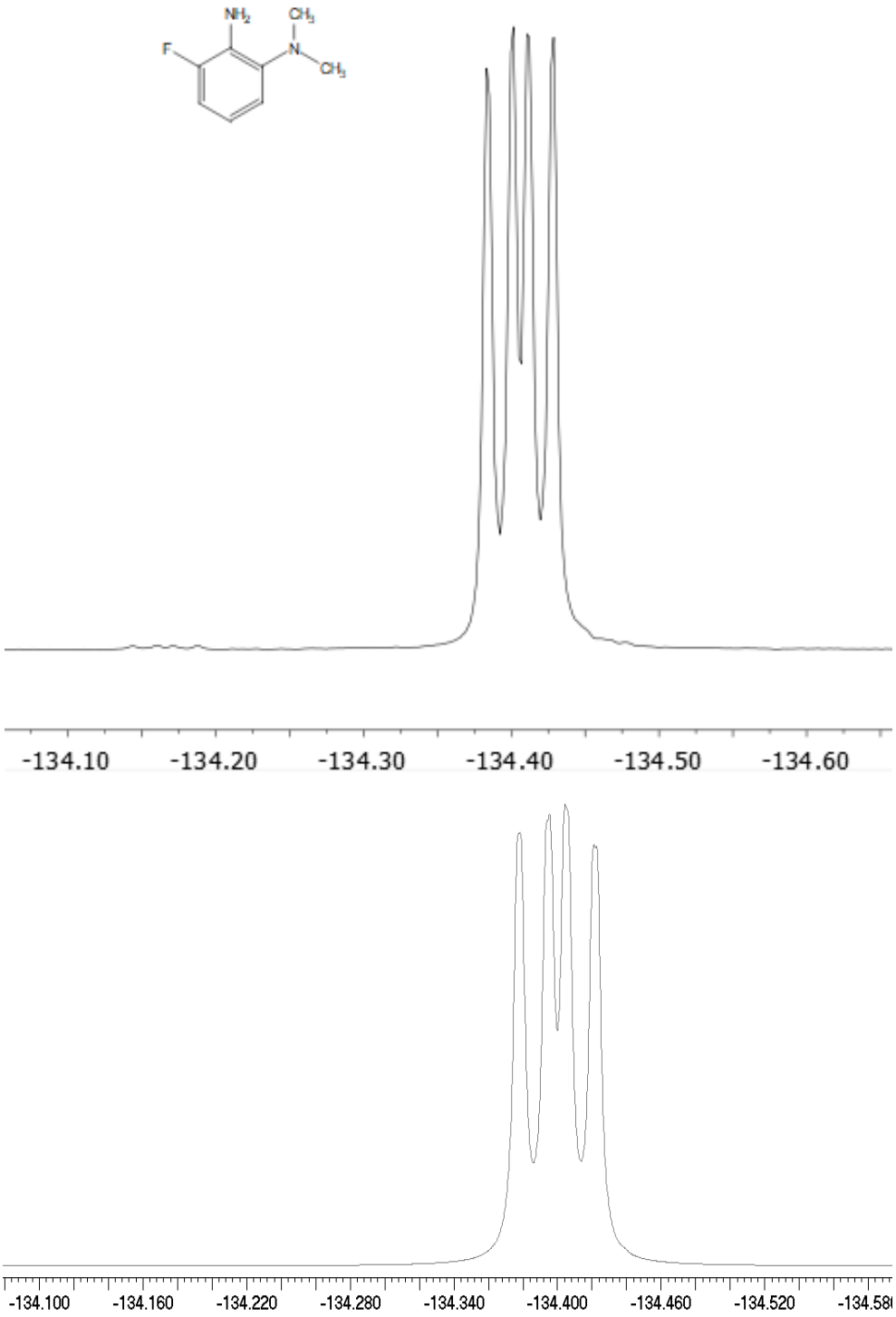

Figure 3.23: ^{19}F NMR spectra ($CDCl_3$, 376 MHz, expansion) of 2-dimethylamino-6-fluoroaniline (**2d**). **Upper**: Experimental spectrum with polynomial baseline correction applied. **Lower**: Simulated (a natural linewidth of 1.8 Hz was estimated.)

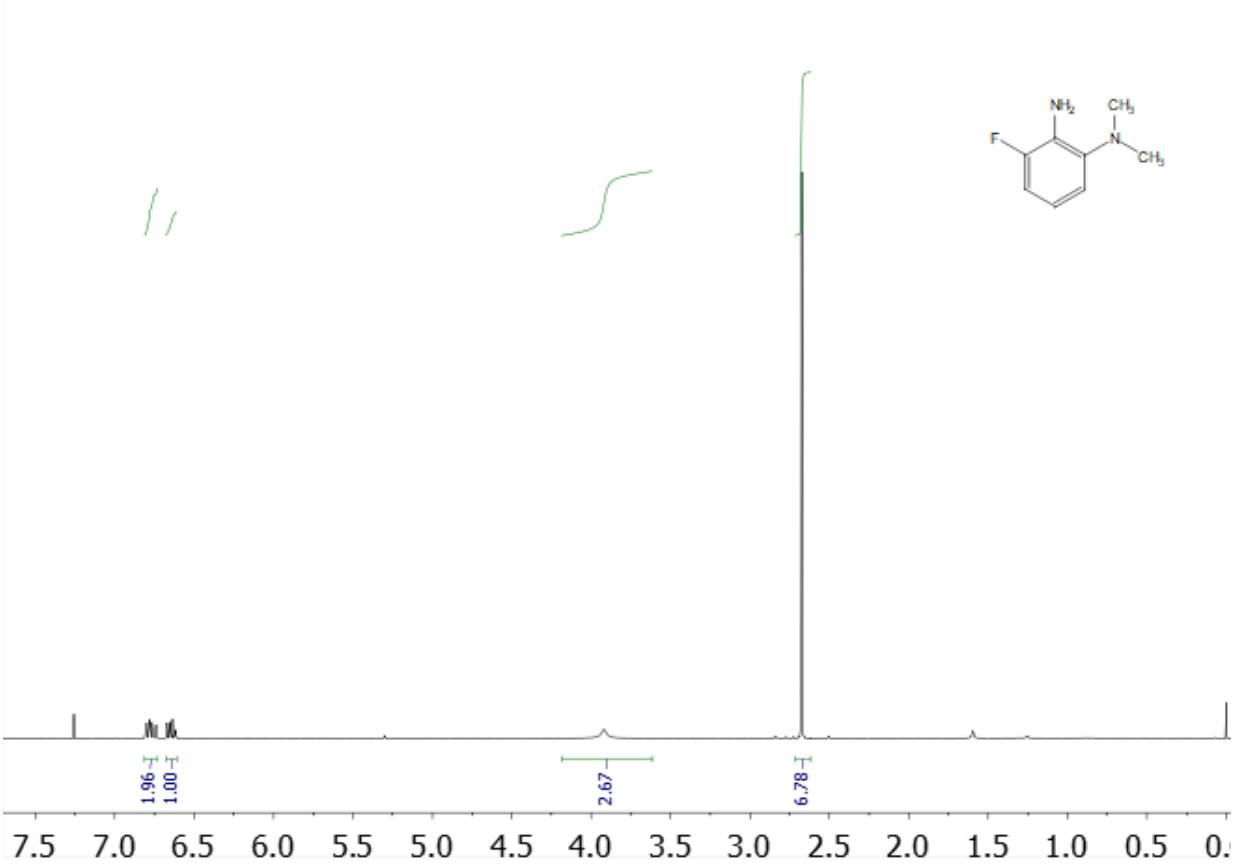

Figure 3.24: ^{1}H NMR spectrum ($CDCl_3$, 400 MHz) of column-purified 2-dimethylamino-6-fluoroaniline (**2d**), δ 6.77 (2 CH), 6.64 (CH), 3.92 (NH_2), 2.67 ppm (NMe_2). $CHCl_3$ is also present at 7.26 ppm. CH_2Cl_2 (chromatography solvent) is visible at 5.28 ppm and adventitious water at 1.6 ppm).

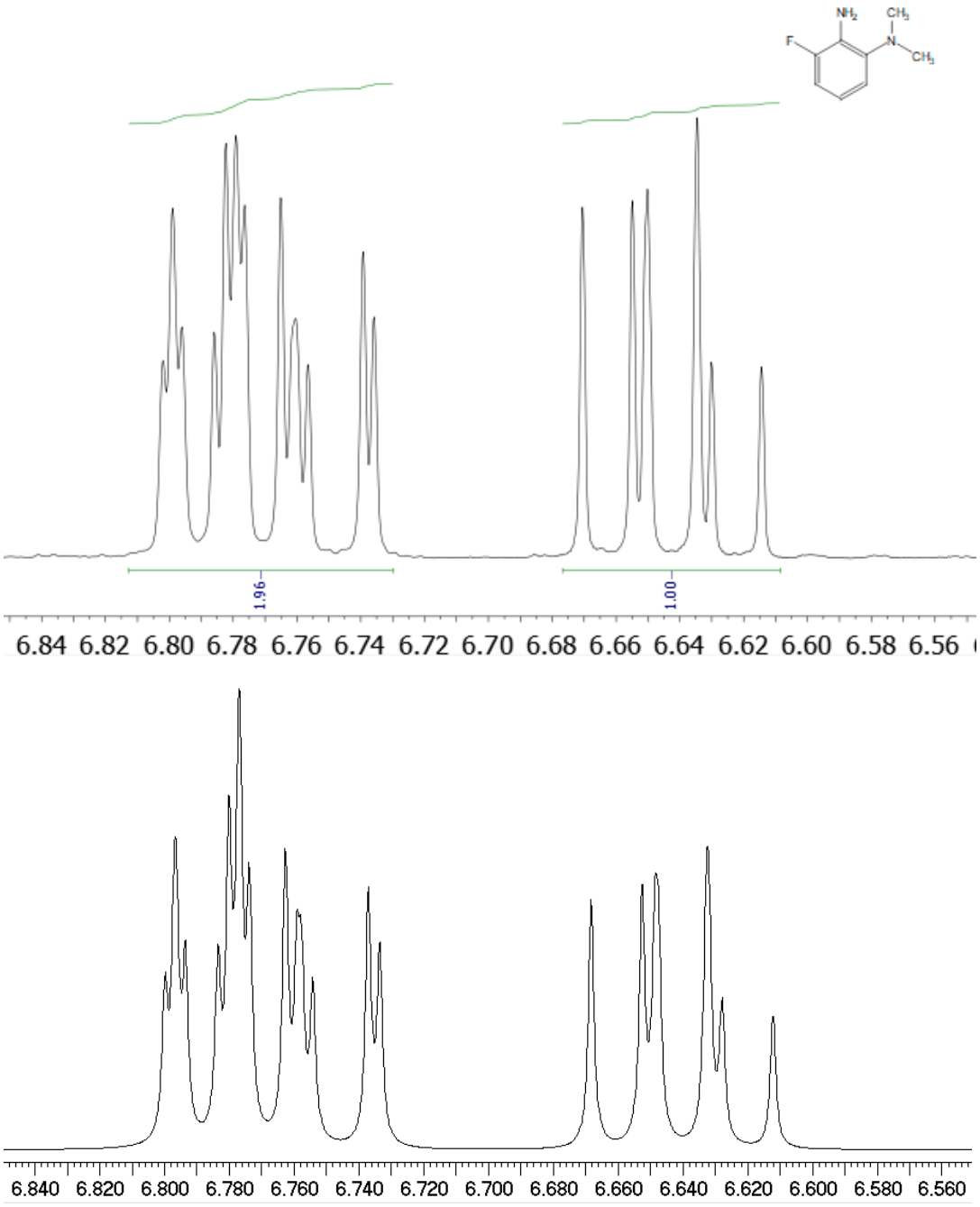

Figure 3.25: ^{1}H NMR spectra ($CDCl_3$, 400 MHz, expansion) of aromatic region of 2-dimethylamino-6-fluoroaniline (**2d**). **Upper:** Experimental spectrum. **Lower**: Simulated; a natural linewidth of 0.8 Hz was estimated.

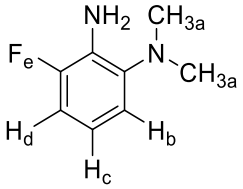

Figure 3.26: Structure of 2-dimethylamino-6-fluoroaniline (**2d**) showing nuclei labeled for the simulation described in Table 3.4.

Table 3.4: Chemical shifts and coupling constants for 2-dimethylamino-6-fluoroaniline used to generate the simulated spectra shown in Figures 3.21 through 3.25.

		Coupling Constants (Hz)				
Nucleus	Chemical Shift (ppm)	a	b	c	d	e
a (NMe_2)	2.67					
b (H)	6.786	0.0				
c (H)	6.64	0.0	8.0			
d (H)	6.758	0.0	1.3	8.3		
e (F)	−135.5	0.0	1.0	6.3	10.3	
NH_2	3.92					

Note that the model shown in Table 3.4 uses two chemical shifts that are adjusted at the ±0.001 ppm level. This fine adjustment was necessary to model the non-first-order features of the spectra.

2,6-Bis(dimethylamino)-3-fluoroaniline, 2-dimethylamino-3,6-Difluoroaniline, and 6-Dimethylamino-2,3-difluoroaniline

These compounds were considered as a group because they arise from a common substrate.

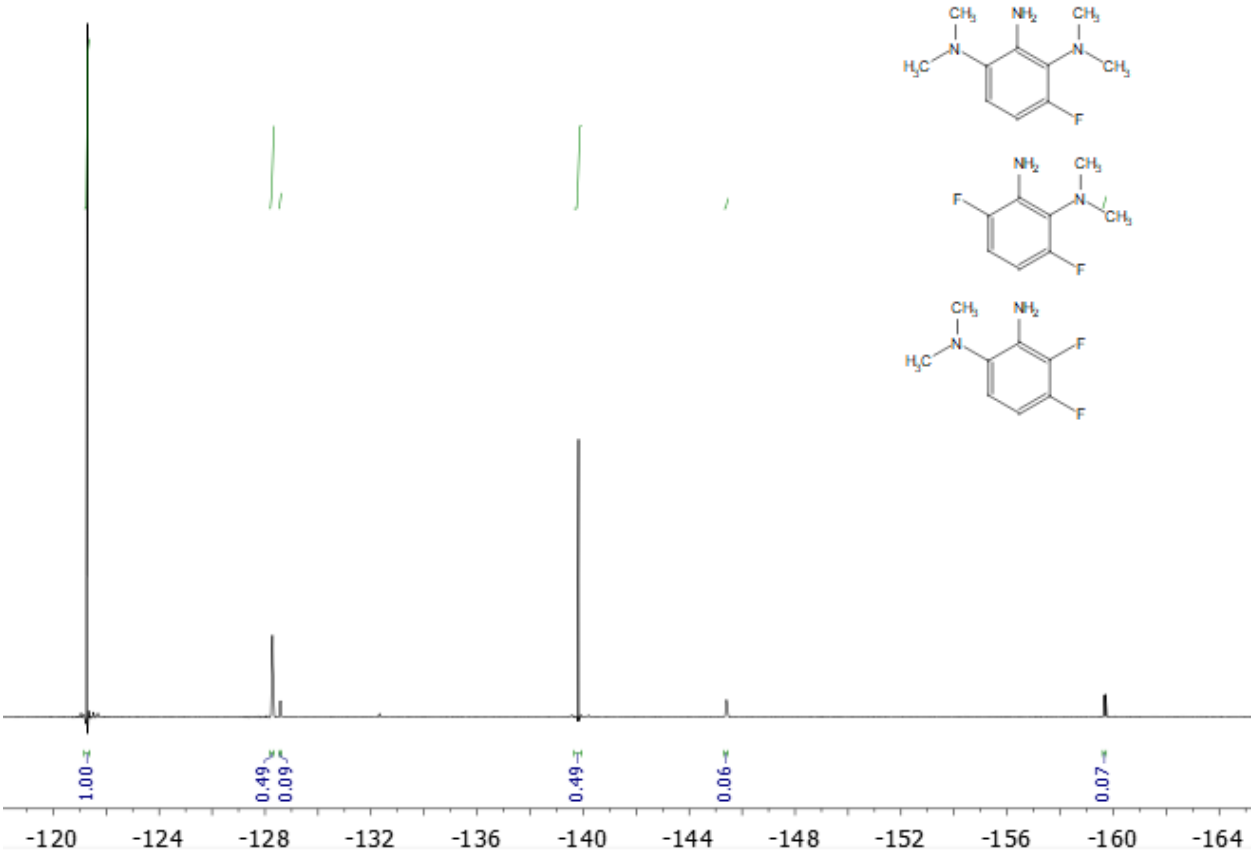

Figure 3.27: ^{19}F NMR spectrum ($CDCl_3$, 376 MHz) of the <u>crude</u> mixture of 2,6-bis(dimethylamino)-3-fluoroaniline (**3e**) (−128.6 ppm), 2-dimethylamino-3,6-fluoroaniline (**2e**) (−128.3 ppm and −139.8 ppm), and 6-dimethylamino-2,3-fluoroaniline (***iso*-2e**) (−145.4 ppm and −159.7 ppm). Also present is bis(4-fluorophenyl) ether at -121.3 ppm.

2-Dimethylamino-3,6-difluoroaniline

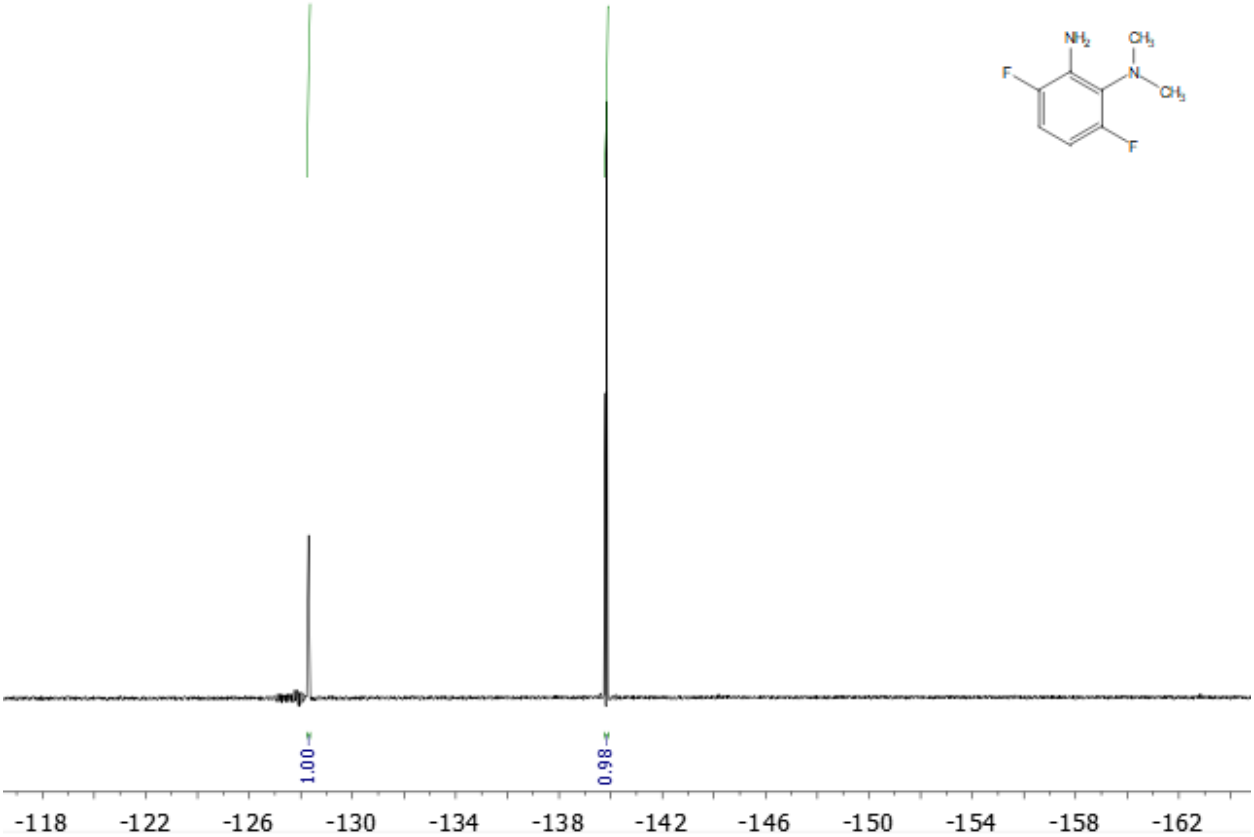

Figure 3.28: ^{19}F NMR spectrum ($CDCl_3$, 376 MHz) of column-purified 2-dimethylamino-3,6-difluoroaniline (**2e**). A polynomial baseline correction was applied to the frequency-domain spectrum.

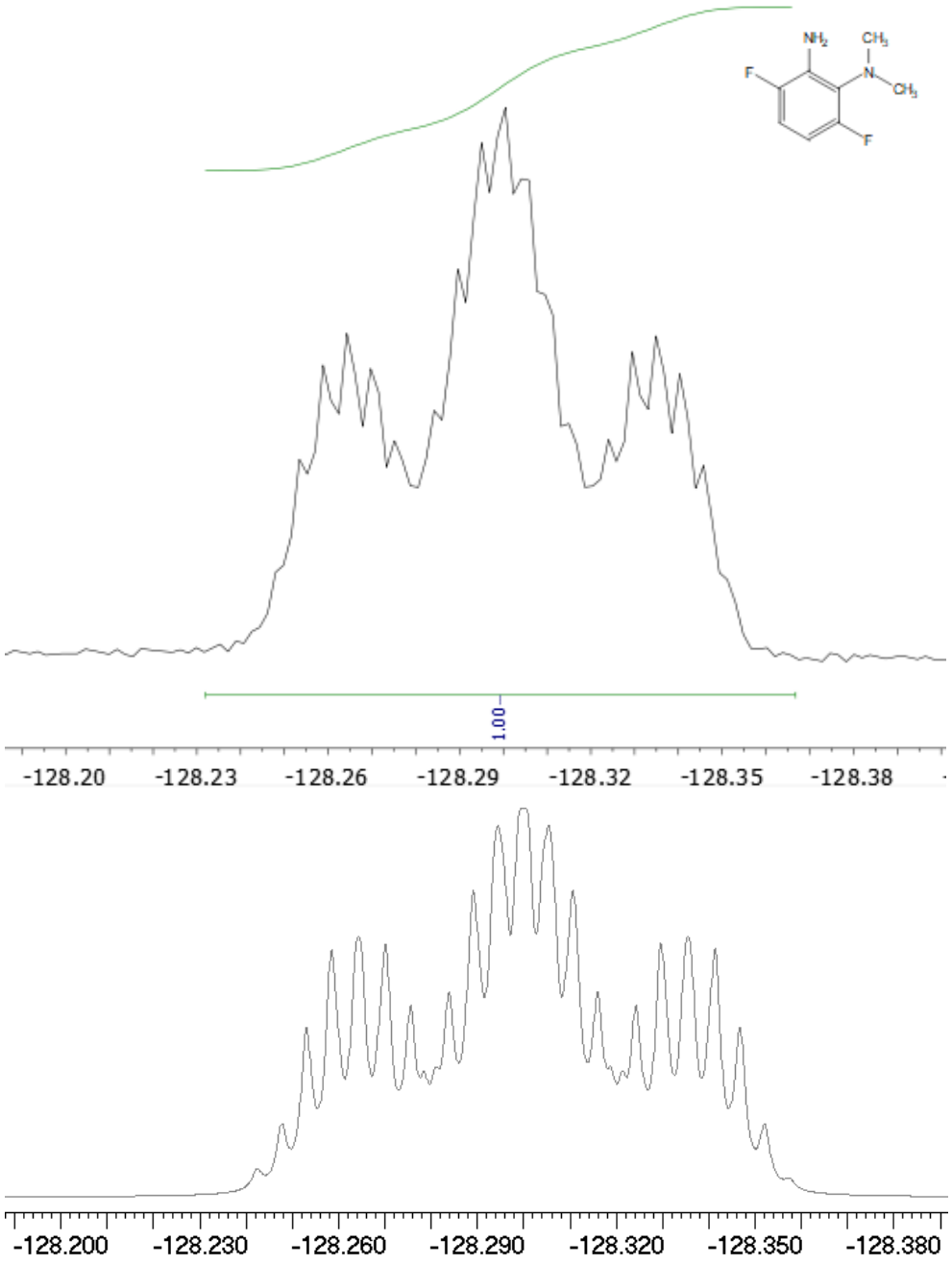

Figure 3.29: ^{19}F NMR spectra ($CDCl_3$, 376 MHz, expansion) of −128.3 ppm peak of 2-dimethylamino-3,6-difluoroaniline (**2e**). **Upper**: Experimental spectrum with polynomial baseline correction applied. **Lower**: Simulated (A natural linewidth of 1.0 Hz was estimated.) This signal is assigned to the 3-fluorine because of the observation of coupling to the NMe_2 group.

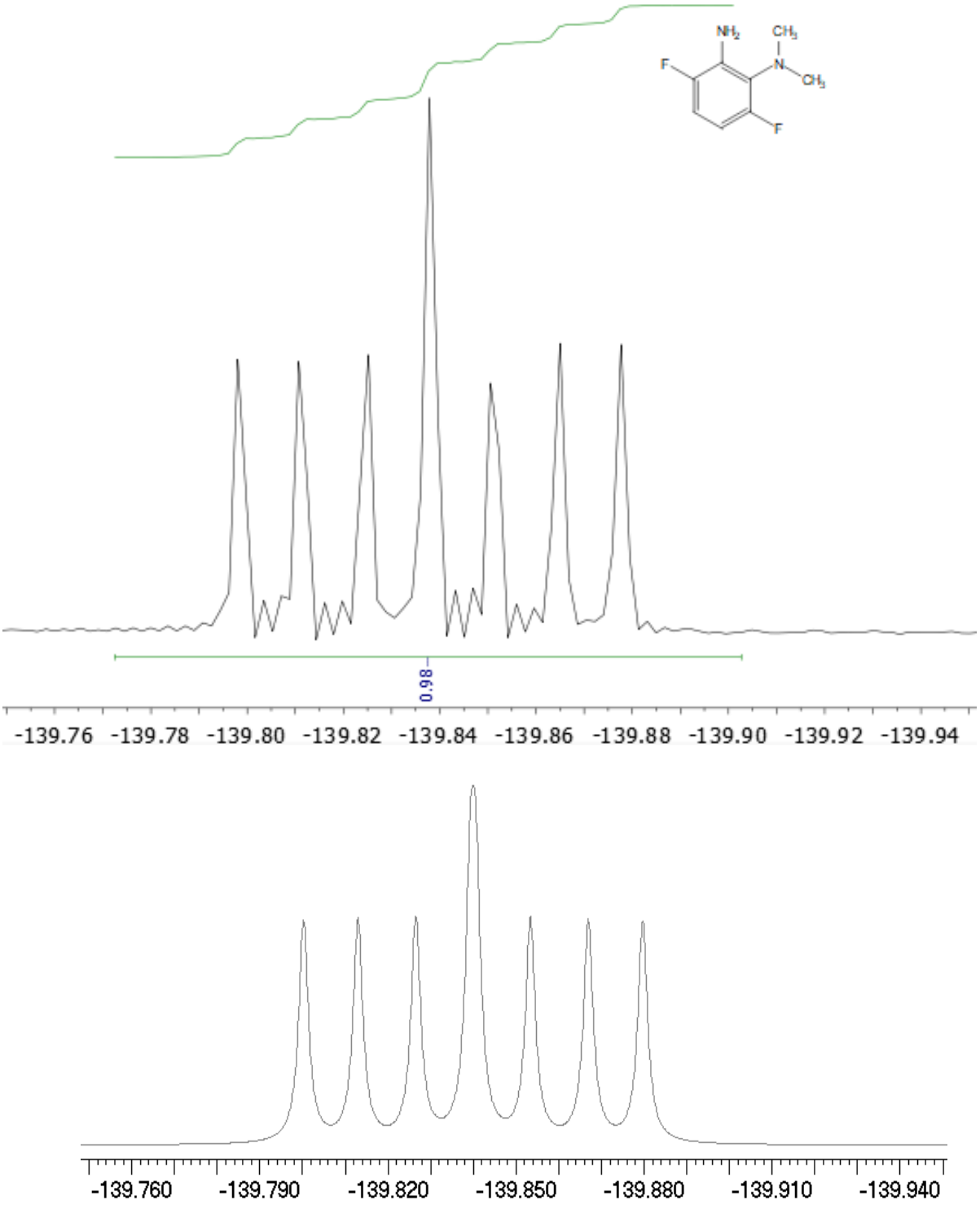

Figure 3.30: ^{19}F NMR spectra ($CDCl_3$, 376 MHz, expansion) of −139.8 ppm peak of 2-dimethylamino-3,6-difluoroaniline (**2e**). **Upper**: Experimental spectrum with polynomial baseline correction applied. **Lower**: Simulated (A natural linewidth of 1.0 Hz was estimated.)

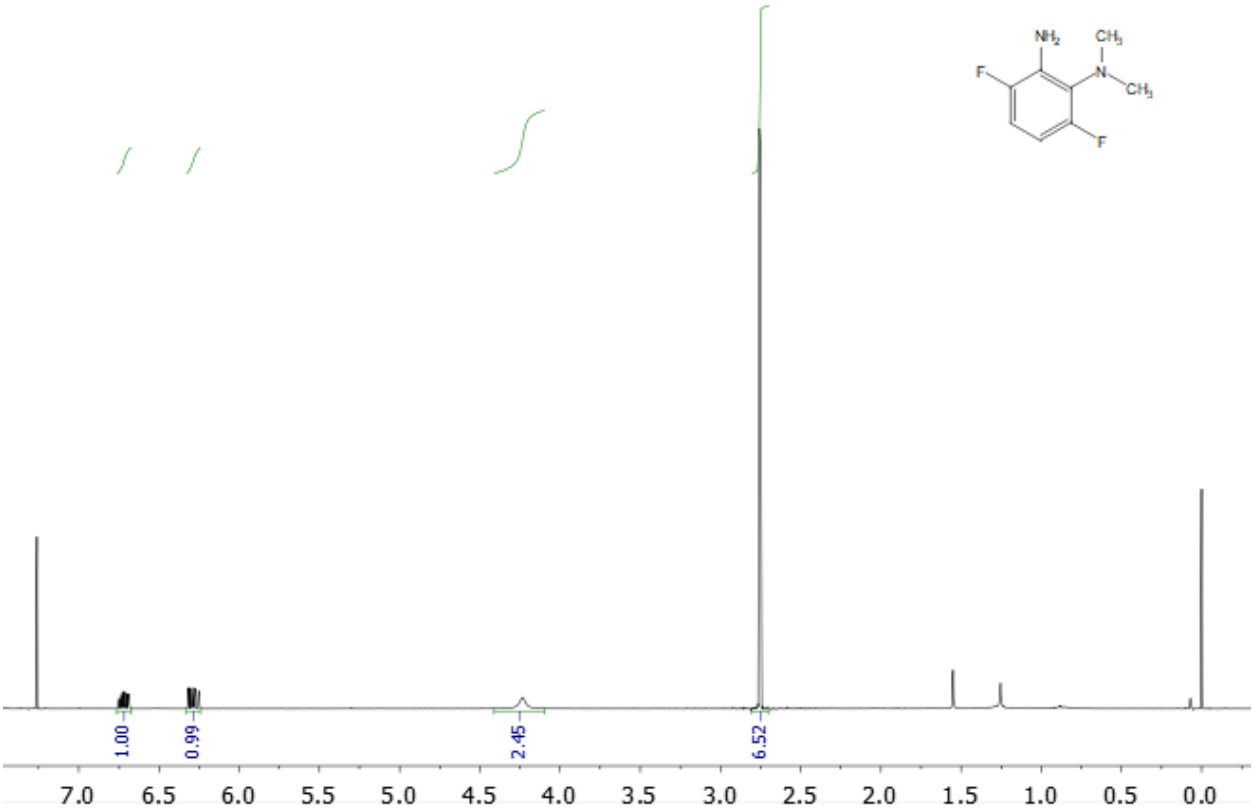

Figure 3.31: ^{1}H NMR spectrum ($CDCl_3$, 400 MHz) of column-purified 2-dimethylamino-3,6-difluoroaniline (**2e**), δ 6.72 (CH), 6.28 (CH), 4.23 (NH_2), 2.75 (NMe_2). Also present is $CHCl_3$ (7.26 ppm).

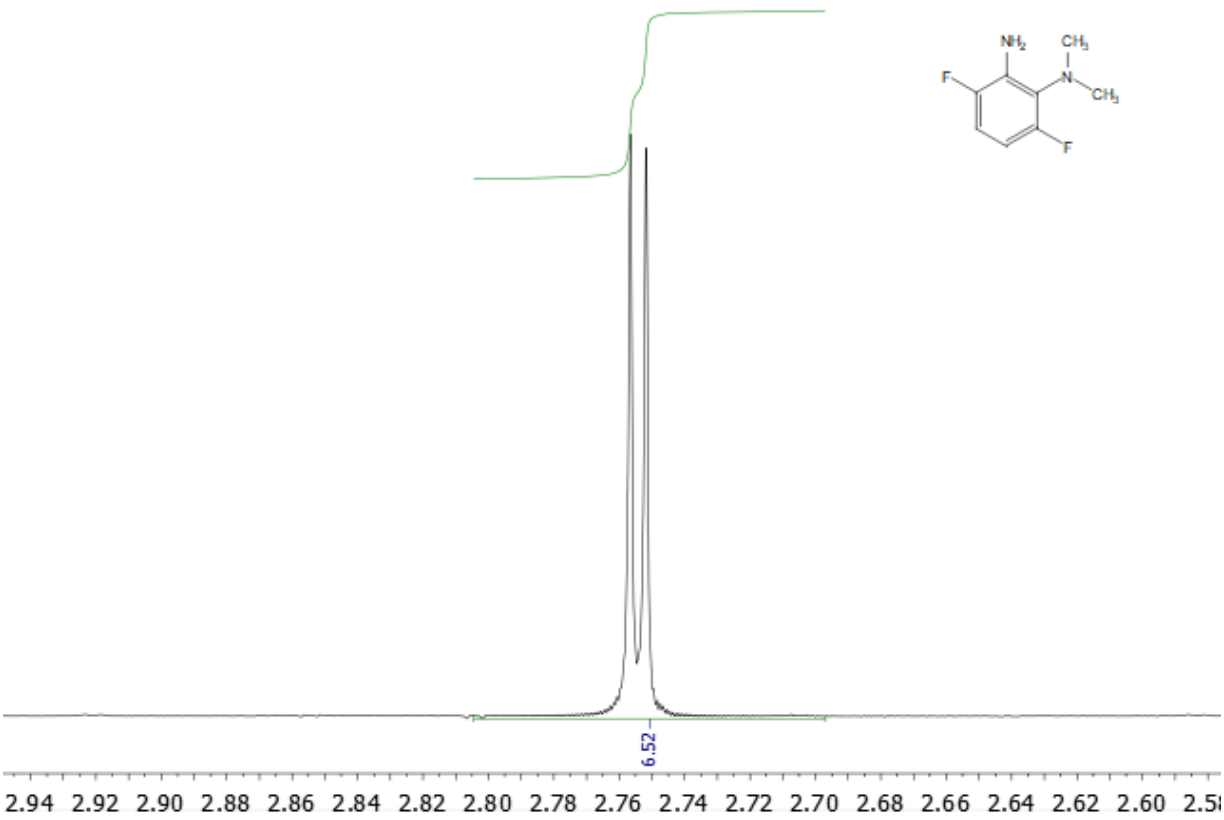

Figure 3.32: ^{1}H NMR spectrum ($CDCl_3$, 400 MHz), of purified 2-dimethylamino-3,6-difluoroaniline (**2e**). Expansion shows NMe_2 group.

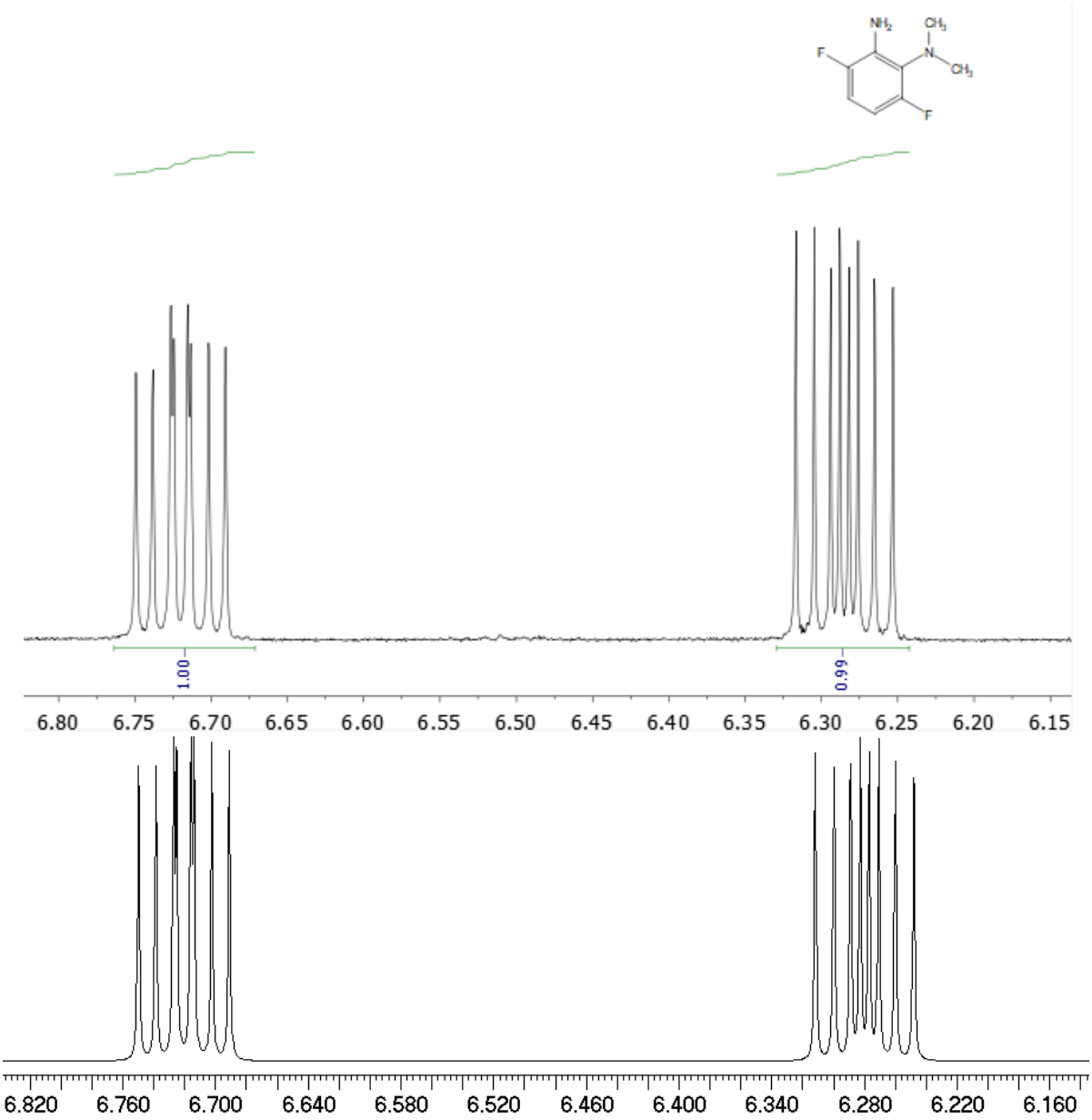

Figure 3.33: ^{1}H NMR spectra ($CDCl_3$, 400 MHz, expansion) of aromatic region of 2-dimethylamino-3,6-difluoroaniline (**2e**). **Upper**: Experimental spectrum. **Lower**: Simulated; a natural linewidth of 0.5 Hz was estimated.

6-Dimethylamino-2,3-difluoroaniline

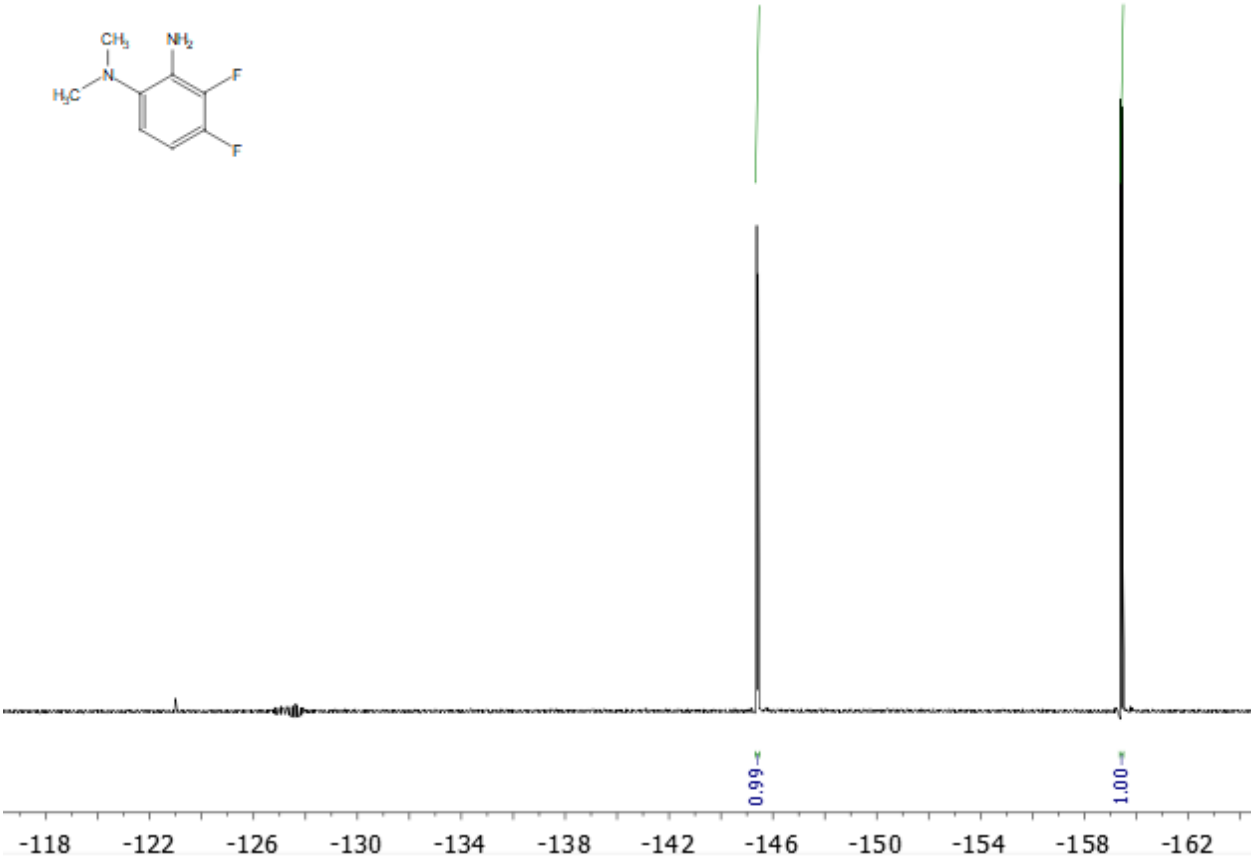

Figure 3.34: ^{19}F NMR spectrum ($CDCl_3$, 376 MHz) of column-purified 6-dimethylamino-2,3-difluoroaniline **(*iso*-2e)**. A polynomial baseline correction was applied to the frequency-domain spectrum.

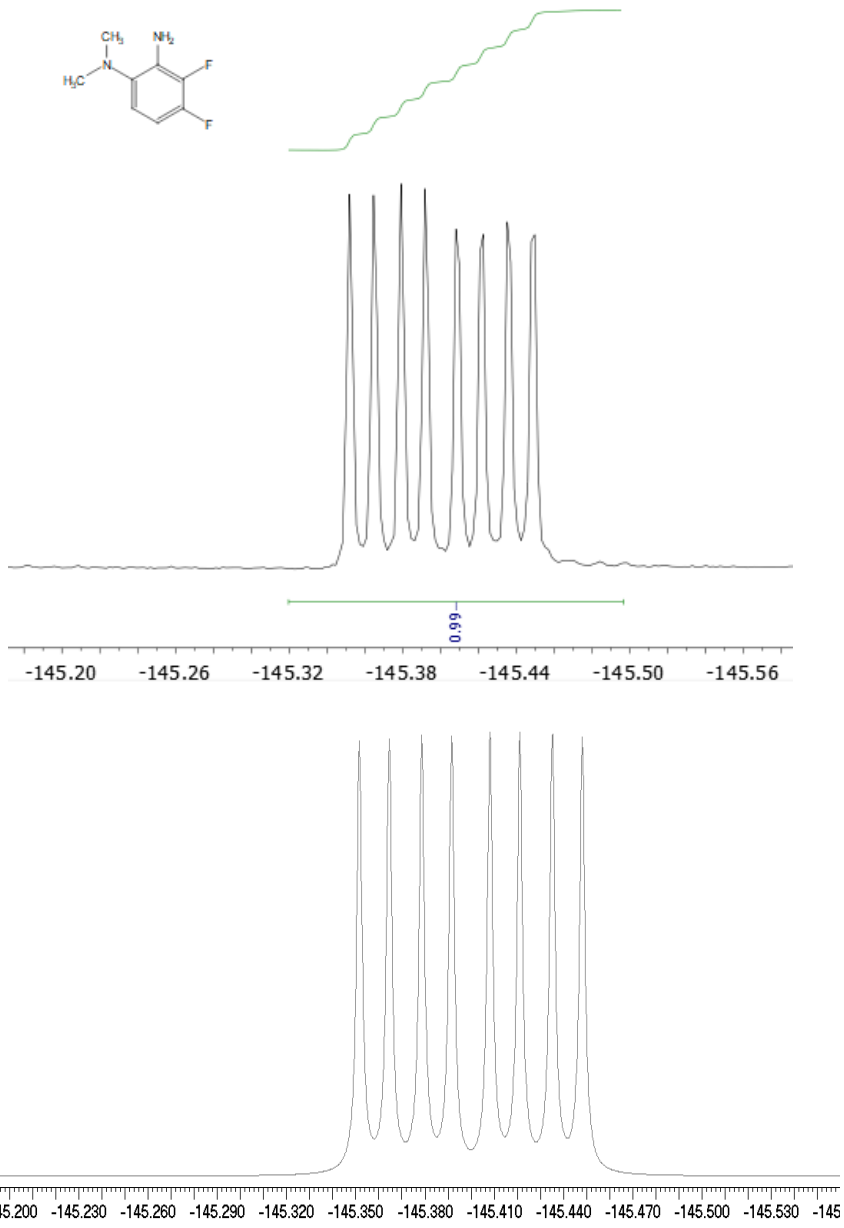

Figure 3.35: ^{19}F NMR spectra ($CDCl_3$, 376 MHz, expansion) of −145.4 ppm peak of 6-dimethylamino-2,3-difluoroaniline ***(iso*-2e)**. **Upper**: Experimental spectrum with polynomial baseline correction applied. **Lower**: Simulated (A natural linewidth of 1.5 Hz was estimated.)

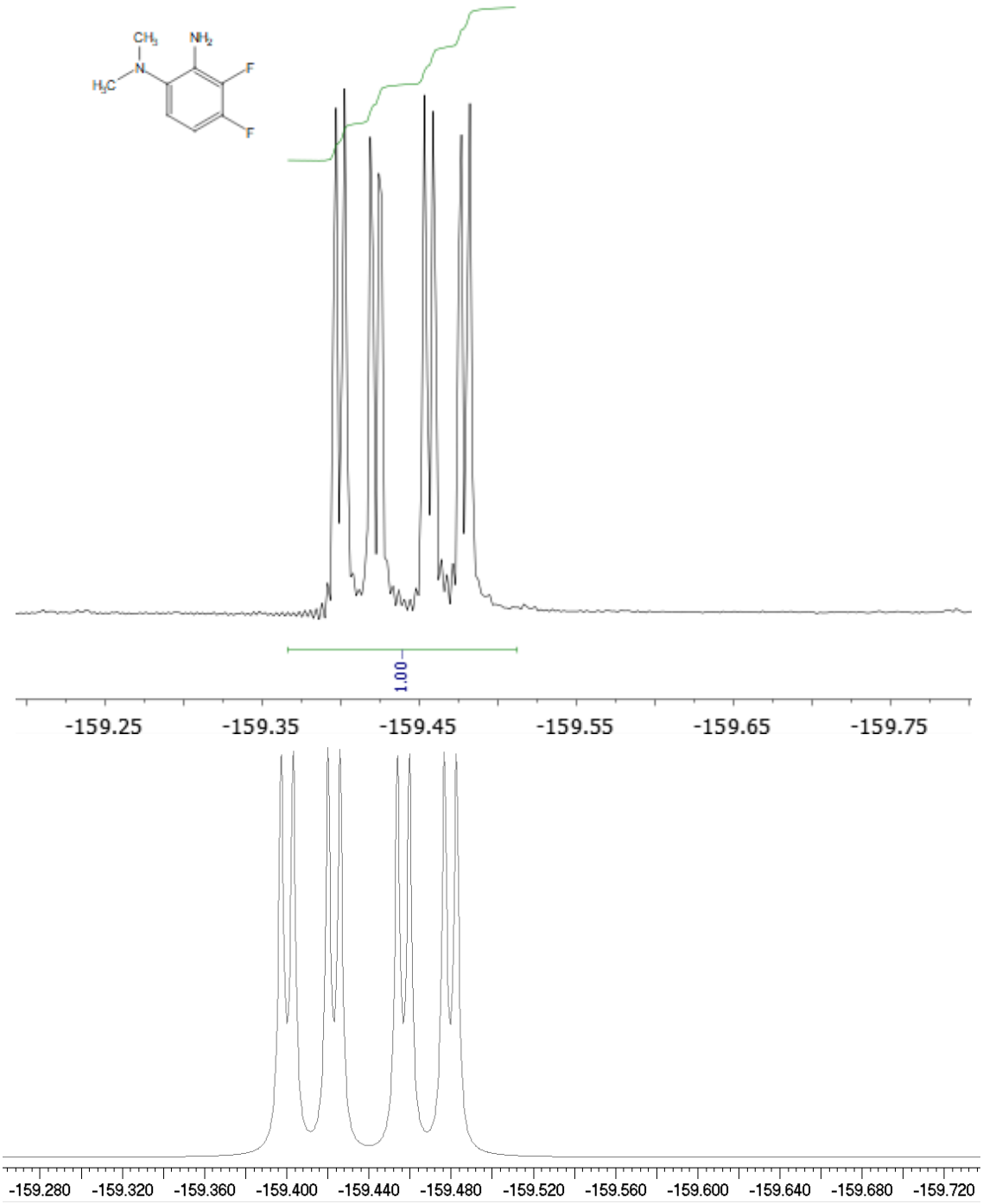

Figure 3.36: ^{19}F NMR spectra ($CDCl_3$, 376 MHz, expansion) of −159.4 ppm peak of 6-dimethylamino-2,3-difluoroaniline ***(iso*-2e)**. **Upper**: Experimental spectrum with polynomial baseline correction applied. **Lower**: Simulated (a natural linewidth of 1.5 Hz was estimated.)

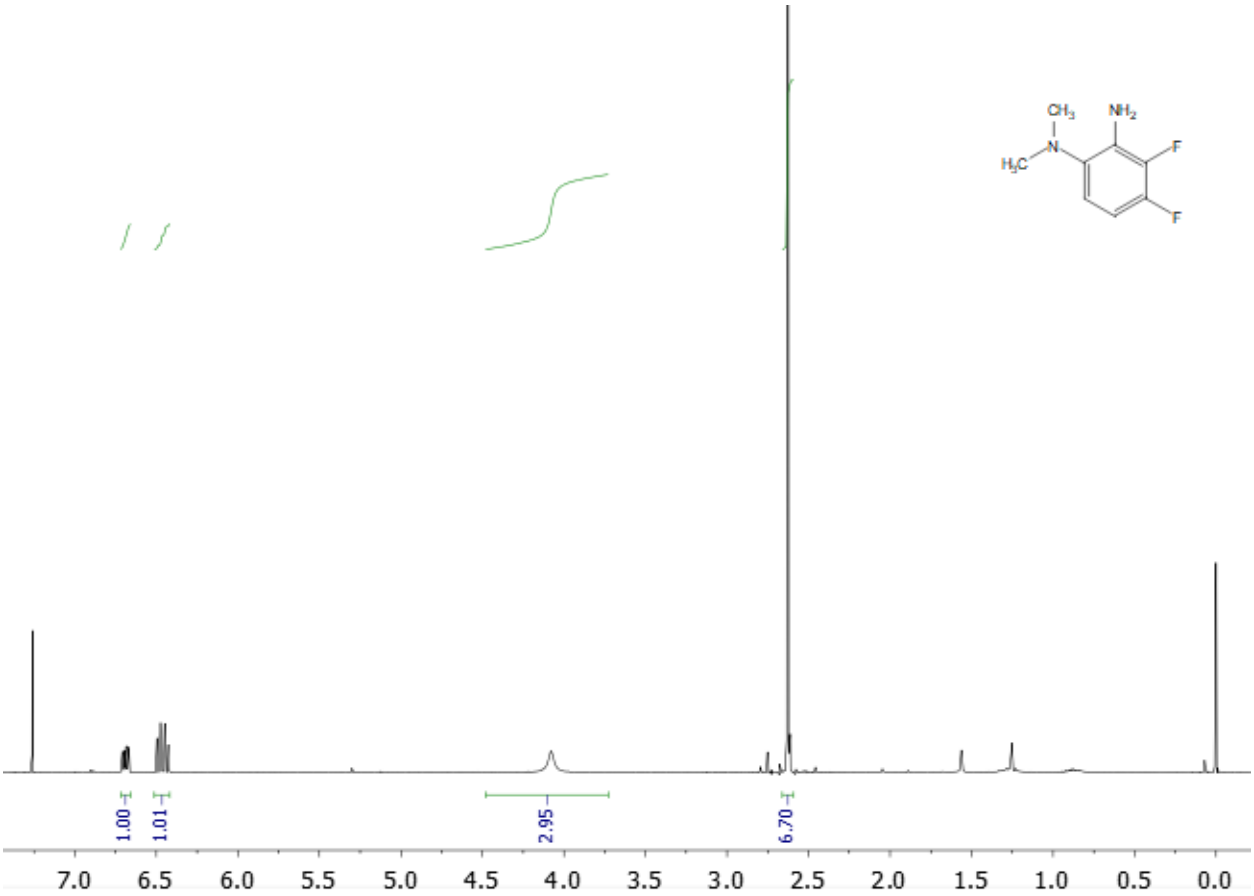

Figure 3.37: ^{1}H NMR spectrum ($CDCl_3$, 400 MHz) of column-purified 6-dimethylamino-2,3-fluoroaniline ***(iso*-2e)**, δ 6.69 (CH), 6.46 (CH), 4.08 (NH_2), 2.63 (NMe_2). Also present is $CHCl_3$ (7.26 ppm). Sample is referenced to TMS (0.00 ppm).

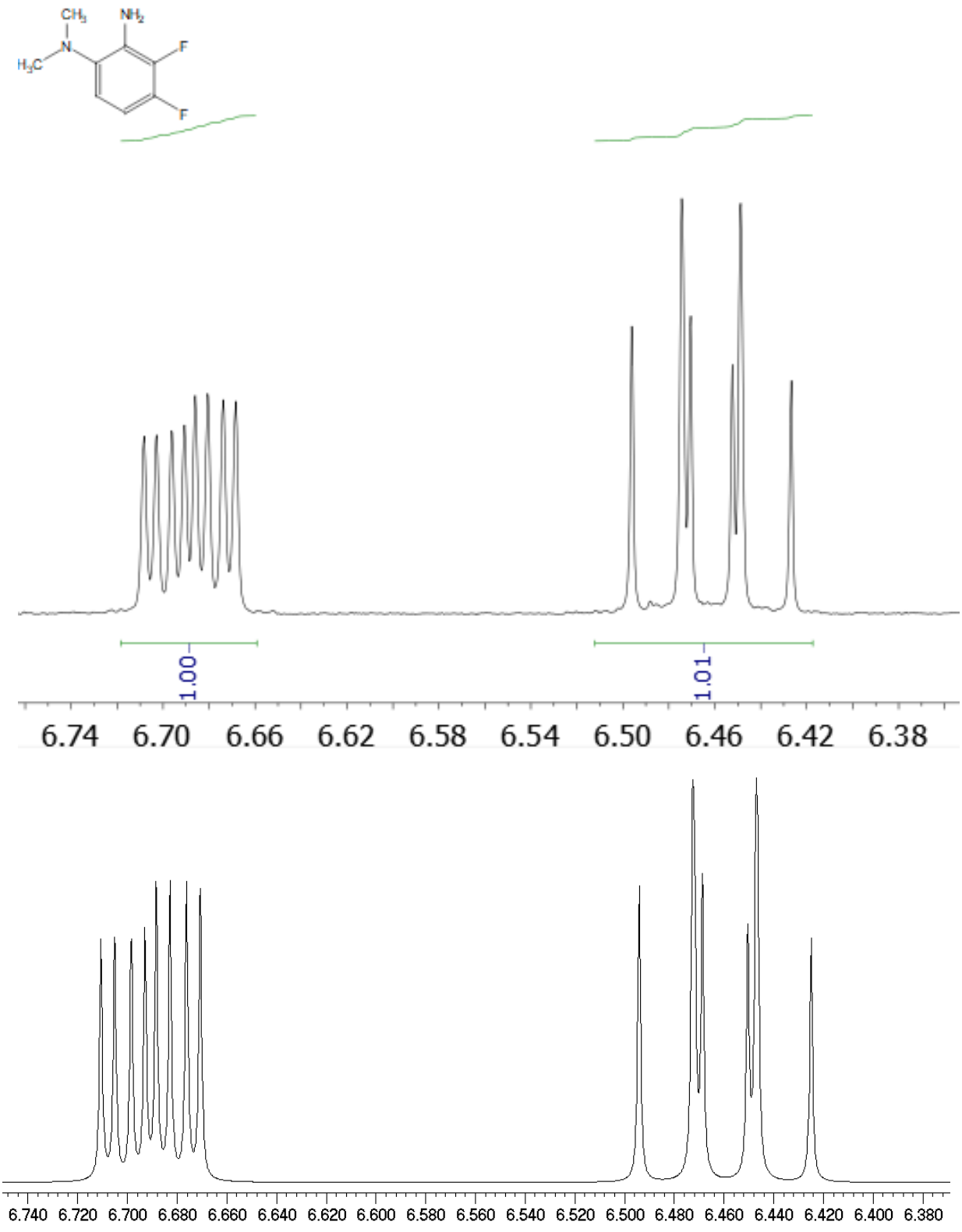

Figure 3.38: ^{1}H NMR spectra ($CDCl_3$, 400 MHz, expansion) of aromatic region of 6-dimethylamino-2,3-difluoroaniline **(*iso*-2e)**. **Upper**: Experimental spectrum. **Lower**: Simulated; a natural linewidth of 0.5 Hz was estimated.

2,6-Bis(dimethylamino)-3-fluoroaniline

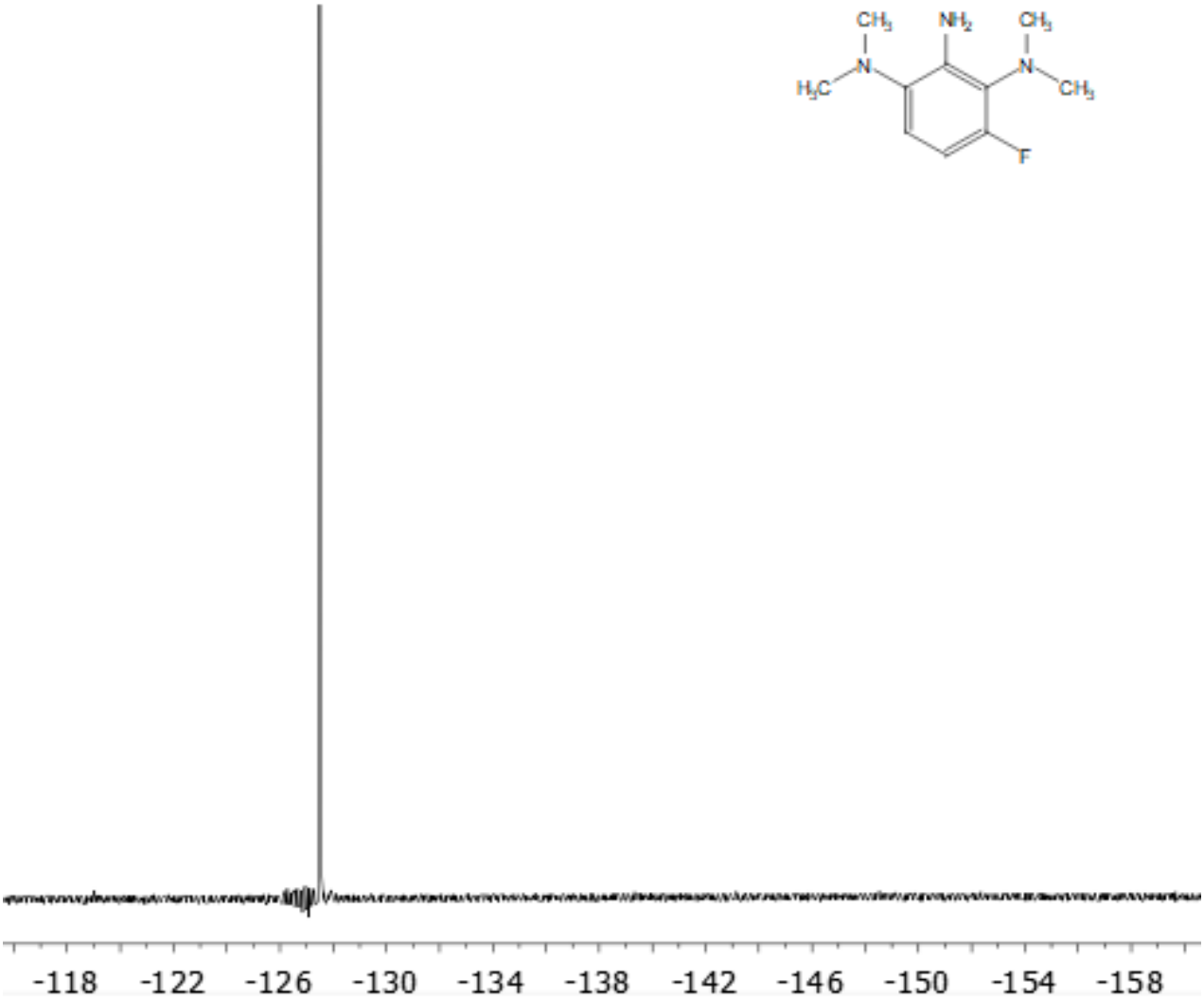

Figure 3.39: ^{19}F NMR spectrum ($CDCl_3$, 376 MHz) of column-purified 2,6-bis(dimethylamino)-3-fluoroaniline (**3e**). This compound was isolated from the mixture shown in Figure 3.27. A polynomial baseline correction was applied to the frequency-domain spectrum. The feature in the baseline at −127 ppm is an FT artifact.

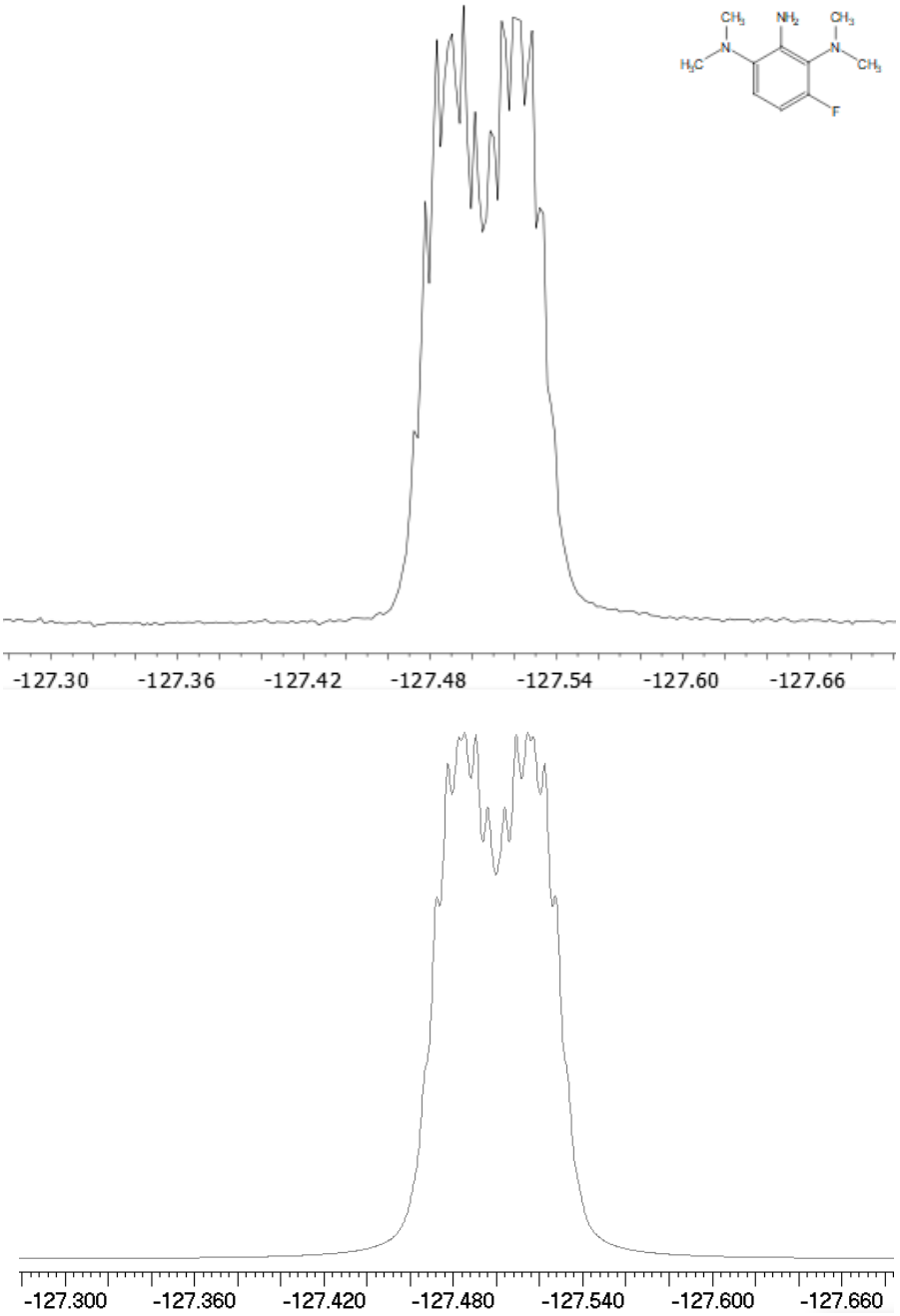

Figure 3.40: ^{19}F NMR spectra ($CDCl_3$, 376 MHz, expansion) of 2,6-bis(dimethylamino)-3-fluoroaniline (**3e**). **Upper**: Experimental spectrum with polynomial baseline correction applied. **Lower**: Simulated (a natural linewidth of 2.0 Hz was estimated.)

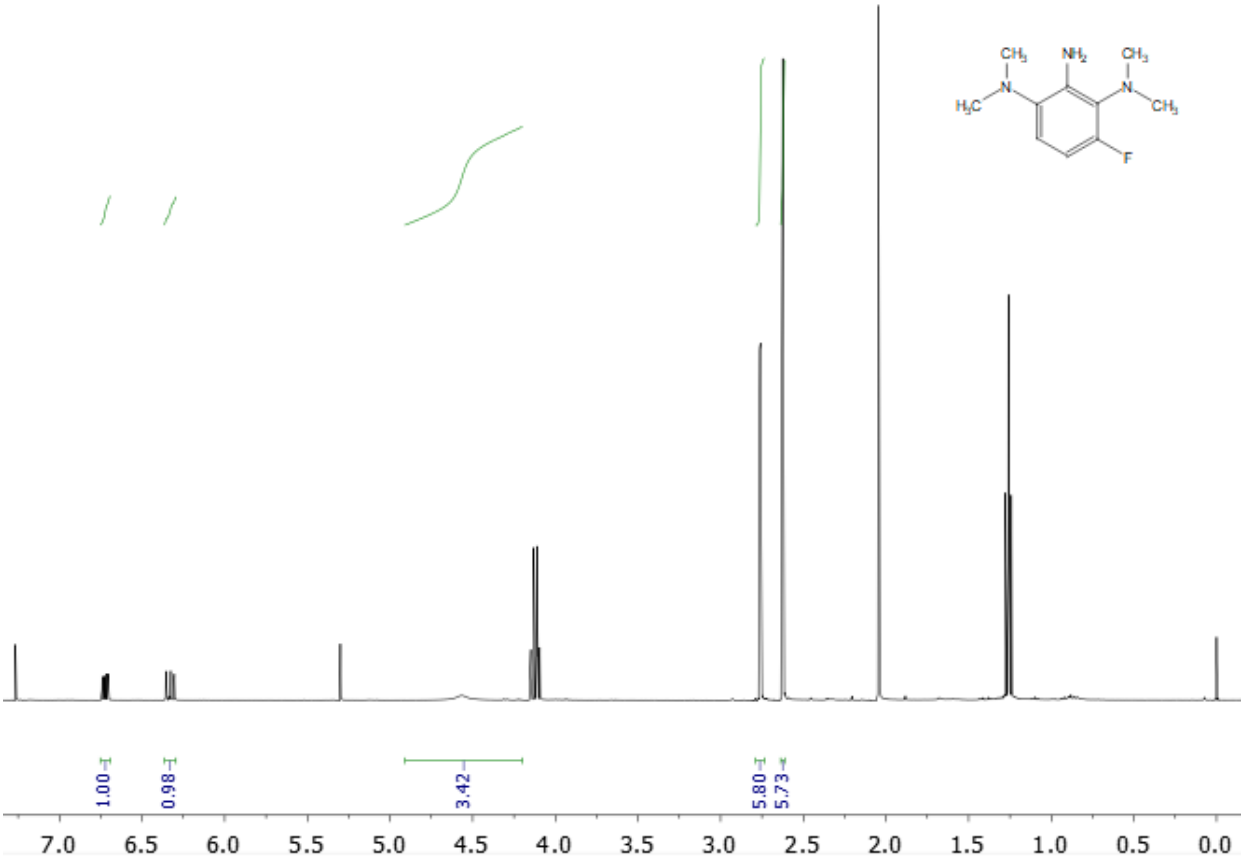

Figure 3.41: ^{1}H NMR spectrum ($CDCl_3$, 400 MHz) of column-purified 2,6-bis(dimethylamino)-3-fluoroaniline (**3e**), δ 6.72 (CH), 6.33 (CH), 4.56 (NH_2), 2.76 (NMe_2), 2.62 (NMe_2). Dichloromethane (5.30 ppm), $CHCl_3$ (7.26 ppm), and ethyl acetate (4.12 ppm, 2.05 ppm, and 1.26 ppm) are also present.

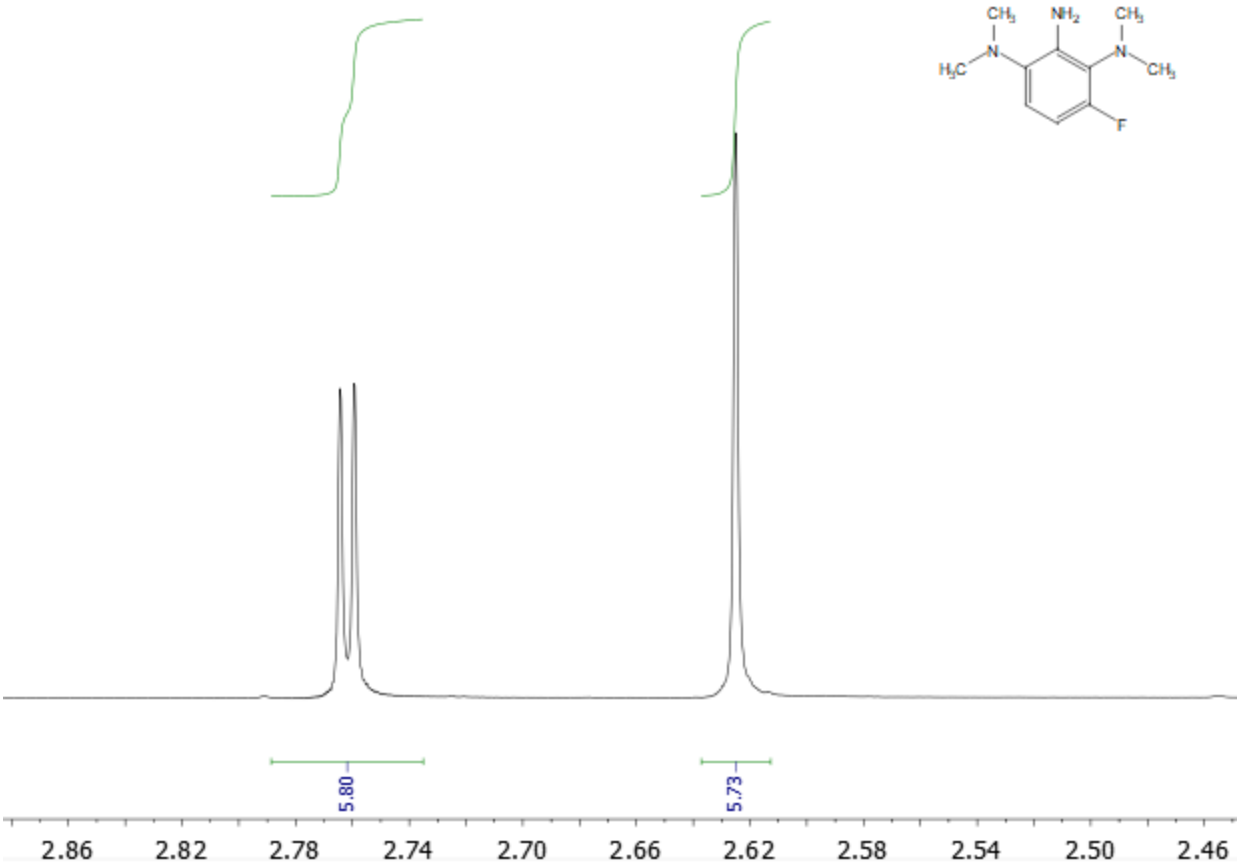

Figure 3.42: ^{1}H NMR spectrum ($CDCl_3$, 400 MHz) of column-purified 2,6- bis(dimethylamino)-3-fluoroaniline (**3e**). This expansion shows the two NMe_2 groups. The downfield doublet corresponds to the NMe_2 group in the 2 position (relative to NH_2); this assignment is based on observation of coupling to the 3-fluorine.

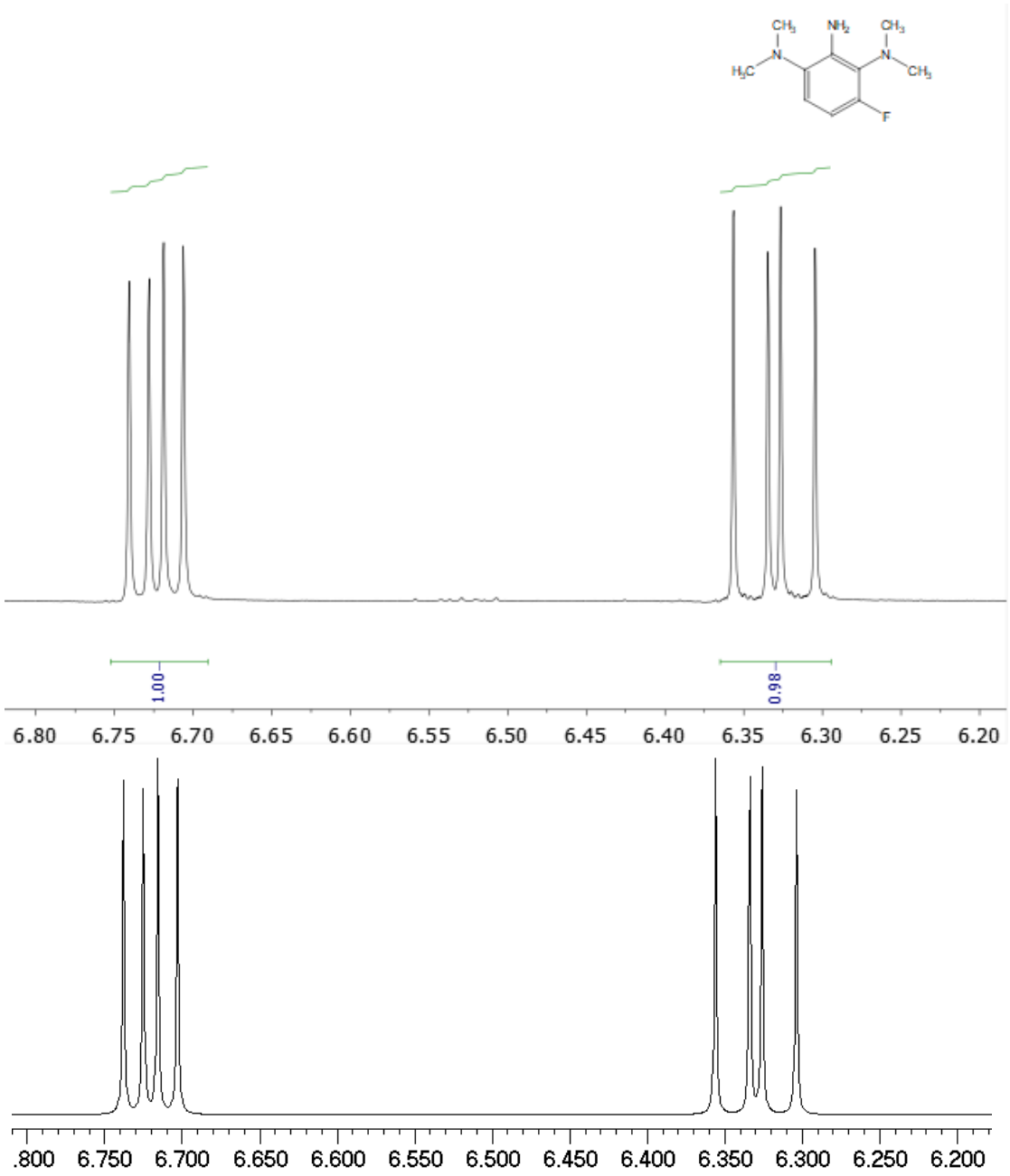

Figure 3.43: ^{1}H NMR spectra ($CDCl_3$, 400 MHz, expansion) of aromatic region of 2,6-bis(dimethylamino)-3-fluoroaniline (**3e**). **Upper**: Experimental spectrum. **Lower**: Simulated; a natural linewidth of 0.5 Hz was estimated.

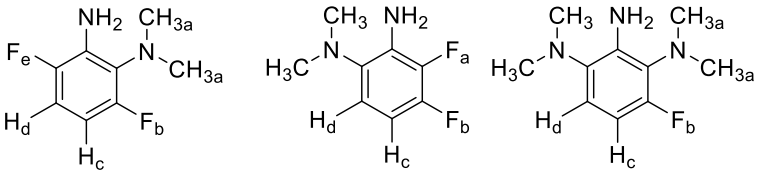

2e ***iso*-2e** **3e**

Figure 3.44: Structures of 2-dimethylamino-3,6-difluoroaniline **(2e)**, 6-dimethylamino-2,3-difluoroaniline ***(iso*-2e),** and 2,6-bis(dimethylamino)-3-fluoroaniline **(3e)**, labeled for simulations (Tables 3.5-3.7).

Table 3.5: Peak assignments for **2e** used to generate the simulated spectra shown in Figures 3.38 through 3.33.

		Coupling Constants (Hz)				
Nucleus	Chemical Shift (ppm)	a	b	c	d	e
a (NMe_2)	2.75					
b (F)	−128.3	2.0				
c (H)	6.28	0.0	11.6			
d (H)	6.72	0.0	4.5	9.1		
e (F)	-139.8	0.0	15.2	4.8	9.9	
NH_2	4.23					

Table 3.6: Peak assignments for ***iso*-2e** used to generate the simulated spectra shown in Figures 3.34 through 3.38.

		Coupling Constants (Hz)				
Nucleus	Chemical Shift (ppm)	a	b	c	d	e
a (F)	−159.7					
b (F)	−145.4	21.0				
c (H)	6.46	8.6	10.2			
d (H)	6.69	2.2	4.9	8.9		
e (NMe_2)	2.63	0.0	0.0	0.0	0.0	
NH_2	4.08					

Table 3.7: Peak assignments for **3e** used to generate the simulated spectra shown in Figures 3.39 through 3.43.

		Coupling Constants (Hz)				
Nucleus	Chemical Shift (ppm)	a	b	c	d	e
a (NMe_2)	2.76					
b (F)	−128.5	2.0				
c (H)	6.33	0.0	12.0			
d (H)	6.72	0.0	5.1	8.9		
e (NMe_2)	2.62	0.0	0.0	0.0	0.0	
NH_2	4.56					

2-Dimethylamino-3,4-difluoroaniline

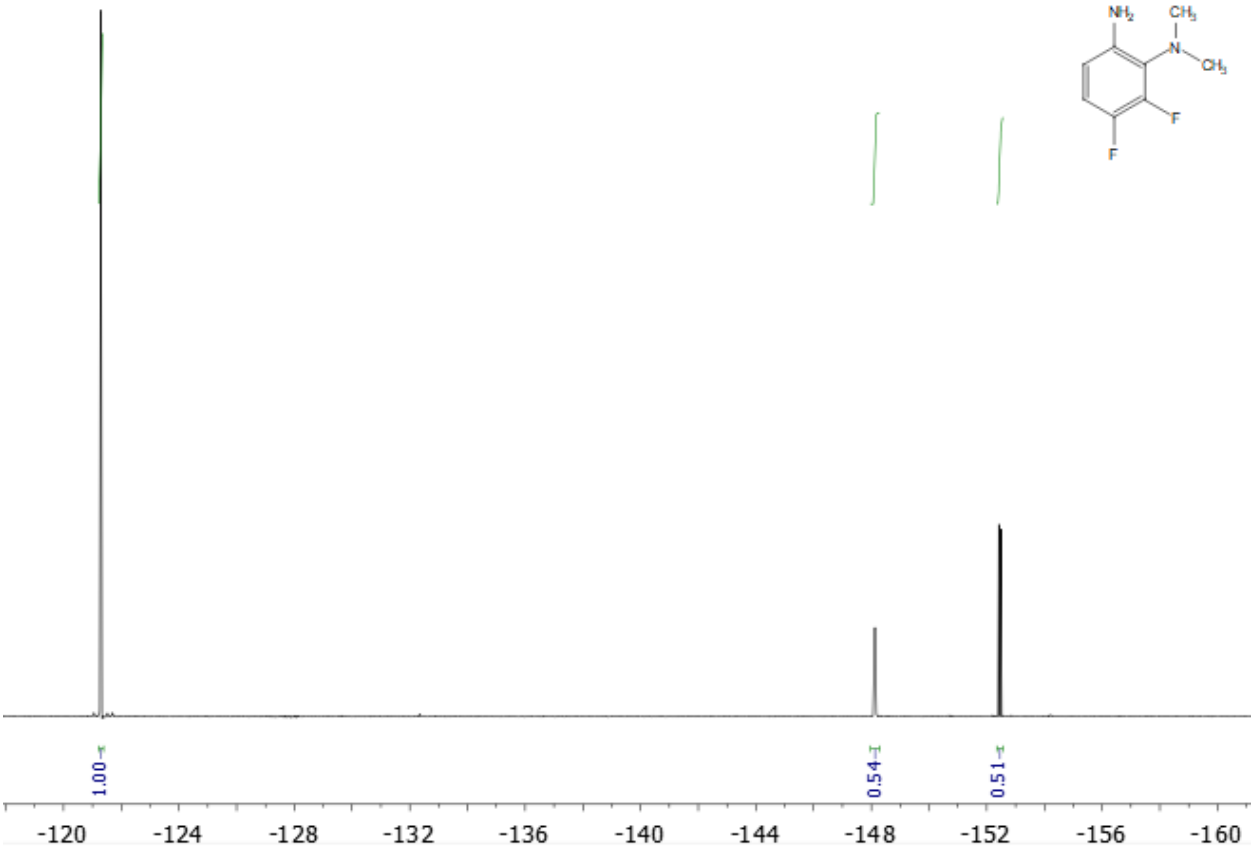

Figure 3.45: ^{19}F NMR spectrum ($CDCl_3$, 376 MHz) of <u>crude</u> 2-dimethylamino-3,4-difluoroaniline (**2f**) (present at −148.1 ppm and –152.4 ppm). Also present is bis(4-fluorophenyl) ether at −121.3 ppm.

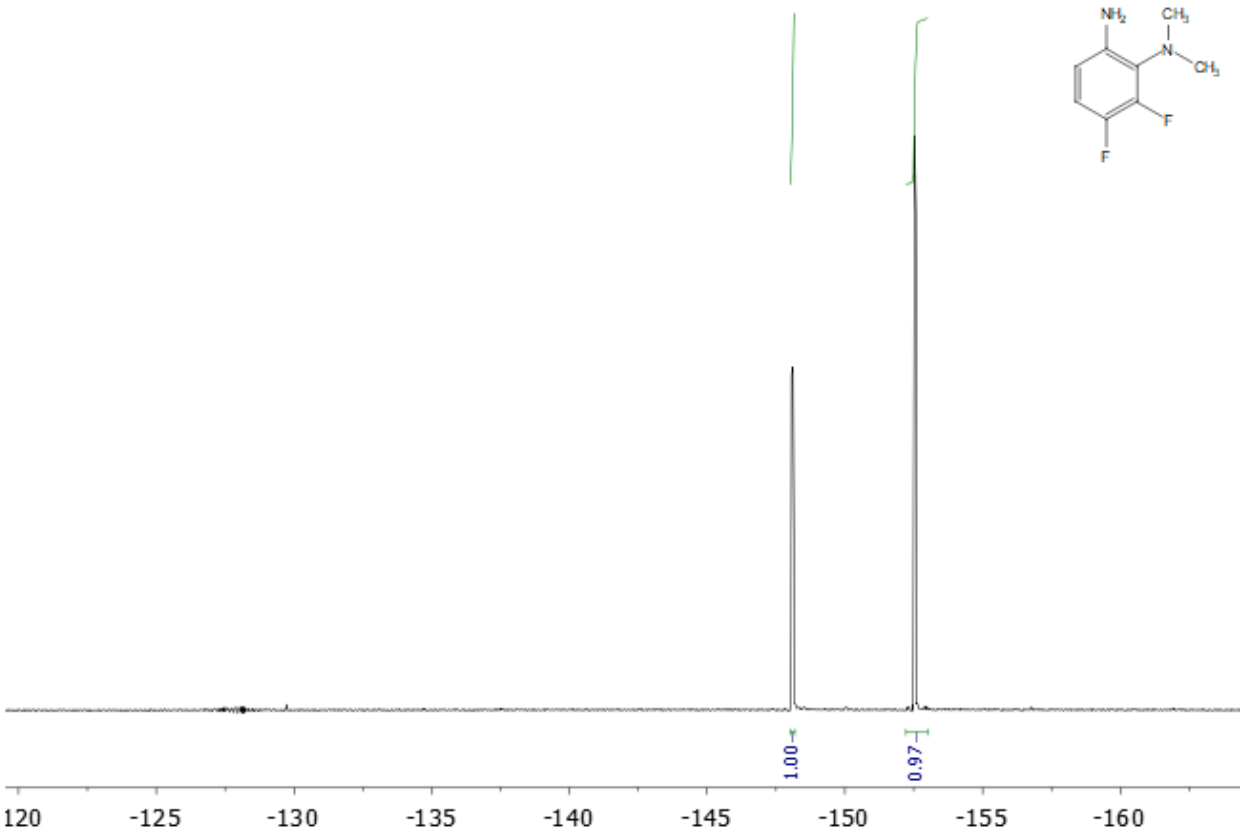

Figure 3.46: ^{19}F NMR spectrum ($CDCl_3$, 376 MHz) of column-purified 2-dimethylamino-3,4-difluoroaniline (**2f**). Line-broadening apodization (0.5 Hz) was applied to the FID and a polynomial baseline correction was applied to the frequency-domain spectrum.

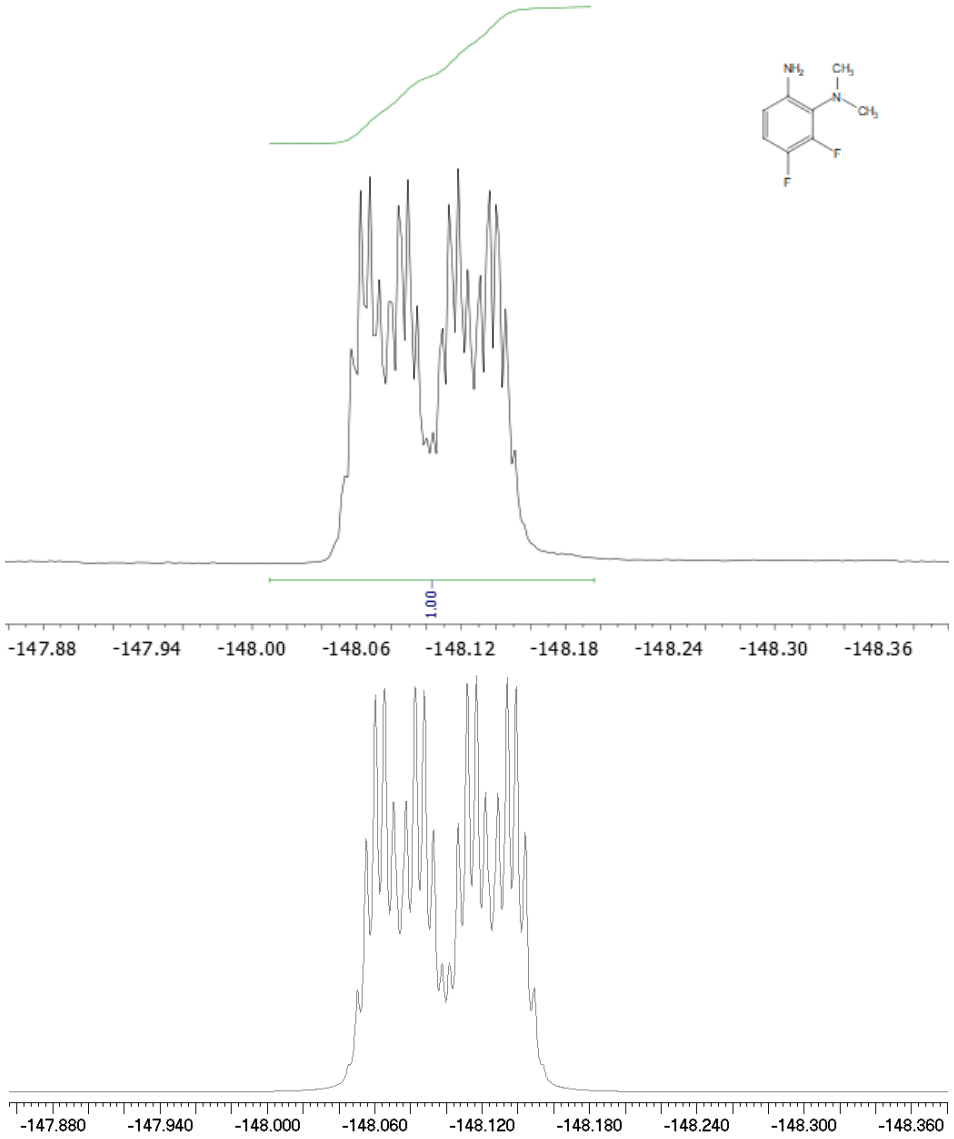

Figure 3.47: ^{19}F NMR spectra ($CDCl_3$, 376 MHz, expansion) of the downfield peak of 2-dimethylamino-3,4-difluoroaniline (**2f**) at −148.1 ppm. **Upper**: Experimental spectrum with polynomial baseline correction and 0.5 Hz of line broadening applied. **Lower**: Simulated: A natural linewidth of 1.0 Hz was estimated.

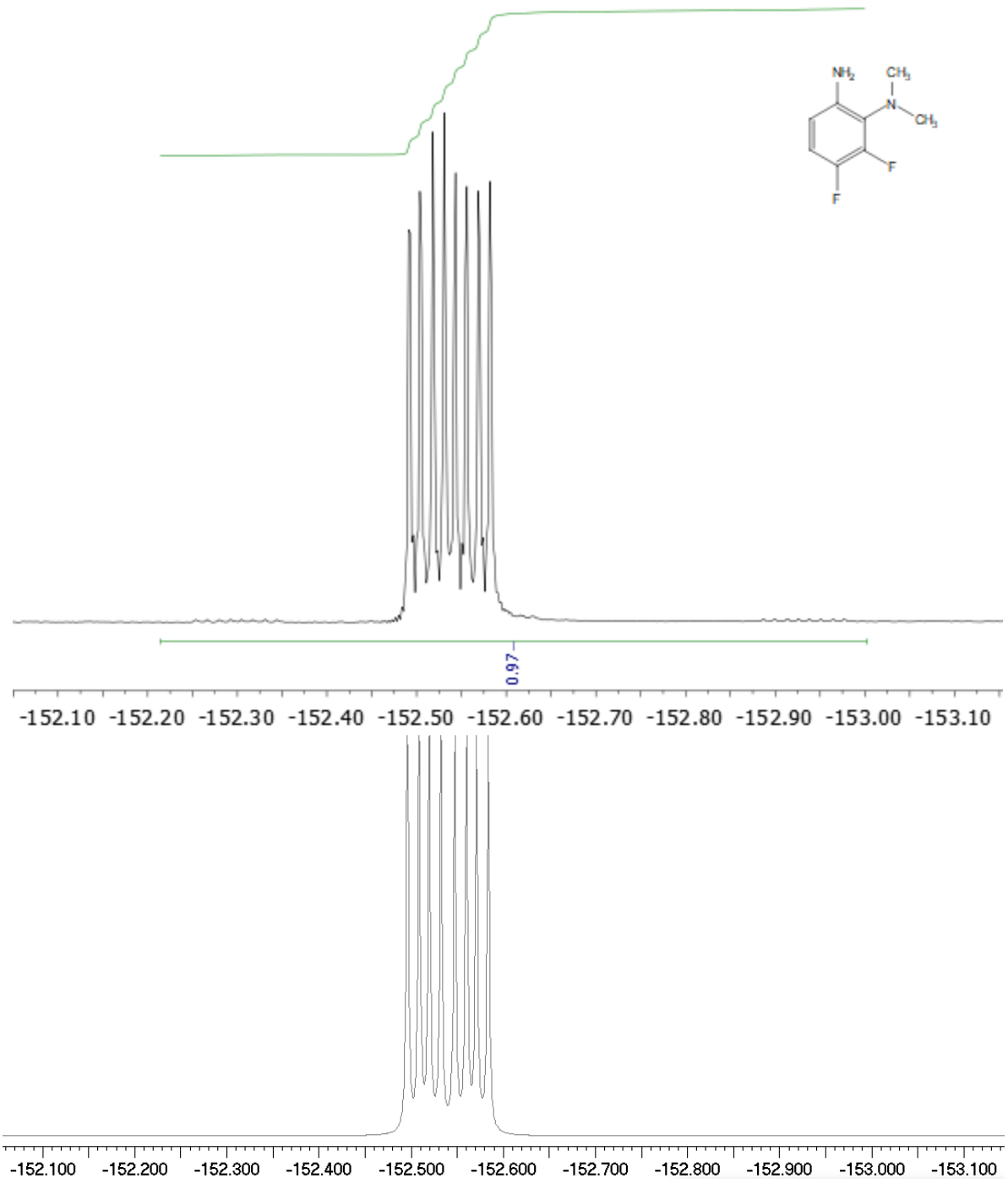

Figure 3.48: ^{19}F NMR spectra ($CDCl_3$, 376 MHz, expansion) of the upfield peak of 2-dimethylamino-3,4-difluoroaniline (**2f**) at −152.5 ppm. **Upper**: Experimental spectrum with polynomial baseline correction and 0.5 Hz of line broadening applied. **Lower**: Simulated: A natural linewidth of 1.0 Hz was estimated.

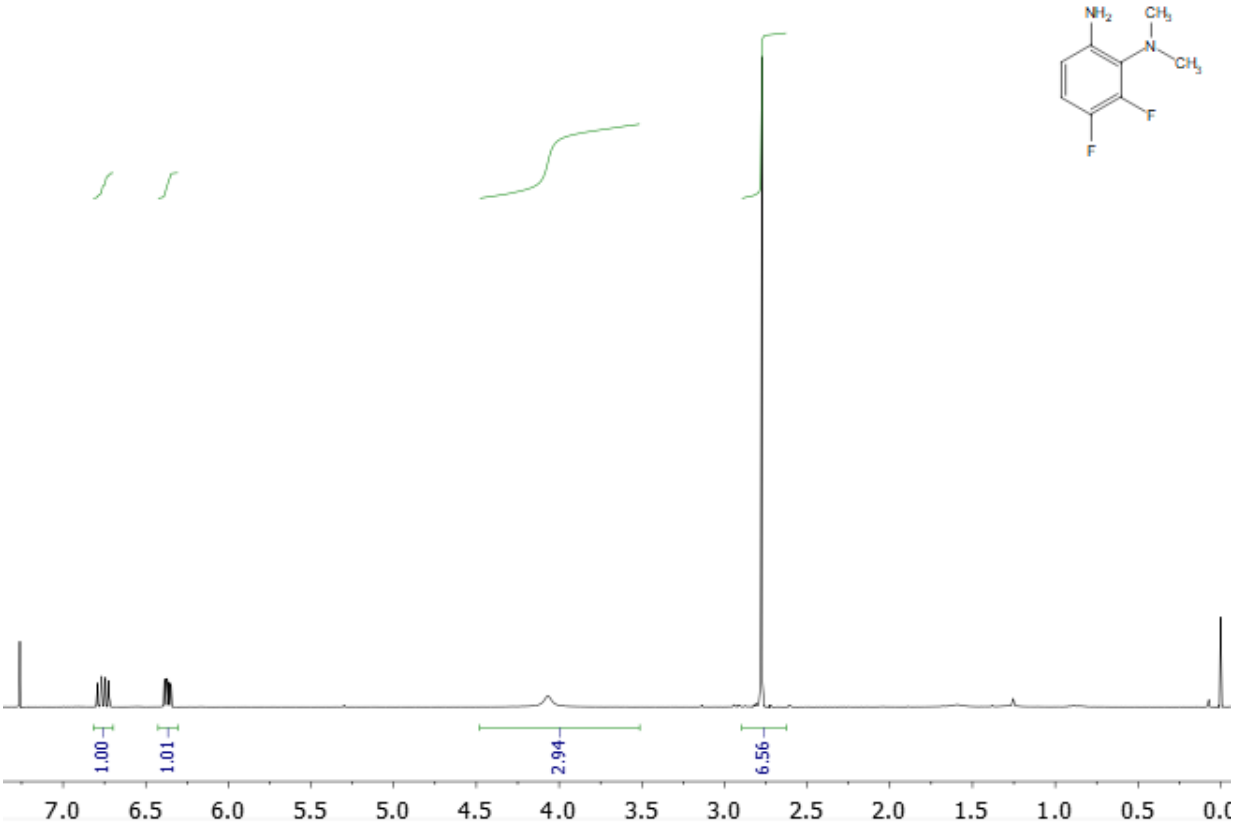

Figure 3.49: ^{1}H NMR spectrum ($CDCl_3$, 400 MHz) of column-purified 2-dimethylamino-3,4-difluoroaniline (**2f**), δ 6.76 (CH), 6.37 (CH), 4.07 (NH_2), 2.78 (NMe_2). $CHCl_3$ is also present (7.26 ppm). Sample is referenced to TMS (0.00 ppm).

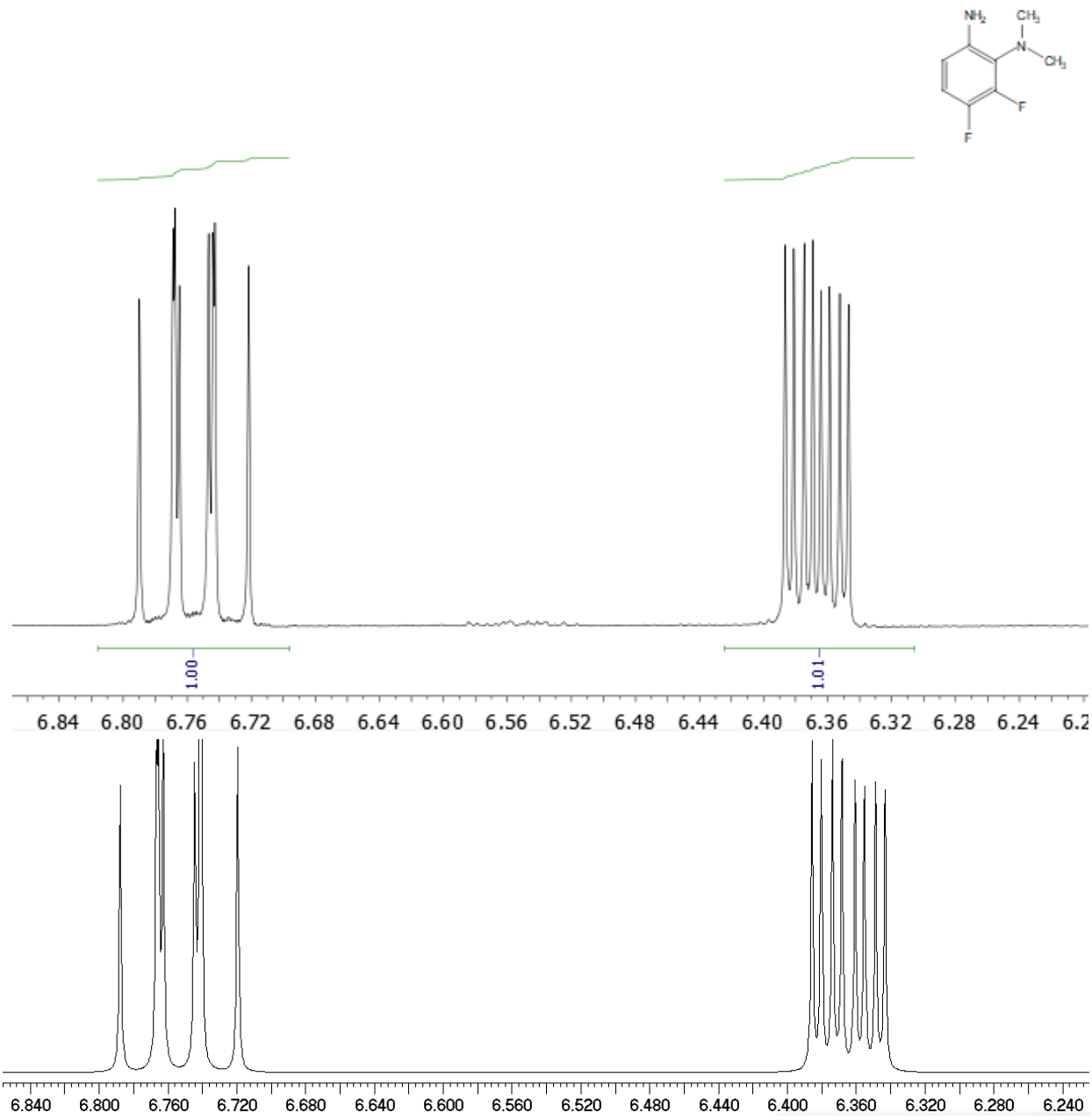

Figure 3.50: ^{1}H NMR spectra ($CDCl_3$, 400 MHz, expansion) of aromatic region of 2-dimethylamino-3,4-difluoroaniline (**2f**). **Upper**: Experimental spectrum. **Lower**: Simulated; a natural linewidth of 0.5 Hz was estimated.

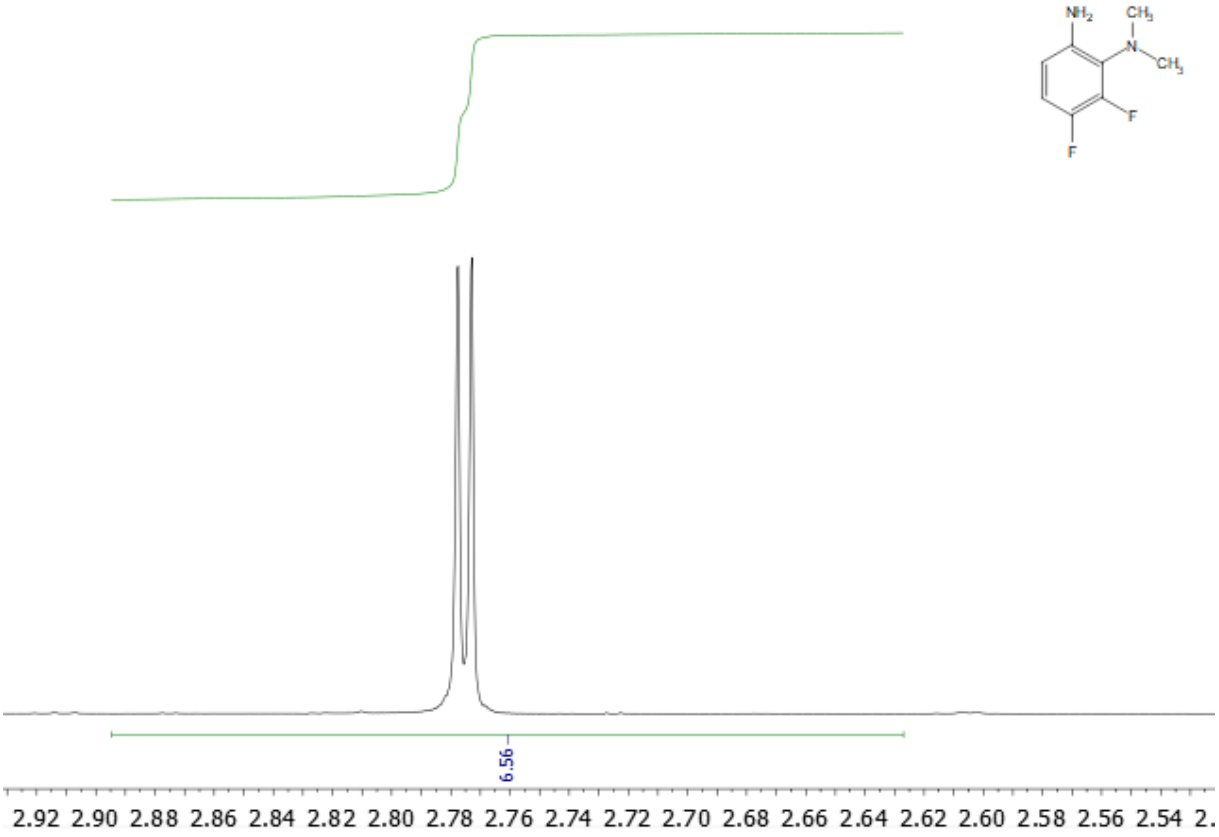

Figure 3.51: ^{1}H NMR spectrum ($CDCl_3$, 400 MHz), NMe_2 signal of column-purified 2-dimethylamino-3,4-difluoroaniline (**2f**) showing coupling to the 3-fluorine.

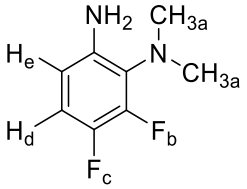

Figure 3.52: Structure of 2-dimethylamino-3,4-difluoroaniline (**2f**) showing nuclei labeled for the simulation described in Table 3.8.

Table 3.8: Chemical shifts and coupling constants for 2-dimethylamino-3,4-difluoroaniline used to generate the simulated spectra shown in Figures 3.45 through 3.51.

		Coupling Constants (Hz)				
Nucleus	Chemical Shift (ppm)	a	b	c	d	e
a (NMe_2)	2.78					
b (F)	−148.1	1.85				
c (F)	−152.4	0.0	19.0			
d (H)	6.76	0.0	8.4	8.9		
e (H)	6.37	0.0	1.9	4.8		
NH_2	4.07					

2-Dimethylamino-4,5-difluoroaniline

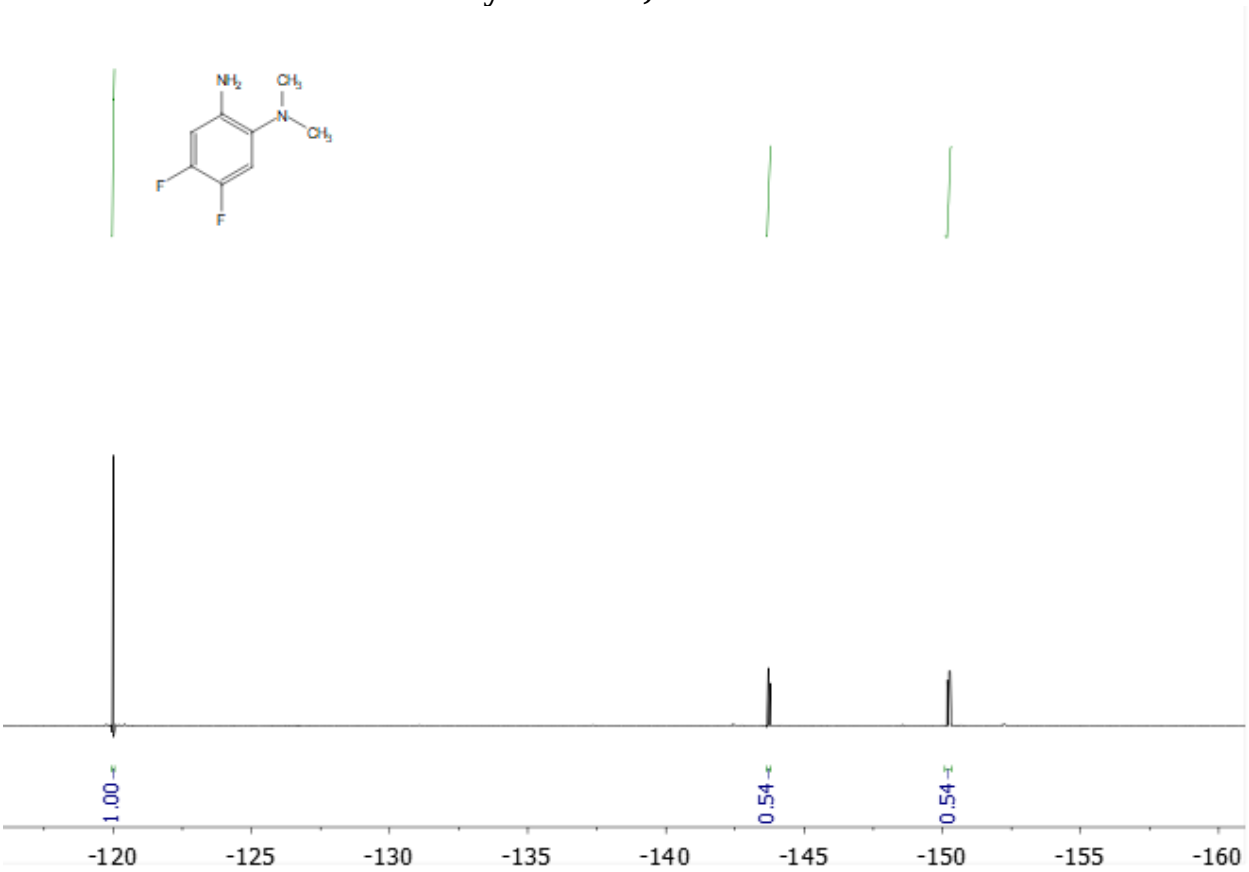

Figure 3.53: ^{19}F NMR spectrum ($CDCl_3$, 376 MHz) of <u>crude</u> 2-dimethylamino-4,5-difluoroaniline **(2g)** (present at −145.0 ppm and −151.5 ppm). Bis(4-fluorophenyl)ether is present at −121.3 ppm.

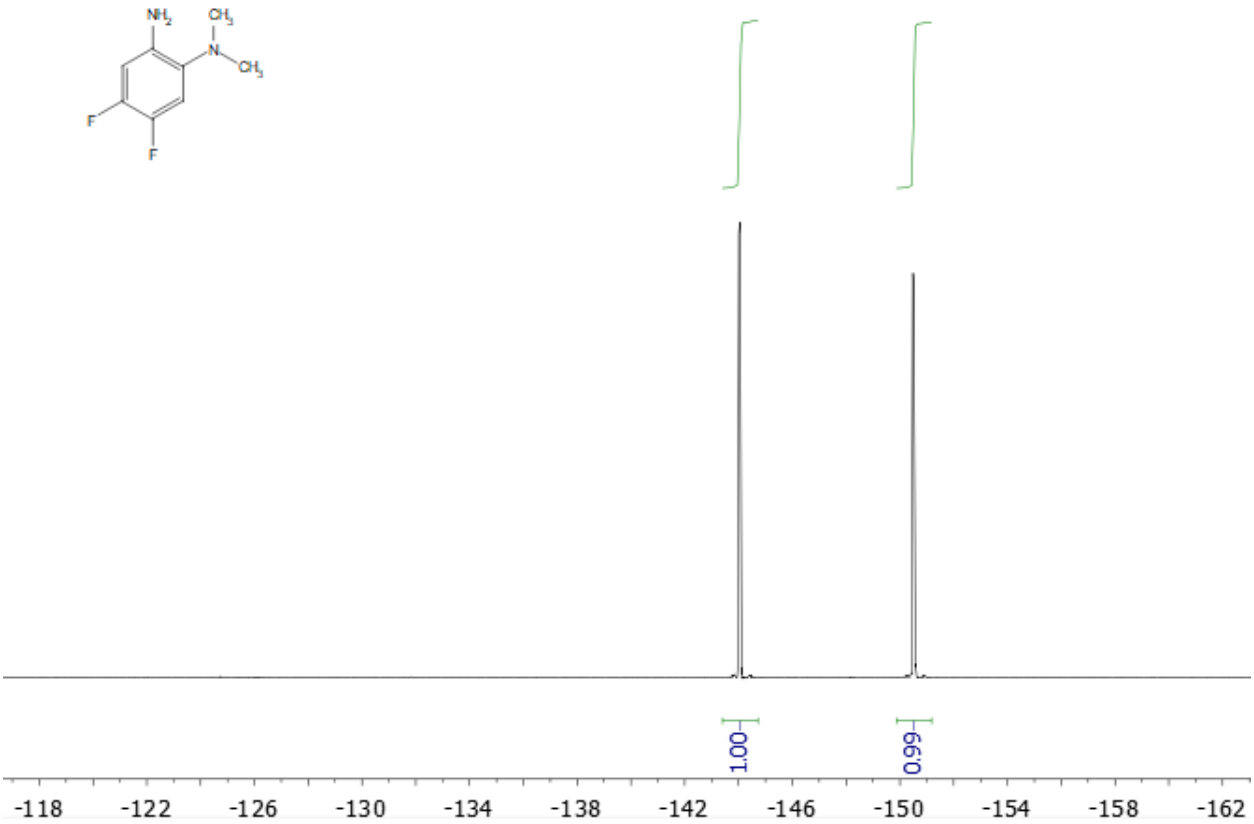

Figure 3.54: ^{19}F NMR spectrum ($CDCl_3$, 376 MHz) of column-purified 2-dimethylamino-4,5-difluoroaniline **(2g)**.

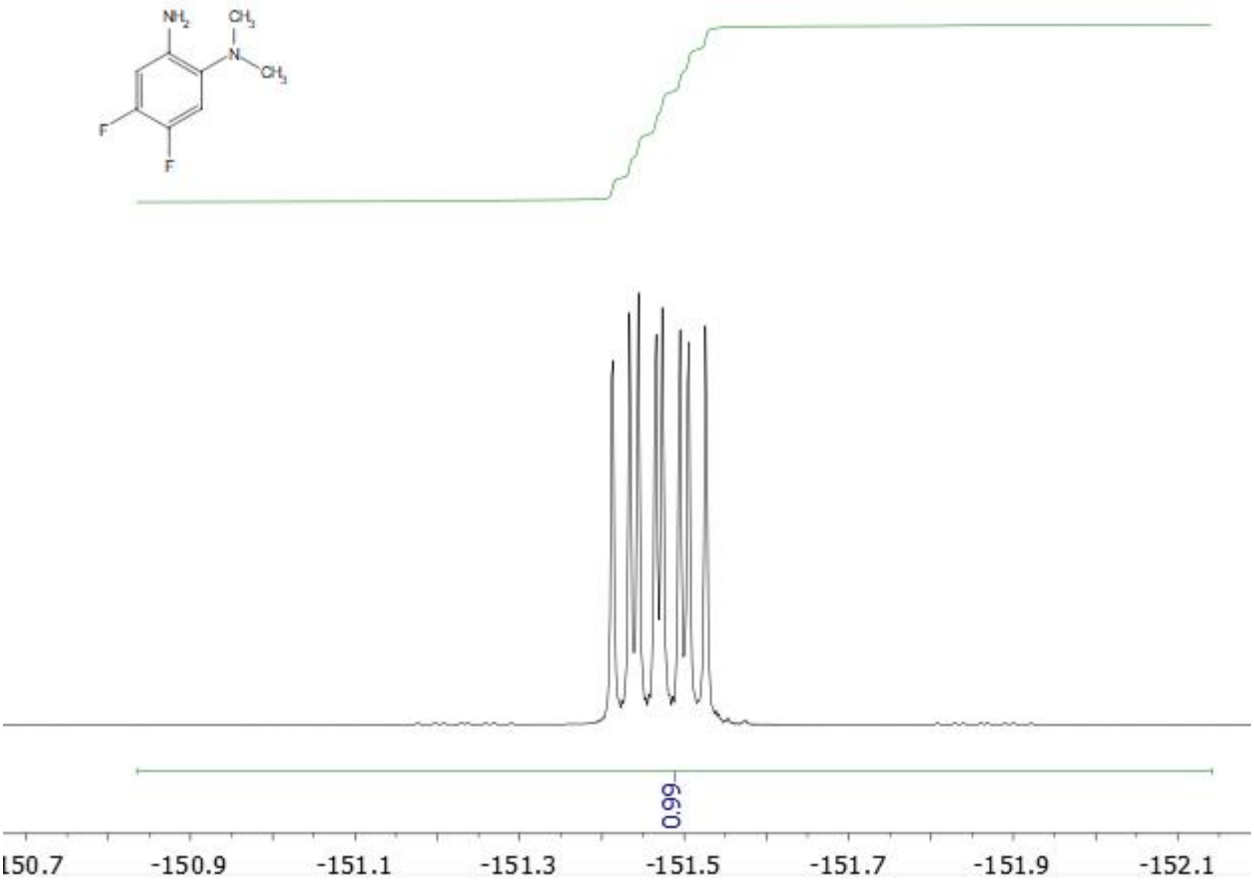

Figure 3.55: ^{19}F NMR spectrum ($CDCl_3$, 376 MHz) of purified 2-dimethylamino-4,5-difluoroaniline **(2g)**, expansion of upfield signal. Simulation was not needed because the spectrum shows simple first-order ddd splitting.

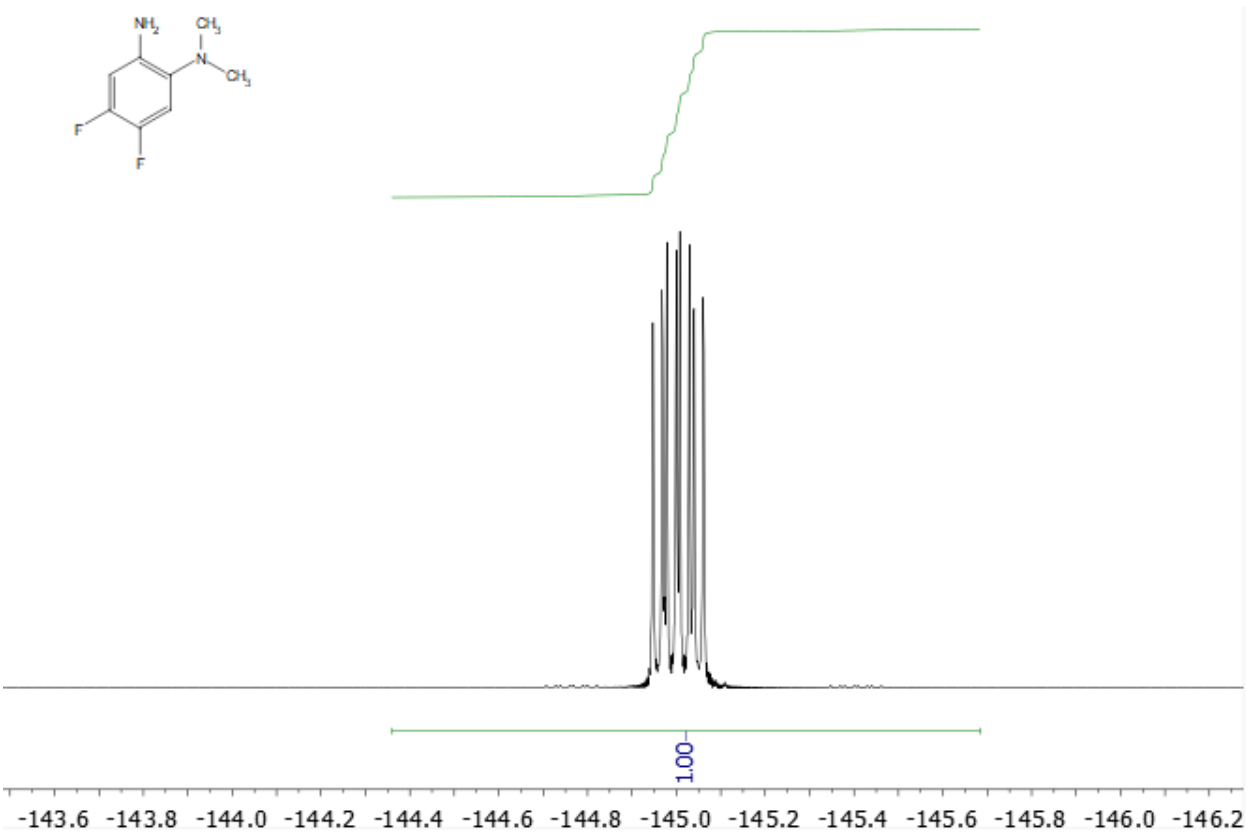

Figure 3.56: ^{19}F NMR spectrum ($CDCl_3$, 376 MHz) of purified 2-dimethylamino-4,5-difluoroaniline **(2g)**, expansion of upfield signal. Simulation was not needed because the spectrum shows simple first-order ddd splitting.

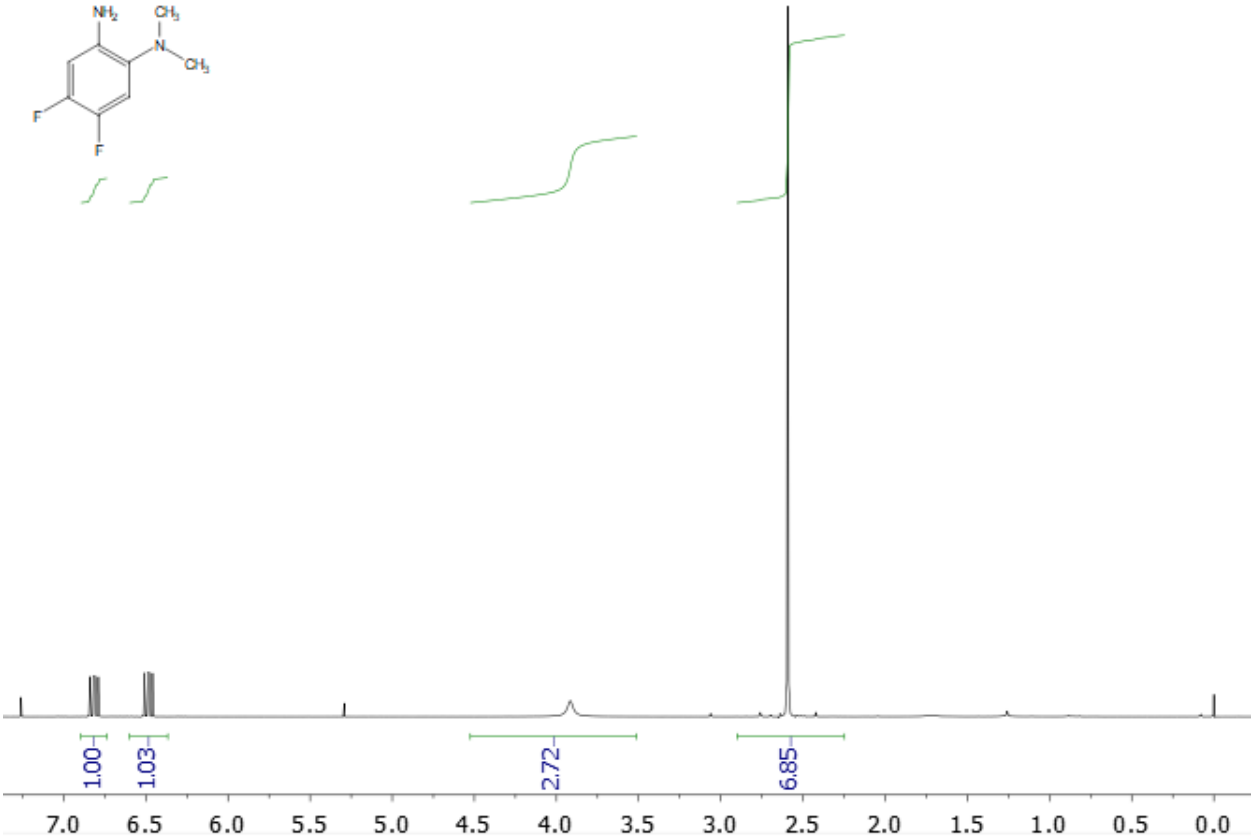

Figure 3.57: ^{1}H NMR spectrum ($CDCl_3$, 400 MHz) of column-purified 2-dimethylamino-4,5-difluoroaniline **(2g)**, δ 6.81 (CH), 6.48 (CH), 3.92 (NH_2), 2.59 (NMe_2). Also present are dichloromethane (5.29 ppm) and $CHCl_3$ (7.26 ppm).

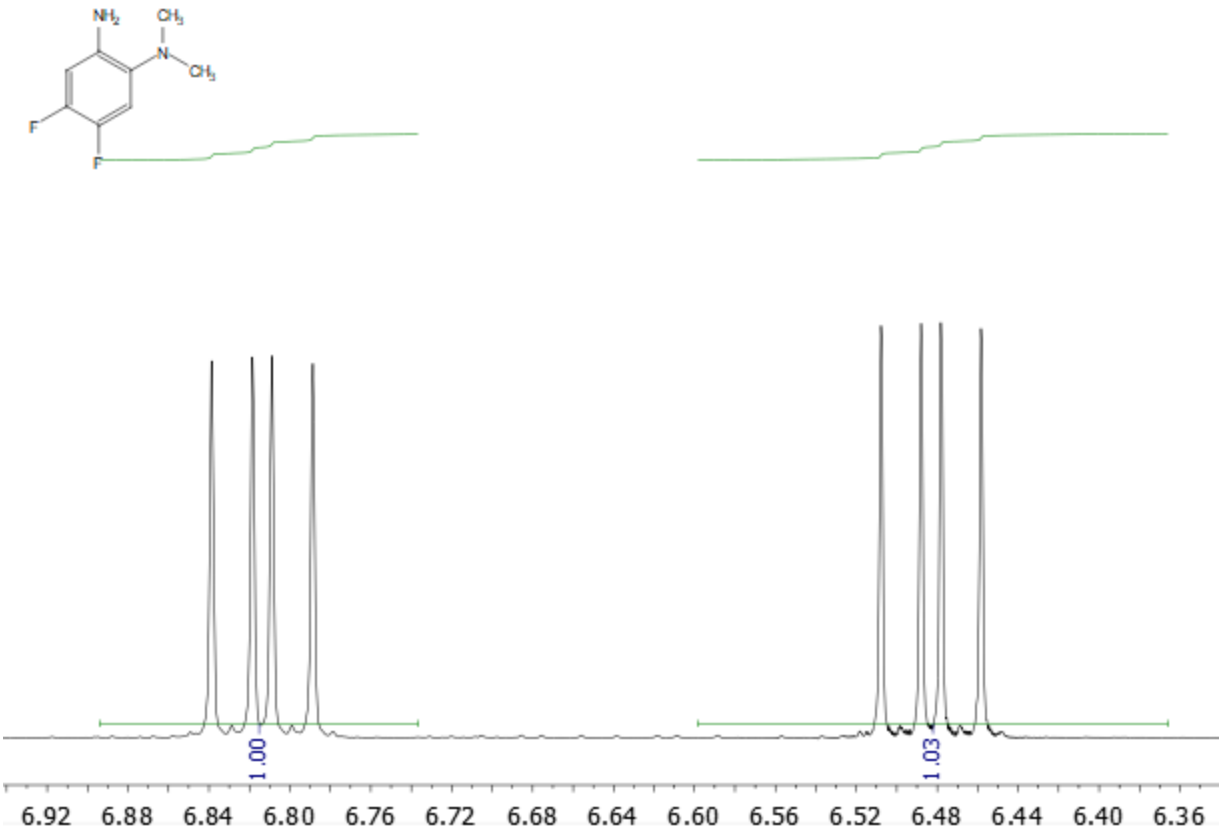

Figure 3.58: ^{1}H NMR spectrum ($CDCl_3$, 400 MHz), aromatic region of purified 2-dimethylamino-4,5-difluoroaniline **(2g)**. Simulation was not needed because these spin systems are simple first-order dd.

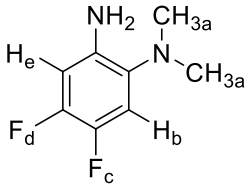

Figure 3.59: Structure of 2-dimethylamino-4,5-difluoroaniline **(2g)** showing nuclei labeled for the simulation described in Table 3.9.

Table 3.9: Peak assignments and coupling constants based on experimental spectra shown in Figures 3.53 through 3.58.						
		Coupling Constants (Hz)				
Nucleus	Chemical Shift (ppm)	a	b	c	d	e
a (NMe_2)	2.59					
b(e) (H)	6.48	0.0				
c(d) (F)	−145.0	0.0	11.9			
d(c) (F)	−151.5	0.0	8.3	23.0		
e(b) (H)	6.81	0.0	0.0	7.9	12.0	
NH_2	3.92					

Note that our model cannot assign the chemical shifts of H_b vs H_e or F_c vs F_d. However the *relative* nuclear positions are well established by the observed coupling constants. Since these spectra display simple dd patterns, we saw no purpose in subjecting the spectra to computational modeling. The large J_{FF} signal is consistent with vicinal F-F coupling, while no H-H coupling is observed, which is only consistent with the structure shown.

2-Dimethylamino-3,4,6-trifluoroaniline, 2,6-Bis(dimethylamino)-3,4-difluoroaniline, and 6-Dimethylamino-2,3,4-trifluoroaniline

These compounds were considered as a group because they arise from a common substrate. A mixture of the first two compounds was obtained by reaction of 2,3,4,6-tetrafluoroaniline with $Ti(NMe_2)_4$ at 120 °C for 23 h. A mixture of the second and third compounds was obtained by reaction at 90 °C for 3 h (please see Figure3.75).

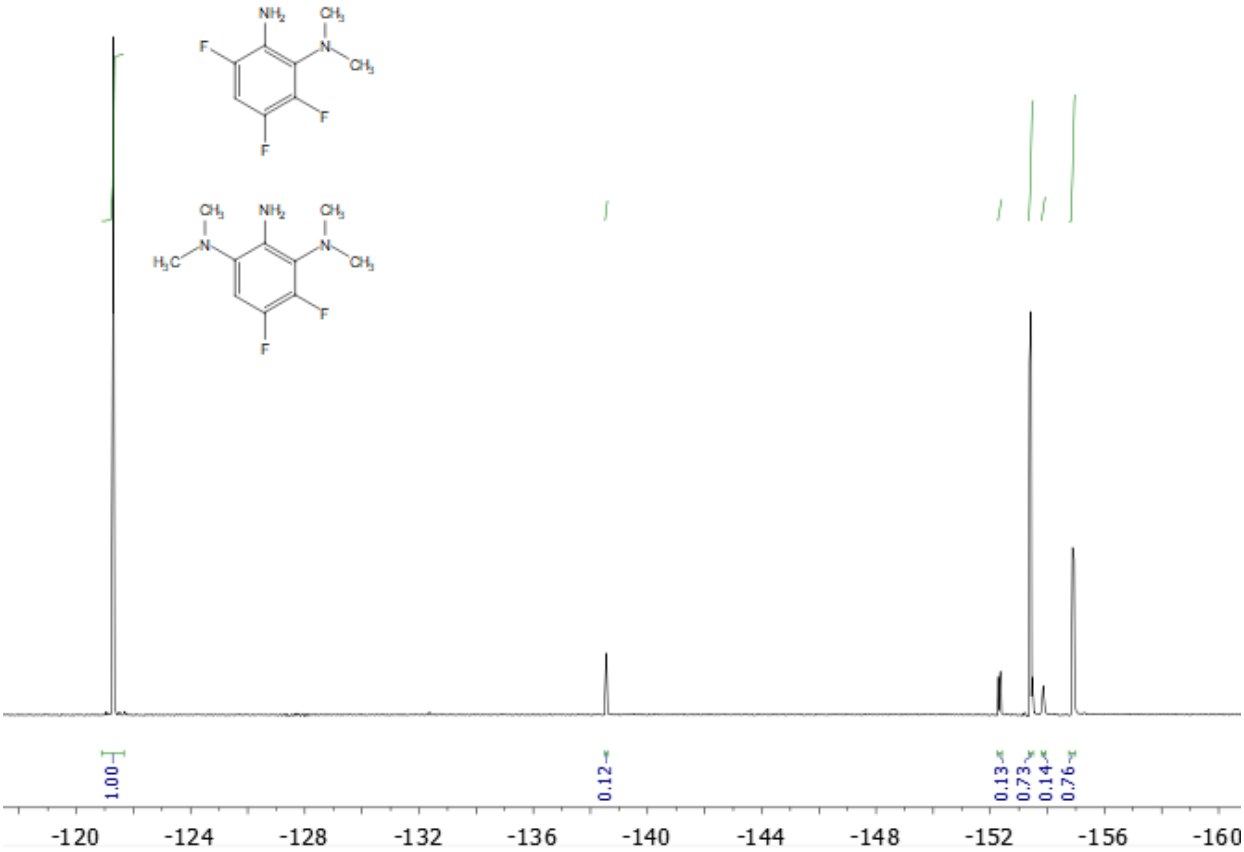

Figure 3.60: ^{19}F NMR spectrum ($CDCl_3$, 376 MHz) of the crude mixture of 2-dimethylamino-3,4,6-trifluoroaniline (**2h**) (−138.6 ppm, −152.3 ppm, and −153.9 ppm) and 2,6-bis(dimethylamino)-3,4-difluoroaniline (**3h**) (−153.4 ppm and −154.9 ppm). Bis(4-fluorophenyl)ether is present at −121.3 ppm.

2-dimethylamino-3,4,6-trifluoroaniline

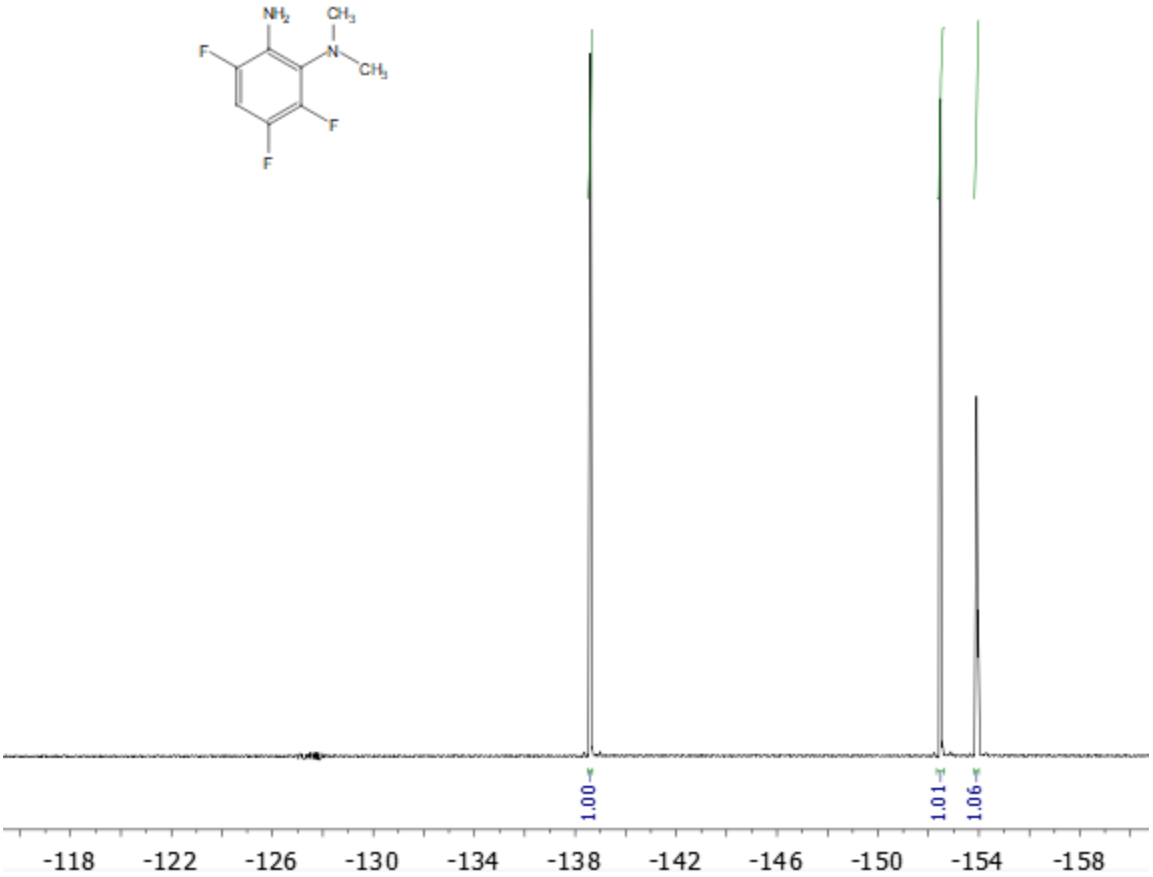

Figure 3.61: ^{19}F NMR spectrum ($CDCl_3$, 376 MHz) of column-purified 2-dimethylamino-3,4,6-trifluoroaniline (**2h**). The FID was subjected to 0.3 Hz of line-broadening apodization; a polynomial baseline correction was applied to the frequency-domain spectrum.

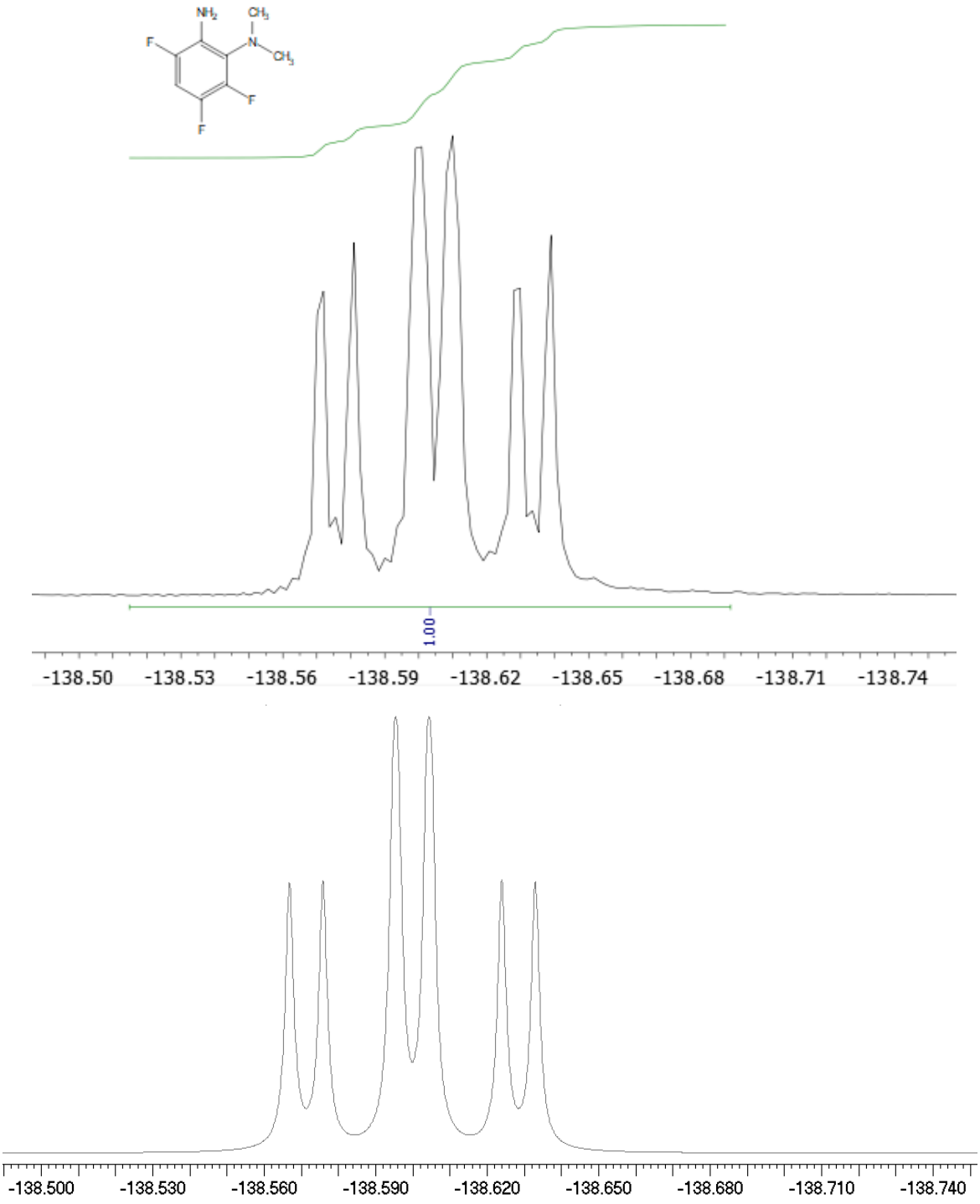

Figure 3.62: ^{19}F NMR spectra ($CDCl_3$, 376 MHz, expansion) of 2-dimethylamino-3,4,6-trifluoroaniline peak at −138.6 ppm (**2h**). **Upper**: Experimental spectrum with polynomial baseline correction and 0.3 Hz line broadening applied. **Lower**: Simulated (a natural linewidth of 1.0 Hz was estimated.)

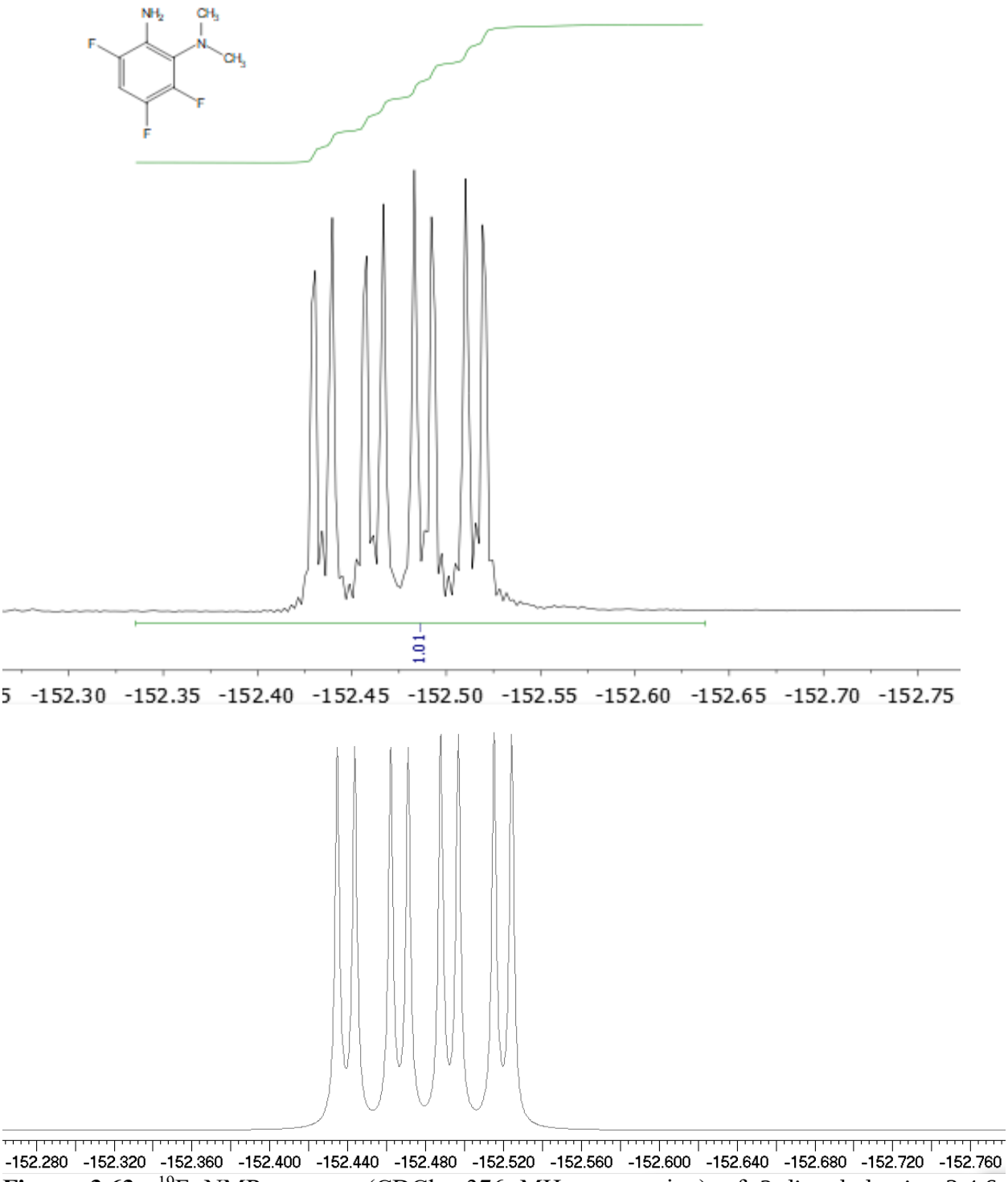

Figure 3.63: ^{19}F NMR spectra ($CDCl_3$, 376 MHz, expansion) of 2-dimethylamino-3,4,6-trifluoroaniline peak at −152.5 ppm (**2h**). **Upper**: Experimental spectrum with polynomial baseline correction and 0.3 Hz line broadening applied. **Lower**: Simulated (A natural linewidth of 1.0 Hz was estimated.)

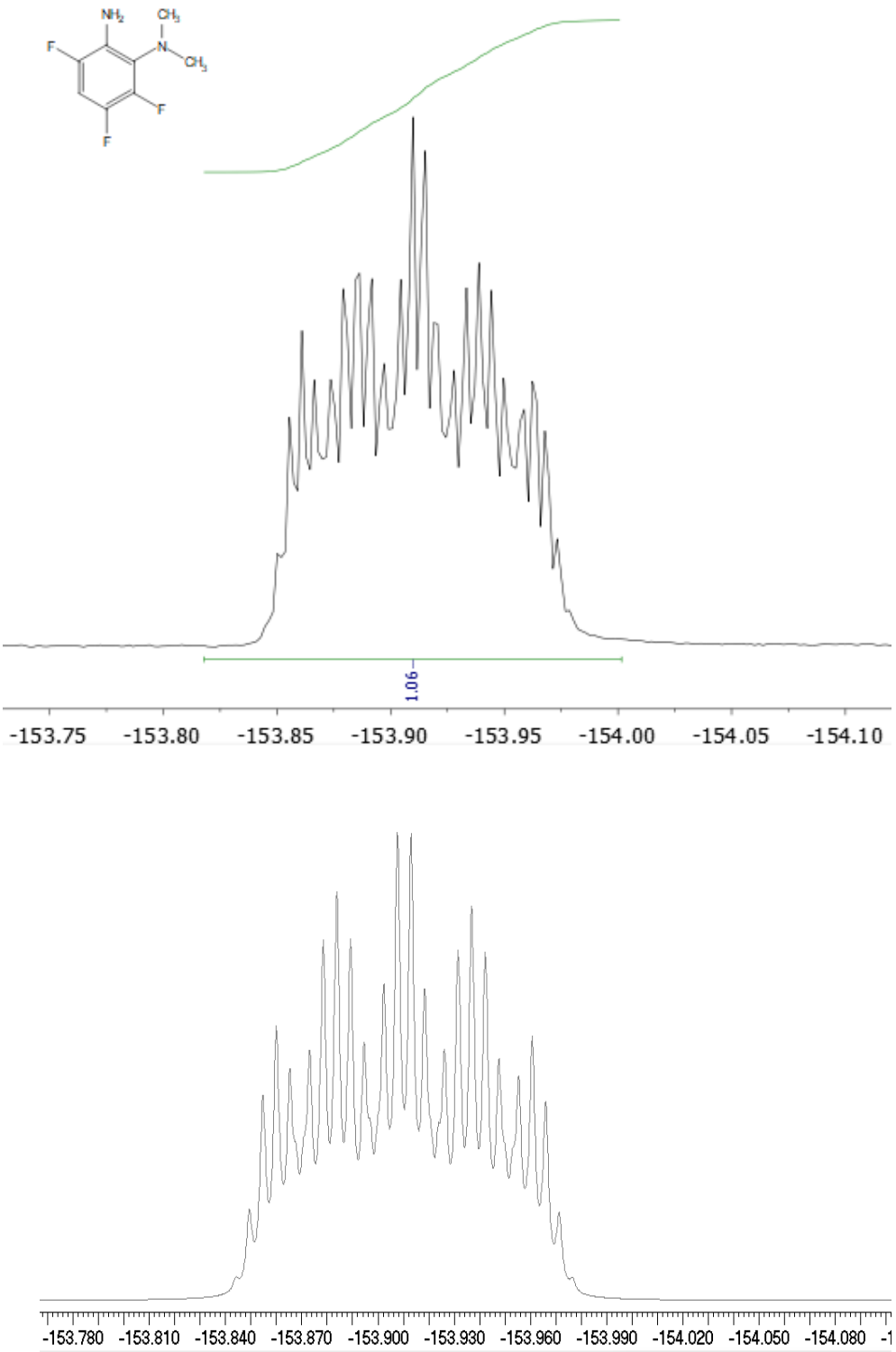

Figure 3.64: ^{19}F NMR spectra ($CDCl_3$, 376 MHz, expansion) of 2-dimethylamino-3,4,6-trifluoroaniline peak at −153.9 ppm (**2h**). **Upper**: Experimental spectrum with polynomial baseline correction and 0.3 Hz line broadening applied. **Lower**: Simulated (a natural linewidth of 1.0 Hz was estimated.)

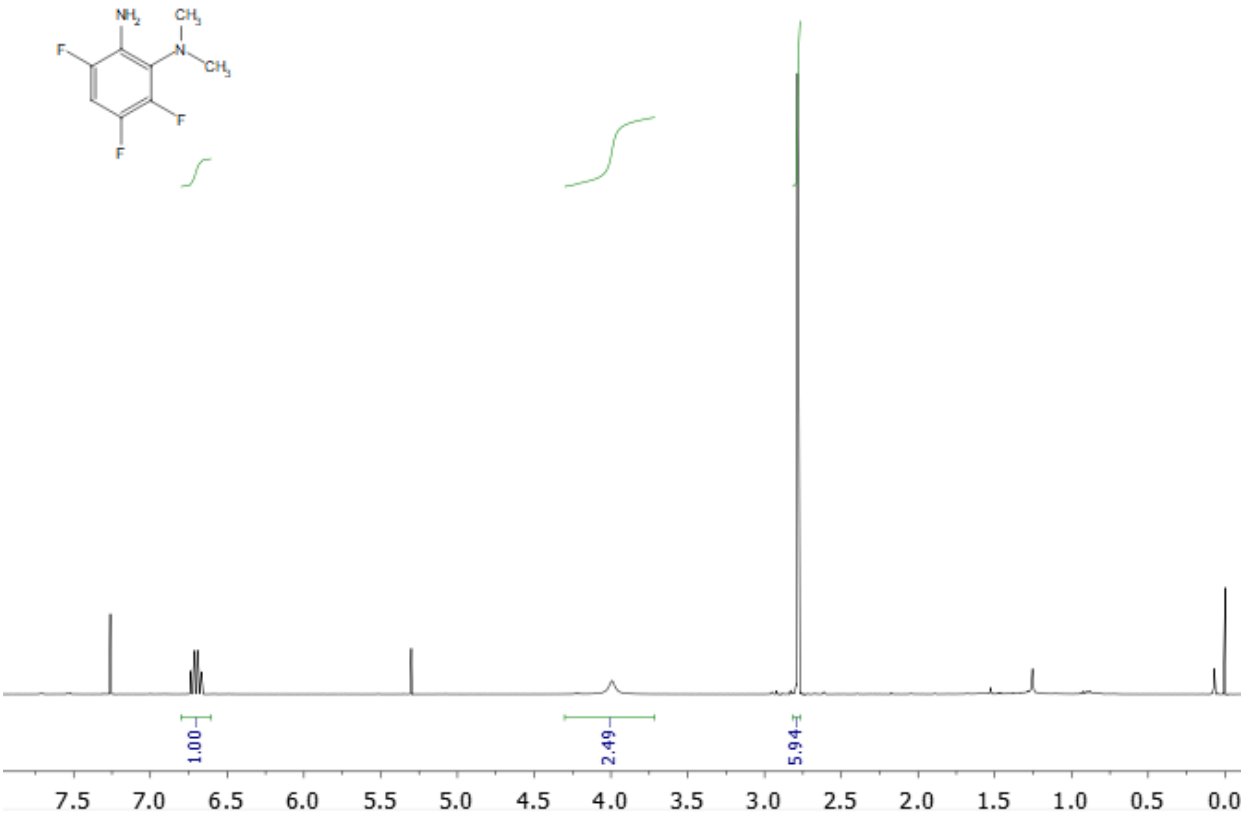

Figure 3.65: ^{1}H NMR spectrum ($CDCl_3$, 400 MHz) of column-purified 2-dimethylamino-3,4,6-trifluoroaniline (**2h**), δ 6.70 (CH), 3.99 (NH_2), 2.79 (NMe_2). Also present are dichloromethane (chromatography solvent, 5.30 ppm) and $CHCl_3$ (7.26 ppm).

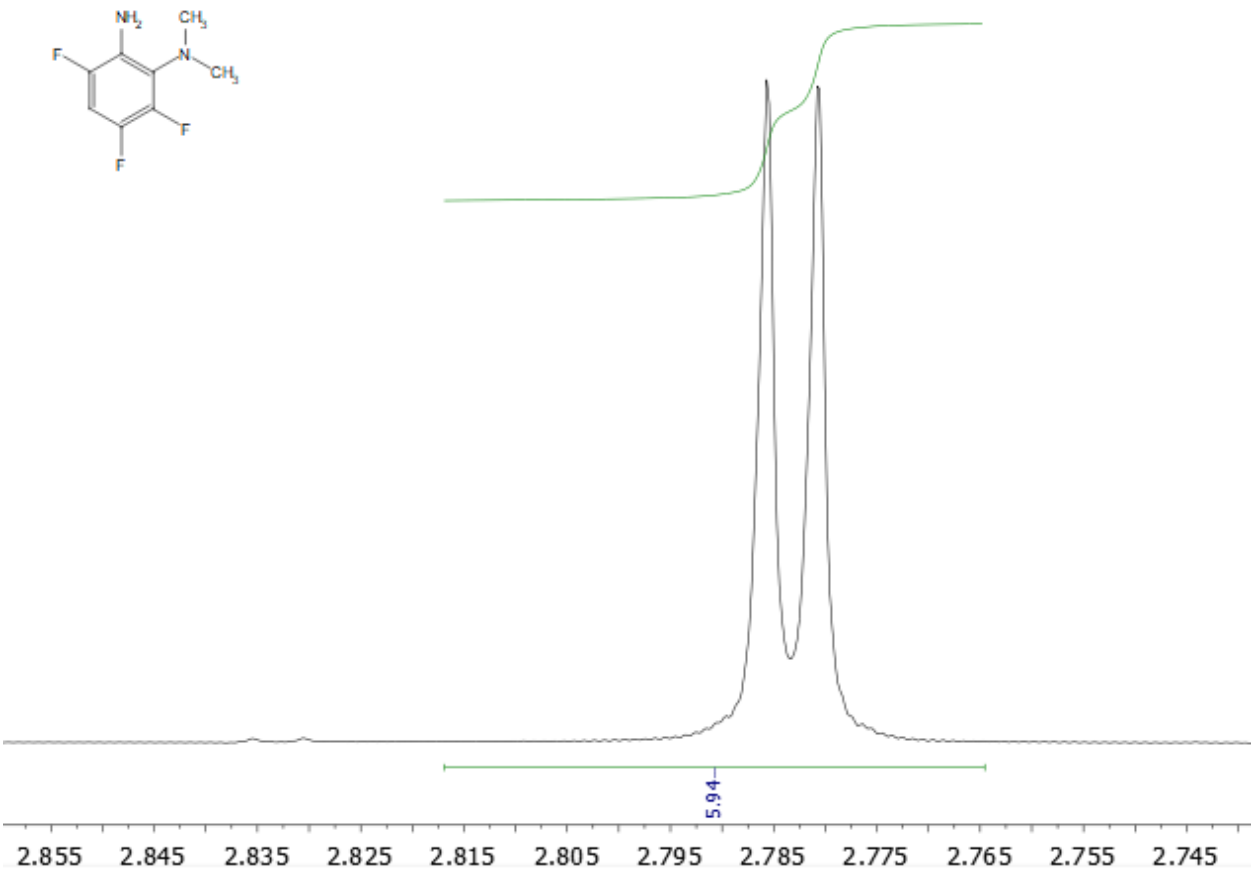

Figure 3.66: ^{1}H NMR spectrum ($CDCl_3$, 400 MHz), NMe_2 signal of column-purified 2-dimethylamino-3,4,6-trifluoroaniline (**2h**). The doublet feature arises from coupling to the 3-fluorine.

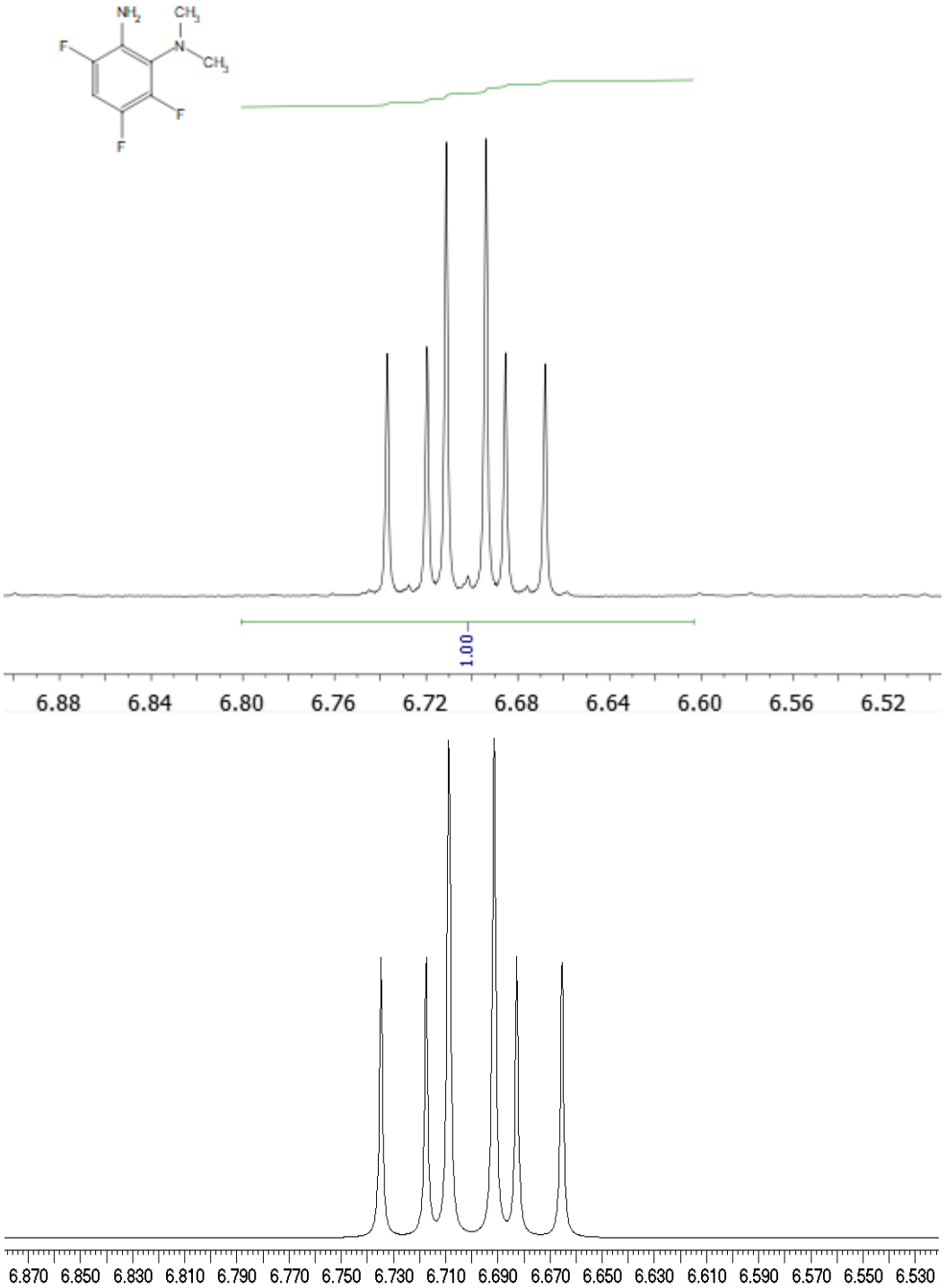

Figure 3.67: ^{1}H NMR spectra ($CDCl_3$, 400 MHz, expansion) of aromatic region of 2-dimethylamino-3,4,6-trifluoroaniline (**2h**). **Upper**: Experimental spectrum. **Lower**: Simulated; a natural linewidth of 0.5 Hz was estimated.

2,6-Bis(dimethylamino)-3,4-difluoroaniline

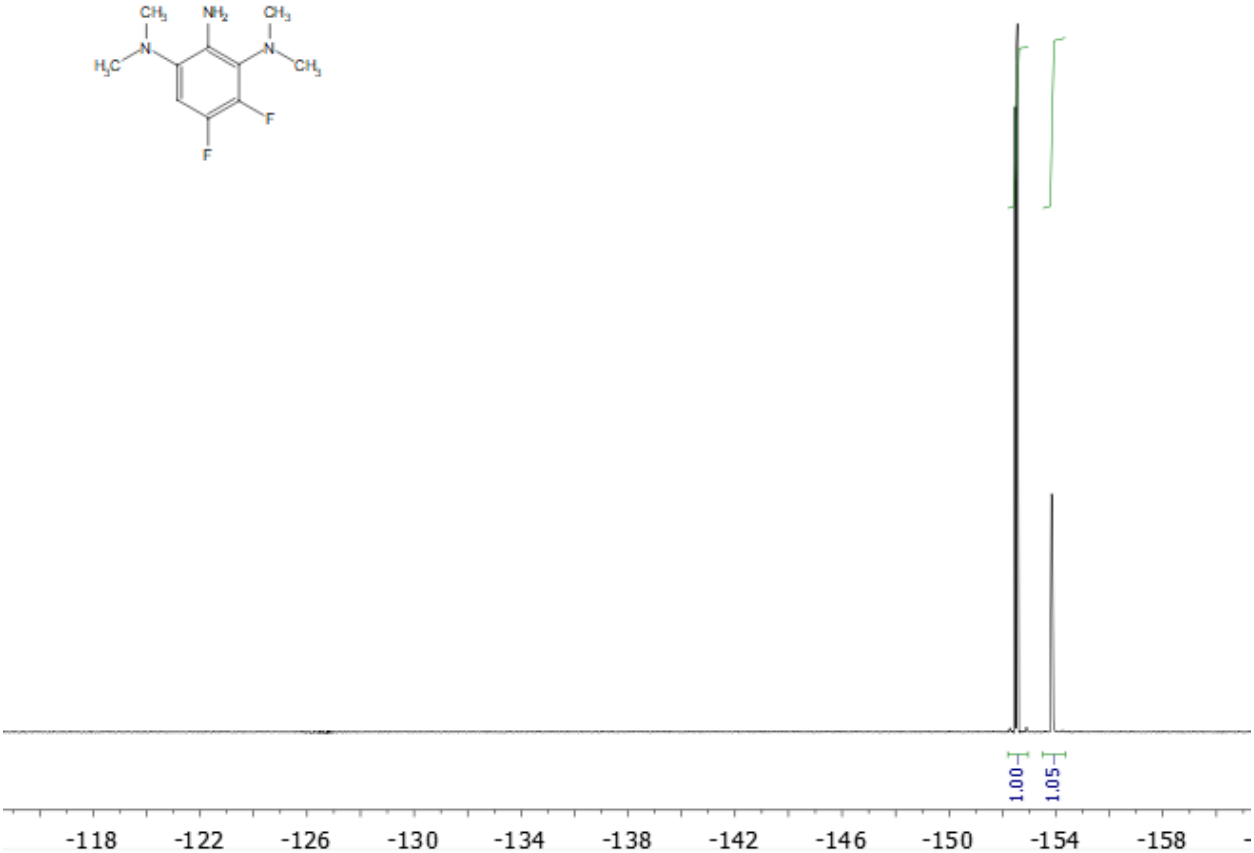

Figure 3.68: ^{19}F NMR spectrum ($CDCl_3$, 376 MHz) of column-purified 2,6-bis(dimethylamino)-3,4-difluoroaniline (**3h**).

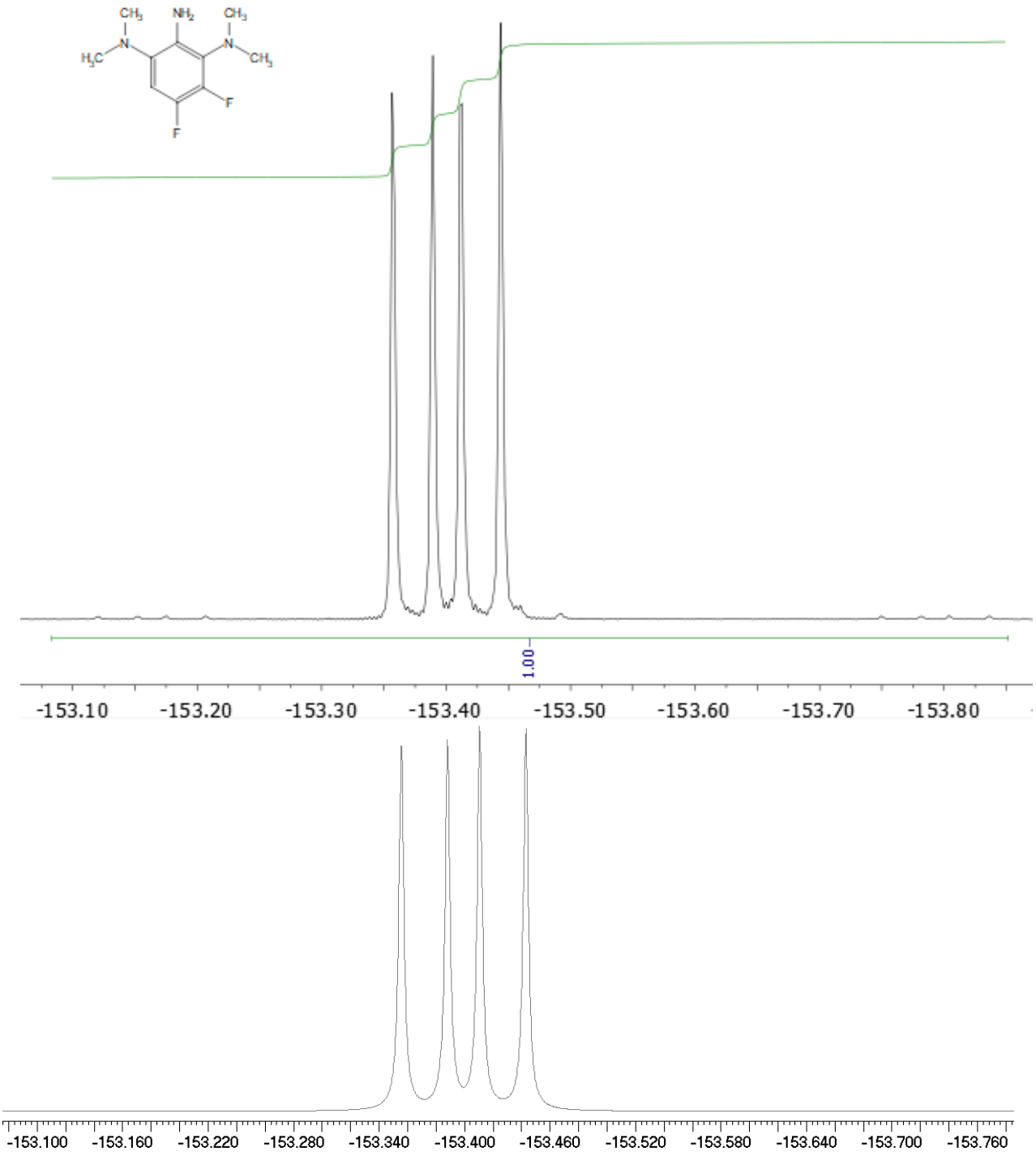

Figure 3.69: ^{19}F NMR spectra ($CDCl_3$, 376 MHz, expansion) of 2,6-bis(dimethylamino)-3,4-difluoroaniline peak at −153.4 ppm (**3h**). **Upper**: Experimental spectrum with polynomial baseline correction applied. **Lower**: Simulated (a natural linewidth of 1.5 Hz was estimated.)

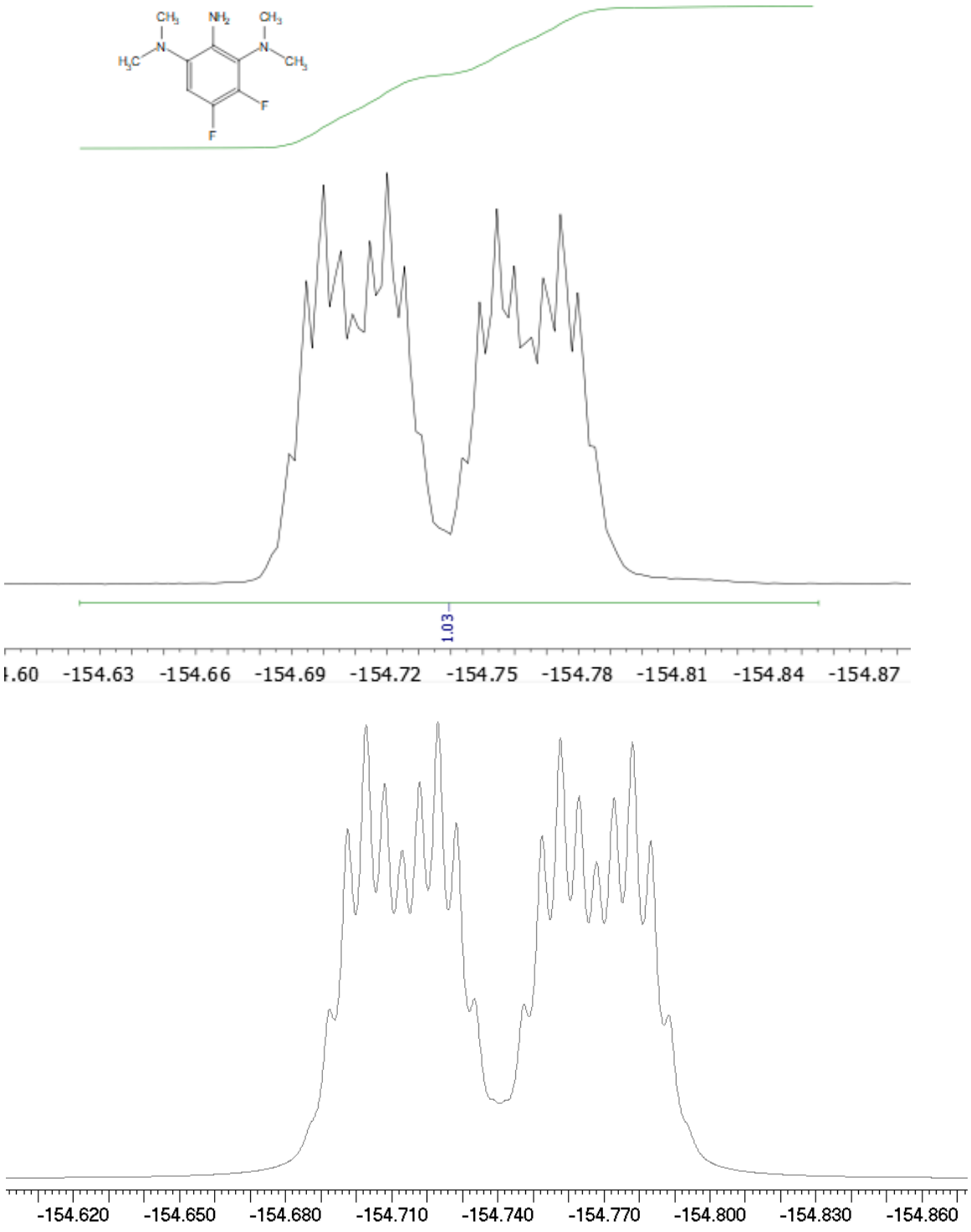

Figure 3.70: ^{19}F NMR spectra ($CDCl_3$, 376 MHz, expansion) of 2,6-bis(dimethylamino)-3,4-difluoroaniline peak at −154.7 ppm (**3h**). Upper: Experimental spectrum with polynomial baseline correction applied. Lower: Simulated (a natural linewidth of 1.5 Hz was estimated.)

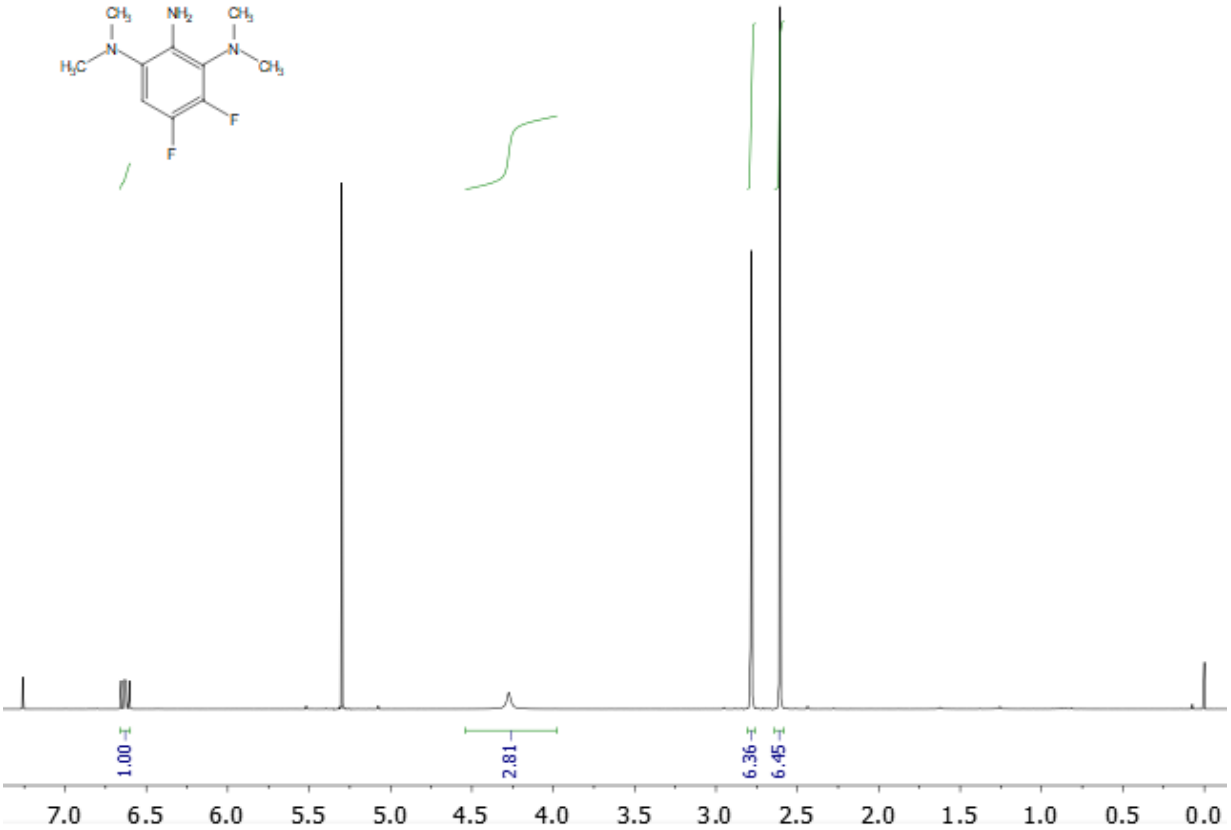

Figure 3.71: ^{1}H NMR spectrum ($CDCl_3$, 400 MHz) of column-purified 2,6-bis(dimethylamino)-3,4-difluoroaniline (**3h**), δ 6.63 (CH), 4.27 (NH_2), 2.78 (NMe_2), 2.61 (NMe_2). Dichloromethane (5.30 ppm) and $CHCl_3$ (7.26 ppm) are also present.

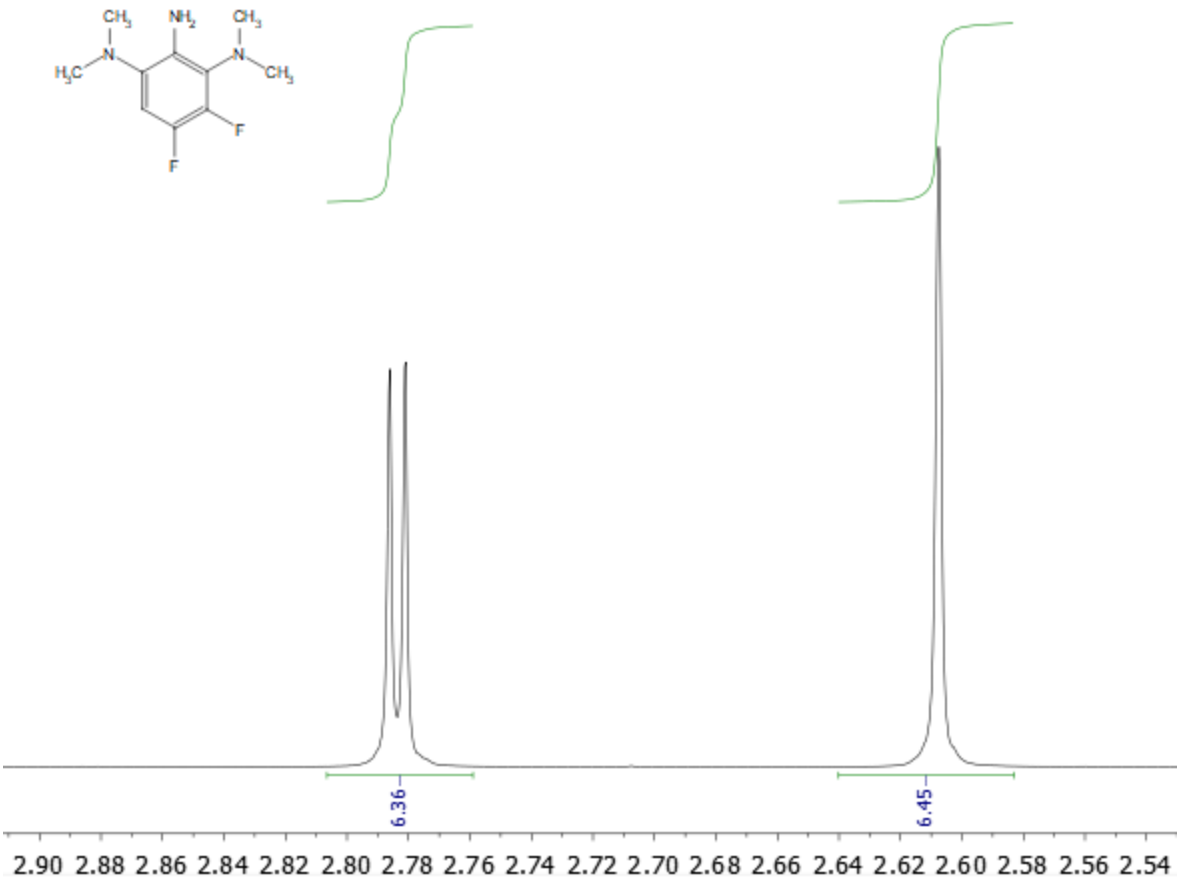

Figure 3.72: ^{1}H NMR spectrum ($CDCl_3$, 400 MHz), methyl signal of column-purified 2,6-bis(dimethylamino)-3,4-difluoroaniline (**3h**). The downfield doublet is assigned to the NMe_2 group in the 2-position (relative to NH_2) because of the coupling to the 3-fluorine.

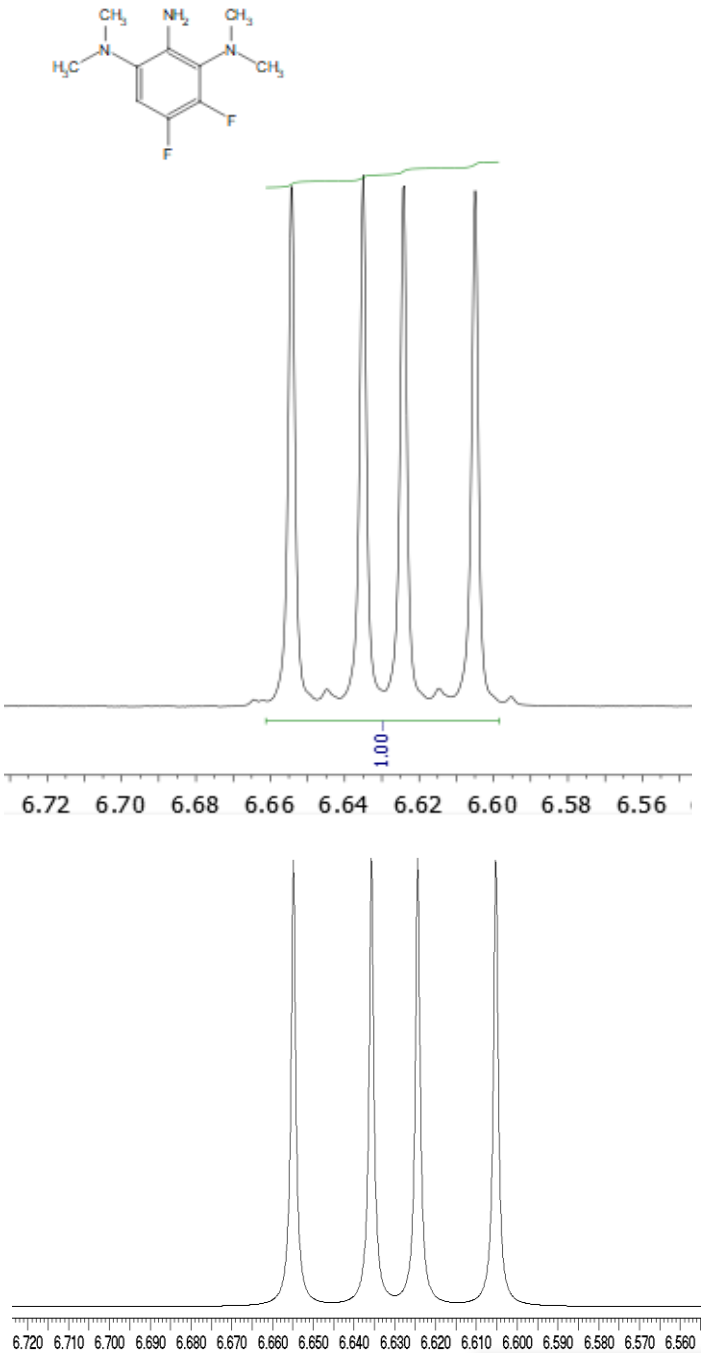

Figure 3.73: ^{1}H NMR spectra ($CDCl_3$, 400 MHz, expansion) of aromatic region of 2,6-bis(dimethylamino)-3,4-difluoroaniline (**3h**). **Upper**: Experimental. **Lower**: Simulated; a natural linewidth of 0.5 Hz was estimated.

6-dimethylamino-2,3,4-trifluoroaniline

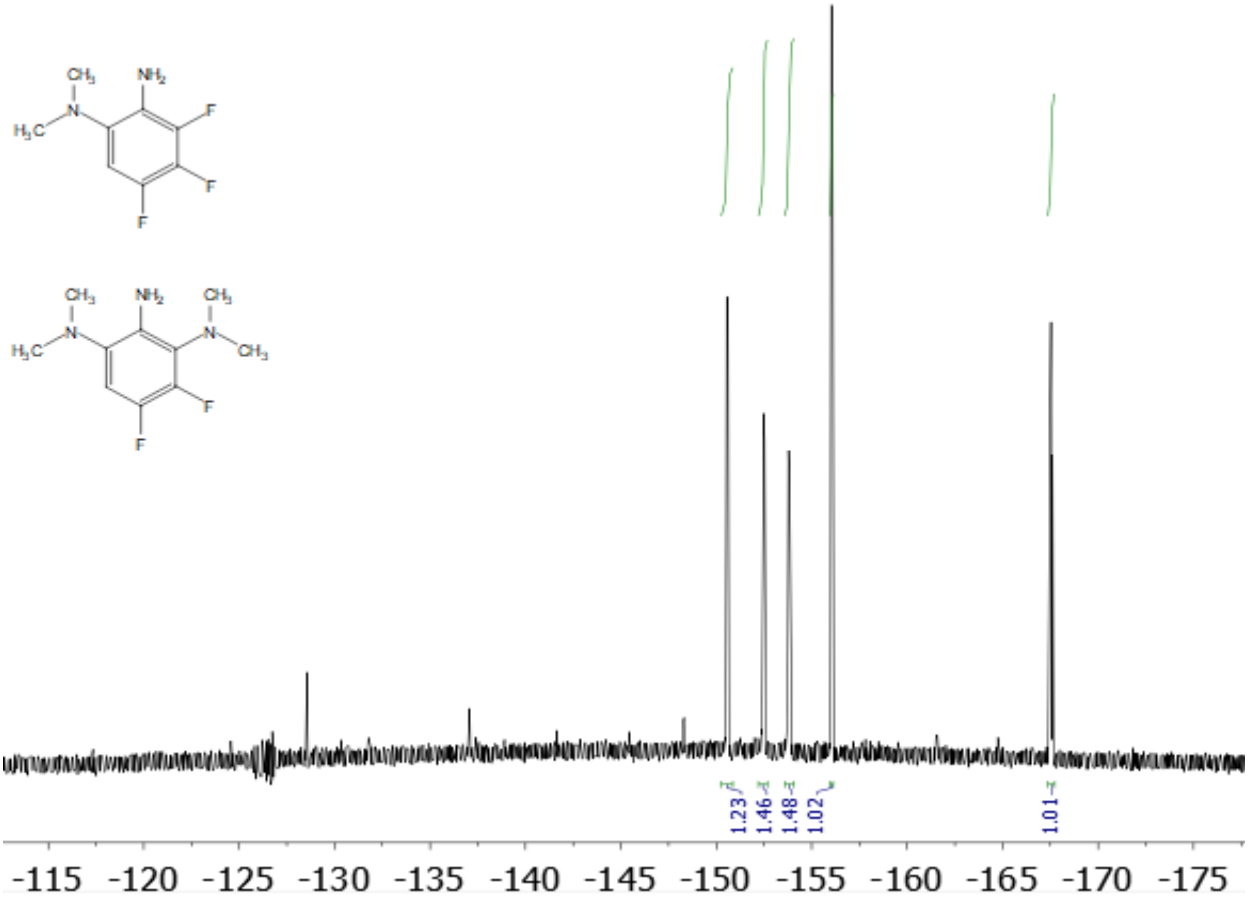

Figure 3.74: ^{19}F spectrum ($CDCl_3$, 400 MHz), of co-eluted 6-dimethylamino-2,3,4-trifluoroaniline (***iso*-2h**) (present at −150.6 ppm, −156.1, −167.5 ppm) and 2,6-bis(dimethylamino)-3,4-difluoroaniline (**3h**). The FID was zero-filled to 256k and a polynomial baseline correction was applied to the frequency-domain spectrum. The latter compound was isolated from a different reaction (see Figure 3.68 and characterized completely as described in Figures 3.60-3.73Note that we were not able to separate 6-dimethylamino-2,3,4-trifluoroaniline from either of the two product mixtures that we obtained, so we characterized 6-dimethylamino-2,3,4-trifluoroaniline from this mixture.

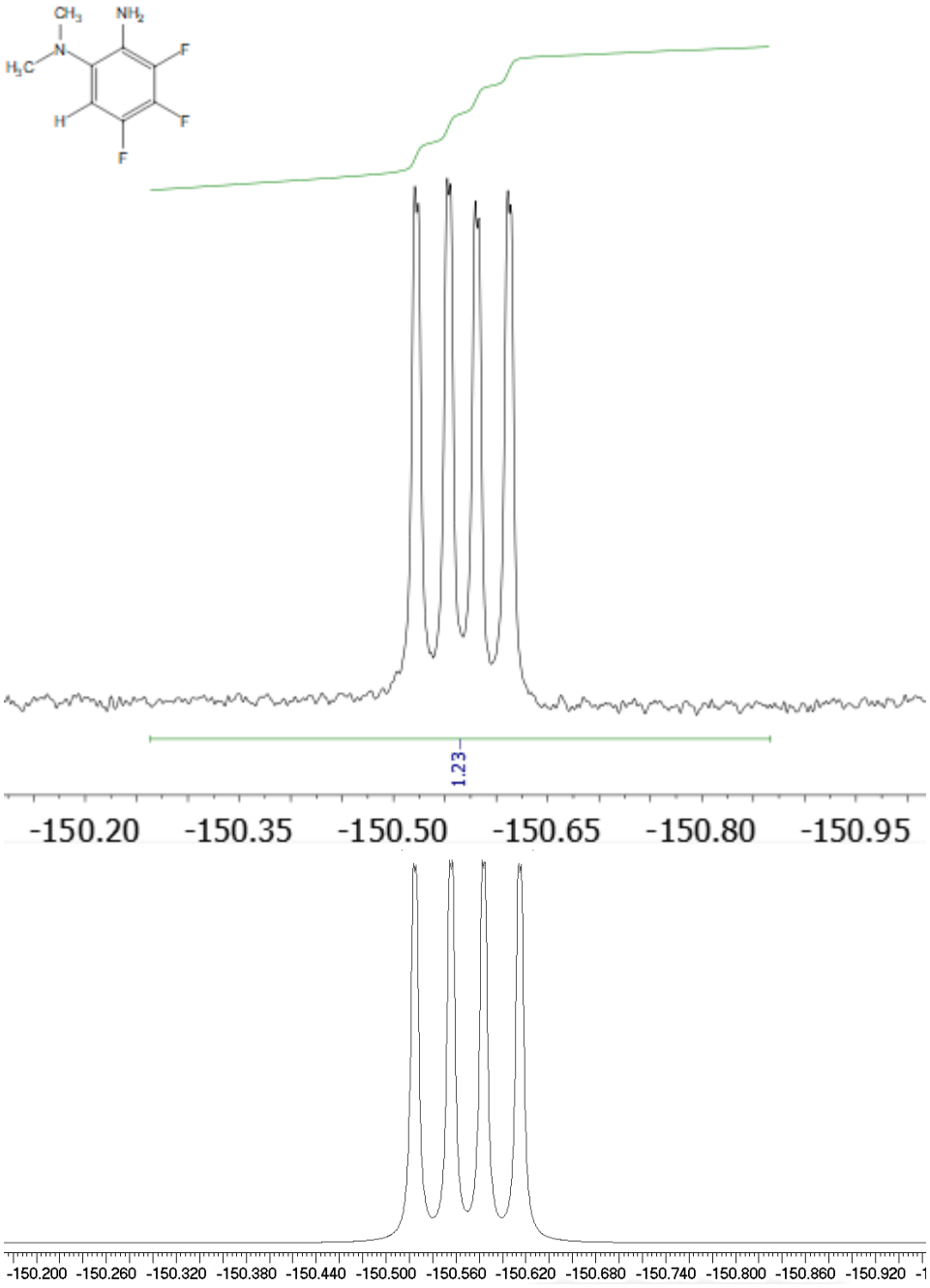

Figure 3.75: ^{19}F NMR spectra ($CDCl_3$, 376 MHz, expansion) of −150.6 ppm peak of 6-dimethylamino-2,3,4-trifluoroaniline (***iso*-2h**). **Upper**: Experimental spectrum zero-filled to 256k, with polynomial baseline correction applied. **Lower**: Simulated (a natural linewidth of 1.7 Hz was estimated.)

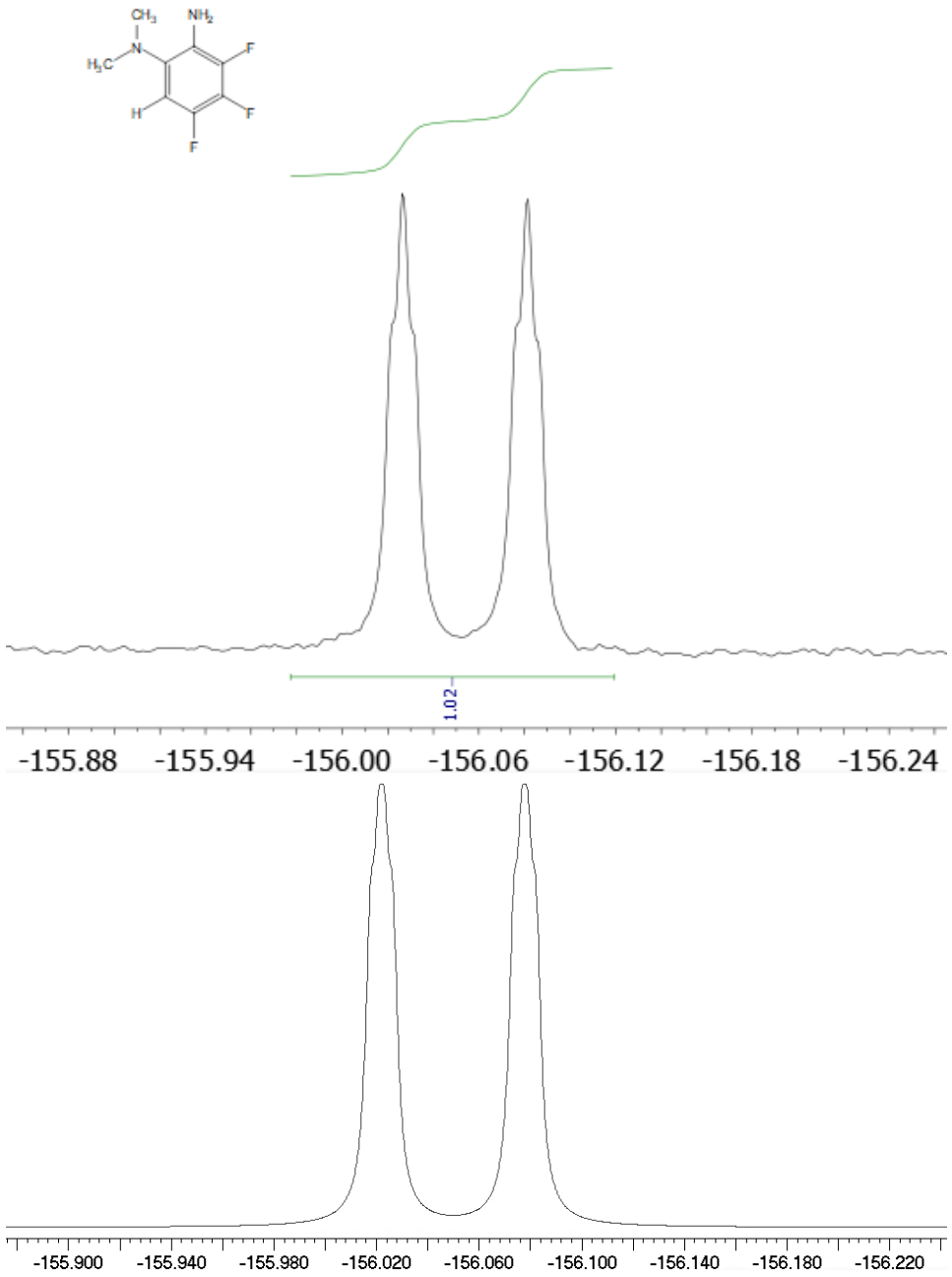

Figure 3.76: ^{19}F NMR spectra ($CDCl_3$, 376 MHz, expansion) of −150.1 ppm peak of 6-dimethylamino-2,3,4-trifluoroaniline (***iso*-2h**). **Upper**: Experimental spectrum zero-filled to 256k, with polynomial baseline correction applied. **Lower**: Simulated (a natural linewidth of 1.7 Hz was estimated.)

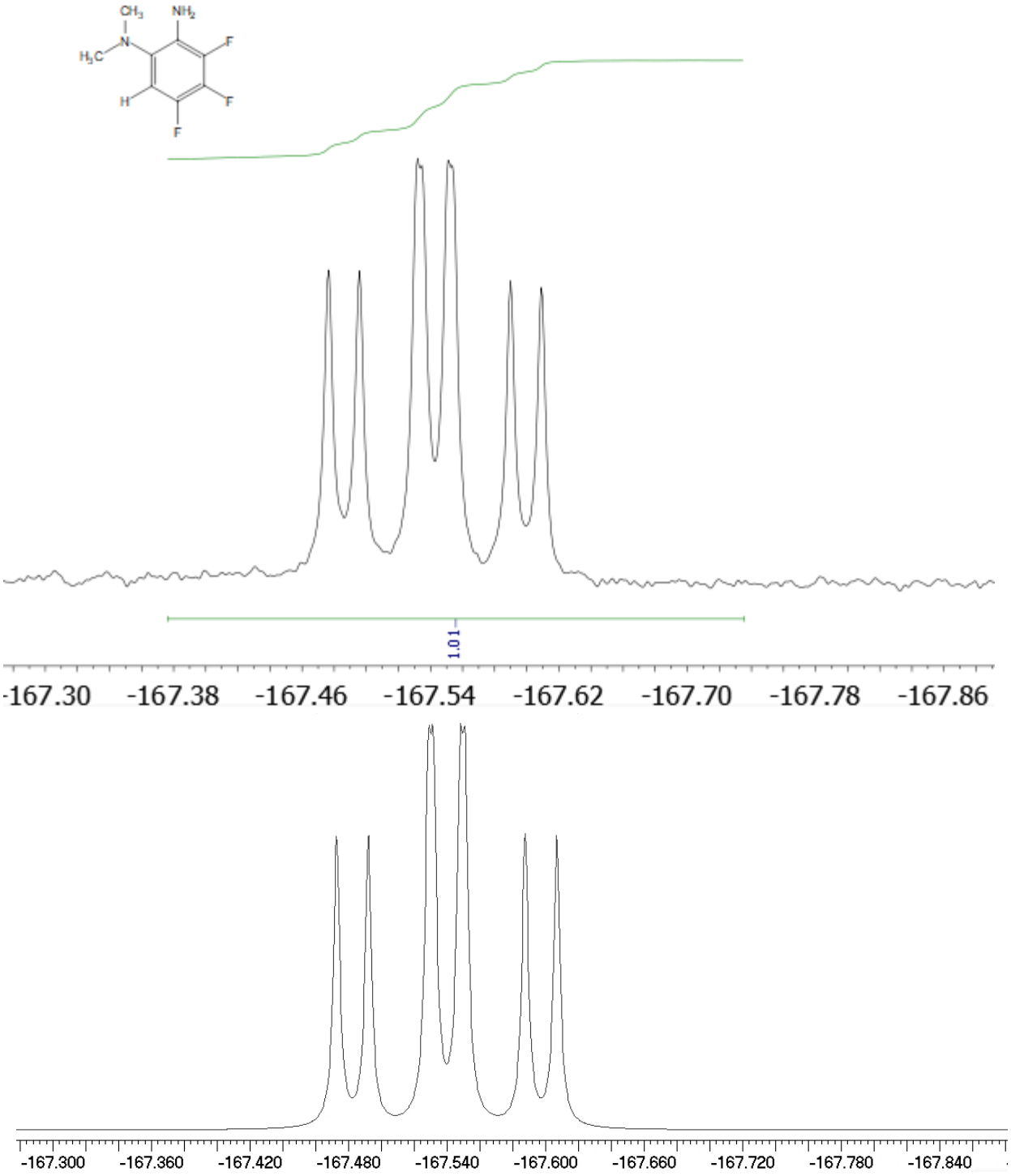

Figure 3.77: ^{19}F NMR spectra ($CDCl_3$, 376 MHz, expansion) of −167.5 ppm peak of 6-dimethylamino-2,3,4-trifluoroaniline (***iso*-2h**). **Upper**: Experimental spectrum zero-filled to 256k, with polynomial baseline correction applied. **Lower**: Simulated (a natural linewidth of 1.7 Hz was estimated.)

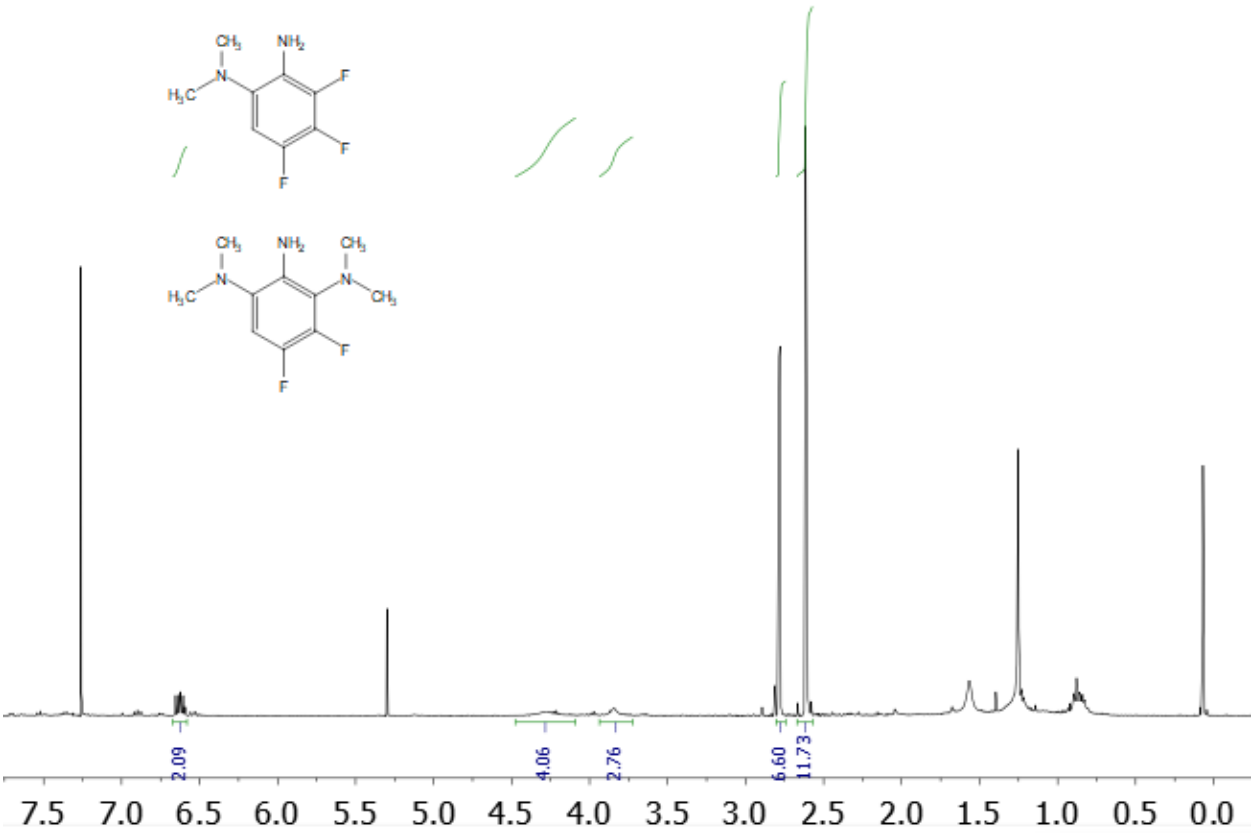

Figure 3.78: ^{1}H NMR spectrum ($CDCl_3$, 400 MHz), of co-eluted 6-dimethylamino-2,3,4-trifluoroaniline (***iso*-2h**) and 2,6-bis(dimethylamino)-3,4-difluoroaniline (**3h**). Signals of 6-dimethylamino-2,3,4-trifluoroaniline are present at 6.55 ppm, 3.78 ppm, and 2.54 ppm. Also present is dichloromethane (5.30 ppm).

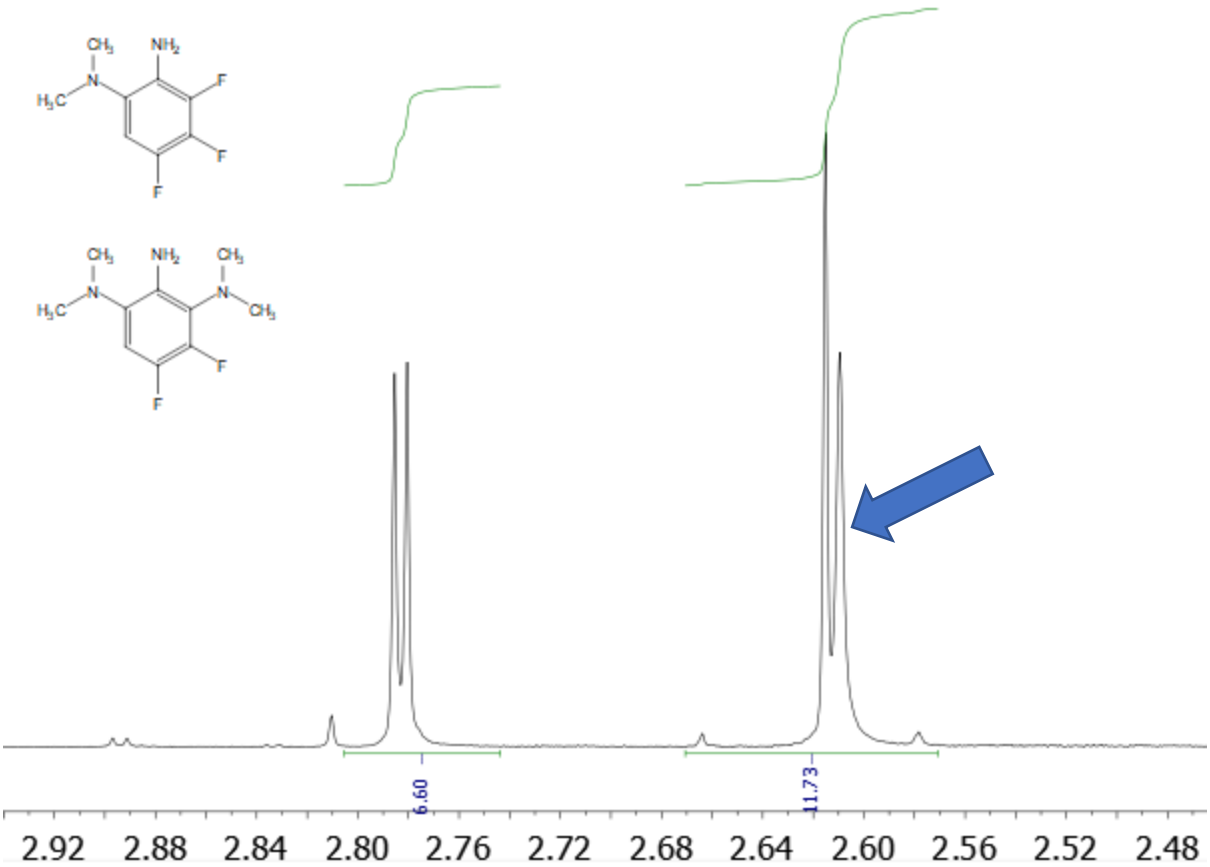

Figure 3.79: ^{1}H NMR spectrum ($CDCl_3$, 400 MHz), methyl signals of coeluted 6-dimethylamino-2,3,4-trifluoroaniline (***iso*-2h**) and 2,6-bis(dimethylamino)-3,4-difluoroaniline **(3h)**. The NMe_2 group of 6-dimethylamino-2,3,4-trifluoroaniline is indicated by the arrow. The other signals arise from 2,6-bis(dimethylamino)-3,4-difluoroaniline.

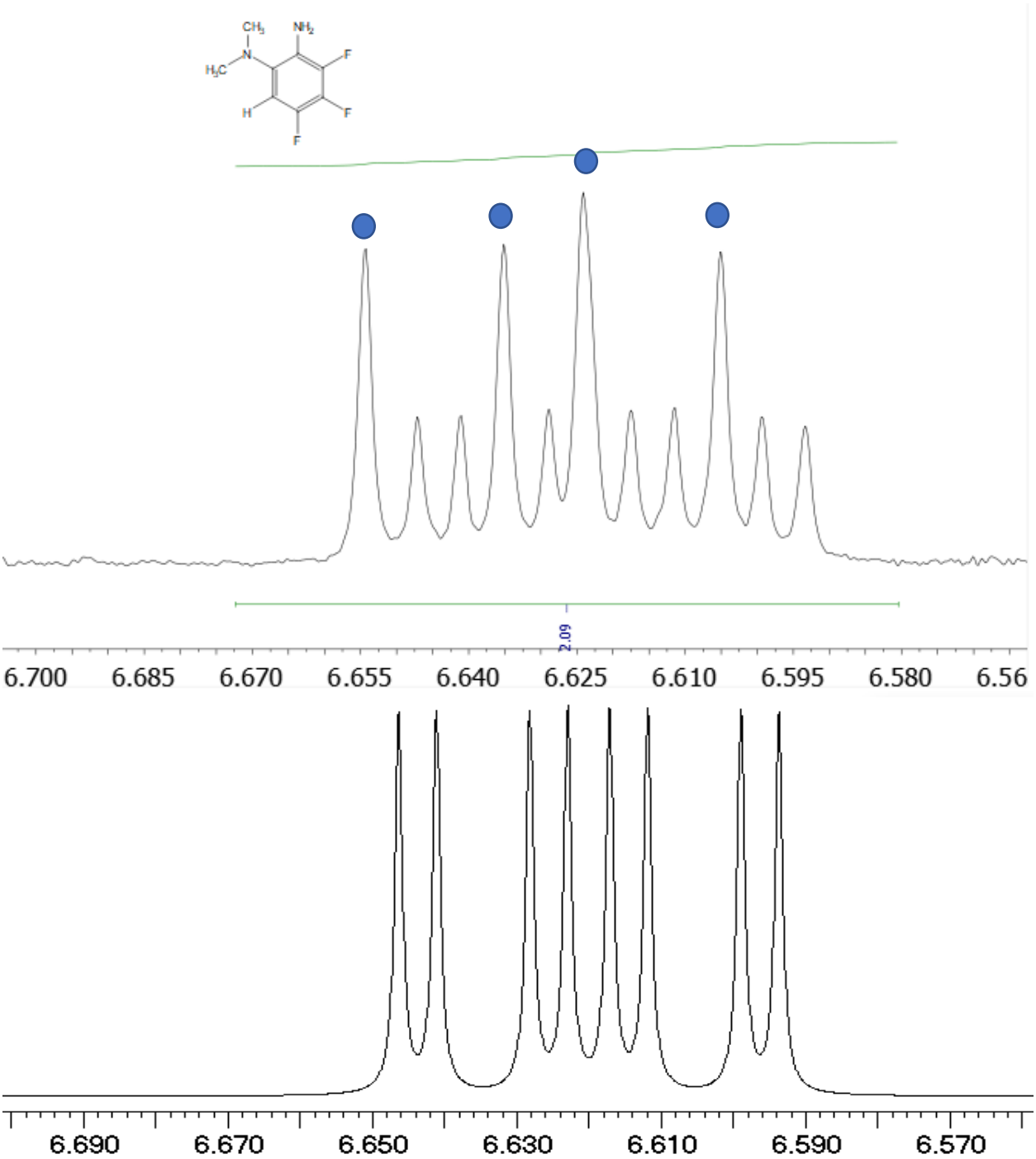

Figure 3.80: ^{1}H NMR spectra ($CDCl_3$, 400 MHz, expansion) of aromatic region of 6-dimethylamino-2,3,4-trifluoroaniline (***iso-2h***). **Upper**: Experimental spectrum, coeluted with 2,6-bis(dimethylamino)-3,4-difluoroaniline (**3h**) (doublet of doublets indicated by blue dots). **Lower**: Simulated; a natural linewidth of 0.5 Hz was estimated.

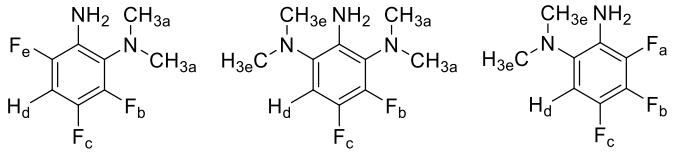

2h **3h** ***iso*-2h**

Figure 3.81: Structures of 2-dimethylamino-3,4,6-trifluoroaniline (**2h**), 2,6-bis(dimethylamino)-3,4-difluoroaniline (**3h**), and 6-dimethylamino-2,3,4-trifluoroaniline (***iso*-2h**) showing nuclei labeled for the simulations described in Table 3.10 through 3.12.

Table 3.10: Peak assignments for **2h** used to generate the simulated spectra shown in Figures 3.61 through 3.67.

		Coupling Constants (Hz)				
Nucleus	Chemical Shift (ppm)	a	b	c	d	e
a (NMe_2)	2.78					
b (F)	−153.9	2.0				
c (F)	−152.5	0.0	20.0			
d (H)	6.70	0.0	6.9	10.3		
e (F)	−138.6	0.0	11.0	3.0	10.5	
NH_2	3.99					

Table 3.11: Peak assignments for **3h** used to generate the simulated spectra shown in Figures 3.68 through 3.73.

		Coupling Constants (Hz)				
Nucleus	Chemical Shift (ppm)	a	b	c	d	e
a (NMe_2)	2.78					
b (F)	−154.7	2.0				
c (F)	−153.4	0.0	21.0			
d (H)	6.63	0.0	7.6	12.2		
e (NMe_2)	2.61	0.0	0.0	0.0	0.0	
NH_2	4.27					

Table 3.12: Peak assignments for ***iso*-2h** used to generate the simulated spectra shown in Figures 3.74 through 3.80.

		Coupling Constants (Hz)				
Nucleus	Chemical Shift (ppm)	a	b	c	d	e
a (F)	−156.1					
b (F)	−167.6	21.0				
c (F)	−150.6	1.2	22.0			
d (H)	6.62	2.1	7.3	11.7		
e (NMe_2)	2.61	0.0	0.0	0.0	0.0	
NH_2	3.84					

2-Dimethylamino-3,4,5,6-tetrafluoroaniline, and 2,6-Bis(dimethyl)-3,4,5-trifluoroaniline

These compounds were considered as a group because they arise from a common substrate. A mixture containing the first compound was obtained by reaction of 2,3,4,5,6-pentafluoroaniline with 2,3,4,6-tetrafluoroaniline with $Ti(NMe_2)_4$ at 120 °C for 18 h. A mixture of the second and third compounds was obtained by reaction at 90 °C for 3 h.

2-dimethylamino-3,4,5,6-tetrafluoroaniline

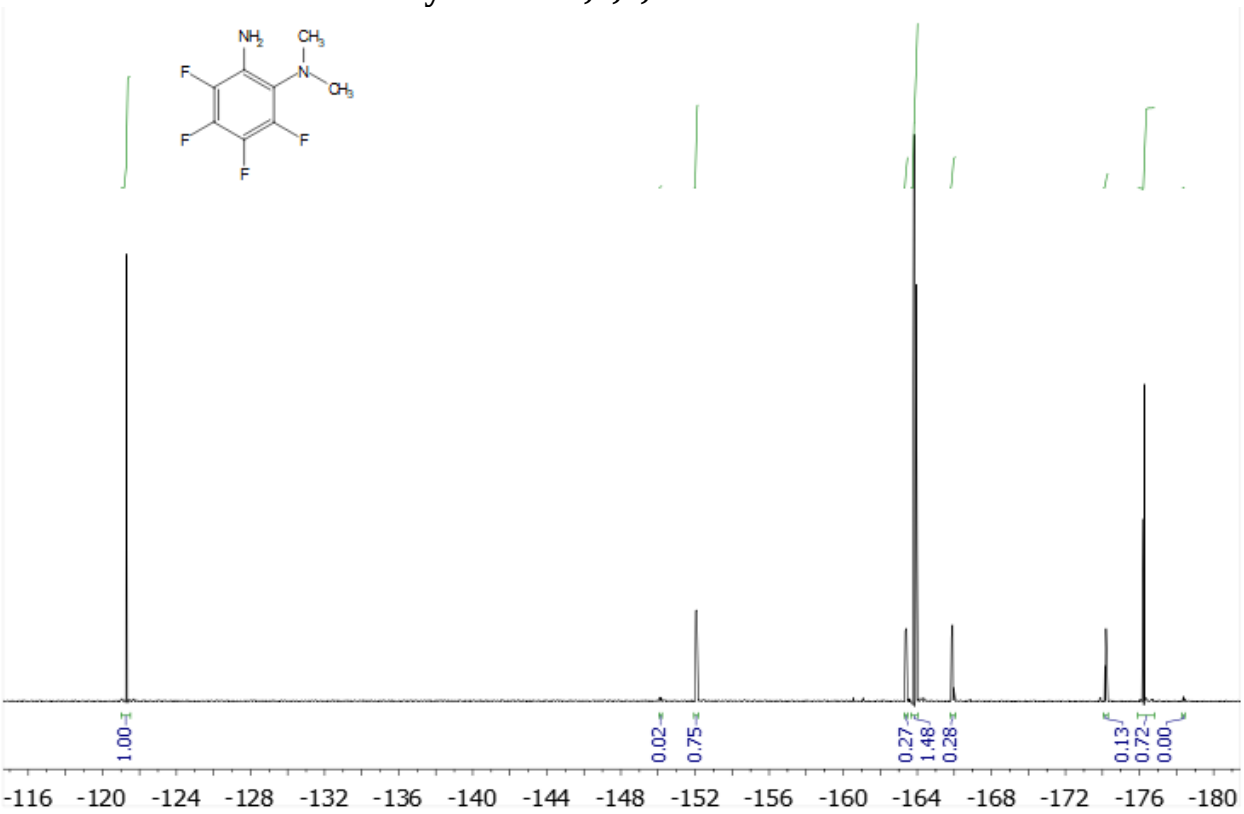

Figure 3.82: ^{19}F NMR spectrum ($CDCl_3$, 376 MHz) of the <u>crude</u> mixture of 2-dimethylamino-3,4,5,6-tetrafluoroaniline (**2i**) (-152.0 ppm, -163.8 ppm, -163.9 ppm, -176.3 ppm), as well as starting material (-163.4 ppm, -165.9 ppm, -174.2 ppm), and trace amounts of 2,6-bis(dimethylamino)-3,4,5-trifluoroaniline (-150.1 ppm, -178.4 ppm). Bis(4-fluorophenyl)ether is present at −121.3 ppm. Polynomial baseline correction applied.

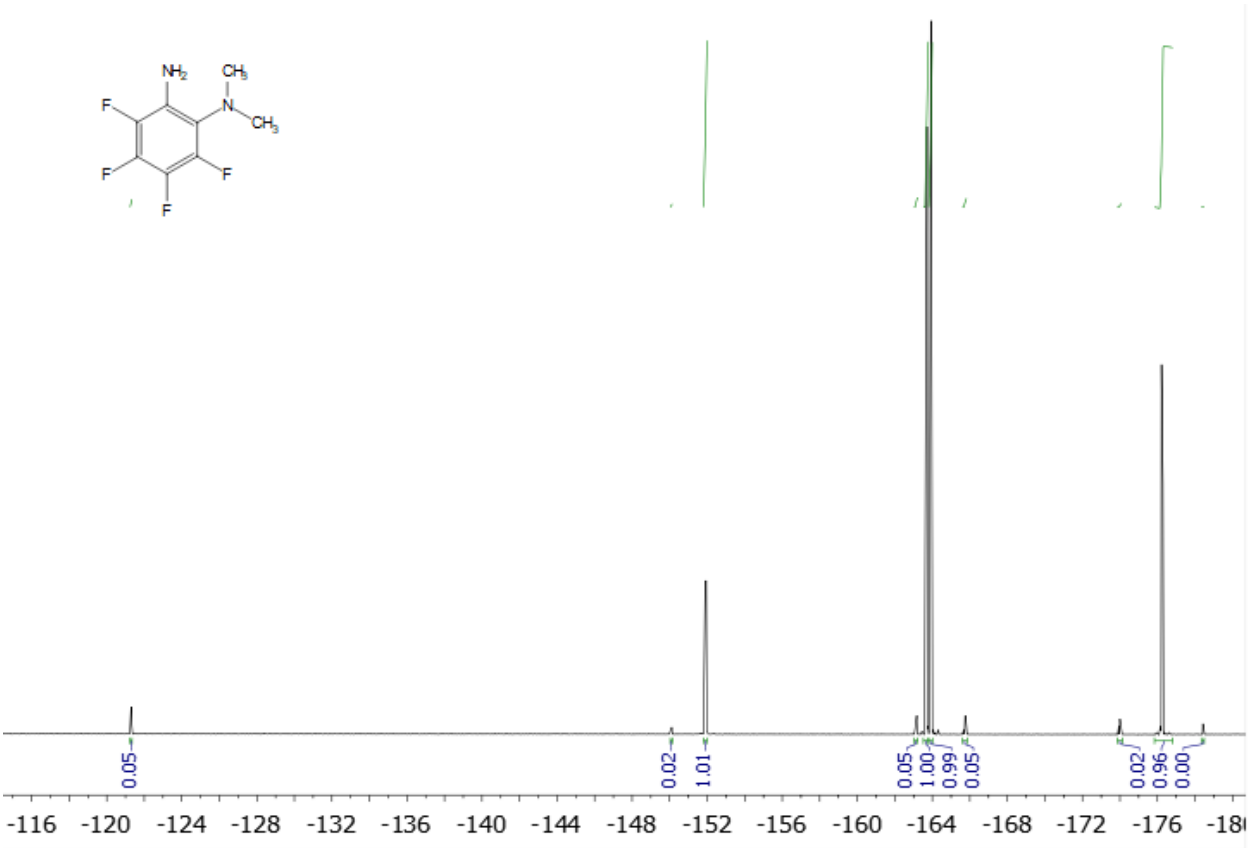

Figure 3.83: ^{19}F spectrum ($CDCl_3$, 400 MHz), of co-eluted 2-dimethylamino-3,4,5,6-tetrafluoroaniline (**2i**) (present at -151.9 ppm, -163.7 ppm, -163.9 ppm, and -176.2 ppm), as well as internal standard (referenced at –121.3 ppm, trace amounts of pentafluoroaniline starting material (-163.1 ppm, -165.7 ppm, -174.0 ppm) and trace amounts of 2,6-bis(dimethylamino)-3,4,5-trifluoroaniline (-151.9 ppm and -178.4 ppm). The latter compound was isolated from a different reaction (see Figure 3.89) and characterized as described in Table 3.13. The FID was zero-filled to 256k and 0.5 Hz of line broadening was added.

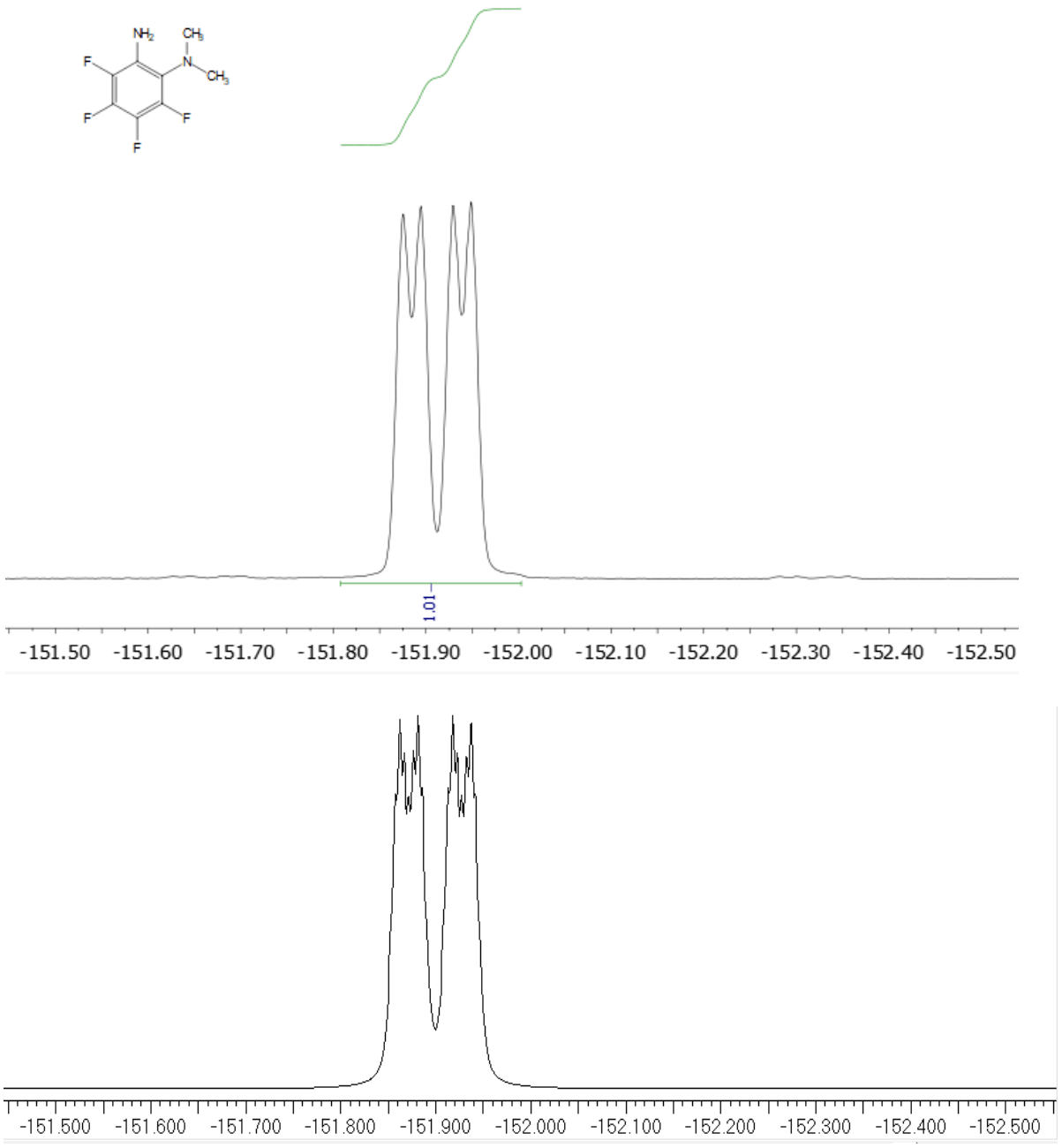

Figure 3.84: ^{19}F NMR spectra ($CDCl_3$, 376 MHz, expansion) of −151.9 ppm peak of 2-dimethylamino-3,4,5,6-tetrafluoroaniline (**2i**). **Upper**: Experimental spectrum zero-filled to 256k. **Lower**: Simulated (a natural linewidth of 1.0 Hz was estimated.)

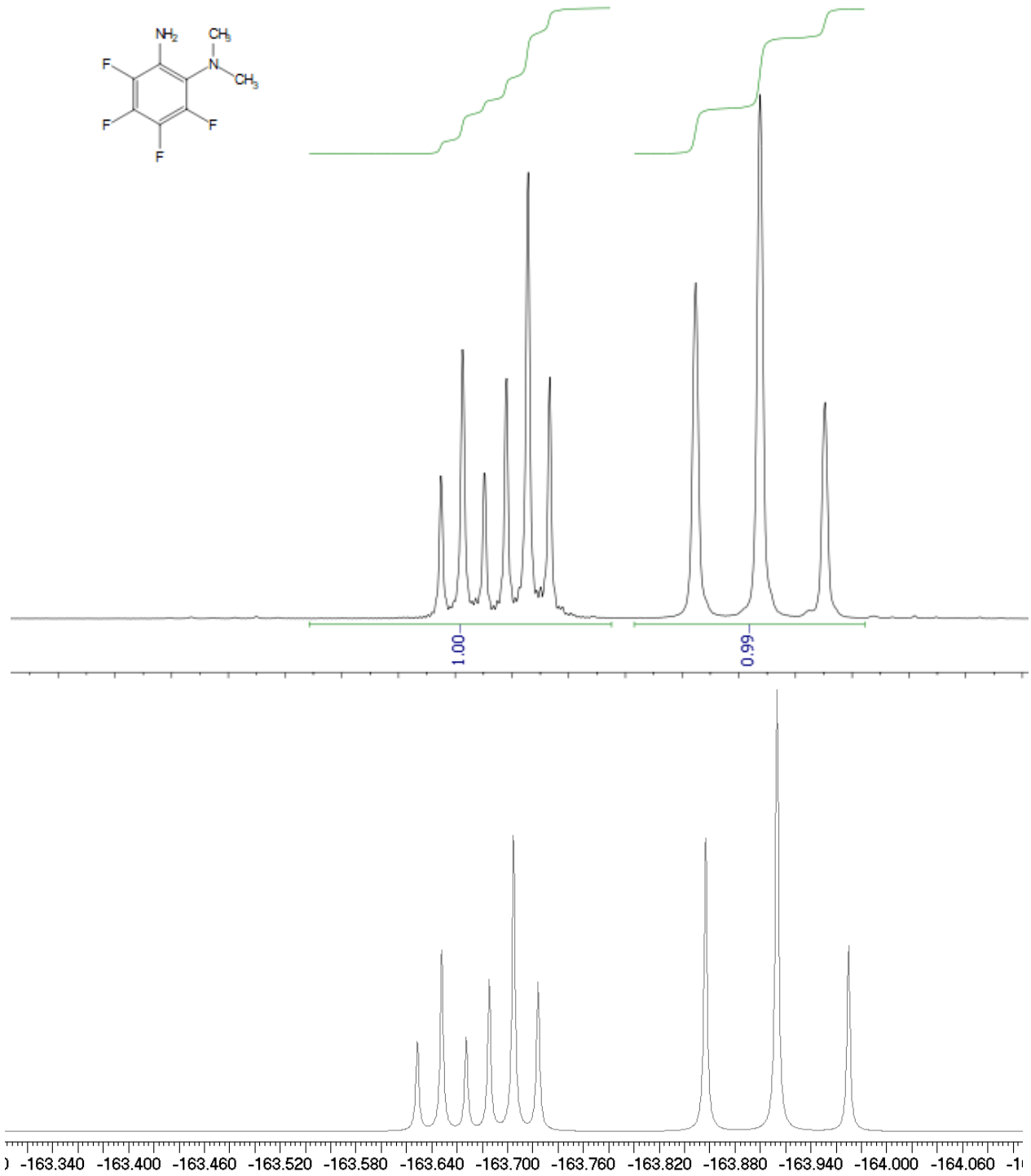

Figure 3.85: ^{19}F NMR spectra ($CDCl_3$, 376 MHz, expansion) of -163.7 ppm and -163.9 ppm peaks of 2-dimethylamino-3,4,5,6-tetrafluoroaniline (**2i**). **Upper**: Experimental spectrum zero-filled to 256k. **Lower**: Simulated (a natural linewidth of 1.0 Hz was estimated.)

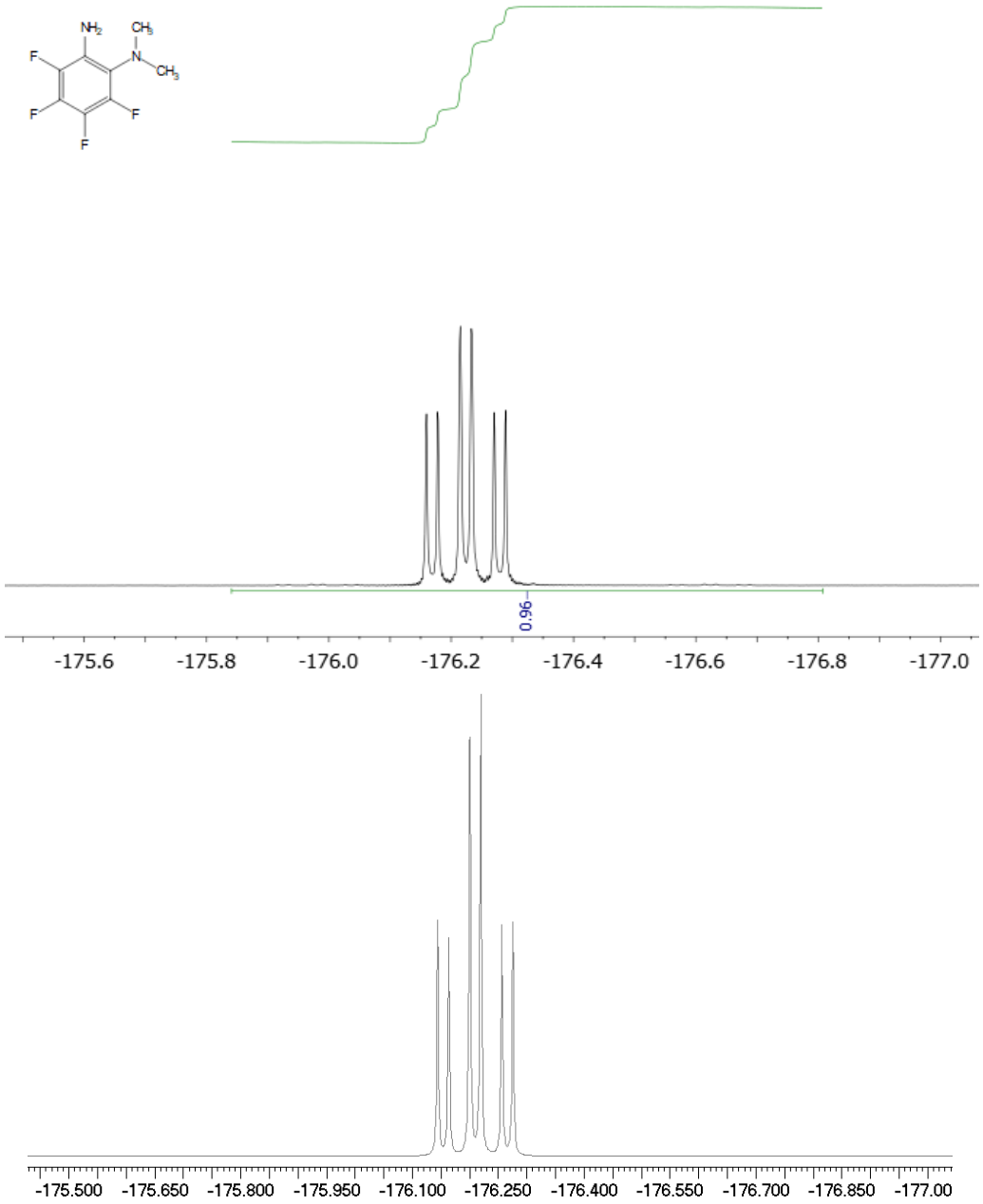

Figure 3.86: ^{19}F NMR spectra ($CDCl_3$, 376 MHz, expansion) of peak at −176.2 ppm of 2-dimethylamino-3,4,5,6-tetrafluoroaniline (**2i**). **Upper**: Experimental spectrum zero-filled to 256k. **Lower**: Simulated (a natural linewidth of 1.0 Hz was estimated.)

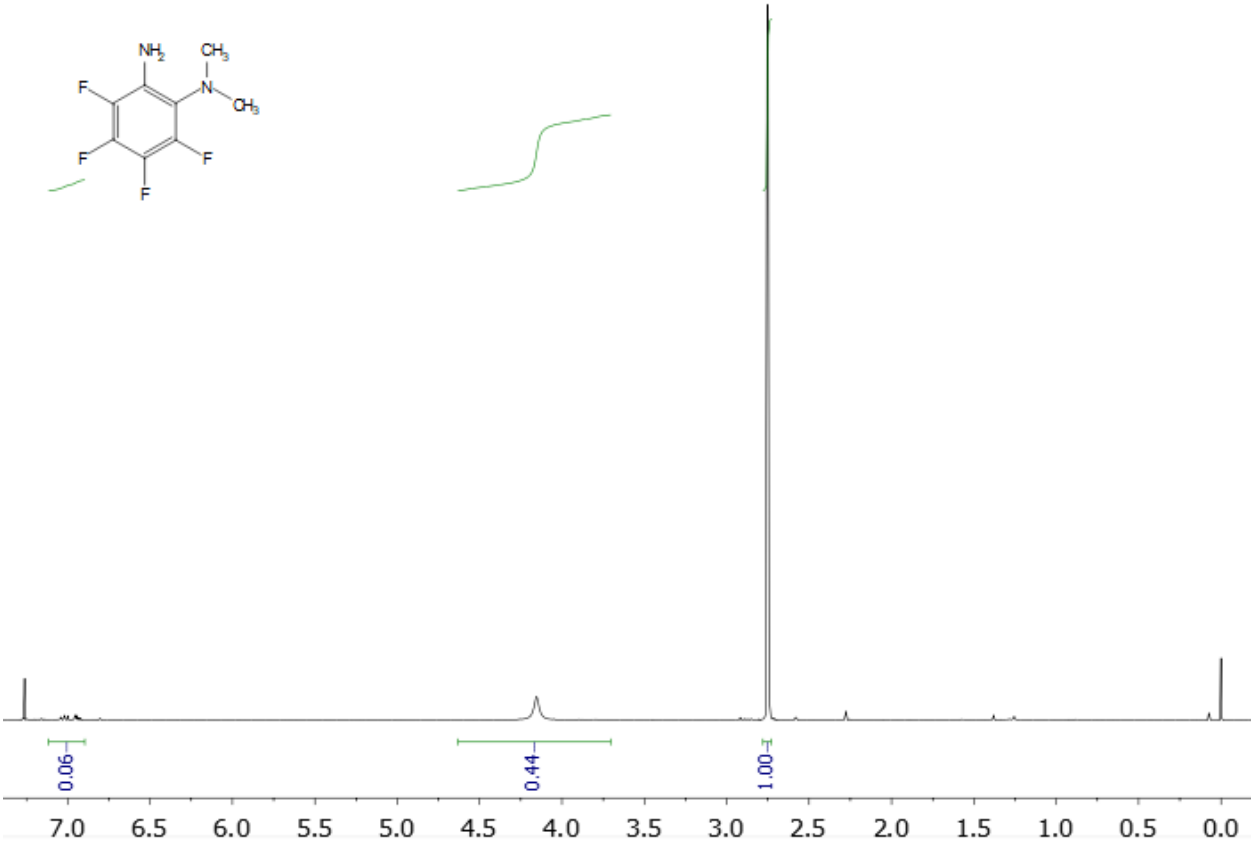

Figure 3.87: ^{19}F spectrum ($CDCl_3$, 400 MHz), of co-eluted 2-dimethylamino-3,4,5,6-tetrafluoroaniline (**2i**), bis(4-fluorophenyl) ether, 2,6-bis(dimethylamino)-3,4,5-trifluoroaniline, and pentafluoroaniline. 2-dimethylamino-3,4,5,6-tetrafluoroaniline is present at 2.74 ppm and 4.15 ppm. Signal from bis(4-fluorophenyl)ether present at 6.94 ppm. Sample referenced to TMS (0.00 ppm).

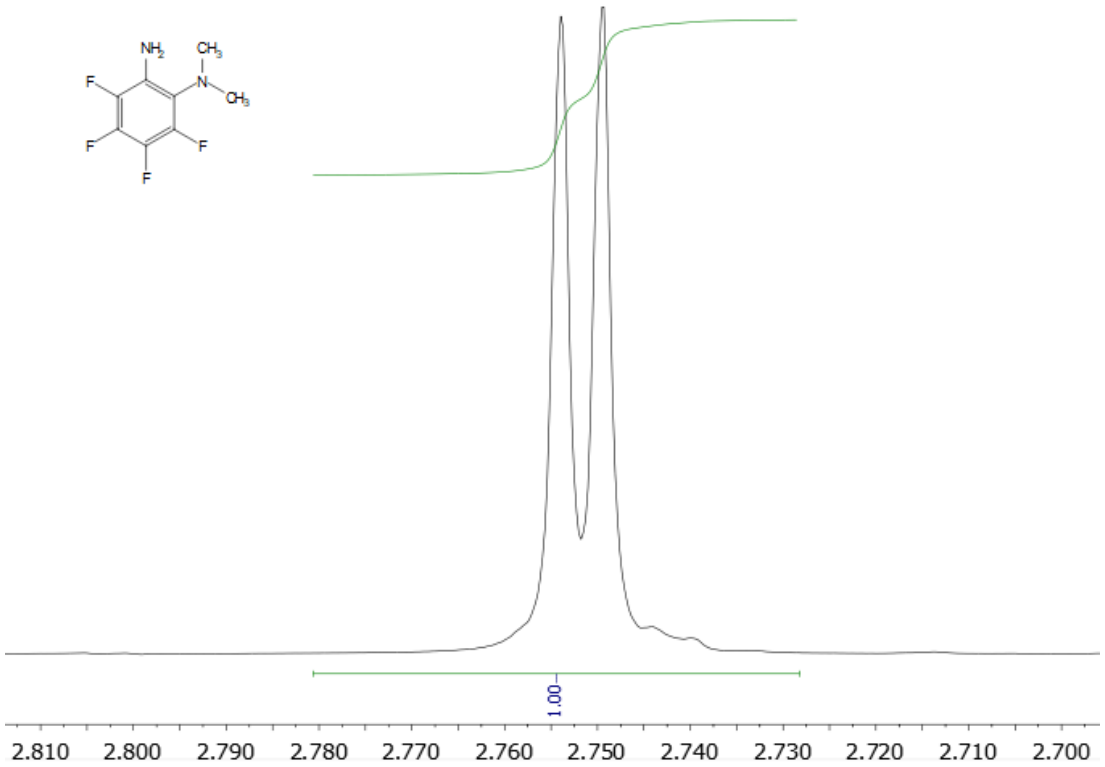

Figure 3.88: ^{1}H NMR spectrum ($CDCl_3$, 400 MHz), methyl signals of coeluted 2-dimethylamino-3,4,5,6-tetrafluoroaniline (major signal, 2.75 ppm) and 2,6-bis(dimethylamino)-3,4,5-trifluoroaniline (minor signal, 2.74 ppm). Both exhibit coupling to their respective 3-fluorines.

2,6-Bis(dimethylamino)-3,4,5-trifluoroaniline

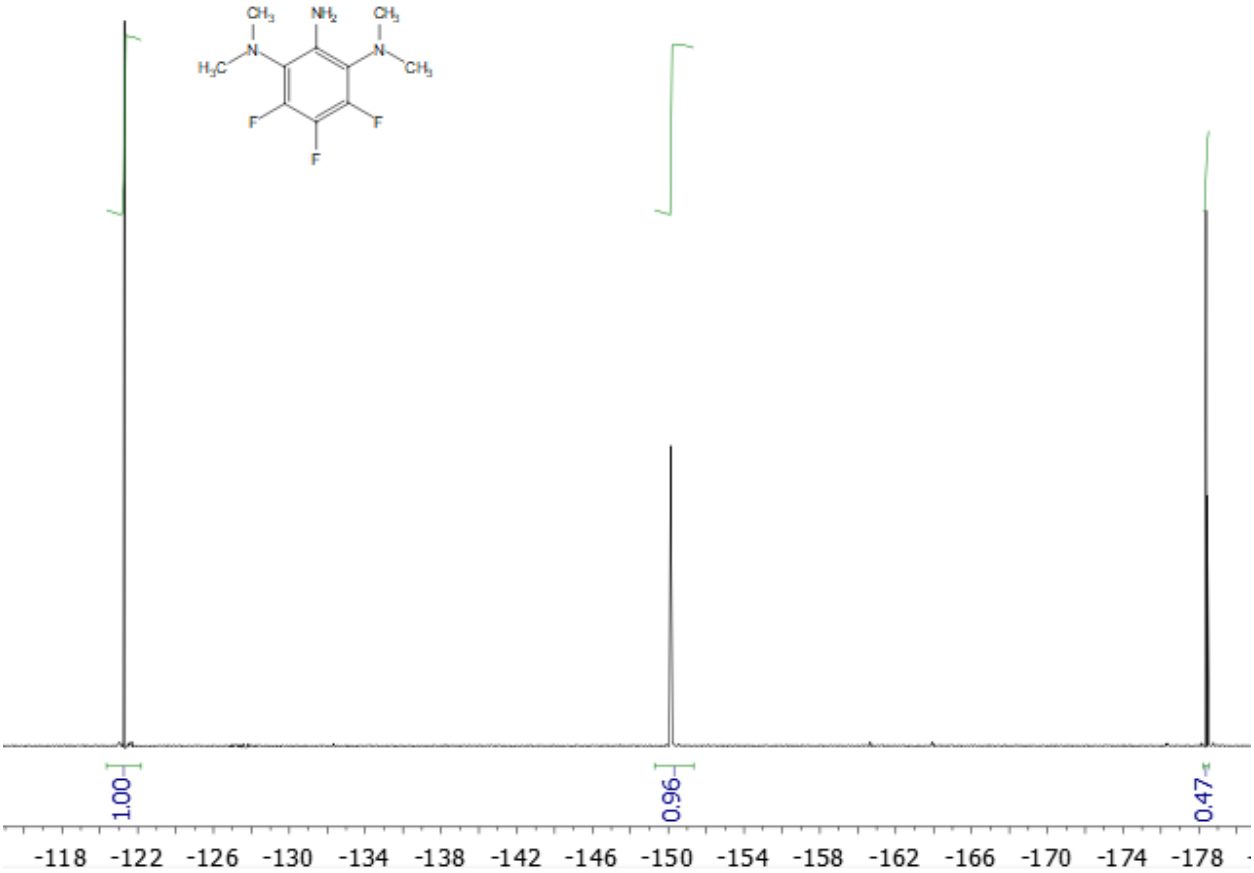

Figure 3.89: ^{19}F NMR spectrum ($CDCl_3$, 376 MHz) of <u>crude</u> 2,6-bis(dimethylamino)-3,4,5-trifluoroaniline (**3i**) (present at −150.2 and −178.4 ppm). Bis(4-fluorophenyl)ether is present at −121.3 ppm.

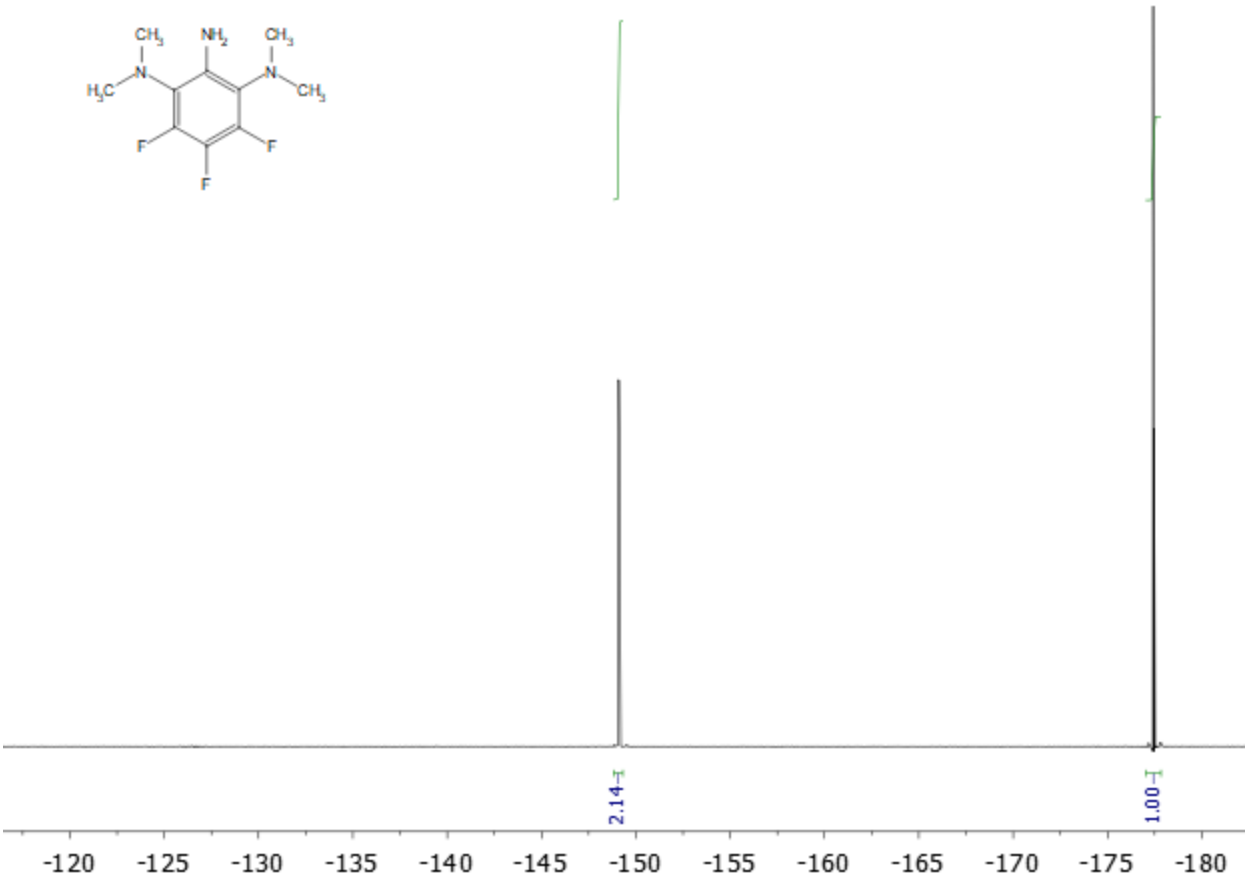

Figure 3.90: ^{19}F NMR spectrum ($CDCl_3$, 376 MHz) of purified 2,6-bis(dimethylamino)-3,4,5-trifluoroaniline (**3i**).

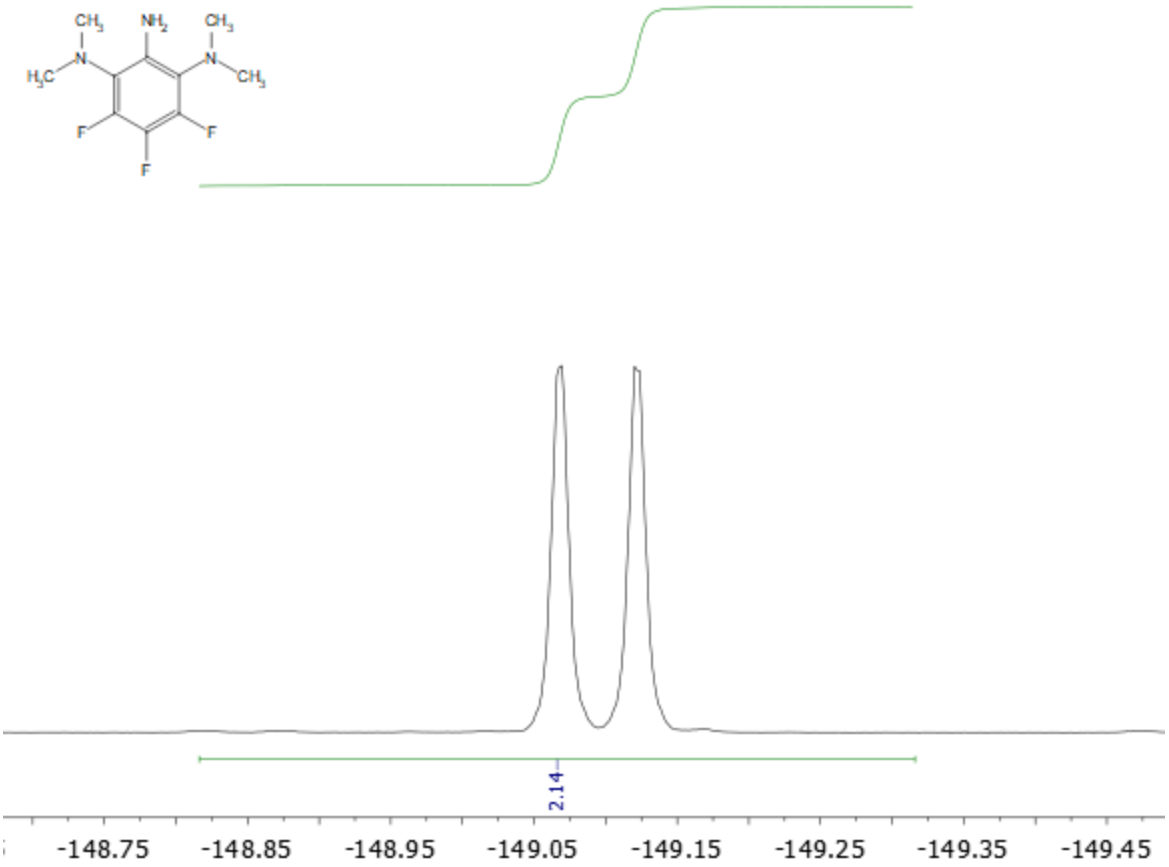

Figure 3.91: ^{19}F NMR spectrum ($CDCl_3$, 376 MHz, expansion) of downfield peak of 2,6-bis(dimethylamino)-3,4,5-trifluoroaniline (**3i**). Simulation was not needed because the spectrum is first-order.

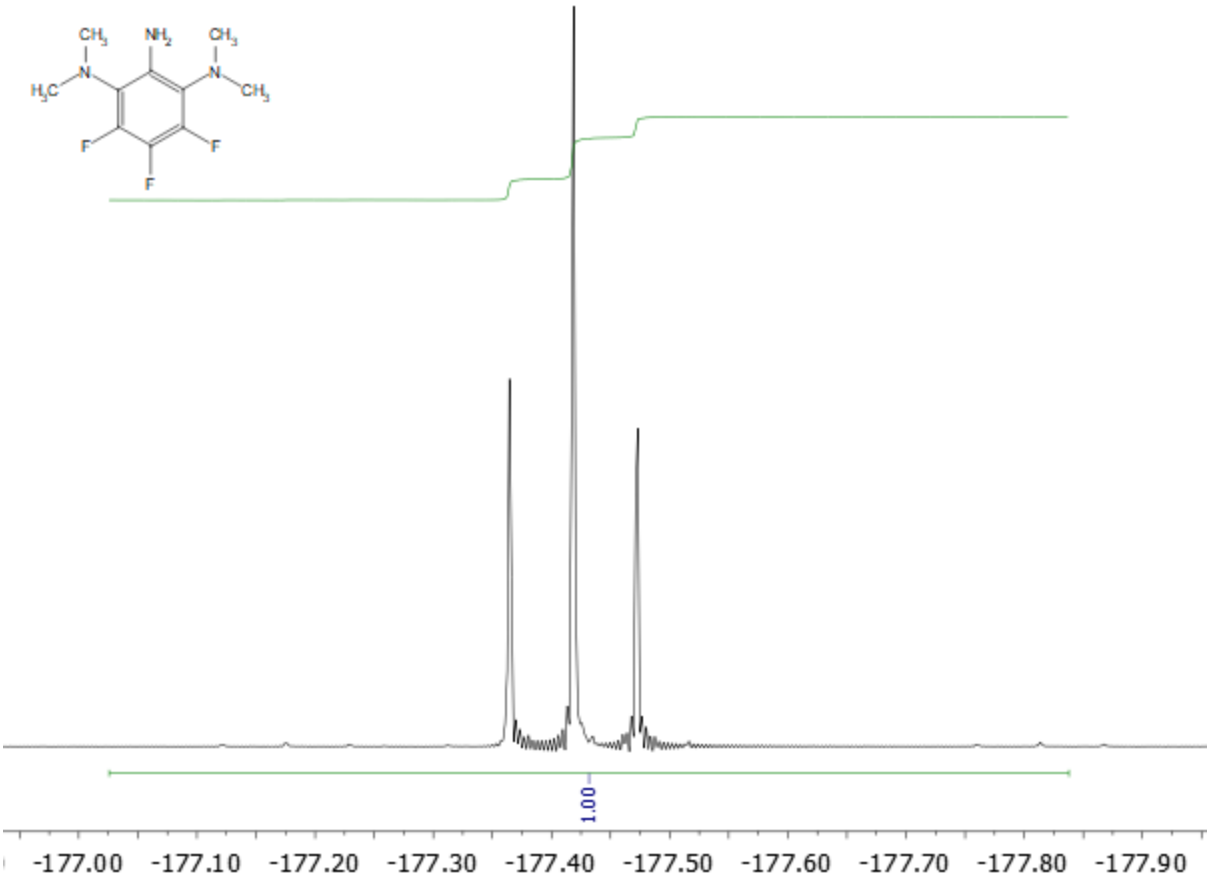

Figure 3.92: ^{19}F NMR spectrum ($CDCl_3$, 376 MHz, expansion) of upfield peak of 2,6-bis(dimethylamino)-3,4,5-trifluoroaniline (**3i**). Simulation was not needed because the spectrum is first-order.

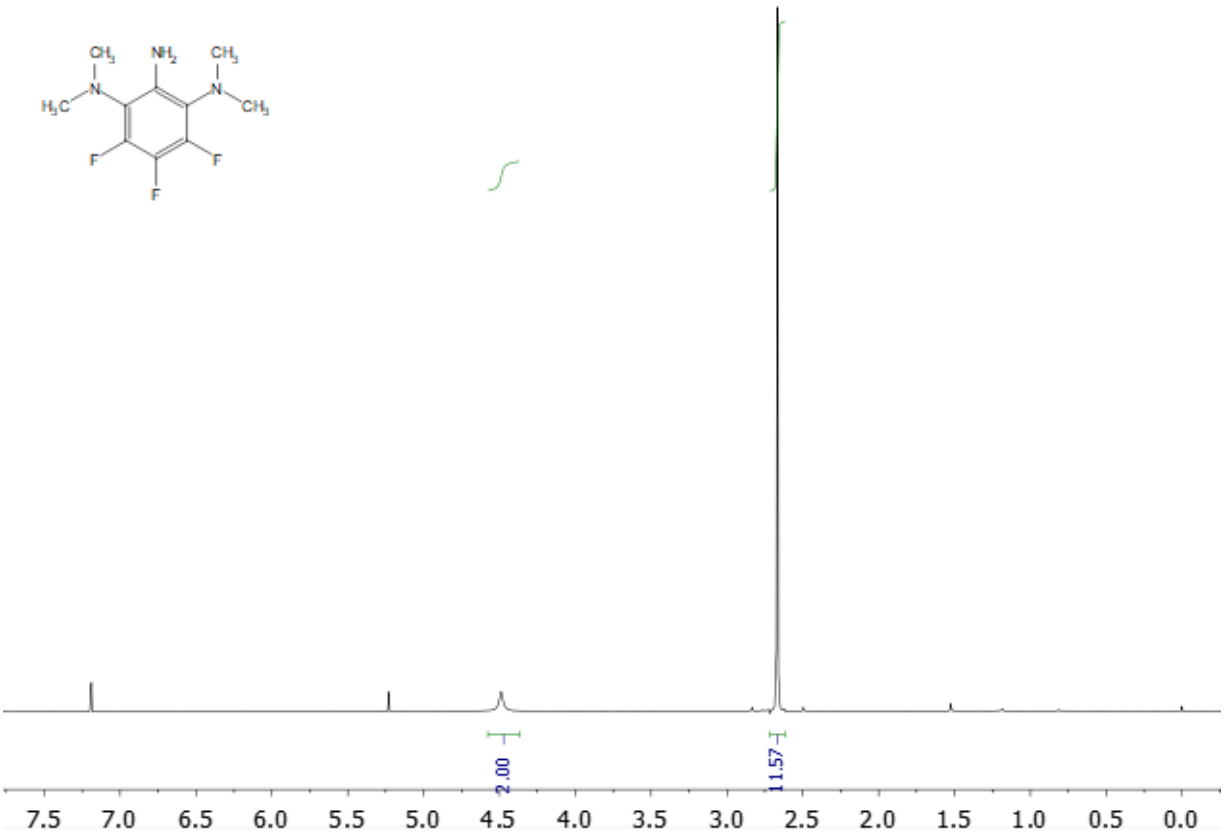

Figure 3.93: ^{1}H NMR spectrum ($CDCl_3$, 400 MHz), of purified 2,6-bis(dimethylamino)-3,4,5-trifluoroaniline (**3i**), with peaks present at 2.74 and 4.56 ppm. Also present is Cl_2CH_2 at 5.30 ppm. Sample is referenced to $CHCl_3$ (7.26 ppm).

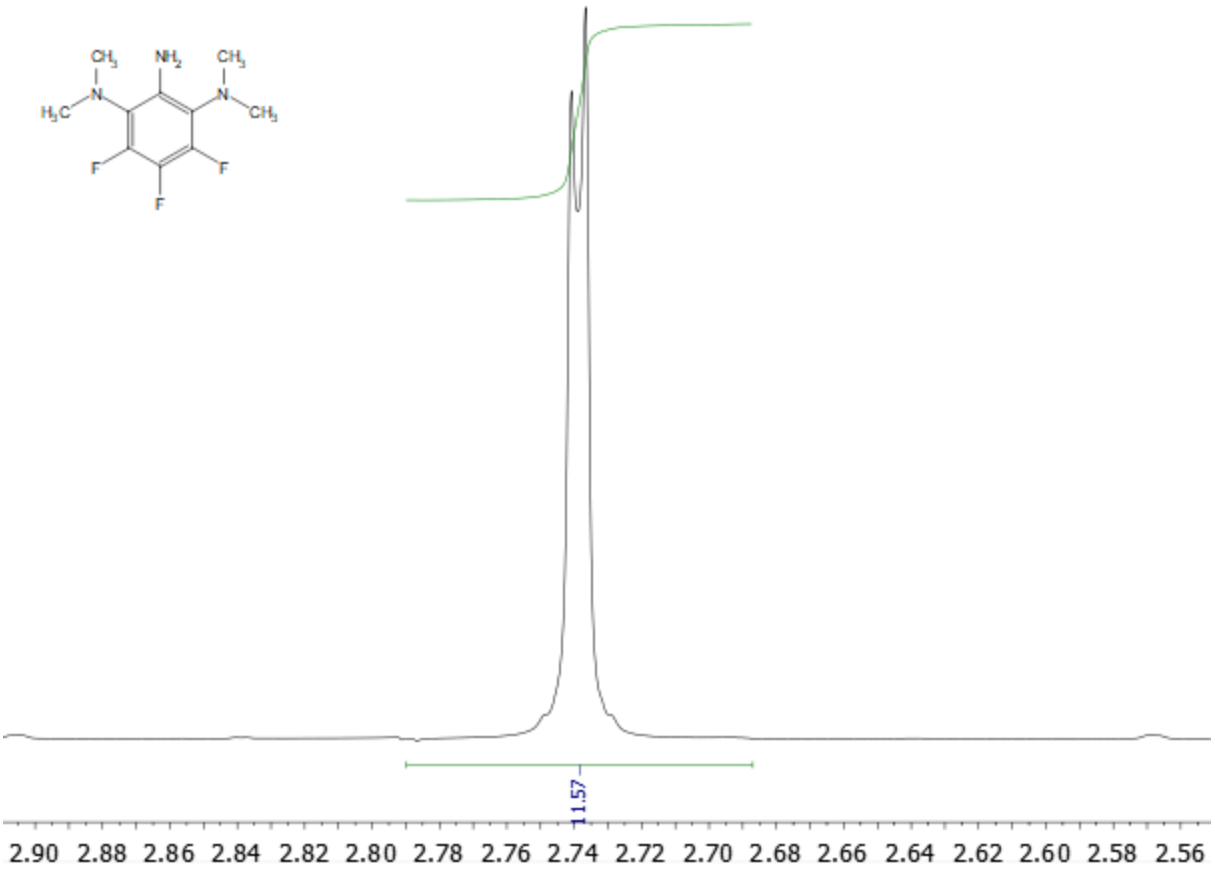

Figure 3.94: ^{1}H NMR spectrum ($CDCl_3$, 400 MHz), methyl signal of purified 2,6-bis(dimethylamino)-3,4,5-trifluoroaniline (**3i**). Coupling to the 3-fluorine is observed.

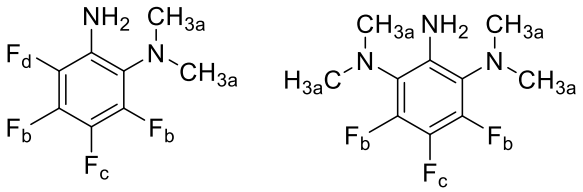

2i **3i**

Figure 3.95: Structures of 2-dimethylamino-3,4,5,6-tetrafluoroanilne (**2i)** and2,6-bis(dimethylamino)-3,4,5-trifluoroaniline (**3i**) showing nuclei labeled for the simulations described in Tables 3.13 and 3.14.

Table 3.13: Chemical shifts and coupling constants for **2i** used to generate the simulated spectra shown in Figures 3.82 through 3.88.

		Coupling Constants (Hz)				
Nucleus	Chemical Shift (ppm)	a	b	c	d	e
a (NMe_2)	2.75					
b (F)	-151.9	1.8				
c (F)	-176.2	0.0	21.0			
d (F)	-163.9	0.0	0.0	21.4		
e (F)	-163.7	0.0	7.4	7.1	21.4	
NH_2	4.15					

Table 3.14: Chemical shifts and coupling constants for **3i** used to generate the simulated spectra shown in Figures 3.89 through 3.94.

		Coupling Constants (Hz)		
Nucleus	Chemical 3.hift (ppm)	a	b	c
a (NMe_2)	2.74			
b (F)	−150.2	2.0		
c (F)	−178.4	0.0	21.0	
NH_2	4.56			

2-Dimethylamino-*N*-ethyl-6-fluoroaniline

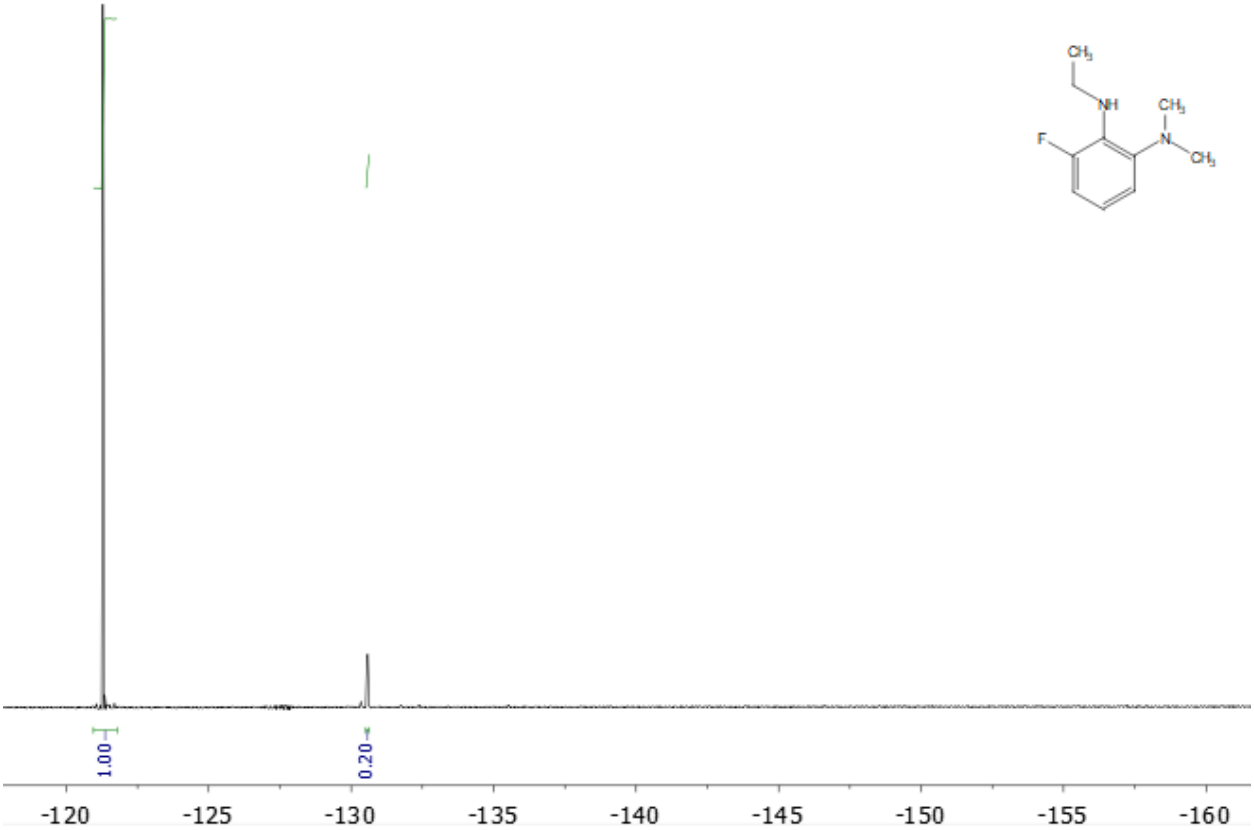

Figure 3.96: ^{19}F NMR spectrum ($CDCl_3$, 376 MHz) of <u>crude</u> 2-dimethylamino-*N*-ethyl-6-fluoroaniline (**8**) with product at −130.6 ppm. Bis(4-fluorophenyl)ether is present at −121.3 ppm.

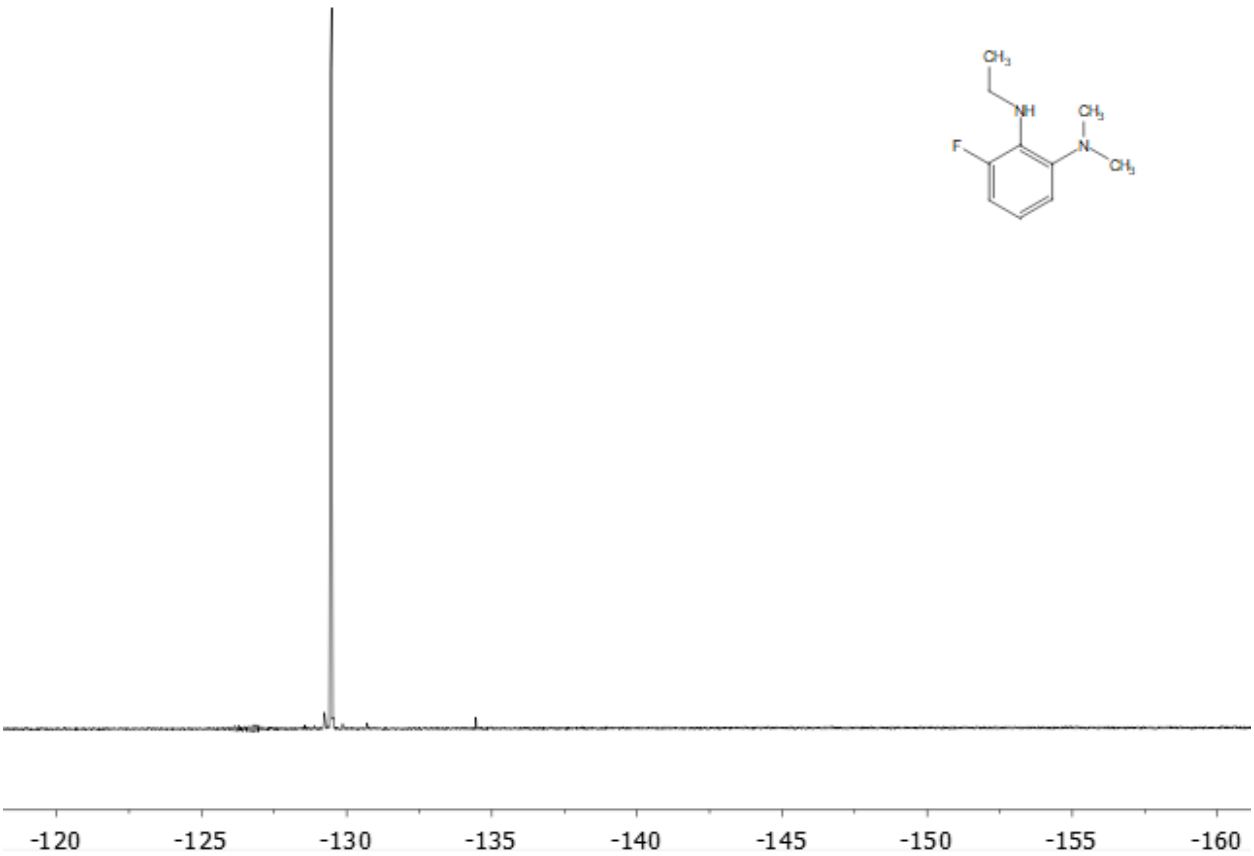

Figure 3.97: ^{19}F NMR spectrum ($CDCl_3$, 376 MHz) of column-purified 2-dimethylamino-N-ethyl-6-fluoroaniline (**8**).

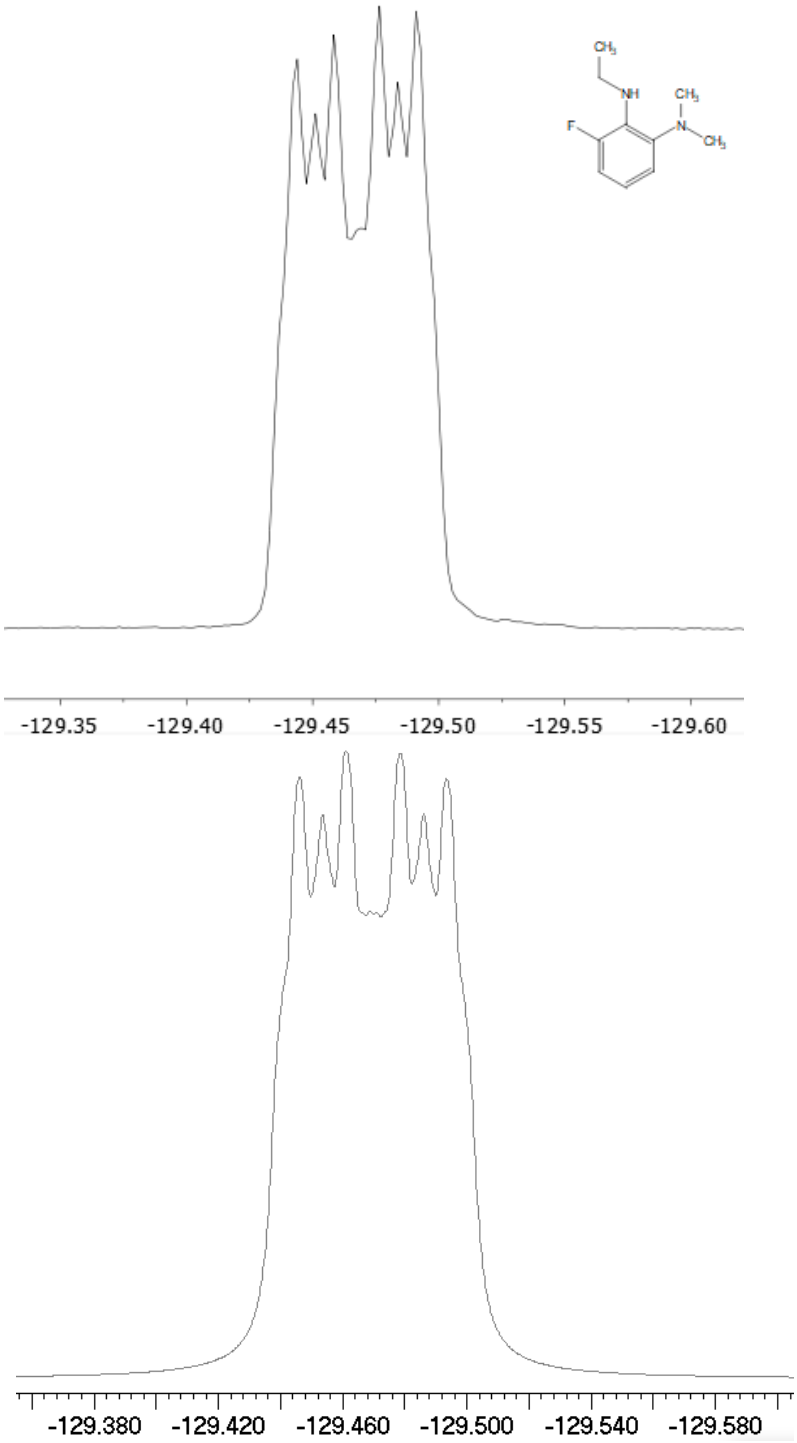

Figure 3.98: ^{19}F NMR spectra ($CDCl_3$, 376 MHz, expansion) of of 2-dimethylamino-N-ethyl-6-fluoroaniline (**8**). **Upper**: Experimental spectrum with polynomial baseline correction applied. **Lower**: Simulated (a natural linewidth of 1.9 Hz was estimated.)

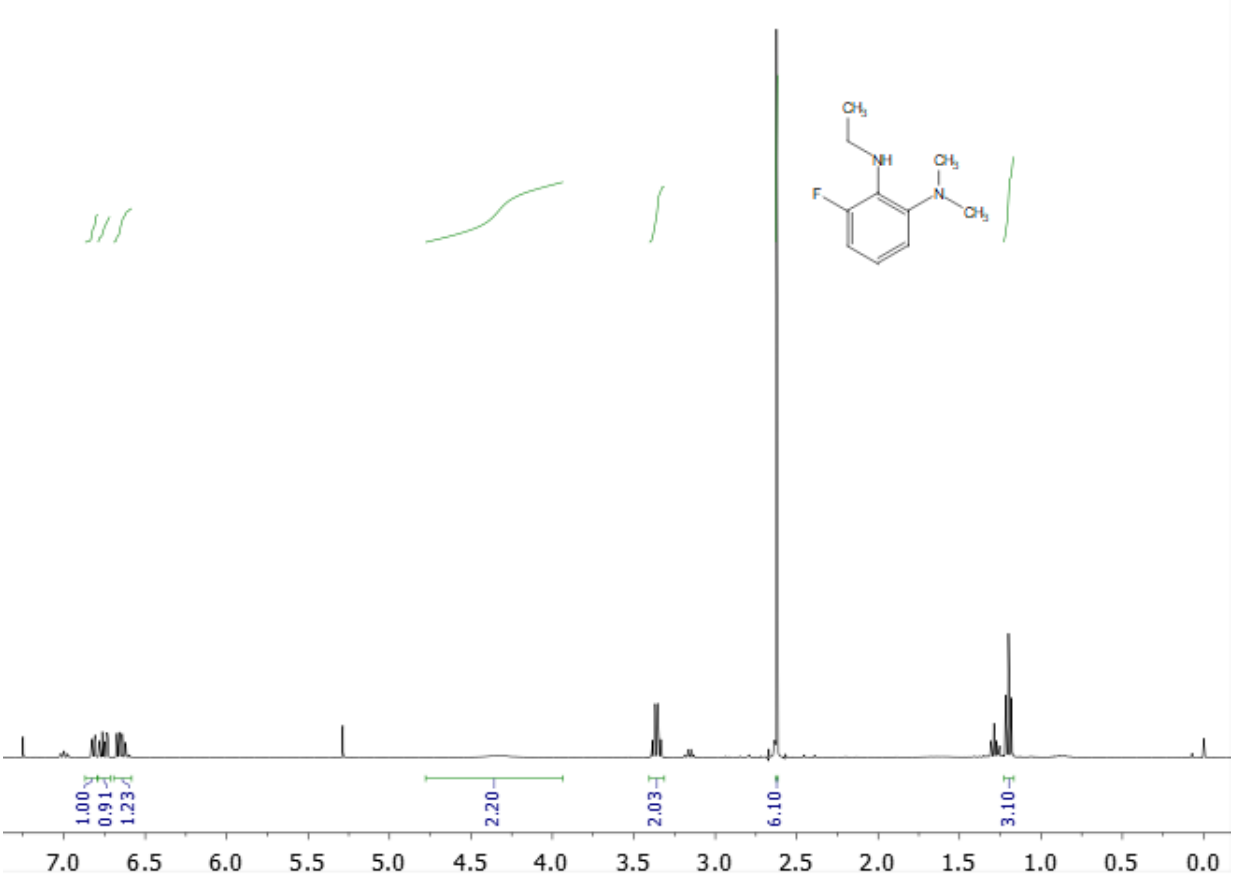

Figure 3.99: ^{1}H NMR spectrum ($CDCl_3$, 400 MHz), of column-purified 2-dimethylamino-*N*-ethyl-6-fluoroaniline (**8**), δ 6.82 (CH), 6.76 (CH), 6.65 (CH), 4.33 (NH_2), 3.36 (CH_2), 2.62 (NMe_2), 1.20 (CH_3). Peaks at 7.00 ppm, 3.16 ppm, and 1.29 ppm arise from unidentified impurities. Also present are $CHCl_3$ at 7.25 ppm and Cl_2CH_2, at 5.29 ppm.

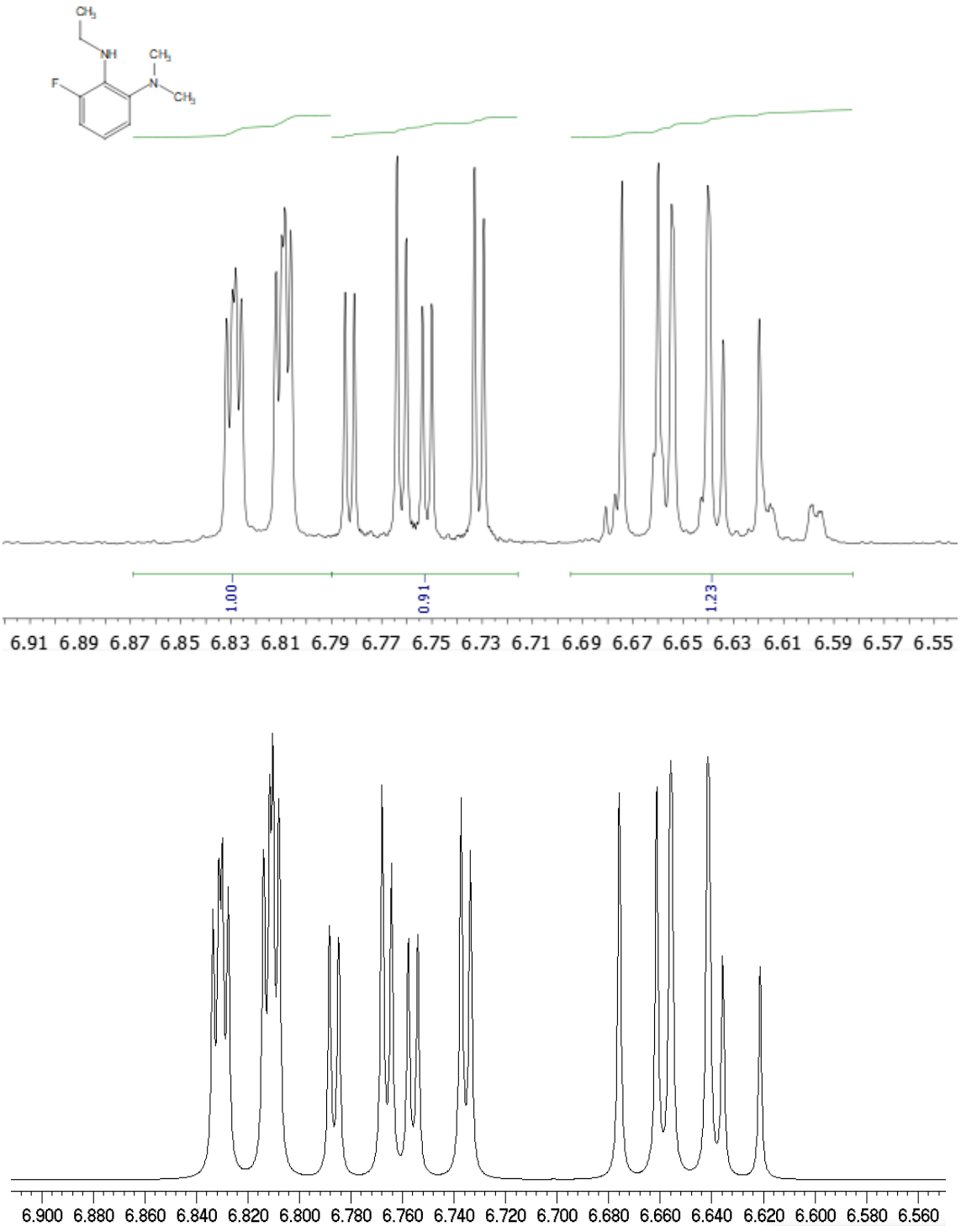

Figure 3.100: ^{1}H NMR spectra ($CDCl_3$, 400 MHz, expansion) of aromatic region of 2-dimethylamino-N-ethyl-6-fluoroaniline (**8**). **Upper**: Experimental spectrum with polynomial baseline correction applied. Unidentified impurities are visible in the range 6.69-6.59 ppm. **Lower**: Simulated; a natural linewidth of 0.5 Hz was estimated.

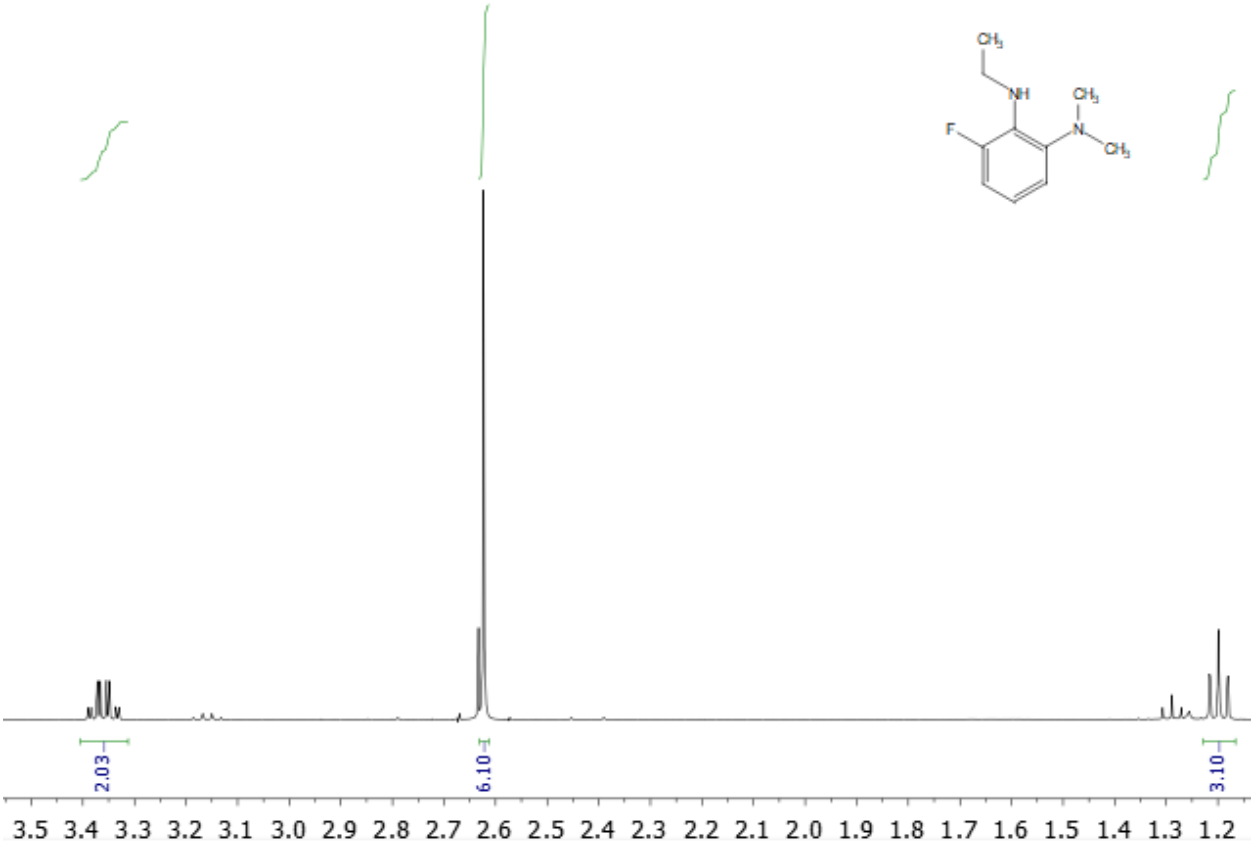

Figure 3.101: ^{1}H NMR spectrum ($CDCl_3$, 400 MHz), expansion of the aliphatic signal of 2-dimethylamino-*N*-ethyl-6-fluoroaniline (**8**). Unidentified impurities are visible.

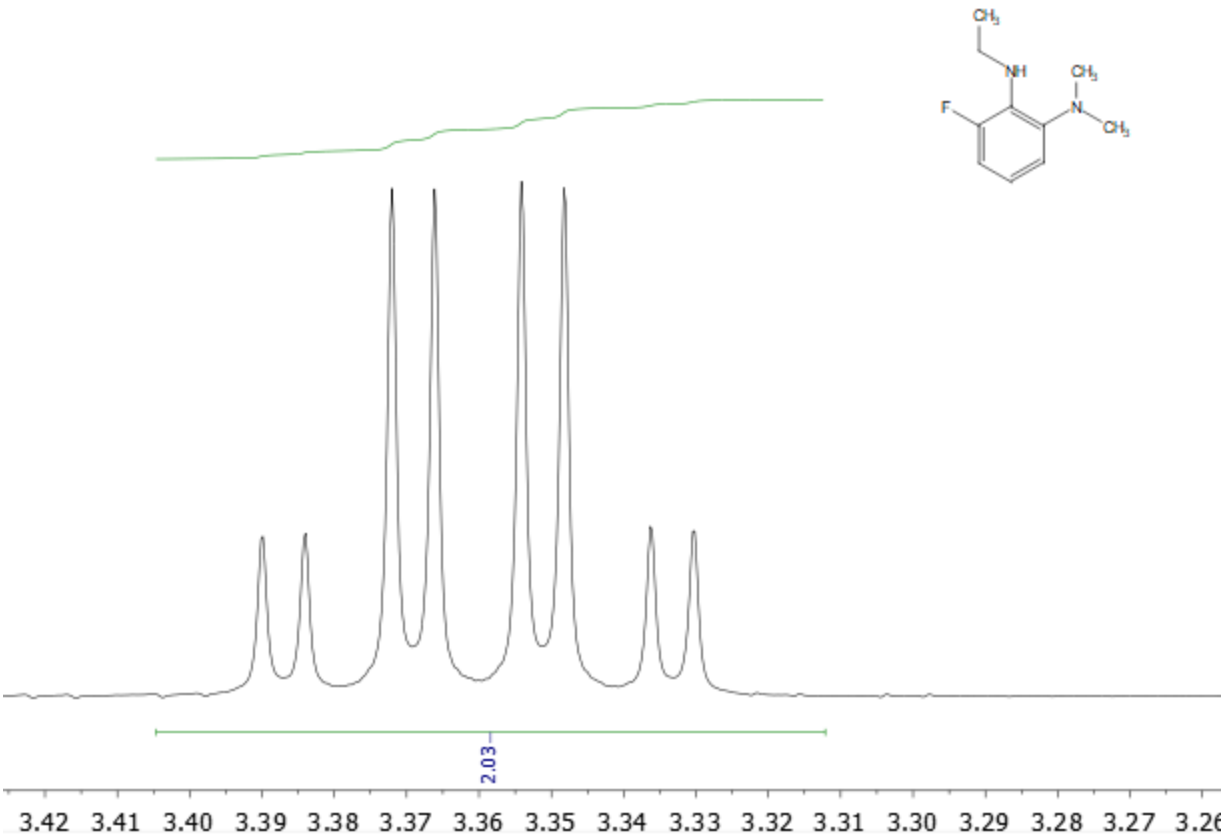

Figure 3.102: ^{1}H NMR spectrum ($CDCl_3$, 400 MHz) of 2-dimethylamino-*N*-ethyl-6-fluoroaniline; expansion of the methylene signal (**8**).

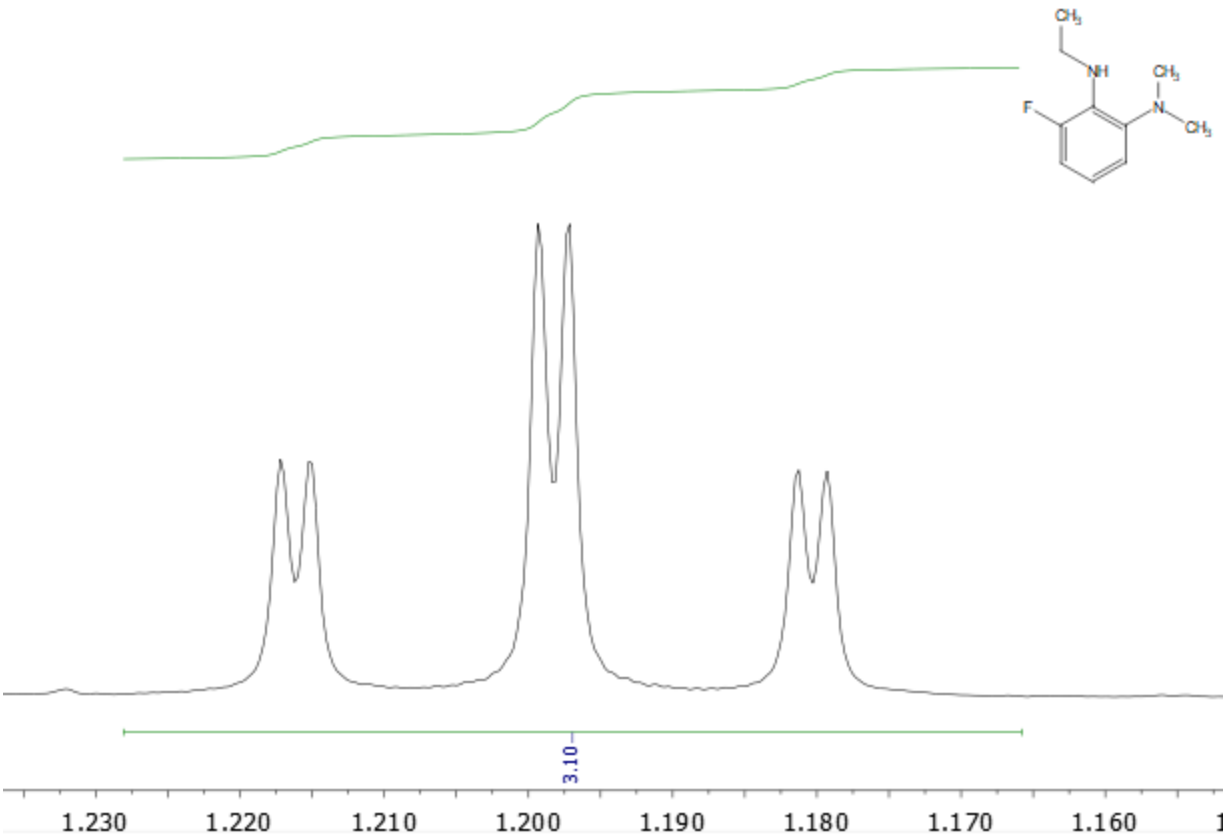

Figure 3.103: ^{1}H NMR spectrum ($CDCl_3$, 400 MHz), expansion of the methyl signal of 2-dimethylamino-*N*-ethyl-6-fluoroaniline (**8**).

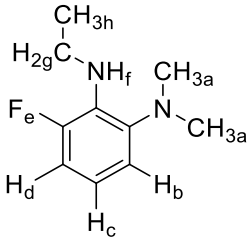

Figure 3.104: Structure of 2-dimethylamino-N-ethyl-6-fluoroaniline (**8**) showing nuclei labeled for the simulation described in Table 3.15.

Table 3.15: Chemical shifts and coupling constants for 2-dimethyl-amino-*N*-ethyl-6-fluoroaniline used to generate the simulated spectra shown in Figures 3.96 through 3.103.

		Coupling Constants (Hz)						
Nucleus	Chemical Shift (ppm)	a	b	c	d	e	f	g
a (NMe_2)	2.62							
b (H)	6.82	0.0						
c (H)	6.65	0.0	8.0					
d (H)	6.76	0.0	1.4	8.2				
e (F)	−121.3	0.0	0.9	5.7	12.4			
f (NH)	4.33							
g (CH_2)	3.36	0.0	0.0	0.0	0.0	2.4		
h (CH_3)	1.20	0.0	0.0	0.0	0.0	0.8		7.2

2-Dimethylamino-6-fluorophenol

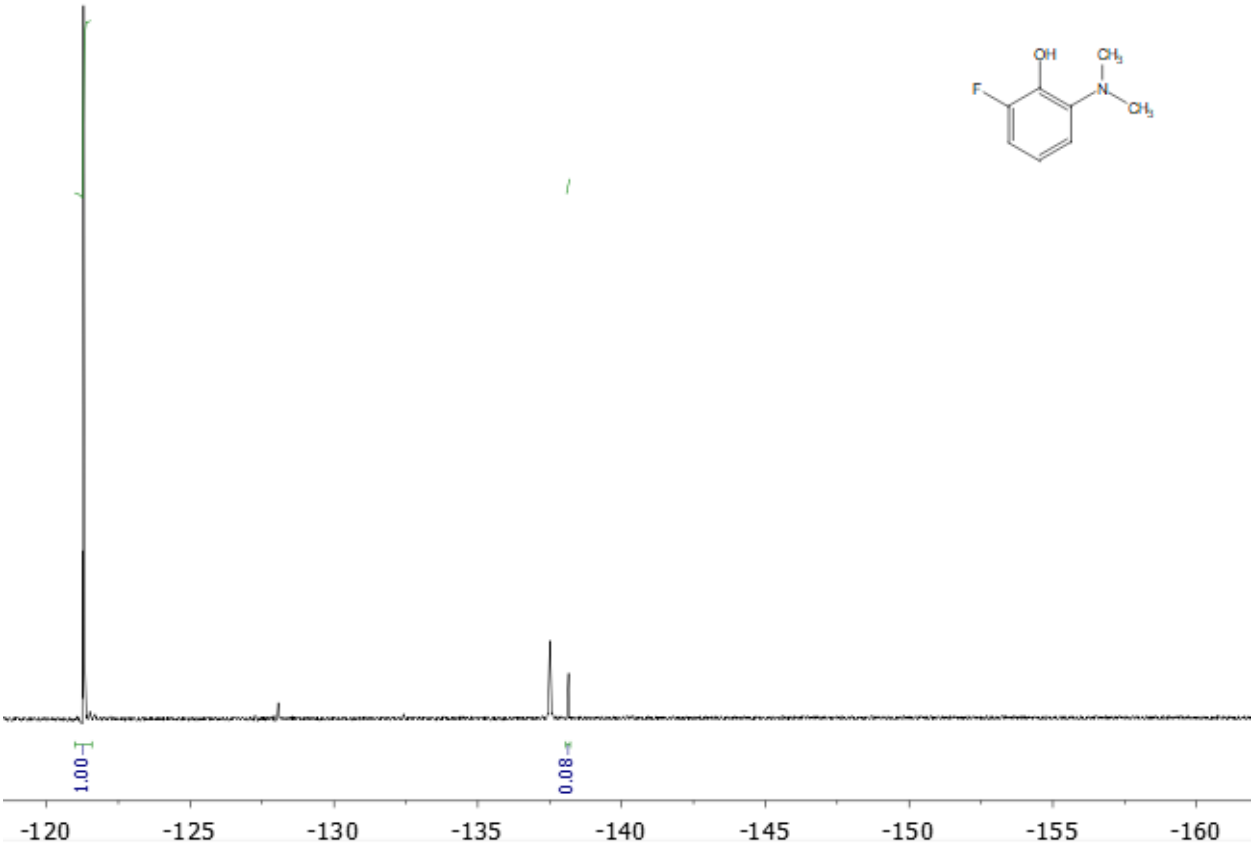

Figure 3.105: ^{19}F NMR spectrum ($CDCl_3$, 376 MHz) of <u>crude</u> 2-dimethylamino-6-fluorophenol (**10**) with product at −137.1 ppm. Bis(4-fluorophenyl)ether is present at −121.3 ppm.

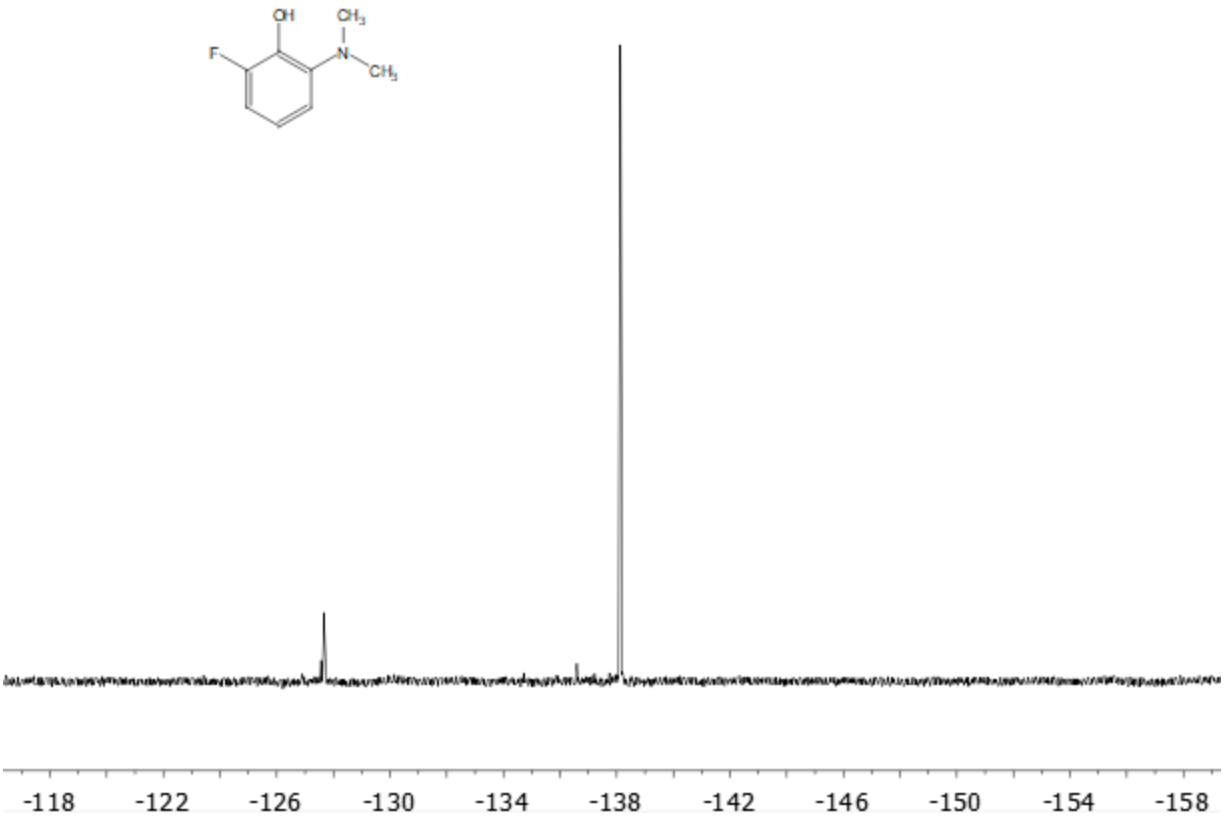

Figure 3.106: ^{19}F NMR spectrum ($CDCl_3$, 376 MHz) of column-purified 2-dimethylamino-6-fluorophenol (**10**). A multipoint baseline correction was applied to the frequency-domain spectrum.

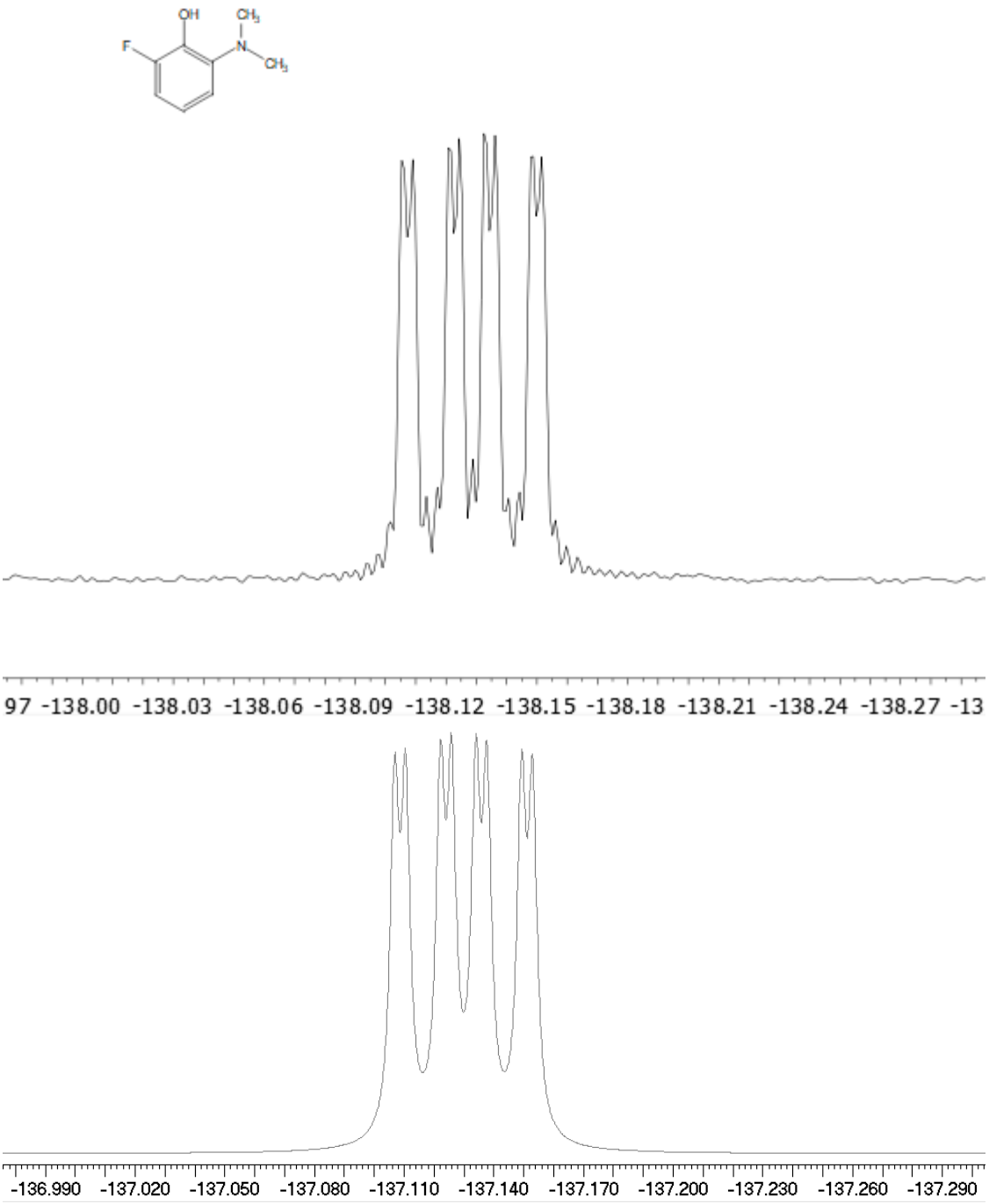

Figure 3.107: ^{19}F NMR spectra ($CDCl_3$, 375 MHz, expansion) of 2-dimethylamino-6-fluorophenol (**10**). **Upper**: Experimental spectrum with multipoint polynomial baseline correction, zero-filled to 256k, and with 0.25 Hz of line broadening apodization applied to the FID. **Lower**: Simulated; a natural linewidth of 1.3 Hz was estimated.

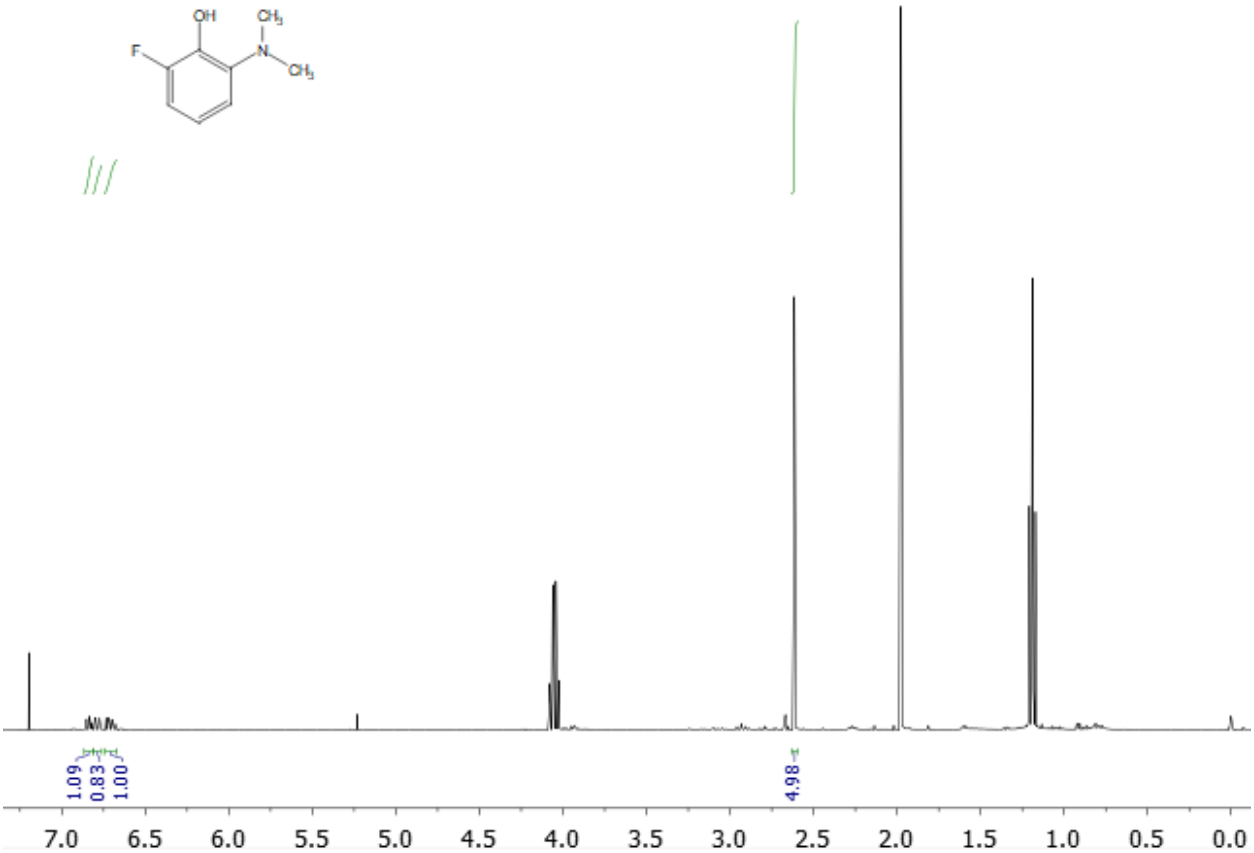

Figure 3.108: ^{1}H NMR spectrum ($CDCl_3$, 400 MHz), of purified 2-dimethylamino-6-fluorophenol (**10**), δ 6.90 (CH), 6.86 (CH), 6.78 (CH), 2.68 (NMe_2). Also present is Cl_2CH_2, at 5.30 ppm, $CHCl_3$, and ethyl acetate (4.12 ppm, 2.05 ppm, and 1.26 ppm).

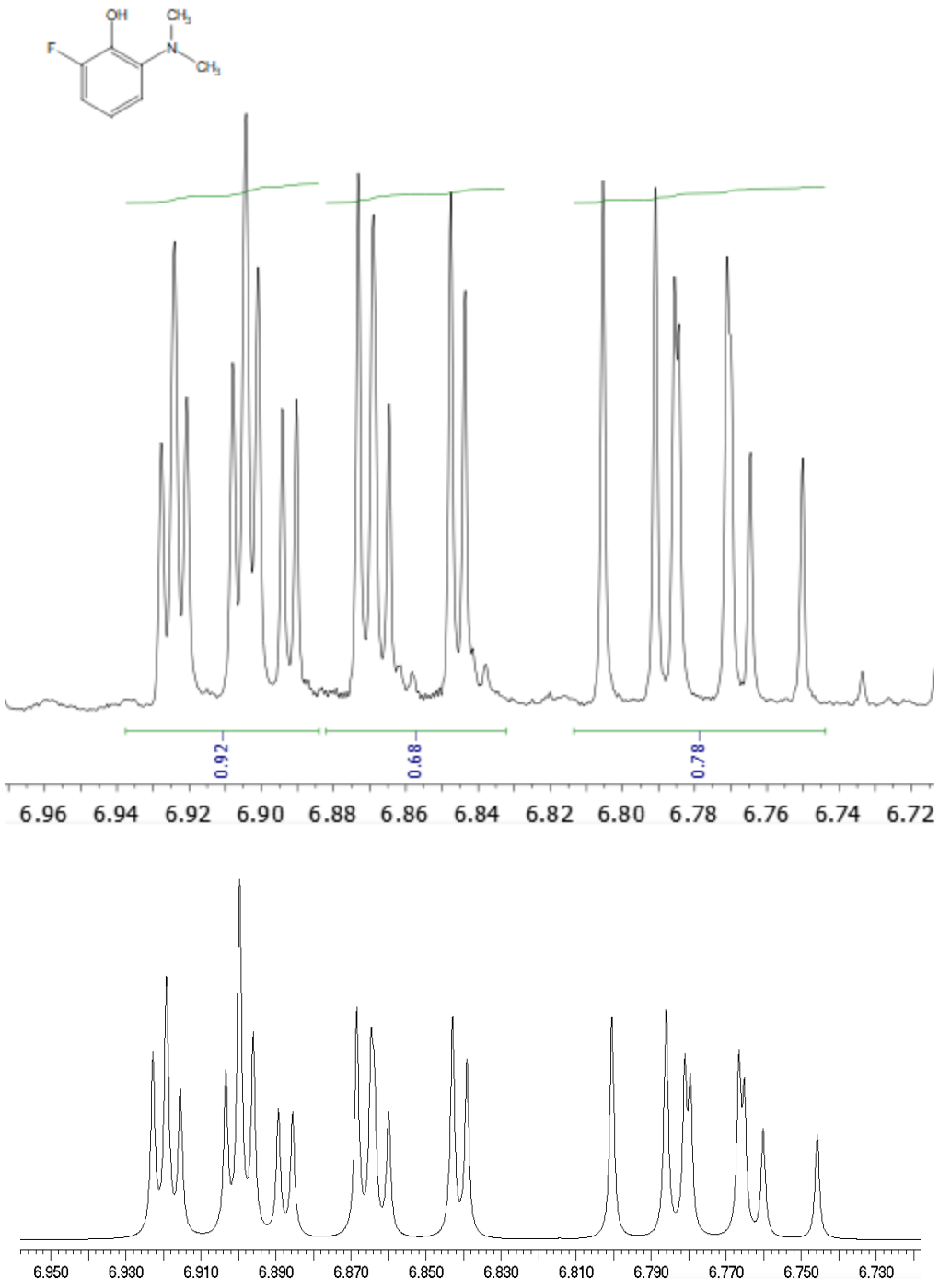

Figure 3.109: ^{1}H NMR spectra ($CDCl_3$, 400 MHz, expansion) of aromatic region of 2-dimethylamino-6-fluorophenol (**10**). **Upper**: Experimental spectrum with multipoint polynomial baseline correction applied. **Lower**: Simulated; a natural linewidth of 0.5 Hz was estimated.

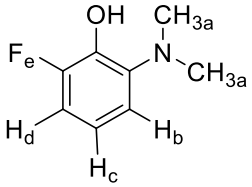

Figure 3.110: Structure of 2-dimethylamino-6-fluorophenol (**10**) showing nuclei labeled for the simulation described in Table 3.16.

Table 3.16: Chemical shifts and coupling constants for 2-dimethylamino-6-fluorophenol used to generate the simulated spectra shown in Figures 3.105 through 3.109.

		Coupling Constants (Hz)				
Nucleus	Chemical Shift (ppm)	a	b	c	d	e
a (NMe_2)	2.68					
b (H)	6.909	0.0				
c (H)	6.78	0.0	7.9			
d (H)	6.863	0.0	1.4	8.3		
e (F)	−137.1	0.0	1.4	5.7	10.3	
OH	4.12					

Note that the model shown in Table 3.16 uses two chemical shifts that are adjusted at the ±0.001 ppm level. This fine adjustment was necessary to model the non-first-order features of the spectra.

Spectra for Competitive Reaction-Rate Experiments

Difluoroanilines

Nominally equal quantities of the four difluoroanilines were reacted with a ten-fold excess of $Ti(NMe_2)_4$ over the course of four hours at 80 °C.

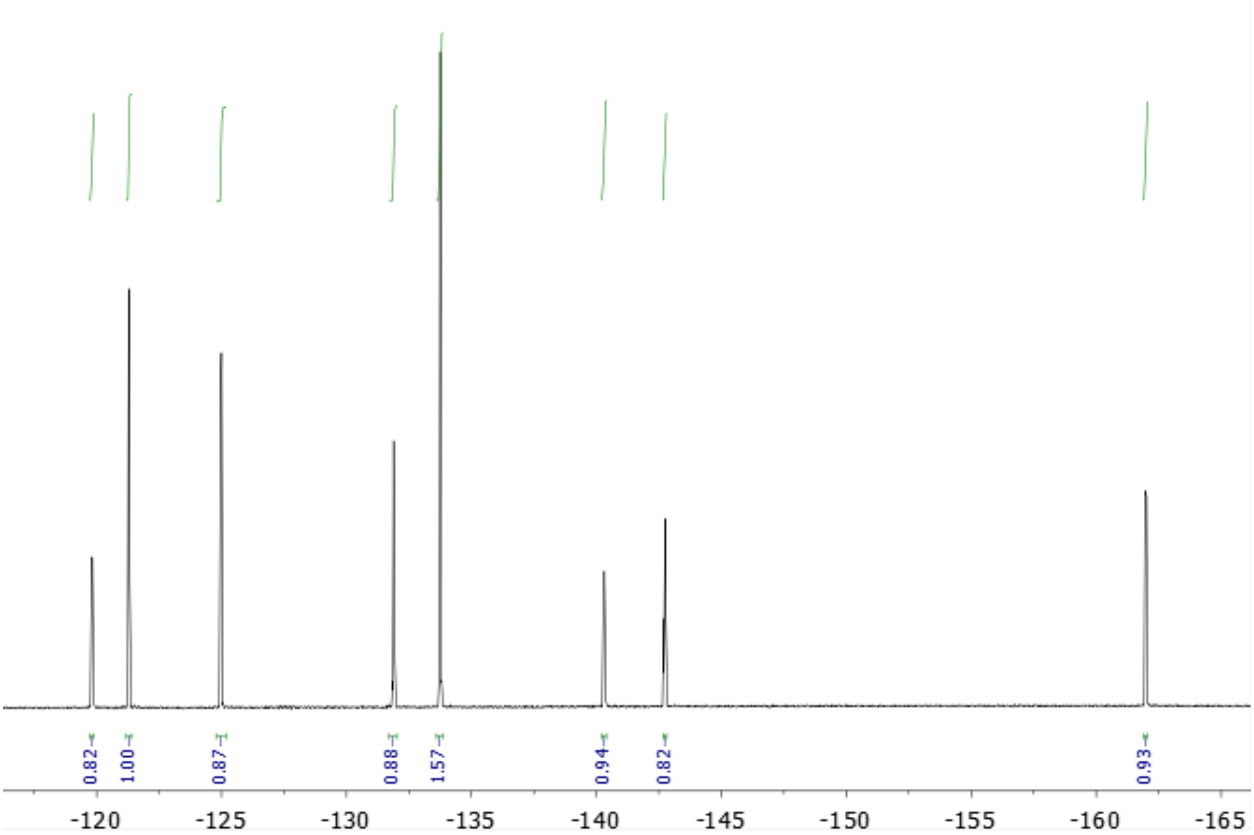

Figure 3.111: ^{19}F NMR spectrum ($CDCl_3$, 376 MHz) of the starting material for the competitive kinetics experiment, referenced to bis(4-fluorophenyl)ether (−121.29 ppm). Present are 2,3-difluoroaniline (−140.3 ppm and −162.0 ppm), 2,4-difluoroaniline (−125.0 ppm and −131.9 ppm), 2,5-difluoroaniline (−119.8 ppm −140.3 ppm), and 2,6-difluoroaniline (−133.8 ppm).

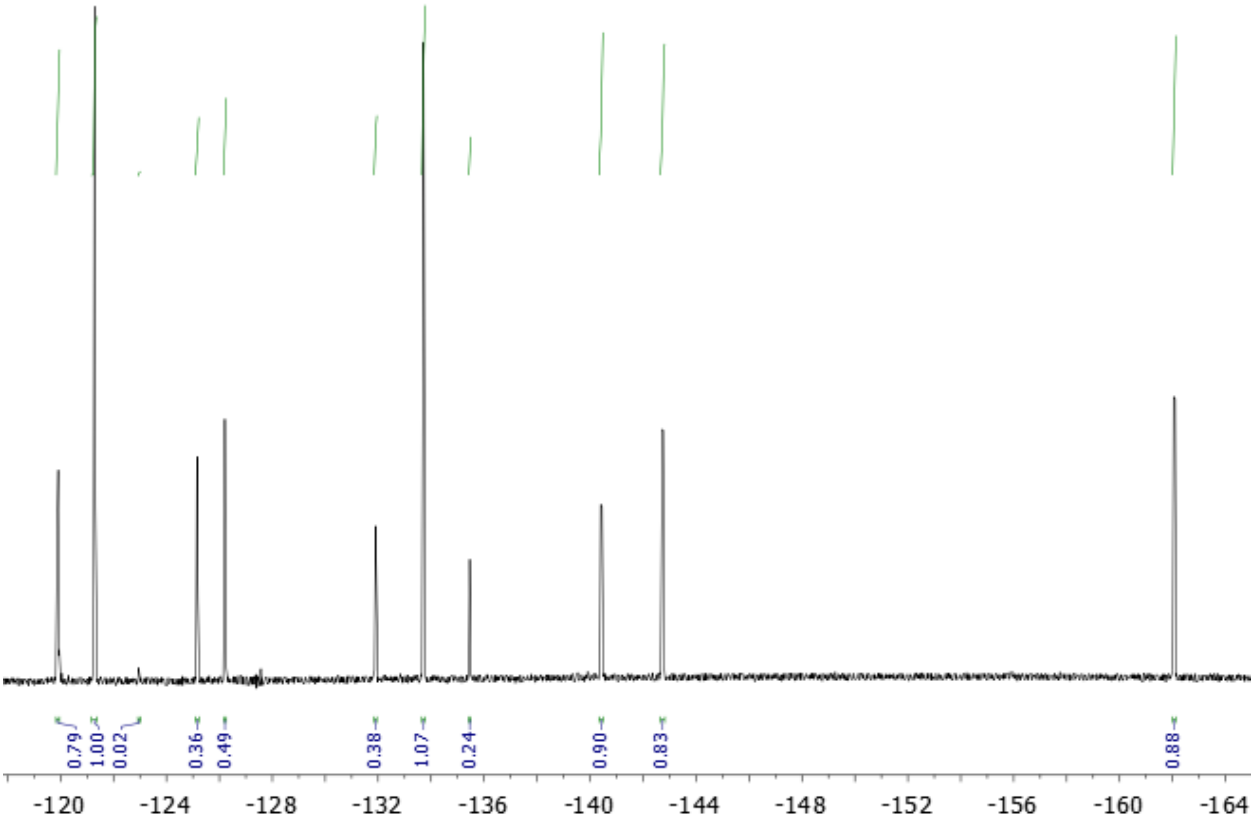

Figure 3.112: ^{19}F NMR spectrum ($CDCl_3$, 376 MHz), of the competitive reaction after 1 h, referenced to bis(4-fluorophenyl)ether (−121.3 ppm). Present are 2,3-difluoroaniline (−140.4 ppm and −162.1 ppm), 2,4-difluoroaniline (−125.2 ppm and −131.9 ppm), 2-dimethylamino-4-fluoroaniline (−126.2 ppm), 2,5-difluoroaniline (−119.9 ppm and −142.7 ppm), 2,6-difluoroaniline (−133.7 ppm), 2-dimethylamino-6-fluoroaniline (−135.5 ppm).

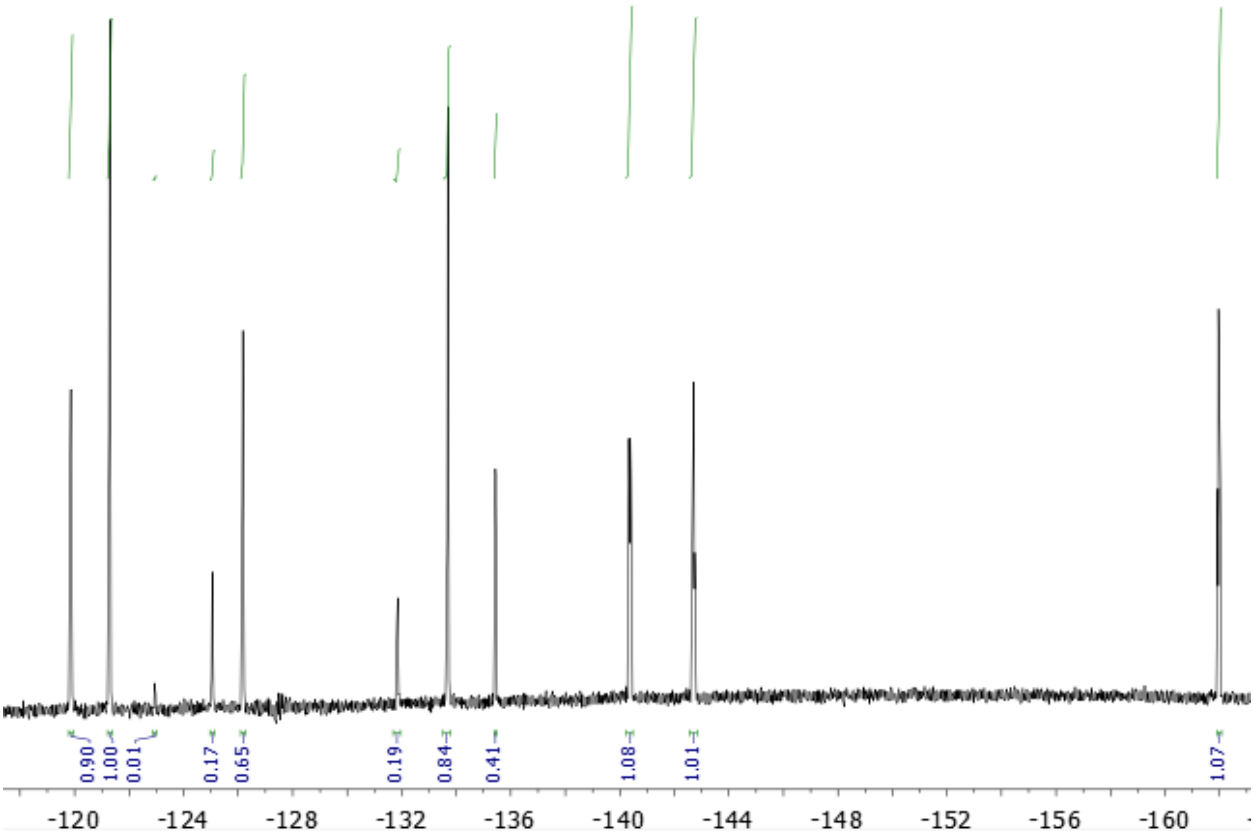

Figure 3.113: ^{19}F NMR spectrum ($CDCl_3$, 376 MHz), of the competitive reaction after 2 h, referenced to bis(4-fluorophenyl)ether (−121.3 ppm). Present are 2,3-difluoroaniline (−140.4 ppm and −162.0 ppm), 2,4-difluoroaniline (−125.1 and −131.9 ppm), 2-dimethylamino-4-fluoroaniline (−126.2 ppm), 2,5-difluoroaniline (−119.9 ppm and −140.7 ppm), 2,6-difluoroaniline (−133.7 ppm), 2-dimethylamino-6-fluoroaniline (−135.4 ppm).

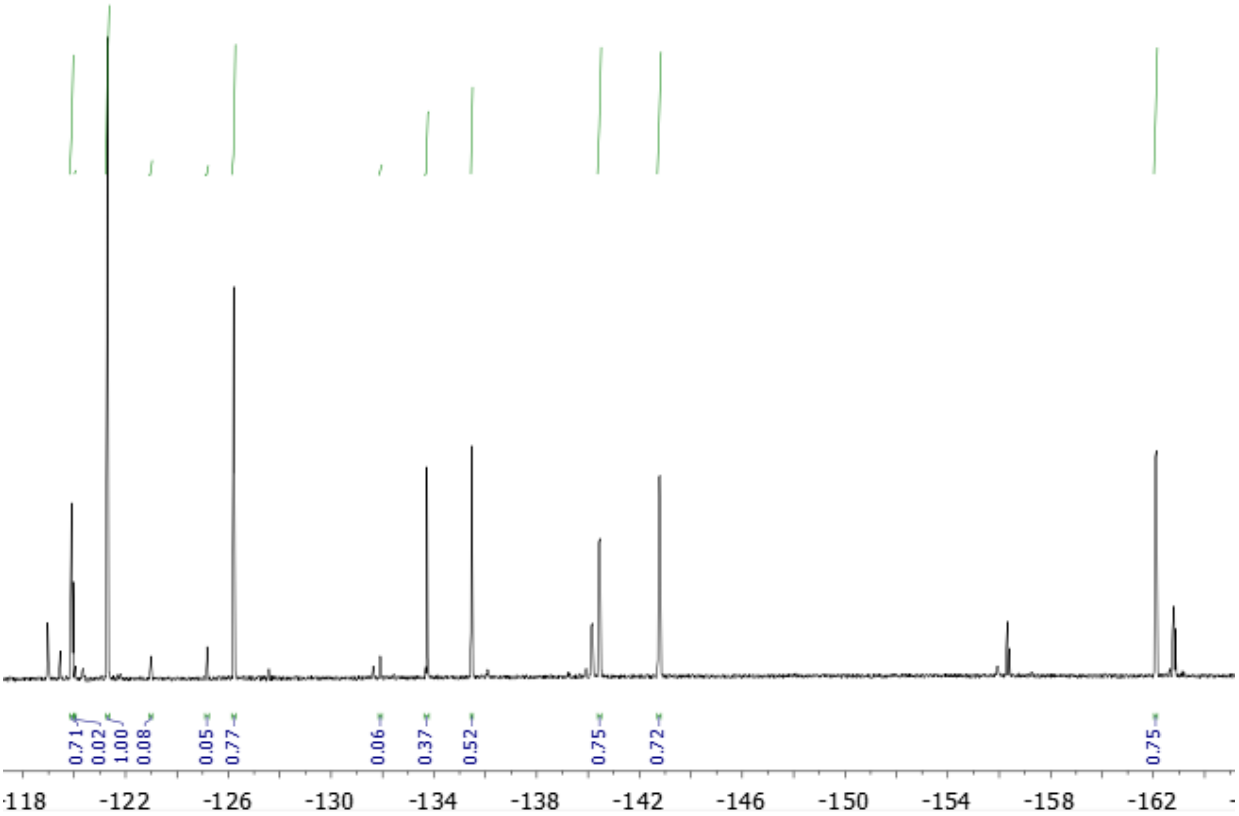

Figure 3.114: ^{19}F NMR spectrum ($CDCl_3$, 376 MHz), of the competitive reaction after 4 h, referenced to bis(4-fluorophenyl)ether (−121.3 ppm). Present are 2,3-difluoroaniline (−140.5 ppm and −162.1 ppm), 2-dimethylamino-3-fluoroaniline (−123.0 ppm), 2,4-difluoroaniline (−125.2 ppm and −139.2 ppm), 2-dimethylamino-4-fluoroaniline (−126.2 ppm), 2,5-difluoroaniline (−119.9 ppm and −142.8 ppm), 2-dimethylamino-5-fluoroaniline (−120.0 ppm), 2,6-difluoroaniline (−133.7 ppm), and 2-dimethylamino-6-fluoroaniline (−135.5 ppm).

Trifluoroanilines

Nominally equal quantities of two trifluoroanilines were reacted with a ten-fold excess of $Ti(NMe_2)_4$ for 1 h at 120 °C.

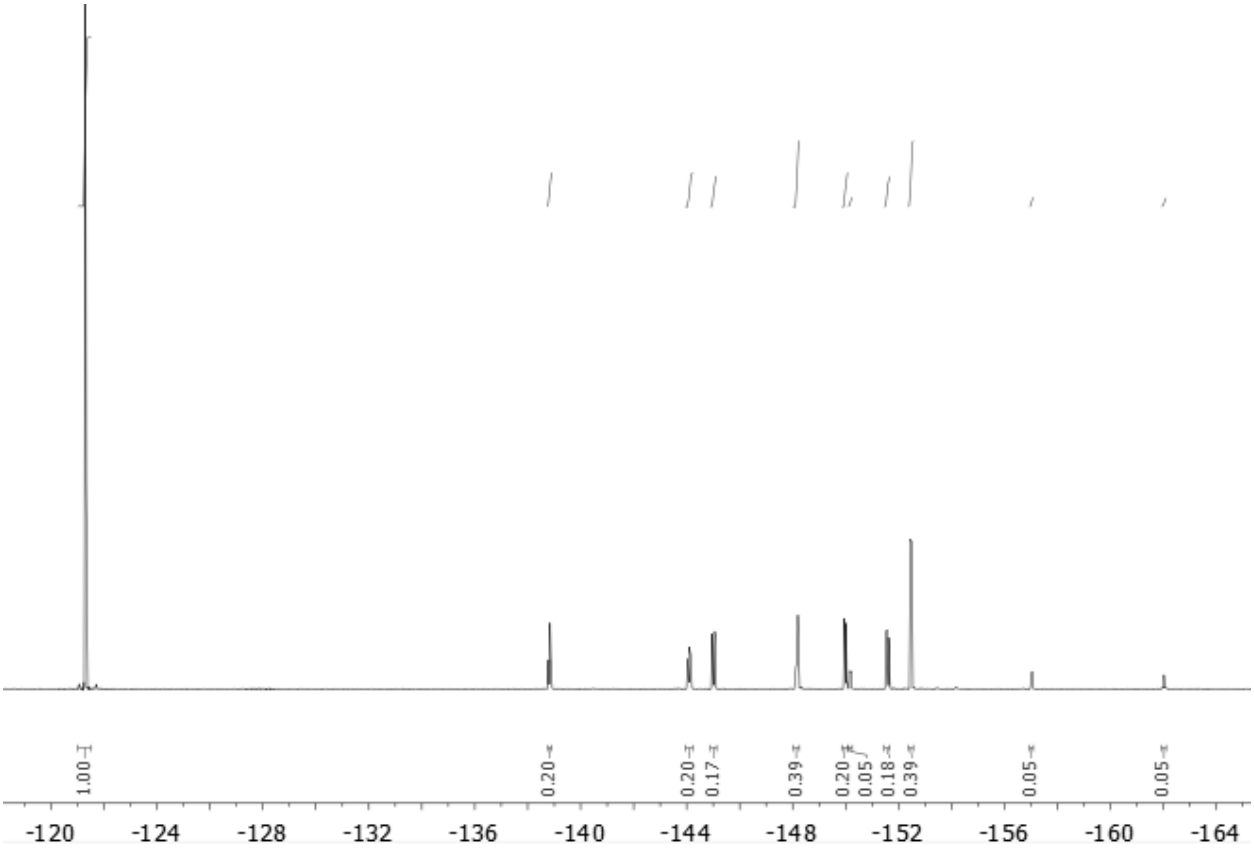

Figure 3.115: ^{19}F NMR spectrum ($CDCl_3$, 376 MHz), of competitive reaction with 2,3,4-trifluoroaniline and 2,4,5-trifluoroaniline after 1 h, referenced to bis(4-fluorophenyl)ether (−121.3 ppm). Also present are 2,3,4-trifluoroaniline (−148.9 ppm, −155.7 ppm, and −160.7 ppm), 2-dimethylamino-3,4-difluoroaniline, (−146.9 ppm and −151.2 ppm), 2,4,5-trifluoroaniline (−137.54 ppm, −142.82, and −148.7 ppm), and 2-dimethylamino-4,5-difluoroaniline (−143.73 ppm and −150.28 ppm).

Active Reaction Mixture Spectra

The following spectra (Figures 3.116 through 3.122) were obtained by combining $Ti(NMe_2)_4$, 2,6-difluoroaniline, and C_6D_6 solvent in an NMR tube and acquiring ^1H and ^{19}F NMR spectra, first at room temperature within one hour of mixing the reactants, and then again after heating the sample at 60 °C for 18 h.

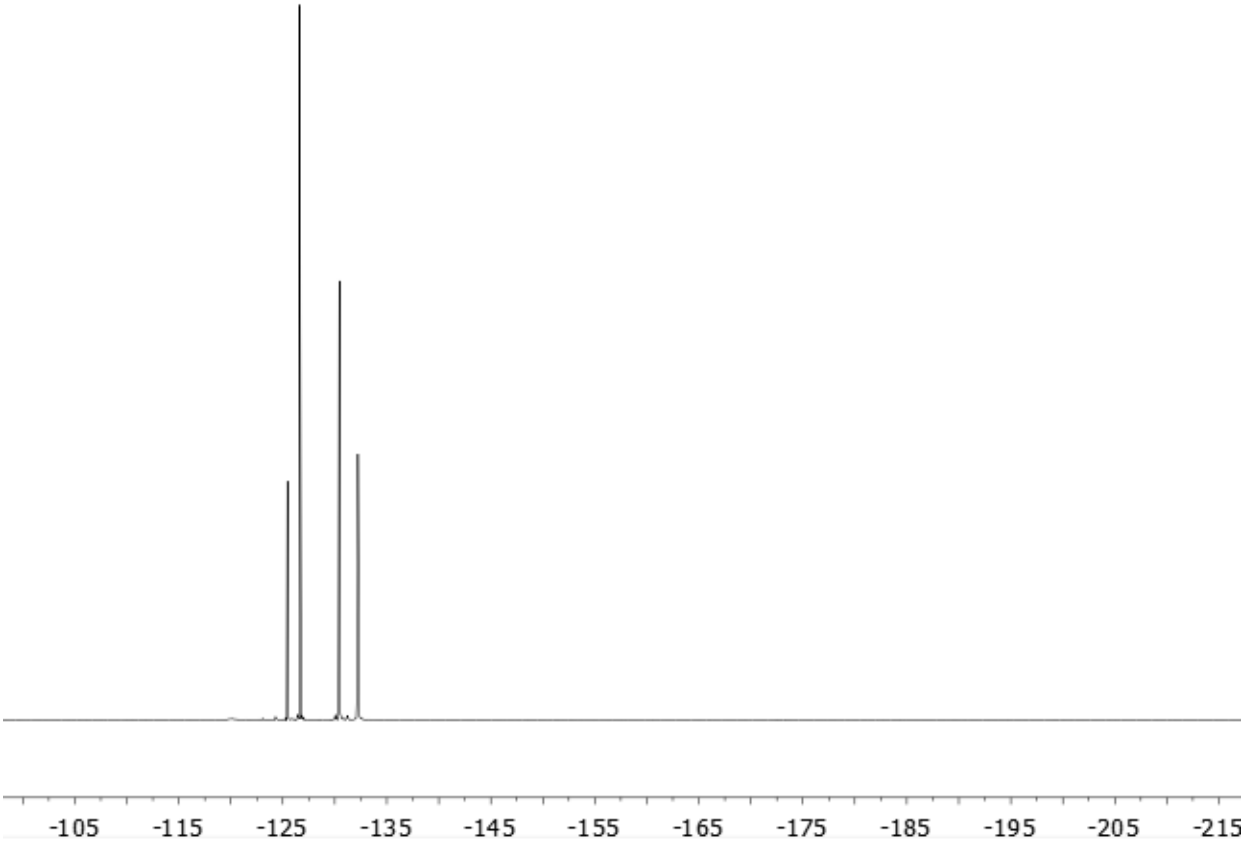

Figure 3.116: ^{19}F NMR spectrum (C_6D_6, 376 MHz) of the $Ti(NMe_2)_4$ + 2,6-difluoroaniline reaction mixture after < 1 h at 25 °C. A polynomial baseline correction was applied to the frequency-domain spectrum.

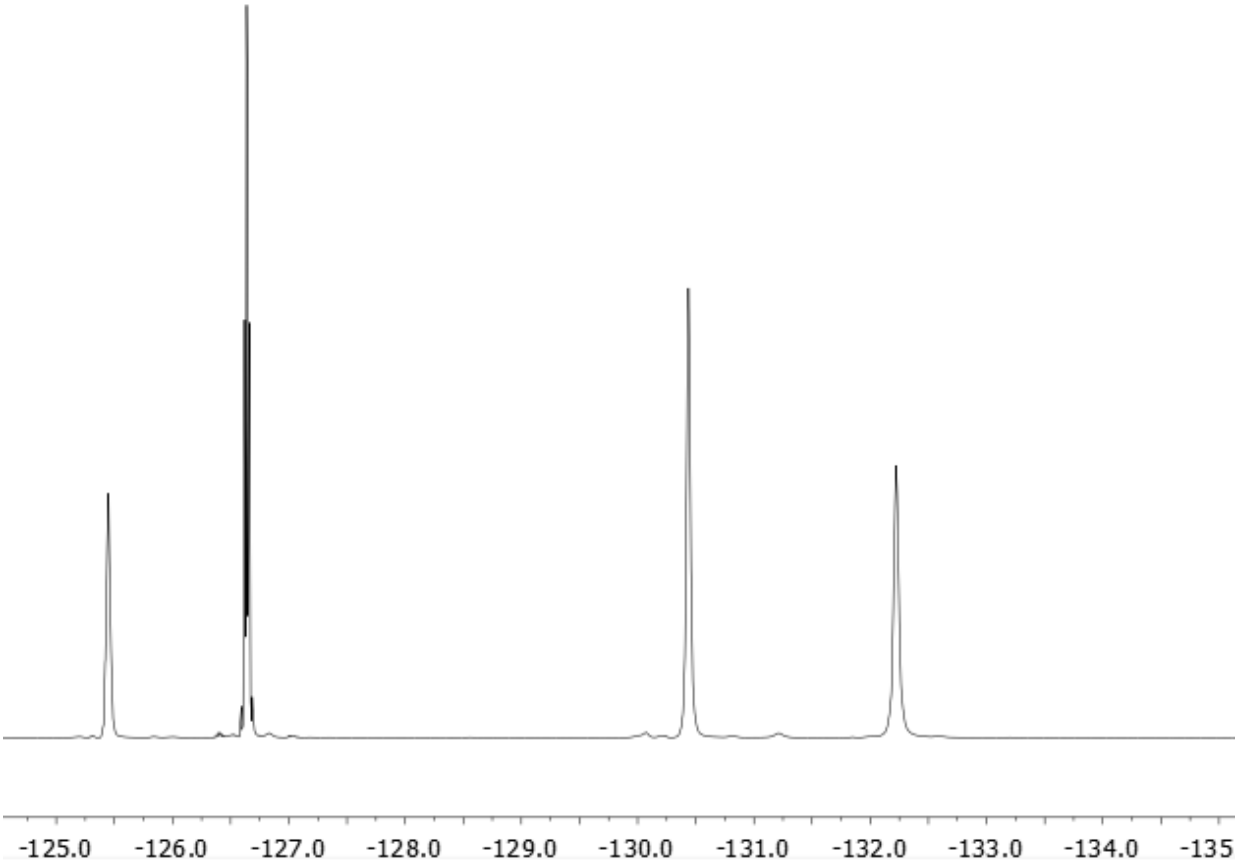

Figure 3.117: ^{19}F NMR spectrum (C_6D_6, 376 MHz), expansion of spectrum shown in Figure 3.116. The signal at −126.64 ppm is tentatively assigned to the starting aniline. This spectrum shows that there are at least three intermediates formed by combining the two reactants, even at room temperature.

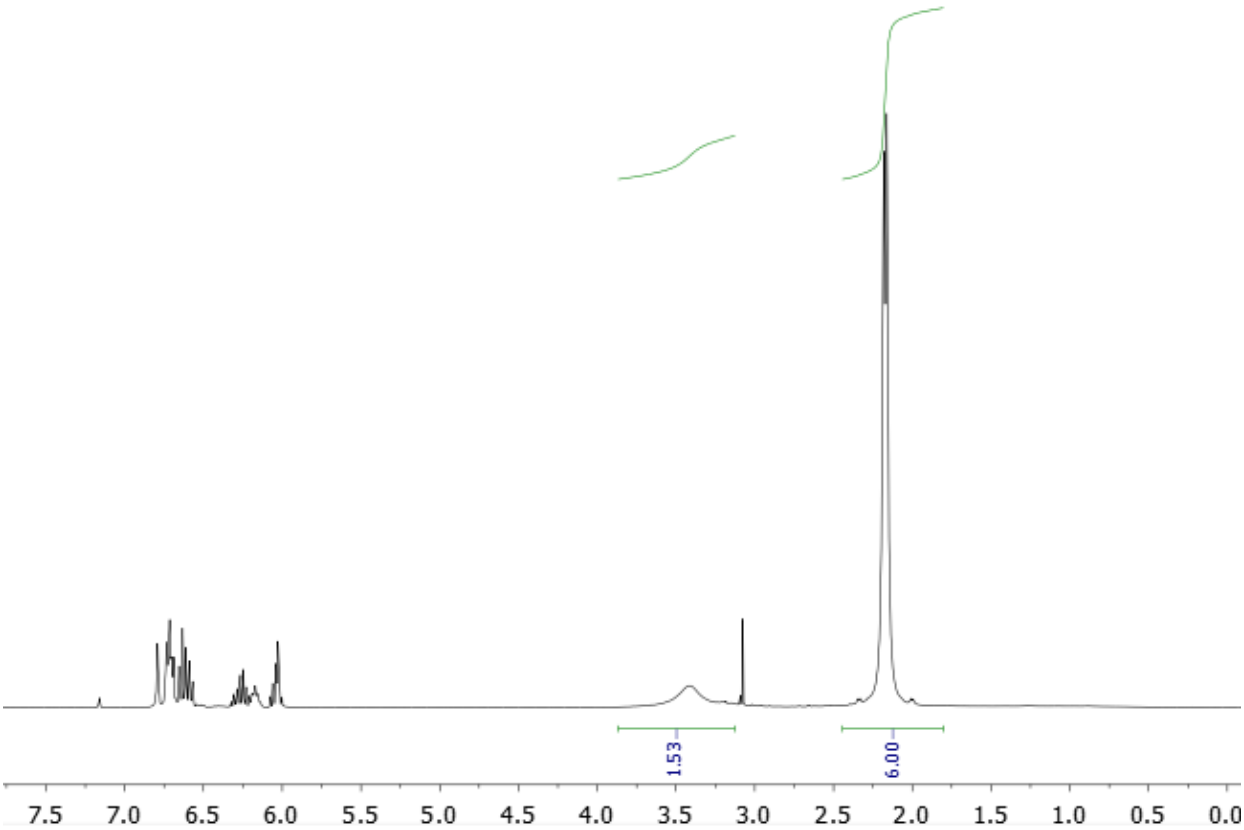

Figure 3.118: ^{1}H NMR spectrum (C_6D_6, 400 MHz) of the $Ti(NMe_2)_4$ + 2,6-difluoroaniline reaction mixture after < 1 h at 25 °C. Chemical shift was referenced to the solvent isotopomer, C_6D_5H at 7.16 ppm. The integrated signals are tentatively assigned to dimethylamine (see Figure 3.119).

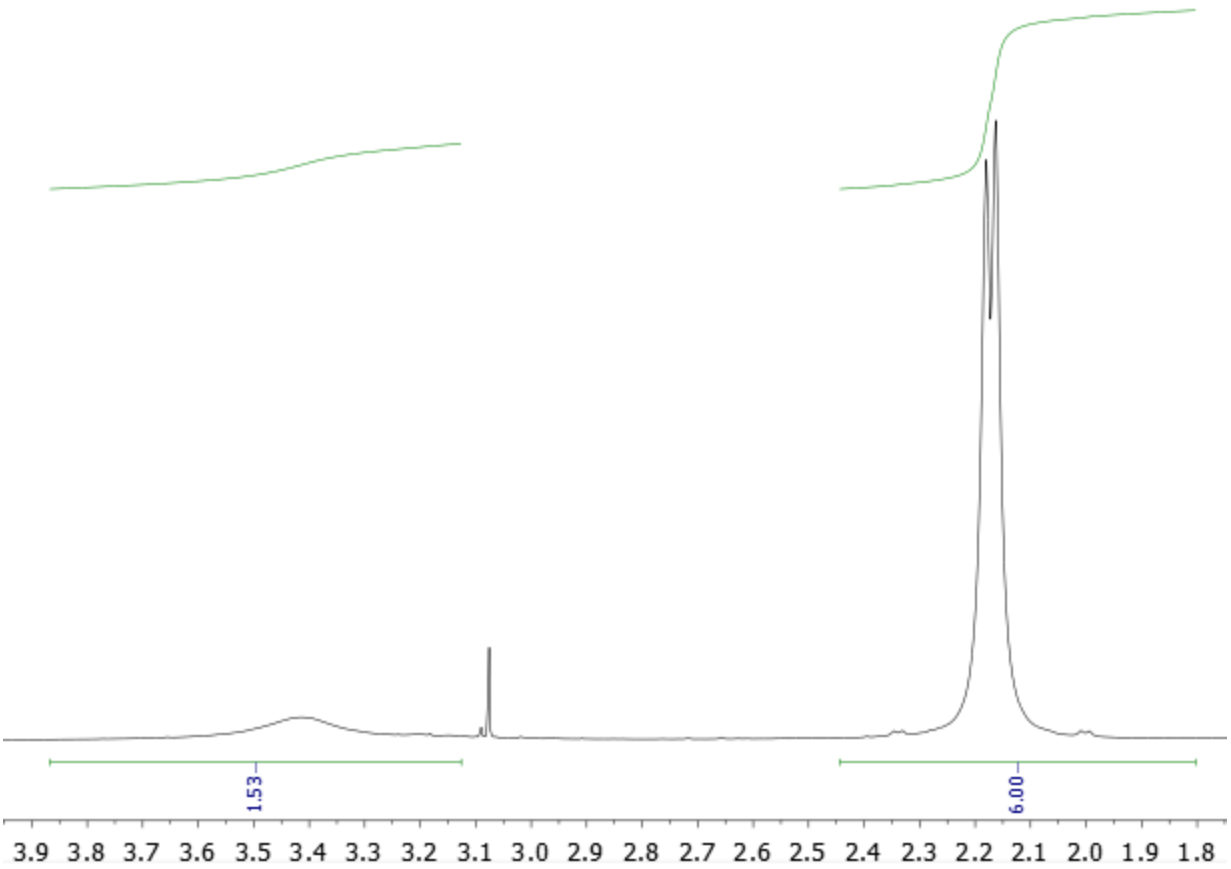

Figure 3.119: ^{1}H NMR spectrum (C_6D_6, 400 MHz), of the $Ti(NMe_2)_4$ + 2,6-difluoroaniline reaction mixture after < 1 h at 25 °C, expansion showing the integrated signals that we tentatively assign to free dimethylamine signals. Note that the coupling constant extracted from the ^{13}C satellites is J_{CH} = 135 Hz, whereas the reported coupling constant for $MeNH_2$ is J_{CH} = 133 Hz.* Importantly, if these signals are assigned to Me_2NH, then the $TiNMe_2$ signals that we expect to observe are conspicuously absent.

* https://www.chem.wisc.edu/areas/reich/nmr/10-cdata-05-jch.htm

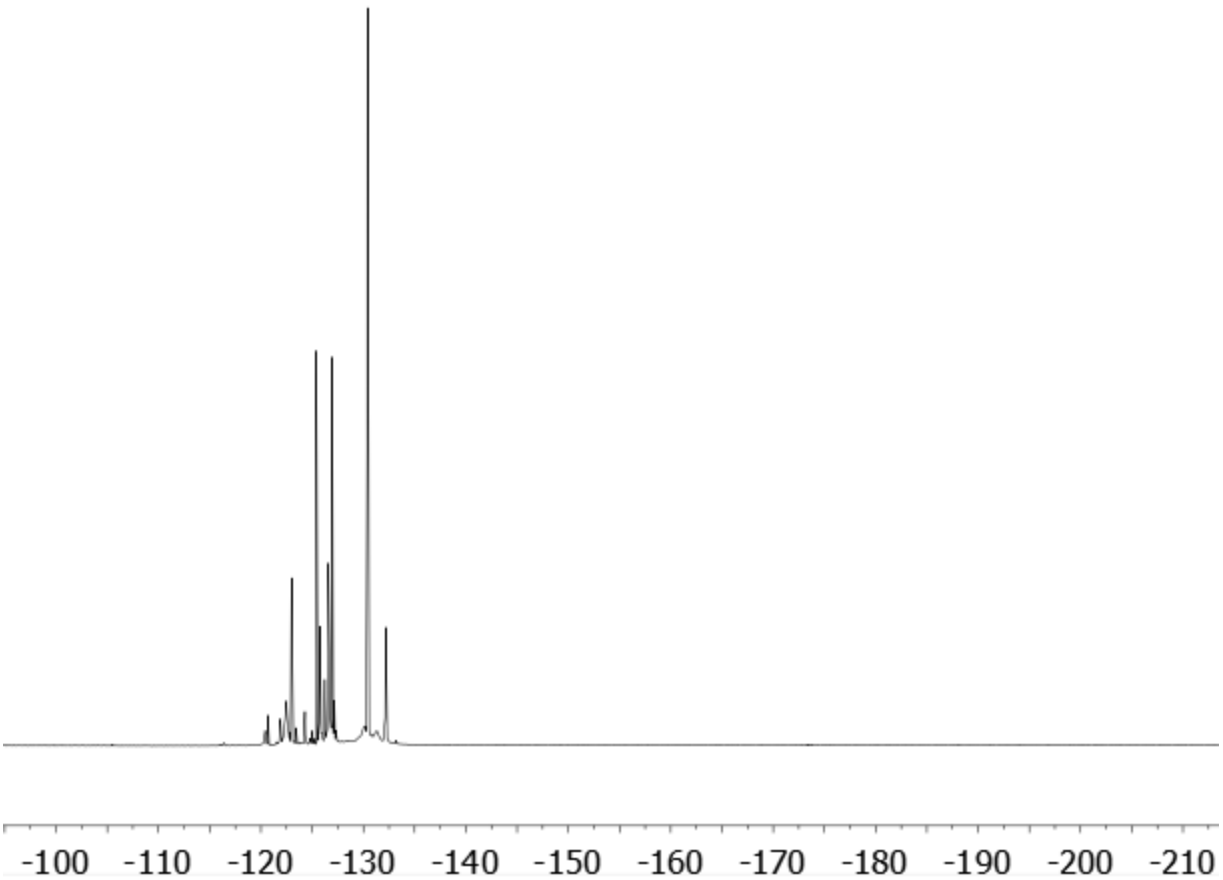

Figure 3.120: ^{19}F NMR spectrum (C_6D_6, 376 MHz) of the $Ti(NMe_2)_4$ + 2,6-difluoroaniline reaction mixture after 18 h at 60 °C. A polynomial baseline correction was applied to the frequency-domain spectrum.

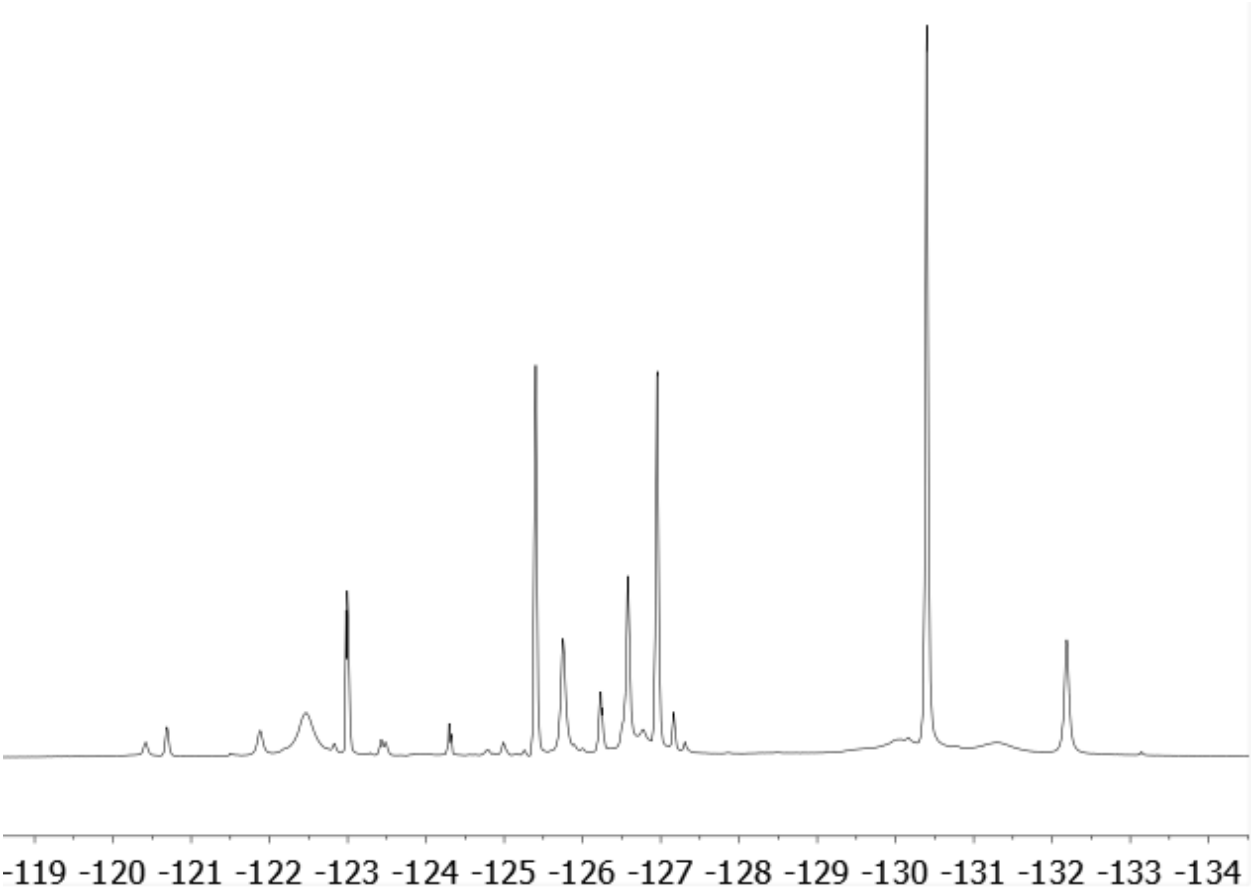

Figure 3.121: ^{19}F NMR spectrum (C_6D_6, 376 MHz), expansion, of the $Ti(NMe_2)_4$ + 2,6-difluoroaniline reaction mixture after 18 h at 60 °C. A polynomial baseline correction was applied to the frequency-domain spectrum.

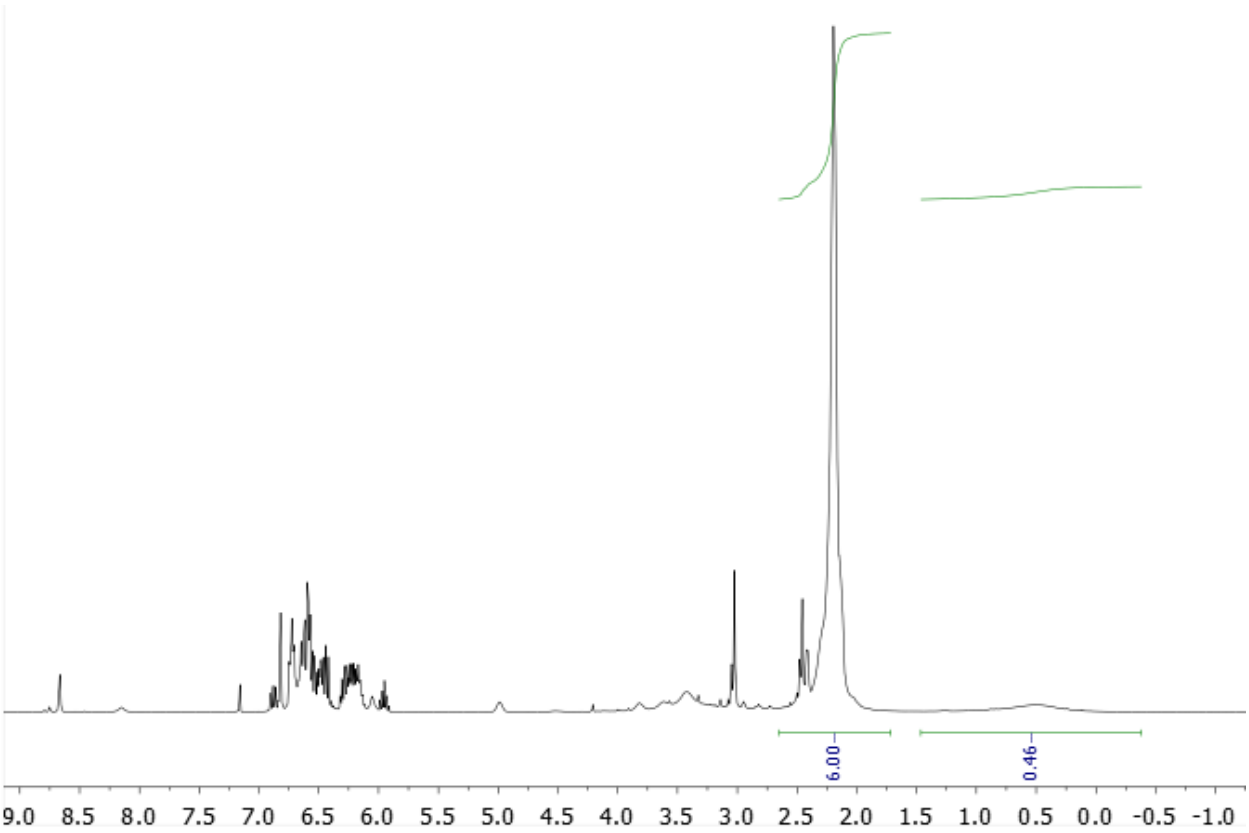

Figure 3.122: ^{1}H NMR spectrum (C_6D_6, 400 MHz) of the $Ti(NMe_2)_4$ + 2,6-difluoroaniline reaction mixture after 18 h at 60 °C.. The FID was zero-filled to 128k, a polynomial baseline correction was applied to the frequency-domain spectrum, and chemical shift was referenced to the solvent isotopomer, C_6D_5H at 7.16 ppm.

High Resolution Mass Spectra

Table 3.17: Exact mass data obtained by ESI-TOF analysis.			
Compound	**Formula (M+H)**	**Calcd (amu)**	**Found (amu)**
2-dimethylamino-3-fluoroaniline	$C_8H_{12}FN_2$	155.0985	155.0972
2-dimethylamino-4-fluoroaniline	$C_8H_{12}FN_2$	155.0985	155.0974
2-dimethylamino-5-fluoroaniline	$C_8H_{12}FN_2$	155.0985	155.0968
2-dimethylamino-6-fluoroaniline	$C_8H_{12}FN_2$	155.0985	155.0985
2-dimethylamino-3,4-difluoroaniline	$C_8H_{11}F_2N_2$	173.0890	173.0901
2,6-bis(dimethylamino)-3-fluoroaniline	$C_{10}H_{17}FN_3$	198.1407	198.1398
2-dimethylamino-3,6-difluoroaniline	$C_8H_{11}F_2N_2$	173.0890	173.0874
6-dimethylamino-2,3-difluoroaniline	$C_8H_{11}F_2N_2$	173.0890	173.0878
2-dimethylamino-4,5-difluoroaniline	$C_8H_{11}F_2N_2$	173.0890	173.0894
2,6-bis(dimethylamino)-3,4-difluoroaniline	$C_{10}H_{16}F_2N_3$	216.1312	216.1309
2-dimethylamino-3,4,5,6-tetrafluoroaniline	$C_8H_9F_4N_2$	209.0702	209.0700
2,6-bis(dimethylamino)-3,4,5-trifluoroaniline	$C_{10}H_{15}F_3N_3$	234.1218	234.1204
2-dimethylamino-N-ethyl-6-fluoroaniline	$C_{10}H_{16}FN_2$	183.1298	183.1284
2-dimethylamino-6-fluorophenol	$C_8H_{10}FNO$	156.0825	156.0824

We were unable to obtain a suitable HRMS of 6-dimethylamino-2,3,4-trifluoroaniline, which was present only as a component of an inseparable mixture. GCMS analysis confirmed its presence with the correct nominal mass. CGMS analysis used an Agilent 7890A fitted with a 30-m HP-5 column. The method used an initial temperature of 40 °C followed by a ramp of 20 °C/min to a final temperature of 180 °C, and held at 180 °C for 2.6 min. The product mixture was diluted with dichloromethane prior to injection.

Chapter 4: Conclusions and Future Work

A selective defluoroamination of *o*-fluoroanilines using stoichiometric amounts of $Ti(NMe_2)_4$ has been reported. The primary way in which this synthesis could be improved would be to turn over the titanium amide. This improvement is unlikely to come easily; per the proposed mechanism, both the aniline and the fluorine remain bound to the metal prior to workup. Potentially, this reaction could be made catalytic with the addition of a fluorine sink, such as Me_3SiNMe_2 or amidoaluminum compounds.

Another limitation of the reported stoichiometric reaction is its high temperature and long reaction time. Alternative transition metal amides such as $Zr(NMe_2)_4$ or $Nb(NMe_2)_5$ have more sterically accessible metal centers and might allow reactions to occur under milder conditions. If a reaction can be contrived that will use secondary amines as the amide source, together with an inexpensive titanium source like $TiCl_4$ in a one-pot procedure, then the scope of the reaction would increase greatly.

Although this reaction offers excellent selectivity and provides moderate to high yields in the context of fluoroanilines, it does not generalize well, as demonstrated by the poor yields obtained in the reactions of $Ti(NMe_2)_4$ with 2,6-difluorophenol and *N*-ethyl-2,6-difluoroaniline. Moreover, 23 h at 120 °C is somewhat forcing and entirely excludes the presence of many other functional groups. However, it is still worth exploring the potential of fluorophenyl thiols as substrates. In addition to potentially expanding substrate scope, sulfur is softer than nitrogen or oxygen, and when bound to titanium(IV), which is quite hard, the softer ligand could potentially form weaker metal-ligand bonds, making it easier to dislodge the substrate and improving the outlook for making the synthesis catalytic.

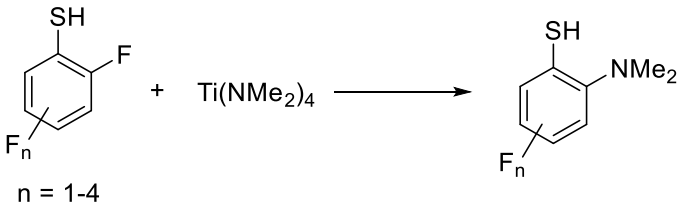

Figure 4.1: Potential substrate expansion, using an *o*-fluorothiol.

A less ambitious possibility is to explore additional aminated substrates. For instance, we have not yet tried reacting 2,6-difluorobenzylamine, or anilines with trifluoromethyl moieties. It might also be interesting to see if a more complex ring system, such as a fluorinated naphthylamine, has comparable reactivity.

References

(1) Barker, A. J.; Gibson, K. H.; Grundy, W.; Godfrey, A. A.; Barlow, J. J.; Healy, M. P.; Woodburn, J. R.; Ashton, S. E.; Curry, B. J.; Scarlett, L.; et al. *Bioorg. Med. Chem. Lett.* **2001**, *11*, 1911–1914.

(2) Ballard, P.; Bradbury, R. H.; Harris, C. S.; Hennequin, L. F. A.; Hickinson, M.; Kettle, J. G.; Kendrew, J.; Klinowska, T.; Ogilvie, D. J.; Pearson, S. E.; et al. *Bioorganic Med. Chem. Lett.* **2006**, *16*, 4908–4912.

(3) Faught, E. *Epilepsy Curr.* **2011**, *11*, 75–78.

(4) Splinter, M. Y. *Clin. Ther.* **2012**, *34*, 1845–1856.

(5) Sánchez, C.; Bøgesø, K.; Ebert, B.; Reines, E.; Braestrup, C. *Psychopharmacology (Berl).* **2004**, *174*, 163–176.

(6) Wang, J.; Sánchez-Roselló, M.; Aceña, J. L.; Del Pozo, C.; Sorochinsky, A. E.; Fustero, S.; Soloshonok, V. A.; Liu, H. *Chem. Rev.* **2014**, *114*, 2432–2506.

(7) Istvan, E. S.; Deisenhofer, J. *Science.* **2016**, *292*, 1160–1164.

(8) Weaver, J.; Senaweera, S. *Tetrahedron* **2014**, *70*, 7413–7428.

(9) Zhou, Y.; Wang, J.; Gu, Z.; Wang, S.; Zhu, W.; Luis, J.; Soloshonok, V. A.; Izawa, K.; Liu, H. *Chem. Rev.* **2016**, *116*, 422–518.

(10) Hagmann, W. K. *J. Med. Chem.* **2008**, *51*, 4359–4369.

(11) Gillis, E. P.; Eastman, K. J.; Hill, M. D.; Donnelly, D. J.; Meanwell, N. A. *J. Med. Chem.* **2015**, *58*, 8315–8359.

(12) O'Hagan, D. *J. Fluor. Chem.* **2010**, *131*, 1071–1081.

(13) Jeschke, P. *ChemBioChem* **2004**, *5*, 1439–4227.

(14) Kuehnel, M. F.; Lentz, D.; Braun, T. *Angew. Rev.* **2013**, *52*, 3328–3348.

(15) Kühnel, M. F.; Lentz, D. *Angew. Chem. Intl. Ed.* **2010**, *49*, 2933–2936.

(16) Rieth, R. D.; Brennessel, W. W.; Jones, W. D. *Eur. J. Inorg. Chem.* **2007**, 2839–2847.

(17) Kraft, B. M.; Lachicotte, R. J.; Jones, W. D. **2001**, *6*, 10973–10979.

(18) Fujita, T.; Fuchibe, K.; Ichikawa, J. *Angew. Chem. Intl. Ed.* **2018**, *58*, 390–402.

(19) Cronin, L.; Higgitt, C. L.; Karch, R.; Perutz, R. N. *Organometallics* **1997**, *16*, 4920–4928.

(20) Jasim, N. A.; Perutz, R. N.; Whitwood, A. C.; Braun, T.; Izundu, J.; Neumann, B.; Rothfeld, S.; Stammler, H. *Organometallics* **2004**, *23*, 6140–6149.

(21) Hu, J.; Zhang, J.; Wang, G.; Sun, H.; Zhang, J. *Inorg. Chem.* **2016**, *55*, 2271–2283.

(22) Ulrike, J.; Klahn, M.; Arndt, P.; Baumann, W.; Spannenberg, A.; Burlakov, V. V; Rosenthal, U. *J. Mol. Catal. A Chem.* **2007**, *261*, 184–189.

(23) Vela, J.; Smith, J. M.; Yu, Y.; Ketterer, N. A.; Flaschenriem, C. J.; Lachicotte, R. J.; Holland, P. L. *J. Am. Chem. Soc.* **2005**, 7857–7870.

(24) Edelbach, B. L.; Jones, W. D. *J . Am. Chem. Soc* **1997**, *7863*, 7734–7742.

(25) Whittlesey, M. K.; Peris, E. *ACS Catal.* **2014**, *4*, 3152–3159.

(26) Sabater, S.; Mata, J. A.; Peris, E. *Nat. Commun.* **2013**, *4*, 1–7.

(27) Li, J.; Zheng, T.; Sun, H.; Li, X. *Dalt. Trans.* **2013**, *42*, 13048–13053.

(28) Hein, N. M.; Pick, F. S.; Fryzuk, M. D. *Inorg. Chem.* **2017**, *56*, 14513–14523.

(29) Breyer, D.; Braun, T.; Kläring, P. *Organometallics* **2012**, *31*, 1417–1424.

(30) Fuchibe, K.; Ohshima, Y.; Mitomi, K.; Akiyama, T. *J. Fluor. Chem.* **2007**, *128*, 1158–1167.

(31) Kiplinger, J. L.; Richmond, T. G. *Chem. Commun.* **1996**, 1115–1116.

(32) Edelbach, B. L.; Rahman, A. K. F.; Lachicotte, R. J.; Jones, W. D. *Organometallics* **1999**, *18*, 3170–3177.

(33) Kim, B.; Woo, H.; Kim, W.; Yun, S.; Hwang, T. *Bull. Korean Chem. Soc.* **2000**, *21*, 211–214.

(34) Kraft, B. M.; Jones, W. D. *J. Org. Chem.* **2002**, *658*, 132–140.

(35) Jones, W. D. *Dalt. Trans.* **2003**, 3991–3995.

(36) Sun, A. D.; Love, J. A. *Org. Lett.* **2011**, *13*, 2750–2753.

(37) Nova, A.; Mas-Ballesté, R.; Lledós, A. *Organometallics* **2012**, *31*, 1245–1256.

(38) Vasil, A. A.; Engman, L.; Storm, J. P. *Organometallics* **1999**, *18*, 1318–1325.

(39) Pearson, A. J.; Ciurea, D. V. *J. Org. Chem.* **2008**, *73*, 760–763.

(40) Chambers, R. D.; Martin, P. A.; Waterhouse, J. S.; Williams, D. L. H.; Anderson, B. *J. Fluor. Chem.* **1982**, *20*, 507–514.

(41) Chambers, R. D.; Seabury, M. J.; Williams, D. L. H.; Hughes, N. *J. Chem. Soc. Perkin. Trans.* **1988**, 251–254.

(42) Chambers, R. D.; Seabury, M. J.; Williams, D. L. H.; Hughes, N. *J. Chem. Soc. Perkin. Trans.* **1988**, 255–257.

(43) Chambers, R. D.; Martin, P. A.; Sandford, G.; Williams, D. L. H. *J. Fluor. Chem.* **2008**, *129*, 998–1002.

(44) Chambers, R. D.; Kenneth, W.; Musgrave, R.; Waterhouse, J. S.; Williams, D. L. H. *J. C. S. Chem. Comm.* **1974**, 239–240.

(45) Diness, F.; Begtrup, M. *Org. Lett.* **2014**, *16*, 3130–3133.

(46) Ivashchuk, O.; Sorokin, V. I. *Tetrahedron* **2009**, *65*, 4652–4658.

(47) Albrecht, M.; Lindner, M. M. *Dalt. Trans.* **2011**, *40*, 8733–8744.

(48) Breitenfeld, J.; Scopelliti, R.; Hu, X. *Organometallics* **2012**, *31*, 2128–2136.

(49) Li, M.; Wang, X.; Luo, Y.; Chen, C. *Angew. Chem. Intl. Ed.* **2017**, *56*, 11604–11609.

(50) Grushin, V. V. *Acc. Chem. Res.* **2010**, *43*, 160–171.

(51) Eisenstein, O.; Milani, J.; Perutz, R. N. *Chem. Rev.* **2017**, *117*, 8710–8753.

(52) Li, B. Z.; Qian, Y. Y.; Liu, J.; Chan, K. S. *Organometallics* **2014**, *3*, 7059–7068.

(53) Vlasov, V. M. *J. Fluor. Chem.* **1993**, *61*, 193–216.

(54) Bume, D. D.; Harry, S. A.; Lectka, T.; Pitts, C. R. *J. Org. Chem.* **2018**, 8803–8814.

(55) Lantaño, B.; Postigo, A. *Org. Biomol. Chem.* **2017**, *15*, 9954–9973.

(56) Yerien, D. E.; Bonesi, S.; Postigo, A. *Org. Biomol. Chem.* **2016**, *14*, 8398–8427.

(57) Sun, H.; Koch, A. S.; DiMagno, S. G. *ACS Symp. Ser.* **2009**, *1003*, 85–104.

(58) Amii, H.; Uneyama, K. *Chem. Rev.* **2009**, *109*, 2119–2183.

(59) Clot, E.; Eisenstein, O.; Jasim, N.; MacGregor, S. A.; McGrady, J. E.; Perutz, R. N. *Acc. Chem. Res.* **2011**, *44*, 333–348.

(60) Baird, D. A.; Jamal, S.; Johnson, S. A. *Organometallics* **2017**, *36*, 1436–1446.

(61) Kwan, E. E.; Zeng, Y.; Besser, H. A.; Jacobsen, E. N. *Nat. Chem.* **2018**, *10*, 917–923.

(62) Senaweera, S. M.; Singh, A.; Weaver, J. D. *J . Am. Chem. Soc* **2014**, *136*, 3002–3006.

(63) Senaweera, S.; Weaver, J. D. *J . Am. Chem. Soc* **2016**, *138*, 1520–1523.

(64) Luo, H.; Wu, G.; Xu, S.; Wang, K.; Wu, C.; Zhang, Y.; Wang, J. *Chem. Commun.* **2015**, *51*, 13321–13323.

(65) Luo, Z.; Zhao, H.; Zhang, X. *Org. Lett.* **2018**, *20*, 2543–2546.

(66) Hughes, R. P.; Lindner, D. C.; Liable-sands, L. M.; Rheingold, A. L. *Organometallics* **2001**, *3*, 363–366.

(67) Park, S.; Pontier-Johnson, M.; Roundhill, D. M. *J . Am. Chem. Soc* **1989**, *111*, 3101–3103.

(68) Deck, P. A.; Konaté, M. M.; Kelly, B. V.; Slebodnick, C. *Organometallics* **2004**, *23*, 1089–1097.

(69) Schrock, R. R.; Adamchuk, J.; Ruhland, K.; Lopez, L. P. H. *Organometallics* **2003**, *22*, 5079–5091.

(70) Cochran, F. V.; Bonitatebus, P. J.; Schrock, R. R. *Organometallics* **2000**, *19*, 2414–2416.

(71) Sousa, F. C.; Bloomer, B. J.; Wengryniuk, S. E. *Tetrahedron* **2018**, *74*, 3278–3282.

(72) Bremond, J. P.; Donnier, M.; Limouzin, Y. *J. Organomet. Chem.* **1975**, *90*, 279–284.

(73) Ahrens, T.; Kohlmann, J.; Ahrens, M.; Braun, T. *Chem. Rev.* **2015**, *115*, 931–972.

(74) Abraham, B. R. J.; Macdonald, D.; Pepper, E. S.; Kline, S. *J. Chem. Soc. B Phys. Org.* **1967**, 835–841.

(75) Abraham, R. J.; Macdonald, D. B.; Pepper, E. S. *Chem. Commun.* **1966**, 542–543.